# Development of sustainable high performance fiber-reinforced concretes by using calcium sulfoaluminate cement

by

**Vahid Afroughsabet**

A thesis submitted in partial fulfillment of the requirements

for the degree of Doctor of Philosophy in Civil Engineering

Politecnico di Milano University

Department of Architecture, Built Environment and Construction Engineering

Supervisor and Tutor: Luigi Biolzi

The chair of the doctoral program: Enrico De Angelis

Doctoral Committee:

Professor Giuseppe Campione

Professor Gaetano Russo

Assistant professor Matteo Maria Gastaldi

Professor Maurizio Orlando

Associate professor Claudio Bernuzzi


POLITECNICO
DI MILANO

March 2018 – Cycle XXX

# ACKNOWLEDGEMENTS

I would like to take this opportunity to express my gratitude toward all individuals who support me during this journey by the hard work, sacrifices, and guidance. Foremost, I would like to express my most profound gratitude to my academic advisors, Professor Luigi Biolzi for his extraordinary enthusiasm, optimism, ideas, insight, encouragement, support, and guidance during this research. Professor Biolzi gave me the opportunity to work on project regarding HPFRC made with CSA cement. Professor Biolzi is a great mentor and a strong role-model as a scholar. A special thank you is also extended to Professor Sara Cattaneo for her willingness to share her experiences regarding the features of HPFRC in this study.

I would also like to thank my dissertation committee members: Professor Giuseppe Campione, Professor Gaetano Russo, Professor Matteo M. Gastaldi, Professor Maurizio Orlando, and Professor Claudio Bernuzzi. I am also immensely grateful to my PhD thesis external examiners: Professor Paulo J. M. Monteiro, and Professor Togay Ozbakkaloglu for their time, helpful advice, and constructive criticism.

I would like to gratefully thank Professor Paulo J.M. Monteiro for his thoughtful comments and suggestions on my research. He has a wealth of knowledge of cement science and has been generously available for scientific discussions. It has been a privilege to work with him on this intriguing subject during my abroad research study at University of California, Berkeley. I would also like to thank Professor Claudia P. Ostertag for her advice on the subject of HPFRC.

I would also like to acknowledge Gian Luca Guerrini who provided his insightful and critical feedback on my research. I should also thank Mr. Paolo Broglia for helping me to conduct my experimental study at the Concrete Materials Laboratory of the Politecnico di Milano, University.

The next group of people who deserve a plenty of appreciation are my friends for accompanying me over the past three years. A special thanks to Fazel Khayatian for his valuable and continuous assistance during this journey.

Above all, I must convey my sincere and special thanks to my fabulous family: my beautiful wife, Bahar Izadi, who has always provided me with a reminder of what is truly important in life, and has been a constant source of strength, inspiration, and love; my mother that if it was not for her efforts, I would not have been in this state now; and my sister who positively supported me.

# Dedication

I would enthusiastically like to dedicate this work to my beloved and amazing wife **Bahar** whose love, support, and patience are the major reasons for me to achieve accomplishments.

# Abstract

Nowadays, the demand for using high performance fiber-reinforced concrete (HPFRC) with improved qualities is widely increased throughout the world. As it is commonly known, for the production of a high performance concrete (HPC) matrix, a large amount of binder is normally used. The production of ordinary Portland cement (OPC) as the binder of concrete accounts for 7% of $CO_2$ emission, in which has a notable environmental impacts, and subsequently results in unsustainable concrete. This study is aimed at replacing OPC with innovative cements like calcium sulfoaluminate cement (CSA) and Type K cement to develop more sustainable HPFRC. Hence, twenty four different concrete mixes were developed and their mechanical, physical, durability and microstructural properties have been assessed.

The first objective of this study is to study the influence of CSA cement on the properties of HPC. Additionally, CSA-blended mixes with OPC, and also ternary mix containing slag were produced to investigate the effect of blended binder on the features of HPC. The second objective of this study is to evaluate the effect of different metallic and non-metallic fibers at constant fiber content of 1% on the properties of HPFRC. Also, the effect of fiber hybridization on the engineering properties of HPFRC was studied. The results of this study indicate that the full replacement of OPC with Type K cement had insignificant influence on the mechanical properties of HPC, while the addition of CSA cement led to an increase in the strengths of HPC. Among different cement based concrete developed in this study, the best performing mix was attained by the concrete containing pure CSA cement. The addition of CSA cement results in a reduced shrinkage deformation, improved durability properties, and enhanced bond between cement matrix and fibers. The results of HPFRC indicate that the addition of double hooked-end (DHE) steel fibers significantly increased the engineering properties of concrete. A deflection-hardening behavior was attained in the flexural performance of HPFRC containing at least 0.5% DHE steel fibers. The findings of this study are of great interest to structural engineers and have the potential to significantly contribute toward expanding the use of HPFRC to different structural applications.

**Keywords:** High performance concrete; Fiber-reinforced concrete; Type K cement; Calcium sulfoaluminate cement; Blended cement mix; Slag; Mechanical properties; Durability properties; Shrinkage deformation; Microstructural properties

# Contents

# List of Figures

# List of Tables

# Glossary

**List of abbreviations:**

| | |
|---|---|
| HPC: | High performance concrete |
| OPC: | Ordinary Portland cement |
| CSA: | Calcium sulfoaluminate cement |
| DHE: | Double hooked-end |
| HE: | Hooked-end |
| PVA: | Polyvinyl alcohol |
| HPFRC: | High performance fiber-reinforced concretes |
| W/C: | Water-cement |
| SEM: | Scanning electron microscopy |
| XRD: | X-ray diffraction |
| $CO_2$: | Carbon dioxide |
| SCM: | Supplementary cementitious materials |
| CAC: | Calcium aluminate cements |
| SHCC: | Shrinkage-compensating concrete |
| ITZ: | Interfacial transition zone |
| FRC: | Fiber-reinforced concrete |
| HSC: | High strength concrete |
| SAC: | Sulfoaluminate cement |
| SRA: | Shrinkage reducing admixture |
| HSFRCC: | High-strength fiber-reinforced cementitous composites |
| PP: | Polypropylene |
| SLS: | Serviceability Limit State |
| RCPT: | Rapid chloride penetration test |
| UHPC: | Ultra-high performance concrete |
| SFRSCC: | Steel fiber-reinforced self-consolidating concrete |
| RMT: | Rapid migration test |
| GGBS: | Ground granulated blast-furnace slag |
| CC: | Conventional concrete |
| SSD: | Saturated surface dry |

| | |
|---|---|
| SCE: | Saturated calomel electrode |
| SE: | Secondary electrons |
| BSE: | Backscattered electrons |
| EDX: | Energy dispersive X-ray spectroscopy |
| HyFRC: | Hybrid-fiber-reinforced concrete |

**List of cement chemistry:**

| | |
|---|---|
| $C_4A_3\$$: | Ye'elimite |
| $C_2S$: | Belite |
| $C_3S$: | Alite |
| $CaSO_4$: | Gypsum |
| $C_3A$: | Tricalcium aluminate |
| AFm: | Monosulfate |
| Aft: | Ettringite |
| C$: | Calcium sulfate |
| CH: | Calcium hydroxide |
| $C_6A\$_3H_{32}$: | Ettringite |
| $AH_3$: | Aluminum hydroxide |
| $C_4A\$H_{12}$: | Monosulfate |
| $C_2ASH_8$: | Strätlingite |
| C-S-H: | Calcium-silicate-hydrate |

# Chapter 1
# Introduction

## 1.1 Problem statement

Portland cement concrete is the most widely used human-made material on the planet; about 25 billion metric tons are produced globally each year. Nowadays the demand for using high performance concrete (HPC) is widely increased throughout the world. As it is commonly known, for the production of a HPC matrix, a large amount of binder is normally used. Even though the reasons for concrete's dominance are diverse, the massive production and consumption cycle of concrete have significant environmental impacts, making the concrete industry unsustainable. Currently, Portland cement concrete production accounts for around 7% of carbon dioxide ($CO_2$) emissions annually. Most of the emissions are attributable to the production of ordinary Portland cement (OPC) clinker. The current approach to overcome this problem is through the reduction of clinker factor, and replacement of OPC with supplementary cementitious materials such as fly ash, slag, silica fume and natural pozzolan. However, due to growing field experience and increasing demand for those materials, there is an essential need to develop concrete made with new generation of cement like calcium sulfoaluminat cement (CSA). CSA clinker can also be blended with OPC to produce Type K cement, which is expansive.

On the other hand concrete is a common building material, generally weak in tension, often ridden with cracks due to plastic and drying shrinkage. Moreover, mechanical loading conditions as well as drying shrinkage can cause the conventional concrete to crack and consequently reduce the overall strength and stiffness of the concrete structure. Once a crack has formed, water and

aggressive agents such as chlorides and sulphates can penetrate quicker and greater into the concrete and subsequently accelerating the corrosion process and reducing the service life of reinforced concrete structures. Hence, introduction of short discrete fibers into the concrete can be used to counteract and prevent the propagation of cracks.

The goal of the current study is to develop sustainable HPC through the replacement of OPC with innovative cement such as CSA cement and Type K cement. Moreover, the properties of CSA blended mixes containing slag as a replacement of OPC are assessed in some mixes. The current research also aims at understanding the effect of introducing different types of fibers like double hooked-end (DHE) steel fibers, hooked-end (HE) steel fibers, and polyvinyl alcohol (PVA) fibers on the mechanical, durability, and microstructural properties of HPC. Therefore, the findings of this research have the potential to significantly contribute toward expanding the use of HPC manufactured with innovative binders and reinforced with fibers to different structural applications.

## 1.2 Objectives and innovative features

The current doctoral thesis is designed to develop a much more sustainable HPC with and without fibers by replacing OPC with CSA cement. The inclusion of CSA cement in concrete has a variety of advantages such as lower carbon footprint, rapid strength gain, and lower shrinkage. However, the variation in the main composition of CSA cement can significantly influence the properties of concrete. Hence after clarifying its features, it can be used for several applications such as bridge decks, airport runways, patching roadways, and sidewalks. The hydration products and microstructure of CSA cement has been already investigated by many researchers. However, to

the knowledge of the author there is very limited data about the effect of blending OPC with CSA cement, and features of ternary mixes including slag. Moreover, the effect of introducing fibers on the properties of CSA-based concretes has not been studied. Therefore, developing high performance fiber-reinforced concretes (HPFRC) containing CSA will be of great interest for cement and concrete producers all over the world. In addition, the features of HPC were fabricated with Type K cement is not well understood by the researchers and further investigation is required to study its properties. The main objectives of the current study are as following:

- Assessment the influence of CSA cement on the mechanical, durability and microstructural properties of HPC. As already discussed, the compositions of CSA cement has a significant influence on the properties of concrete. To the knowledge of the author this is the first study that comprehensively investigates the features of HPC made with CSA cement.
- Investigating the properties of CSA-based concretes in binary and ternary systems containing cementitious materials, such as slag.
- Studying the effect of expansive cement like Type K cement on the properties of HPC, with the aim of improving the bond between fibers and cement matrix and also compensating the shrinkage of concrete.
- Understanding the effect of different fibers including DHE steel fibers, HE steel fibers, and PVA fibers at low fiber volume fraction of 1% on the properties of HPFRC made with CSA cement. Additionally, this study aims at investigating the effect of fiber hybridization and water-cement (w/c) ratio on the characteristics of the HPFRC.

## 1.3 Structure of the dissertation

The current doctoral thesis is composed of eight chapters. The details of each chapter is as follow:

**Chapter 1: Introduction.** This chapter covers the problem statement, objectives and innovative features of this study and structure of the dissertation. The aim of this chapter is to clarify why this research topic should be further investigated by researchers.

**Chapter 2: Research background.** A literature survey of the main topics studied in this dissertation is presented. The essential of using alternative binders such as CSA cement is discussed. An overview on the topic of CSA cement and its effect on the mechanical and durability properties of concrete has been done. Additionally, pervious research on the properties of HPFRC are discussed, and the influence of different fibers on the characteristics of HPFRC is reviewed.

**Chapter 3: Materials and experimental program.** The properties of materials employed in this study, mixing procedure, and testing method are presented in this chapter. Based on the nature of this research that is mainly focused on the experimental program, a set of experiments including compressive, splitting tensile, modulus of elasticity, flexural strength, single fiber pullout, drying shrinkage, water absorption, electrical resistivity, electrochemical potential of fibers in concrete, scanning electron microscopy (SEM), and X-ray diffraction (XRD) are discussed.

**Chapter 4: The influence of expansive cement on the mechanical, physical, and microstructural properties of hybrid-fiber-reinforced concrete.** This chapter presents the results of the mechanical, physical, and microstructural properties of HPFRC made with expansive Type K cement. The results of this chapter has been obtained from the research that was carried out as a study abroad in the University of California, Berkeley.

**Chapter 5: Mechanical, durability, and microstructural properties of high performance CSA-based composites.** The mechanical, durability and microstructural properties of HPC made with CSA cement and fibers are analyzed and discussed in this chapter. Moreover, the effect of combined use of CSA with OPC, and blend mixes containing OPC, CSA, and slag with and without DHE steel fibers are evaluated in this chapter.

**Chapter 6: The influences of different types of fibers and fiber hybridization on the engineering properties of concrete containing CSA cement.** The aim of this chapter is to investigate the effects of addition different types of fibers including DHE steel fibers, conventional HE steel fibers, and PVA fibers and their hybridization on the engineering properties of CSA-based concretes. Hence, different concrete mixes at w/c ratios of 0.35 and 0.28 were developed and their compressive strength, splitting tensile strength, modulus of elasticity, flexural behavior, and dimensional stability have been evaluated. Additionally, the microstructure of concretes were observed by using SEM method.

**Chapter 7: Conclusions and recommendation for future research.** This chapter provides a summary of the major conclusions that can be drawn from the research. Several recommendations for future work that stem from this work are also provided.

**Chapter 8: References.** Generally, a number of most related references that have been used in the body of this dissertation are listed in this chapter.

# Chapter 2
# Research background

## 2.1 Introduction

CSA cement is a new generation of cement industry, and further research are still required to fully understand the properties of concretes were manufactured with CSA cement. This chapter presents a review on the manufacturing and hydration products of CSA cement as well as the properties of concretes made with CSA cement including dimensional stability, mechanical properties, and durability properties. Moreover, a comprehensive review to date is presented to show the effect of different fibers on the mechanical, physical and durability related features of HPFRC.

## 2.2 Need for alternative binders

Concrete, with a yearly consumption of more than 25 billion tons [1], is the most used construction material in the world. Conventional concrete is a composite material that consists of OPC, aggregate, and water at proportions of approximately 12%, 80%, and 8%, respectively [2]. The Portland-based hydraulic cement was annually used about 4 billion tons in 2013 [3], and as is shown in Fig. 2.1, it is expected that its production rapidly grows in countries such as China, India, and some regions in middle East and Northern Africa [4]. It was reported that the Portland cement concrete production has a significant environmental impact due to the emission of carbon dioxide ($CO_2$), in which accounts for around 5-7% emission annually [5]. The production of Portland cement clinker is the main reason leads to the $CO_2$ emissions. The current approach to overcome this problem is through the reducing clinker factor, and replacing OPC with supplementary cementitious materials (SCM) such as fly ash, slag, silica fume and natural pozzolan [6]. However,

due to growing field experience and increasing demand for those materials, there is an essential need to develop concrete made with alternative binders such as calcium aluminate cements (CAC), CSA cement, alkali-activated binders, and supersulfated cements [7]. Recently, CSA cement gained an increased attention due to its lower amount of $CO_2$ emission as compared to that of the OPC [8]. It is reported that the $CO_2$ emission may reduce up to 35% by replacing OPC with CSA cement [9]. Using CSA cement in concrete results in an increased sulfate resistance, high impermeability and chemical resistance, and low chance for alkali-silica reaction [10]. Moreover, depending on CSA cement composition and subsequently its hydration products, different kind of binders like shrinkage-compensating concrete (SHCC), self-stressing concrete, and rapid-hardening concrete can be developed [11-13].

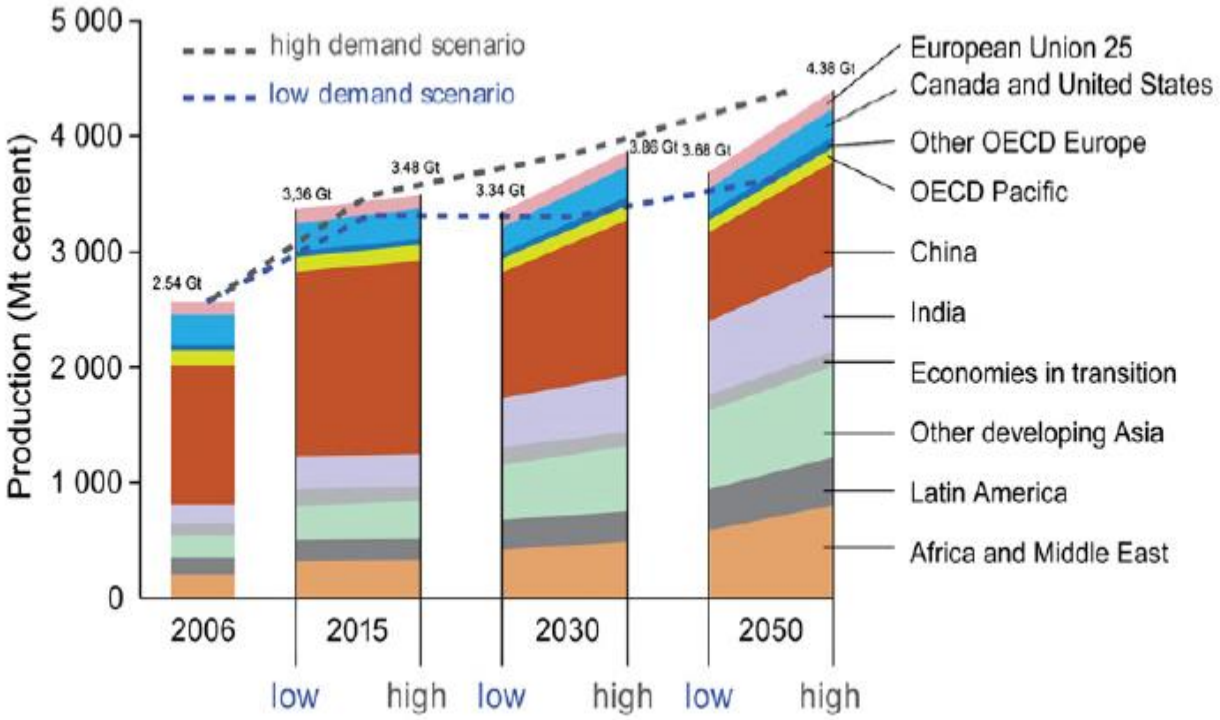


Fig. 2.1 Global cement production [4]

## 2.3 Calcium sulfoaluminate cement (CSA)

### 2.3.1 Manufacturing of CSA cement and its application

CSA cements were first developed by Alexander Klein at the University of California at Berkeley in the 1960s [14]. Thereafter, various kind of CSA cements were successfully produced in China in 1970s and categorized as the "third cement series" [15, 16]. Limestone, a source of aluminum like bauxite or recycled materials, and gypsum are the raw materials for the production of CSA cements that are burned at 1250-1350°C, which resulting in a sulfate-based clinker [17]. The main compounds of the formed clinker are ye'elimite ($C_4A_3\$$), followed by belite ($C_2S$), aluminate and ferrite, depending on the raw materials [18]. The CSA clinker production caused lower amount of $CO_2$ emission over that of the OPC due to the lower firing temperature, and lower used limestone percentage that subsequently contribute toward generating environmental-friendly binder [19]. As can be seen in Fig. 2.2, ye'elimite phase as the major compound of CSA cement releases 0.216 g $CO_2$ per g of cementing phase, while alite ($C_3S$) as the main phase in OPC releases 0.578 g $CO_2$ per g of cementing phase during calcination process [8].

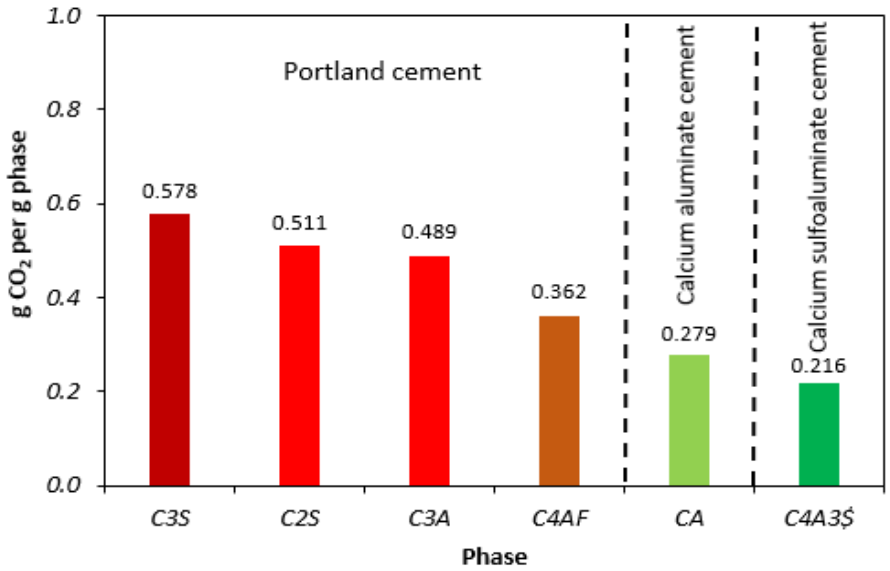


Fig. 2.2 Amount of $CO_2$ released for various cementitious phases during calcination process [8]

Dimensional stability features of CSA cement are significantly influenced by the variation of the gypsum and anhydrite content that were added to the raw mix [20]. The presence of gypsum ($CaSO_4$) content in the range between 18-20%, 22-24%, and higher than 25% resulted in slight shrinkage during setting, minimal dimensional change, and notable expansion, respectively [12]. To develop expansive cement, CSA clinker can be blended with OPC. Expansive cement based on its main components can be classified to three different types of K, M, and S [21], which resulting in shrinkage-compensating concrete and self-stressing concrete [22]. Type K cement is a modified Portland cement containing ye'elimite, gypsum, and lime. The main component of Type M cement is gypsum that appropriately mixed with Portland cement and alumina cement, while high amount of tricalcium aluminate ($C_3A$) is available in Type S cement [23]. The magnitude of the final expansion is the dominant factor that influencing the properties of expansive concrete that is larger in self-stressing concrete [24].

The presence of ye'elimite phase in the CSA cement results in the rapid generation of ettringite, and interlocking and bonding between ettringite crystals consequently caused high early strength [25]. The lower alkalinity of pore solution in CSA cement over that of the OPC make it as a promising binder to develop high performance glass fiber-reinforced composites [26]. Additionally, CSA cements and their blends with OPC have the potential to encapsulate hazardous waste due to their lower porosity, and the ability of ettringite and AFm phases to bind heavy metals [27-29]. CSA cements have several applications based on their performance, and this binder has been successfully used in China for the production of concrete in concrete pipes, bridges, precast concrete, waterproof layers, pre-stressed concrete, shotcrete, and low temperature constructions [30-32].

### 2.3.2 Hydration product of CSA cement

The main compound of CSA cement is ye'elimite that its hydration products can be varied depending on the availability of calcium sulfate and lime [33, 34]. In the presence of both calcium sulfate and lime, it is expected that the ye'elimite hydration forms only ettringite crystals based on the Eq. (2-1):

$$C_4A_3\$ + 8C\$ + 6CH + 90H \longrightarrow 3(C_6A\$_3H_{32}) \quad (2\text{-}1)$$

In the absence of lime, the hydration products consist of ettringite and amorphous aluminum hydroxide (Eq. (2-2)):

$$C_4A_3\$ + 2C\$ + 38H \longrightarrow C_6A\$_3H_{32} + 2AH_3 \quad (2\text{-}2)$$

When calcium sulfate is consumed and in the absence of lime, the ye'elimite hydration will lead to the formation of monosulfate and amorphous aluminum hydroxide (Eq. (2-3)):

$$C_4A_3\$ + 18H \longrightarrow C_4A\$H_{12} + 2AH_3 \quad (2\text{-}3)$$

It is worth noted that the calcium sulfate is always present within commercial formulations of CSA cement in forms of anhydrate in the CSA clinker or added to it as gypsum or anhydrite. The required lime to form ettringite in Eq. (2-1) can be derived from different ways: (1) free CaO sourced from the CSA clinker, (2) calcium hydroxide generated by hydration of belite as the second phase of CSA clinker, (3) calcium hydroxide originated by hydration of OPC blended with the CSA cement, and (4) calcium hydroxide originated by hydration of modified OPC containing $C_4A_3\$$ instead of $C_3S$ [35]. As it can be seen from the above equations, the main hydration product of ye'elimite is ettringite. However, the properties of ettringite formed in Eqs. (2-1) and (2-2) are significantly different. The ettringite formed in the presence of lime exhibit an expansive behavior

(Eq. 2-1) that can contribute toward development of self-stressing and shrinkage-resistant binders [11, 36, 37]. It has been reported that the morphology of these ettringite is different with others and colloidal ettringite with high specific surface are formed through the first reaction pathway [38]. The expansion of CSA cements can be attributed to the adsorption of water molecules whereby colloidal ettringite based on the swelling theory [39, 40]. On the other hand, the absence of lime (Eq. 2-2) caused to the formation of non-expansive large ettringite crystals, which subsequently resulted in a high early mechanical strength [41, 42]. Lower drying shrinkage and solution alkalinity as well as high impermeability and chemical resistance are other promising features of these dimensionally stable and rapid-hardening cements [12, 43].

Moreover, the presence of belite as the second phase in CSA cement results in the formation of strätlingite ($C_2ASH_8$) based on the Eq. (2-4). Winnefeld and Lothenbach [44] used a thermodynamic modeling to determine the phase development with ongoing hydration of CSA cement containing belite as shown in Fig. 2.3.

$$C_2S + AH_3 + 5H \longrightarrow C_2ASH_8 \qquad (2\text{-}4)$$

In binary mix containing OPC and CSA cements, in which CSA has been added at more than 50% of the total binder, the hydration of OPC compounds takes place after several hydration days [45]. The hydration of alite as the main component of OPC results in the formation of strätlingite and portlandite based on the Eq. (2-5). However, if the content of CSA in blended mix with OPC is low, the calcium-silicate-hydrate (C-S-H) and portlandite will be produced. Additional ettringite crystals also expected to be formed through the reaction of $C_3A$ as the accessory phase in OPC based on the Eq. (2-6):

$$C_3S + AH_3 + 6H \longrightarrow C_2ASH_8 + CH \quad (2\text{-}5)$$

$$C_3A + C\$ + 32H \longrightarrow C_6A\$_3H_{32} \quad (2\text{-}6)$$

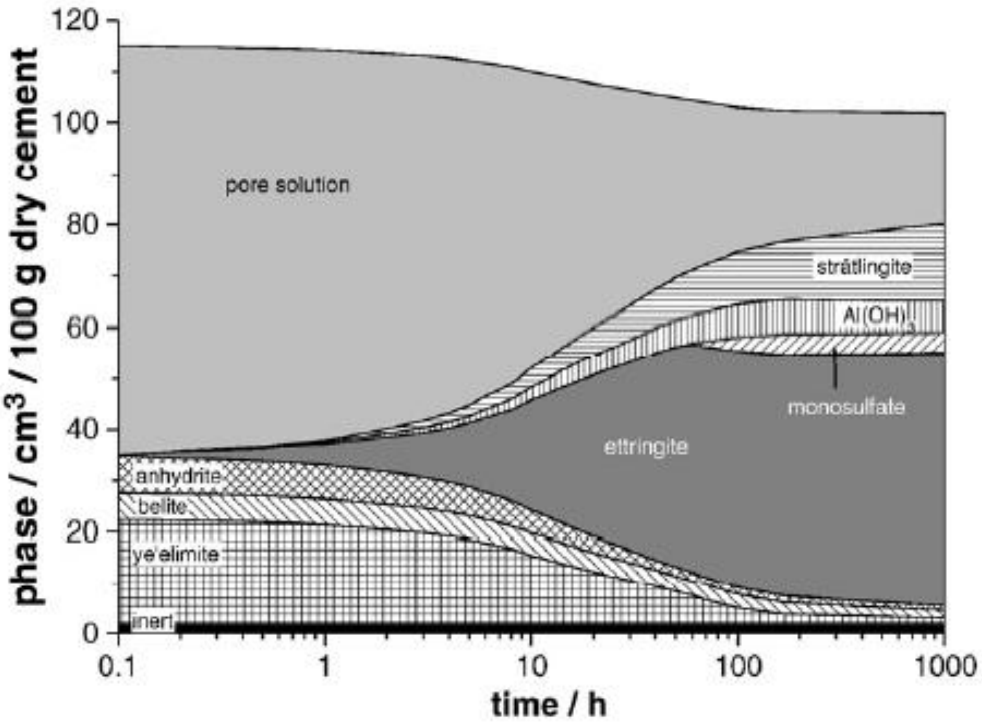


Fig. 2.3 Phase development of a CSA cement with a water-cement ratio of 0.8 as a function of hydration time calculated by thermodynamic modeling [44]

### 2.3.3 Dimensional stability of CSA cement and expansion mechanism

Volumetric changes of cementitious materials are unavoidable due to their ongoing hydration. Dimensional stability of concrete is closely linked to the properties of cement paste, in which pore structure, specifically pore size is principal factor. At the beginning, these porosities are saturated with water. However, ongoing hydration of cementitious materials results in self-desiccation jointly with external evaporation. As a result of that, capillary stresses will develop in cement matrix and consequently leads to macroscopic shrinkage [46, 47]. Shrinkage cracking in concrete structures may accelerate other forms of damage in concrete such as corrosion, freeze/thaw

damage, and subsequently shorten the service life of structures [48]. Hence, expansive cement like CSA cement are developed to overcome this weakness and compensate the shrinkage of concrete. The dominant factors influencing the magnitude of expansion in CSA cement are the content of ye'elimite and added calcium sulfate, the particle size distribution, the w/c ratio, and lime content [49-51]. There are two main theories that proposed to outline the expansion mechanism of CSA cement as a result of ettringite precipitation.

- **Crystallization pressure theory:** Based on this theory, the expansion of CSA cement can be attributed to the ettringite formation in small pores in a supersaturated pore solution [52-54]. Taber [55] used experiments to show the role of supersaturation in applying stress as shown in Fig. 2.4. He reported that in a saturated solution, a crystal is not always able to lift a given weight. On the other hand, a supersaturated solution provides condition that a crystal can grow and lift a specific weight as a result of crystallization stress generated due to the crystal growth. Additionally, in a supersaturated solution and in the presence of one loaded crystal and one unloaded crystal, the experiment indicate that the unloaded crystal grows to consume the supersaturation. In absence of evaporation in a saturated solution, the unloaded crystal grows while the loaded crystal would dissolve. This clearly reveals the contribution of pressure on solubility of the crystal. It should be taken into account that these experiments were conducted under equilibrium conditions and the effect of ions transport and kinetics were not considered.

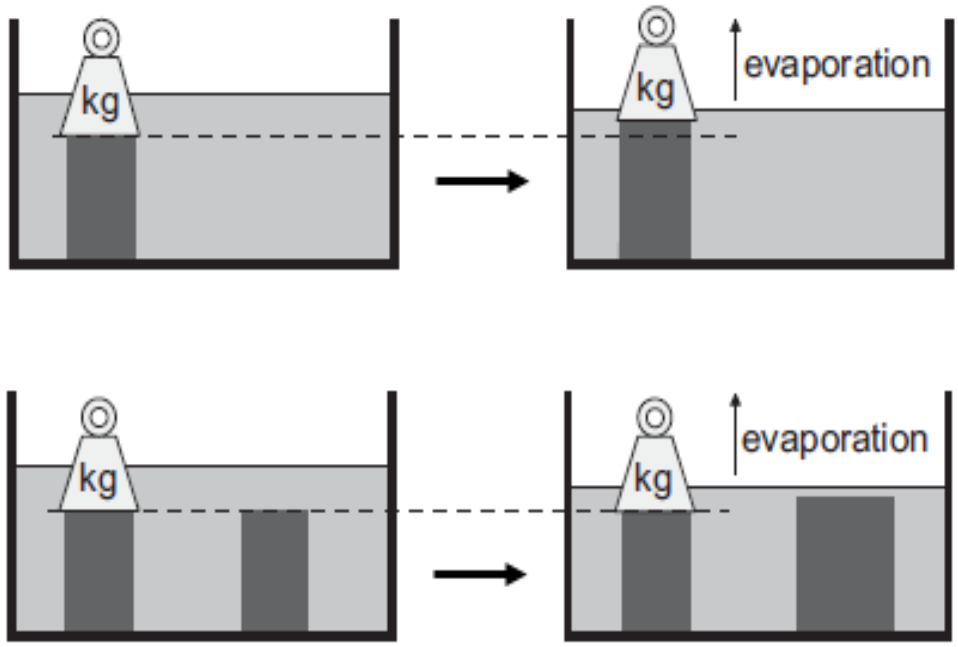


Fig. 2.4 Experiments conducted by Taber to show the role of supersaturation in exerting pressure [55]

- **Swelling theory:** According to the swelling theory proposed by Mehta [11], the expansion of CSA cement is directly linked to the swelling behavior of fine ettringite crystal. It was reported that the presence of lime changed the morphology of ettringite crystal (Fig. 2.5), in which resulting in finer colloidal ettringite crystals that tend to adsorb polar molecules of water and consequently cause an expansion [56, 57]. There are also studies [58, 59] pointed out that the both described theories can result in an expansion in CSA cement. Additionally, Mather [60] proposed that the expansion can be attributed to the increased solid volume. However, there exist no convincing evidence to support this hypothesis and correlate the expansion of cement matrix to the total content of ettringite crystals [61].

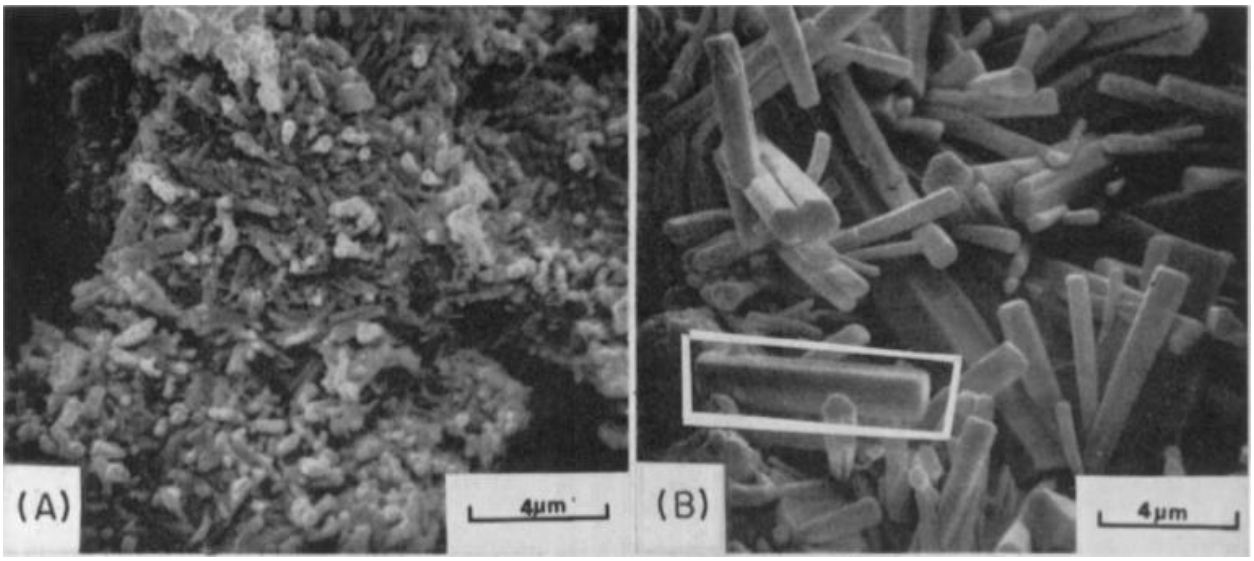


Fig. 2.5 SEM micrographs indicating different ettringite crystals in $C_4A_3$\$-C\$ system: (a) colloidal ettringite in the presence of lime, (b) prismatic long ettringite in the absence of lime [57]

### 2.3.4 Mechanical properties of CSA cement

Generally, the same factors that affecting the dimensional stability of CSA cement can also alter its mechanical properties. The cement particle size distribution, w/c ratio, curing condition, clinker phase assemblage, and the content of added calcium sulfate are variables that affect the properties of concrete produced with CSA cement. Concrete made with finer cement particle size distribution gained faster strength development due to the presence of greater surface area of the cement to react. A suitable curing condition is essential for any kind of cements to exploit hydration reactions and develop concrete with enhanced strength. Using wet plastic sheets or external water as well as the addition of curing compound can provide conditions that promote hydration of cement particles and subsequently lead to improved strength. There is a direct correlation between the porosity and w/c ratio of concrete. The strength of concrete increases by lowering the w/c ratio due to the reduced capillary porosity. Pores are not able to carry the load, and their reduction causes a strength development. On the contrary, high w/c ratios result in an increased porosity in the microstructure

of cement matrix that consequently cause lower mechanical strength [62, 63]. It has been reported that the formation of ettringite and monosulfate phases in the CSA cement consumed large volume of water that resulting in a lower porosity over that of the OPC for a given w/c ratio and rate of hydration [64]. To study the hydration reactions of CSA cement, different w/c ratios including very low w/c ratios of 0.35-0.45 [65-67], moderate w/c ratios of 0.5-0.6 [68-70], and very high w/c ratios of 0.7-0.8 [71, 72] were used. A w/c ratio of 0.64 is theoretically required for the hydration of CSA cement through reaction pathway of Eq. (2-2). However, the presence of different minor phases in CSA cement can also affect the hydration products as well as aforementioned w/c ratio. It should be noted that it would not be possible to establish a general theoretical water demand for full hydration of CSA cement due to the large variation in its compositions.

The increase in the content of ye'elimite in the CSA clinker leads to a higher strength at early ages, while an increase in the belite content results in an improvement in the strength at later age. In general, raising the content of calcium sulfate results in a lower strength of concrete [73], while its presence speed up the hydration process of CSA cement [74]. Hence, it is expected to attain higher strength at early ages by addition of calcium sulfate to the CSA cement. However, it should be noted that the addition of calcium sulfate more than 25% can result in reduced strength due to the cracking of cement matrix. Additionally, the type of calcium sulfate added to the CSA cement can significantly change the mechanical properties of concrete. Using reactive calcium sulfate like gypsum improves the early age strength [75], while the addition of low reactive calcium sulfate like anhydrate increases the strength at later age due to the delayed ettringite formation [20].

### 2.3.5 Durability properties of CSA cement

Durability is one of the most important aspects of the concrete due to its fundamental incidence on the serviceability working conditions of concrete structures [76]. It is well understood that a well-formulated CSA cement based concrete is able to resist against different physical and chemical attacks it may subjected during its service life. However, the performance of concretes fabricated with CSA cement is poorer as compared to that of the OPC over time [77]. Carbonation, sulfate attack, and chloride diffusion can result in deterioration of concrete structures made with CSA cement. Basically, ion diffusion is required for all those effects that is related to the microstructural properties of concrete. In CSA cement based concrete, the resistance to diffusion is increased due to the formation of significant amount of hydration products, particularly at early ages that subsequently reduces the interior pore space [78]. Additionally, hydration of CSA cement consumes the free water quickly that consequently hinders the growth of porosity. However, the addition of CSA cement in concrete increases the possibility of carbonation due to the presence of rich amount of ettringite crystals [79]. Carbonation decomposes the ettringite crystals and forms calcium carbonate, calcium sulfate, and alumina gel, which causes a reduction in the strength of concrete [19, 80]. It was reported that the 28-days strength of CSA cement-based concrete was reduced by up to 7.1% as a result of accelerated carbonation [77]. In another study, Mechling et al. [81] studied the carbonation resistance of mortars produced with CSA cement at different w/c ratios and subjected to variable curing conditions. They reported that mortar made with CSA cement specifically at high w/c ratios (i.e. 0.58 and 0.78) were more sensitive to carbonation over that of the mortars containing OPC. However, it was observed that the carbonation resistance was almost equal for both type of mortars at lower w/c ratio of 0.45. Similarly, Zhang and Glasser [17]

reported that reducing the w/c ratio reduces the risk of carbonation in concrete made with CSA cement and comparable results with OPC concrete can be attained.

Lower pH of CSA cement over that of the OPC increases the concern of steel bars corrosion embedded in the concrete. On the other hand, lower pH in CSA cement-based concrete results in a lower risk of alkali-silica reaction compared to that of the OPC concrete [15]. The results of the existing studies on the corrosion resistance of steel bars in concrete made with CSA cement are still contradictory. For instance, Glasser and Zhang [12] pointed out that there was no evidence of corrosion on the surface of steel bars embedded in CSA concrete after 14 years, and they remained passivated. The good performance of concrete with CSA cement against the corrosion can be attributed to the lower permeability as well as the self-desiccation features that subsequently reduces the bleeding water in the vicinity of steel bars. On the contrary, Kalogridis et al. [82] observed that more negative potential was attained in concrete with CSA cement compared to that of the OPC concrete in half-cell potential test. This can be explained by the less alkalinity of pore solutions in concrete fabricated with CSA cement that subsequently increases the risk of bars corrosion.

## 2.4 High performance fiber-reinforced concrete (HPFRC)

### 2.4.1 Mechanics of crack formation and propagation

Concrete usually exhibits large numbers of micro-cracks even before it is subjected to any loads [83]. The aggregate-mortar interface is typically the weakest link in the composite concrete system [84-86]. During loading, cracks will typically form at interfacial transition zone (ITZ), generally the weakest part of most hardened concrete, and influence the mechanical properties of the

concrete. Cement-based materials have a relatively low tensile strength and low tensile strain capacity. Due to its low tensile strain capacity, concrete has a brittle behavior and cracks are almost inevitable in any concrete structure [87, 88]. The applied load surpassing the low tensile strength of the concrete is the primary reason of crack formation [89]. These cracks propagate under loading and contribute to the non-linear behavior at low stress levels and volumetric expansion until failure. The fiber has the ability of transferring stress between the matrix and tensile strains at rupture [90]. This fiber capability, causes an improvement in the post-cracking behavior and the toughness of the concrete [91, 92].

#### 2.4.1.1 Pre-cracking mechanisms (Stress transfer)

Concrete is a heterogeneous material with pores and micro-cracks caused by shrinkage and thermal strains, which have been restrained by coarse aggregates and boundary conditions. Hence, during loading, the matrix transfers part of the load to the fibers before any macro-cracks are initiated [93]. As a consequence, it has been shown that the strength of the concrete can be increased by adding fibers with a higher elastic modulus than that of the matrix [94].

#### 2.4.1.2 Post-cracking mechanisms (Crack bridging)

In fiber-reinforced concrete (FRC), the main effect from fibers comes after the initial cracking of the matrix. The steel fibers are able to bridge the cracks and transfer the stress across the cracks. The presence of steel fibers is also able to limit the propagation of the cracks [95, 96]. The tensile strength of the steel fibers is higher than that of the hardened concrete. Therefore, the failure of a FRC is mainly due to the failure of the bonding between the concrete paste and the fibers. This pullout effect of fibers was observed in the failure of FRC tensile tests. The inclusion of deformed-

end fibers (e.g. hook-end steel fibers) results in a considerable energy dissipation that takes place to straighten and plastically deform the fibers [97-100]. There will be also the combined effect of aggregate and fibers bridging in FRC. Comparing the two types of bridging effect from the aggregate and steel fibers, the effect of steel fibers bridging is significantly greater as it is shown in Fig. 2.6. The process from crack initiation to failure of the specimen can be broadly divided into three zones: 1) a zone of micro-cracking and macro-crack growth, 2) bridging zone and 3) traction-free zone [101]. Depending on the amount of fibers crossing the crack and on the fiber matrix bonding, the post-crack stress can be larger than the cracking load, resulting in a so-called strain hardening behavior where multiple cracks occur. However, for normal fiber content (<1%) the concrete exhibits strain softening behavior, which the damage localizes immediately after initiation of the first crack.

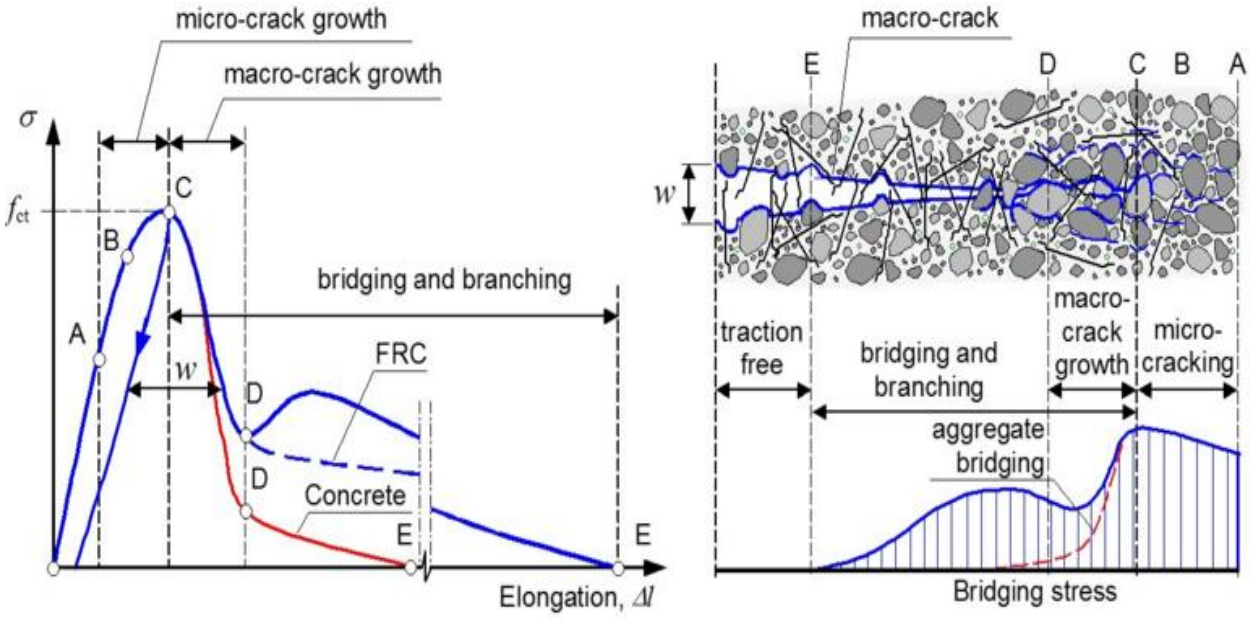


Fig. 2.6 Schematic description of the stress-crack opening relationship for the plain concrete and FRC [101]

### 2.4.2 Fiber orientation and its effect on the mechanical properties of FRC

Efficiency of fibers in enhancing mechanical properties is significantly influenced by their orientation with respect to the cracks formed in concrete [102, 103]. The positive effect of fibers on the performance of FRC is maximized when the fibers are aligned perpendicular to the crack openings in the direction of stress [104, 105]. Mechanical property results of FRC show scatter as a result of variations in the fiber orientation in different specimens [106-110]. The orientation of fibers is generally characterized through the so-called orientation number, $\eta\theta$, which varies from 0.0 to 1.0, denoting fibers parallel and orthogonal to the analyzed cross-section, respectively [111]. The parameters that affect the fiber orientation in composites include the fresh-state properties, casting method, vibration, flow direction, and formwork geometry [112-115]. Among these, the wall-effects produced by the formwork and the fresh-state characteristics of SFRC are recognized as the most influential [116, 117]. There are different techniques to measure the alignment of steel fibers in concrete, which can be classified as destructive and non-destructive methods. Researchers have studied the fiber orientation in the composites by using different techniques, such as the manual counting [118, 119], image analysis [120, 121], electrical AC-Impedance measurement [116, 122-124], electrical resistivity [107, 125, 126], and X-ray computed tomography [108, 127-129]. The last of these techniques is a non-destructive method that investigates the internal structure of materials. This technique has recently become popular among researchers owing to its advantages such as higher accuracy and simplicity over the other techniques [127].

Lin [130] investigated the effect of fiber orientation on the compressive strength of specimens were drilled from a concrete block with dimensions of 1060×1060×300 mm. It was found that the samples taken vertically from the concrete block had a larger compressive strength compared to

that of the specimens taken horizontally. This can be attributed to the fact that fibers were aligned more horizontally in the specimens taken vertically, and consequently they arrested the propagation of vertical cracks created during compression. This is in agreement with the findings of Bonzel and Schmidth [131]. Barnett et al. [107] studied the effect of fiber orientation on the flexural strength of ultra-high performance fiber-reinforced concrete by assessing the effect of flow direction to evaluate the influence of fiber orientation on the results. It was found that the fibers tended to incline perpendicularly to the flow of concrete. It was also shown that panels poured from the center had the highest strength compared to those poured randomly or at several locations around the perimeter of the panel. Edgington and Hannant [132] reported that the flexural strength of specimens that were cast horizontally increased by 75% over that of the specimens cast vertically. In another study, Ponikiewski et al. [128] investigated the effect of fiber orientation on the flexural strength of beams that were cut from a wall with dimensions of 1200×1200×150 mm. In this study, the concrete was pumped from the upper middle section of the formwork to fill the structure. It was shown that the specimens taken from the bottom part of the wall exhibited the best post-cracking behavior, which was also verified by the better dispersion and alignment of fibers seen in the X-ray computed tomography results. As evident from the summary presented in this section, the fiber alignment has a considerable influence on the mechanical properties of FRC, and it should be taken into consideration in the design of different structural elements manufactured with FRC.

### 2.4.3 Mechanical properties of fiber-reinforced concretes

It has been shown that different parameters of fibers such as type, content, aspect ratio, and length affecting the properties of fiber-reinforced concrete. Therefore, it is quite essential to consider the

influence of each factor on the concrete mix design. This chapter was aimed at making a significant contribution toward the understanding of the effect of these important factors on the properties of FRC. A special focus is drawn on the steel fiber-reinforced concrete as their applications are widespread. However, the influence of the other fiber types and fiber hybridization on the properties of concrete including different fibers is also presented to make a comprehensive conclusion.

#### 2.4.3.1 Compressive strength

In general, HPFRC exhibits higher compressive strength than concrete without fiber [133-136]; however, there are instances where conflicting results on the compressive strength of HPFRC are reported in the literature [137].

Song and Hwang [138] studied the effect of steel fiber on the compressive strength of high strength concrete (HSC) at the fiber content including 0.5%, 1.0%, 1.5%, and 2.0% by volume of concrete. The maximum compressive strength was obtained with the inclusion of 1.5% fiber in which the compressive strength was measured to be 15.3% higher than that of the HSC without fiber. In another study by Ding et al. [139], it was reported that steel fiber had no significant influence on the compressive strength of hardened concrete. In their study, they introduced hooked-end steel fiber (L=35 mm and D=0.55 mm) at the dosages of 25 and 50 kg/m$^3$. It has been shown that the compressive strength of HPFRC was almost equal to that of plain concrete. Eren and Çelik [140] pointed out that the content and aspect ratio of fibers are primary factors governing the compressive strength of concrete. In this study, it was observed that the use of steel fiber with higher content and aspect ratio led to a higher increase in the compressive strength. Köksal et al.

[141] also studied the influence of steel fiber on the compressive strength of FRC containing silica fume. To investigate the effect of silica fume, it was used at three different percentages including 5%, 10%, and 15%. Additionally, steel fiber was used with aspect ratios of 65 and 80 at two fiber contents of 0.5% and 1.0%. It was reported that the compressive strength values of concretes having aspect ratio of 80 were higher than that of concretes with aspect ratio of 65 at the same silica fume and steel fiber content. The addition of 1% steel fiber content with aspect ratios of 80 and 65 resulted in an increase up to 117.6% and 113.8%, respectively in the compressive strength of steel fiber-reinforced concretes having 15% silica fume as compared to that of control specimen.

#### 2.4.3.2 Modulus of elasticity

In homogeneous materials, a direct relationship exists between density and modulus of elasticity. In heterogeneous, multiphase materials such as concrete, the density, the modulus of elasticity of the principal constituents, and the characteristics of the transition zone determine the elastic modulus behavior of the composite [142]. The experimental test results indicate that the use of fibers has no significant influence on the modulus of elasticity of concrete, particularly at a low fibers content [143, 144]. It was reported by some researchers [145-149] that introducing fibers, and specifically steel fibers caused an increase in the modulus of elasticity of concrete, whereas other researchers could not comply with it [150-153].

Beigi et al. [154] studied the influence of fiber types on the properties of self-consolidating concrete. Steel fiber at the content of 0.2%, 0.3%, and 0.5%, polypropylene fiber at the content of 0.1%, 0.15%, and 0.2% and glass fiber at the content of 0.15%, 0.2%, and 0.3% were used. It was reported that the inclusion of fibers did not significantly affect the modulus of elasticity of the

concrete and in the most cases a slight reduction in the modulus of elasticity was observed as compared to that of the control concrete. In another study performed by Suhaendi and Horiguchi [155], it was reported that the incorporation of polypropylene fiber led to a reduction in the modulus of elasticity. However, introducing steel fiber in concrete resulted in an increase up to 7% and 22% in the modulus of elasticity of concrete with 0.25% and 0.5% fiber content, respectively as compared to that of the control specimen. Aulia [156] studied the effect of addition PP fiber at the content of 0.2% on the elastic modulus of concretes with different types of aggregate. He showed that the inclusion of polypropylene fiber in concrete did not significantly affect the modulus of elasticity of the HSC. The average increase in the modulus of elasticity of concrete with different aggregates containing polypropylene fiber was up to 6% and the average decrease amounted up to 5%. This indicates that the use of 0.2% polypropylene fiber resulted in a low influence on the modulus of elasticity of concrete rather than the influences contributed by the other compositions of the concrete.

#### 2.4.3.3 Stress-strain curve

Typically, the stress-strain curves of most normal strength concretes are roughly linear to about one-third to one-half of the concrete's ultimate strength [157]. In case of high strength concrete it has been found to be straight up to 85% or more of the peak stress [158]. Such a high linearity of the stress-strain relationship can be attributed to the absence of micro-cracks at low load levels [142, 159], which causes sudden failure and high brittleness behavior of concrete. It was reported that the addition of steel fibers into concrete has little-to-no effect on the ascending part of the stress-strain relationship, while it has a significant effect on the descending branch of the curve [160-163]. However, Ding and Kusterle [94] found that at early age, fiber reinforcement has a

significant effect on the ascending portion of the stress-strain curve. In addition, it has been shown that the descending part of the stress-strain curve is an essential key element in the non-linear analysis and design of reinforced concrete members under compression loads.

Marar et al. [164] indicated that an increase in the content and aspect ratio of fiber led to an increase in the compression toughness of concrete. It was reported that the use of 2% steel fiber content with aspect ratios of 60, 75, and 83 caused the compression toughness energy of concrete to increase by 5.4, 7.0, and 7.6 times, respectively compared to that of the plain HSC. As it is shown in Fig. 2.7, the slope of the descending part decreased as the fiber content increased, which resulted in an increase in the tough-ness. An increase in the fiber content led to an improvement in the post-peak ductility and energy absorption capacity of the high strength FRC. Additionally, the strain at the peak compressive stress was also increased with an increase in the volume of fiber. This finding was in agreement with the results of Ünal et al. [165], Ezeldin et al. [166], Panzera et al. [167] and Nataraja et al. [168].

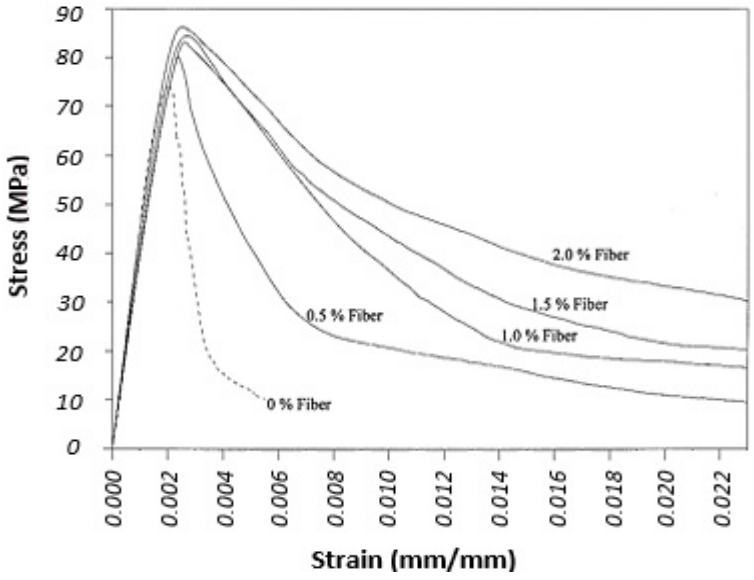


Fig. 2.7 Typical stress-strain relationship for HSC containing steel fiber with aspect ratio of 83 at fiber volume content of 0.5%, 1.0%, 1.5%, and 2.0% [164]

### 2.4.3.4 Splitting tensile strength

The tensile strength of concrete is much lower than the compressive strength, which is normally assumed to be equal to zero and is not considered directly in design [169, 170]. This is demonstrated that under tensile loading, cracks propagate rapidly at much lower stress levels than when compared to compressive stress levels, which cause brittle failure in the concrete [171]. Even for reinforced concrete structural members, due to the low tensile strength of concrete, the concrete cover is likely to be cracked under load. Dewar [172] studied the relationship between the indirect tensile strength (cylinder splitting strength) and the compressive strength of concretes having compressive strengths of up to 85 MPa at 28 days. It has been shown that at low strengths, the indirect tensile strength may be as high as 10% of the compressive strength, but at higher strengths it appears to reduce to 5%. It was observed that the splitting tensile strength was about 8% higher for crushed-rock-aggregate concrete than that of the gravel-aggregate concrete.

Lu and Hsu [173] reported that HSC experienced a brittle splitting tensile failure when the lateral deformation exceeded its tensile capacity, while the steel fiber HSC exhibited more ductility without a sudden breakage of the cylinder, which could be attributed to the reinforcement effect of steel fiber. Previous researchers [174-180] have shown that the addition of steel fibers in very low contents ($V_f \leq 0.5\%$) in concrete resulted in a maximum increase in the splitting tensile strength ranged from 9% to 50% when compared to the concrete without fiber. For low contents ($0.5\% < V_f \leq 1\%$) and higher contents ($1\% < V_f \leq 2\%$) of fibers, an improvement was observed in the splitting tensile strength varied from 15% to 121% and 40% to 143%, respectively. Some other studies investigated the influence of synthetic fibers on the splitting tensile strength of concrete. For instance, Song et al. [181] pointed out that the inclusion of 0.6 kg/m$^3$ nylon and polypropylene

fiber in concrete resulted in an increase up to 17.1% and 9.7% in the splitting tensile strength, respectively as compared to that of the control concrete. Mohammadi et al. [182] conducted an experiment to study the behavior of hybrid fiber-reinforced concrete. As it can be seen in Fig. 2.8, a maximum increase up to 59% was observed in the splitting tensile strength of the concrete with 65% long fiber (L=50 mm and L/D=40) and 35% short fiber (L=25 mm and L/D=20) at a fiber volume fraction of 2% with respect to control specimen.

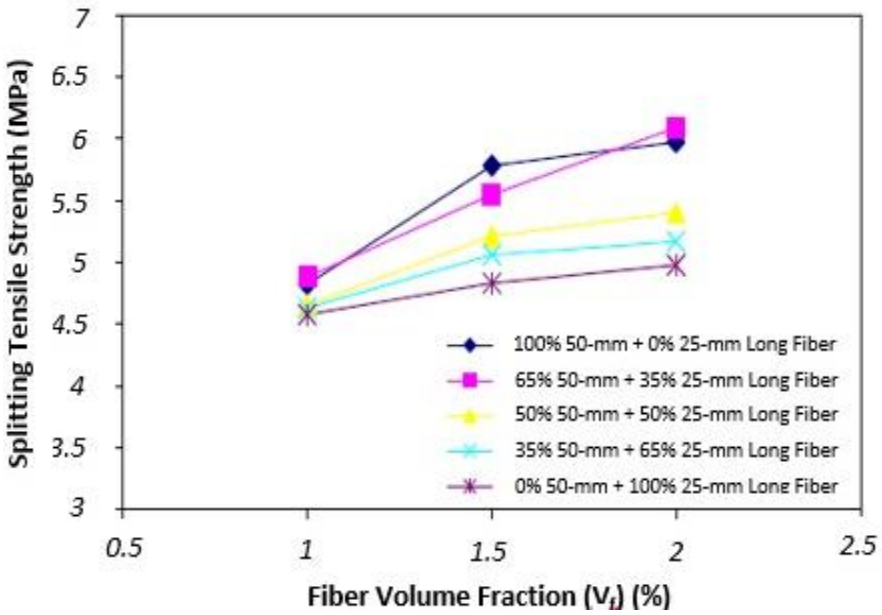


Fig. 2.8 Typical splitting tensile strength of fiber-reinforced concretes with mixed aspect ratio of fibers at different fiber volume fractions [182]

### 2.4.3.5 Flexural strength

It has been reported that the inclusion of fibers in HPC resulted in an increase in the flexural strength of concrete [183-188]. The reason for this increase is that after matrix cracking, the fibers will carry the load that the concrete sustained until cracking by the interfacial bond between the fibers and the matrix. Therefore, the fibers resist the propagation of cracks and tend to reduce the sudden failure of specimen, which causes an increase in the load carrying capacity of concrete

[189, 190]. Balaguru et al. [191] investigated the influence of fiber type, content, and length on the flexural behavior of HSC. It has been shown that the use of hooked-end steel fiber in concrete was very effective in increasing the toughness when compared to other types of fiber. It was also pointed out that the fiber content in the range of 30 to 60 kg/m$^3$ was sufficient to obtain a ductile behavior. Toutanji [192] studied the effect of PP fiber at different fiber volume fractions on the flexural strength of concrete. It has been shown that an increase in the fiber volume fraction resulted in an increase in the post-peak flexural resistance of concrete. A pronounced increase in the flexural strength was noted upon increasing the fiber volume fraction from 0.1% to 0.3% and a relatively smaller increase was observed as a result of the addition 0.5% fiber content. The test results reported by Banthia and Sappakittipakorn [193] are shown in Fig. 2.9. Although hybridization appears to be a promising concept, FRC with hybridization of large and small diameter crimped fibers failed to reach the toughness levels demonstrated by FRC with small diameter fiber alone.

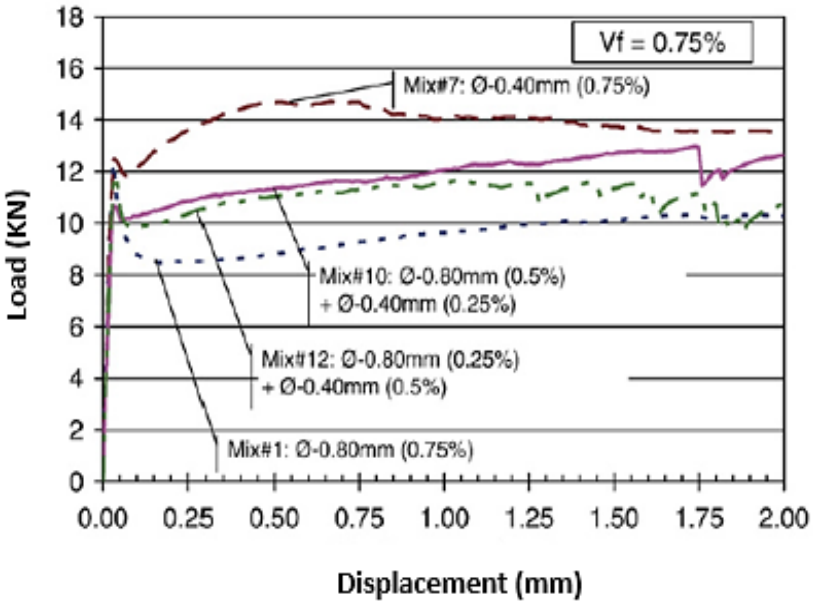


Fig. 2.9 Typical flexural load-deflection curves for single and hybrid steel fibers with diameters of 0.80 mm and 0.40 mm at a volume fraction of 0.75% [193]

Sivakumar and Santhanam [175] reported that the combined use of polypropylene, glass or polyester fibers with steel fiber led to an increase in the pre-peak and post-peak performance of FRC compared to those of the concrete without fiber. Blunt and Ostertag [194] also showed that the use of hybrid fibers was very effective in improving the flexural behavior of concrete when compared to that of the composite with single fiber. As can be seen from Fig. 2.10, the mixture with 1.5% total fiber content (0.8% S2 + 0.5% S1 + 0.2% PVA) showed a significant increase in the post-cracking resistance of the concrete compared to that of the concrete with monotype fiber. It has been shown that the use of fiber hybridization resulted in an increase up to 196% in the maximum flexural strength relative to the control concrete.

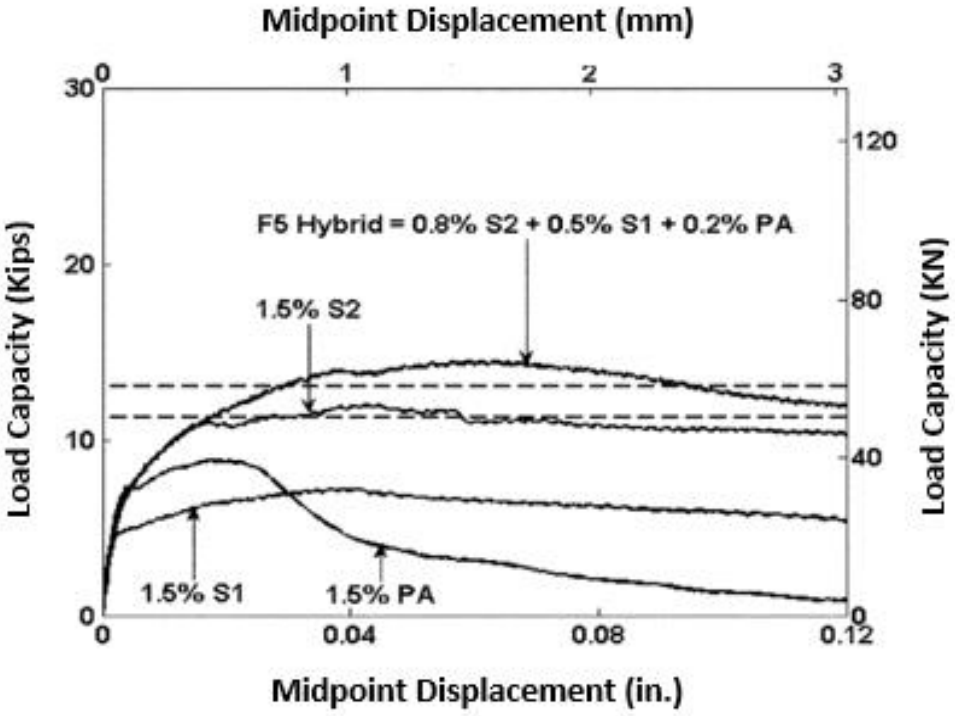


Fig. 2.10 Typical flexural load-displacement of single fiber and hybrid fiber proportions at the same total fiber content [194]

### 2.4.4 Physical and durability properties of fiber-reinforced concretes

In this section, the influence of different parameters such as fiber type, fiber content and fiber aspect ratio on the properties of FRC is discussed. Considering the important effect of mineral admixtures on the properties of concrete, this paper was aimed to address their contribution on the physical and durability behavior of FRC.

#### 2.4.4.1 Drying shrinkage

Drying shrinkage has a serious impact on the structural and durability performance of the concrete. Shrinkage cracking in concrete structures may accelerate other forms of damage in concrete such as corrosion, freeze/thaw damage, and subsequently shorten the service life of structures [195, 196]. Shrinkage of concrete due to loss of water is closely linked to the properties of cement paste, in which pore structure, specifically pore size is principal factor. The shrinkage of concrete is also affected by many different parameters such as composition of the concrete, method of curing, ambient temperature and humidity condition [197].

In one study Cheung and Leung [198] studied the effectiveness of sulfoaluminate cement (SAC) and shrinkage reducing admixture (SRA) on the shrinkage of high-strength fiber-reinforced cementitous composites (HSFRCC) with various water-binder ratios. HSFRCC were manufactured with water-binder ratios of 0.19, 0.3 and 0.4 when OPC was used. Concretes with SAC were developed at water-binder ratios of 0.21, 0.3 and 0.4. Micro-steel fiber (L=13 mm and D=0.16 mm) was used at the volume fraction of 2% in all mixes. It has beenreported that SAC was more effective in reducing the shrinkage of HSFRCC with higher water-binder ratios (0.3 and 0.4), whereas SRA indicated better performance in a lower water-binder ratio. The combined use of

SAC and SRA led to a very significant reduction in the shrinkage of concrete. Drying shrinkage was decreased by over 80% when the water-binder ratio was around 0.2, while the reduction was over 70% for mixes with water-binder ratios of 0.3 and 0.4. Other researches also indicated that the use of SRA in concrete caused a reduction in the shrinkage of cementitious materials [199-202].

Though researchers have been studying the effect of fibers on the drying shrinking of concrete for decades, their results really explored contradictory conclusions [203-205]. Some studies showed that fibers had an insignificant effect on the shrinkage [206-208], while others indicated a real contribution of fibers in reducing the shrinkage of FRC [209-212]. A reduction up to 8% [213], 24% [214], 32% [215], 50% [216], and 65% [217] have also been reported by researchers. Kaïkea et al. [135] studied the effect of mineral admixtures and steel fiber content on the drying shrinkage of HPC. In this study, the cement weight was replaced by 10% or 20% of silica fume or slag, respectively as a supplementary cementitious materials. Corrugated steel fiber (L=55 mm and D=0.8 mm) was added into concrete at fiber volume fraction of 1% and 2%. The water to binder ratio was equal to 0.27. Fig. 2.11 indicates that an increase in the fiber content resulted in a significant reduction in the shrinkage strain of concrete, particularly at 28-day. Specimens with the fiber content of 1% (HPCB1% and HPCS1%) showed a reduction in the shrinkage of concrete varied from 4% to 9% as compared to that of the corresponding plain concrete specimens. Introducing 2% fiber content (HPCB2% and HPCS2%) in concrete led to a reduction in the shrinkage ranged from 15% to 24%. This is in agreement with the results of Mangat and Azari [218] that demonstrate an increase in the steel fiber volume fraction has a significant influence on the reduction of drying shrinkage.

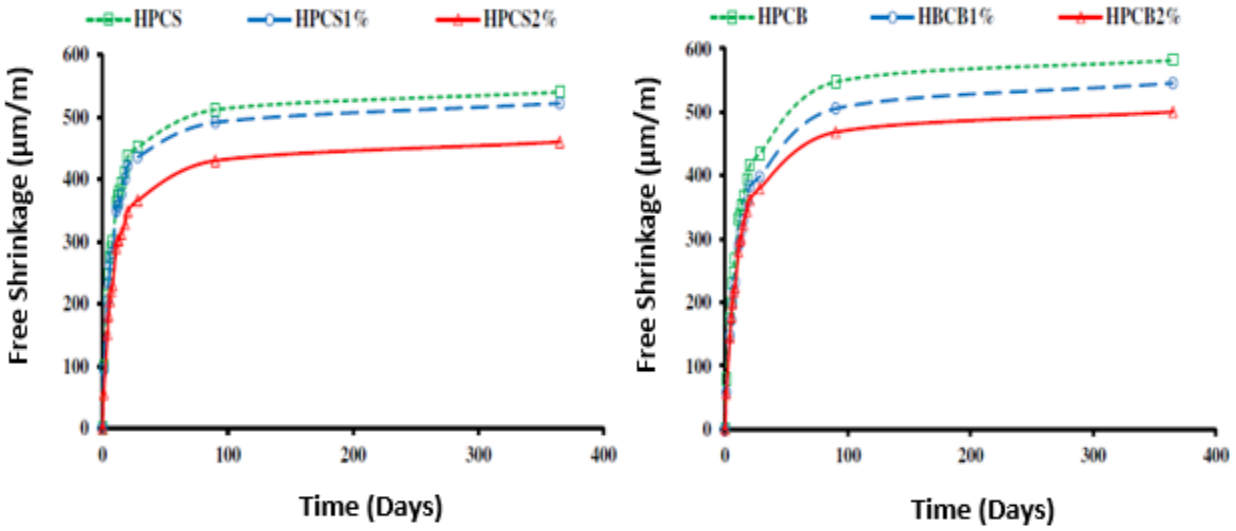


Fig. 2.11 Typical free shrinkage of high performance fiber-reinforced concrete: (a) include silica fume, (b) include blast furnace slag [135]

### 2.4.4.2 Creep

Concrete due to its poor strain capacity and low tensile strength is a brittle material and highly sensitive to cracking. In most cases, cracks can significantly reduce the lifetime of a structure by allowing aggressive agents to move into the cracked areas [219]. The evolution of strains and crack openings through time is fundamental for the durability of concrete structures. Therefore, time-dependent phenomena such as shrinkage and creep must be taken into account along with instantaneous strains and cracking [220, 221]. Concrete is known to deform considerably under constant loading and normal service conditions. Compressive creep strain in conventional concrete can be 1.30 to 4.15 times higher than the initial elastic strain under standard conditions [222, 223]. Rossi et al. [224] conducted a study to compare the creep of concrete in tension and compression. It was pointed out that the basic creep was more important in compression than that of in tension, while the tensile creep and compressive creep in drying conditions were equivalent. It was also reported that there was a greater difference between the basic creep in tension and in compression

when the concrete was younger. Bywalski et al. [215] investigated the influence of steel straight fiber (L=13 mm and D=0.2 mm) on the creep behavior of HSC. Steel fiber with three volume fractions of 1%, 2%, and 3% was used as the reinforcing material. To investigate the creep of HSC, the water-binder ratio of 0.26 was used. As can be seen in Fig. 2.12, the presence of steel fiber had negligible or small effect on the value of creep deformation of HSFRC. Also, the fiber content had no significant influence on the creep deformation of concrete. It was reported that the value of creep deformation depend on the concrete matrix, or to be more exact, its quality. The quality of the concrete matrix is affected by the consolidation of the concrete mixture. This conclusion may be applied in the assumption for estimating the bending rigidity of structural elements, assuming for the purpose of calculations, the creep deformation identical as in the case of HSC without fiber.

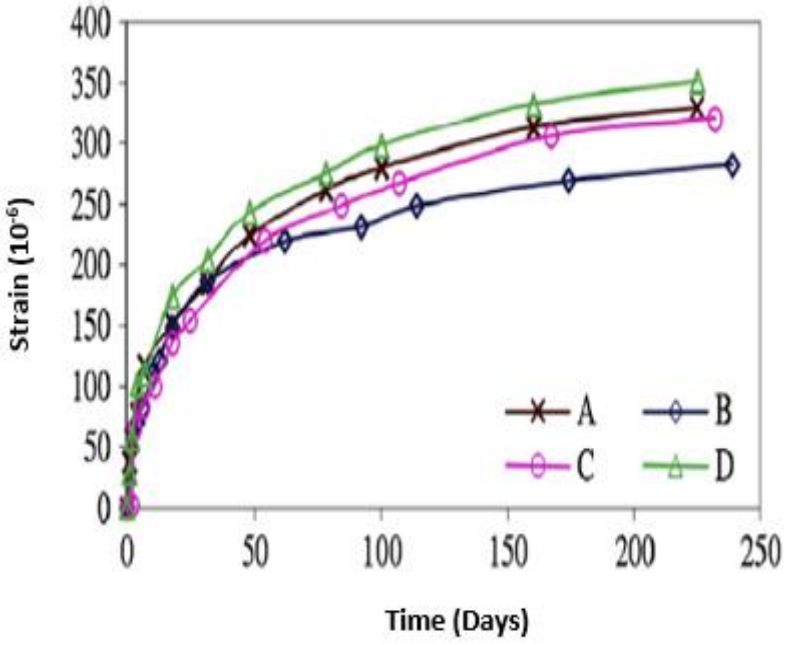


Fig. 2.12 Typical creep deformation of fiber-reinforced concrete after 28 days (Note: A, B, C, and D indicate plain concrete, fiber-reinforced concretes containing 1%, 2%, and 3% steel fibers, respectively) [215]

### 2.4.4.3 Electrical resistivity

Concrete is a multiple-phased material and its microstructure contains many interconnected micro-pores, in which the applied external current can be transferred through the migrating ions. Hence, resistivity measurement is an effective way to explore the microstructure and the features of ions in the micro-pores of concrete [225-228]. This technique is related to chloride ingress because chloride presence can increase electrical current and reduce the resistivity of concrete [229, 230]. Therefore, it can be used to provide information regarding the risk of steel rebar corrosion in the concrete [231-234]. There are some established relationships between the corrosion rate and electrical resistivity of concrete that are shown in Table 2.1 [235], and Table 2.2 [236]. It is suggested that an electrical resistivity of higher than 20 kΩ cm results in a low corrosion rate of steel rebar, whereas an electrical resistivity of less than 5 kΩ cm causes a very high corrosion rate. Resistivity of concrete is influenced by many factors such as concrete composition, w/c ratio, cement content, admixtures, curing condition, moisture content, and ambient humidity [237-239].

Table 2.1 Relationship between concrete resistivity and rebar corrosion rate [235]

| Electrical resistivity (kΩ cm) | Corrosion rate |
|---|---|
| >20 | Low |
| 10–20 | Low to moderate |
| 5–10 | High |
| <5 | Very high |

Table 2.2 Relations between electrical resistivity of concrete and probability of steel corrosion [236]

| Electrical resistivity (kΩ cm ) | Probability of corrosion |
|---|---|
| 12< | Not probable |
| 5-12 | Probable |
| <5 | Inevitable |

Ahmad et al. [233] studied the electrical resistivity of self-consolidating concrete containing different filler materials such as silica fume, natural pozzolan, metakaolin, and limestone powder. It has been shown that all blend mixes had a "low" likelihood of steel bars corrosion. Silica fume was the most effective pozzolan when compared to other fillers to increase the electrical resistivity of concrete. It was reported by Alsadat Sabet et al. [240] that incorporation of mineral admixtures caused a significant increase in the electrical resistivity of concrete mixes, specifically at later ages. They indicated that introducing natural zeolite and fly ash in concrete mixes resulted in an increase in the electrical resistivity in approximately the same level in all ages. The addition of 10% natural zeolite or 20% fly ash in concrete mixes caused the 90-day electrical resistivity to increase from 8.4 kΩ cm for the control mix to 30 kΩ cm and 50 kΩ cm, respectively. At this age, the resistivity of mixes containing 10% and 20% silica fume were 54 kΩ cm and 231 kΩ cm, respectively. The presence of silica fume densifies the microstructure of concrete, while its pozzolanic reaction causes the formation of secondary C-S-H. The C-S-H gel, which is known as a source of strength in concrete, increases the volume of solid phases and reduces the formation of capillary pore systems in concrete. These phenomena result in an improvement in durability properties of concrete, such as concrete resistivity. The positive impact of supplementary cementitious materials on the electrical resistivity of concrete has been proven by other researchers [226, 241-243].

The electrical resistance of concrete is strongly influenced by the electrolytes in the pores structure of composite, and in the case of fiber-reinforced specimens, by the presence of the conductive elements such as steel fibers [244]. Nili and Afroughsabet [245] assessed the effect of steel fiber on the properties of concrete made with silica fume. Steel fiber was used at 0.5% and 1.0% by volume of concrete. Silica fume was introduced at 8% by weight of cement into concrete mixtures that were manufactured with water-binder ratios of 0.46 and 0.36. It was reported that the addition

of steel fiber into specimens led to a considerable decrease in the electrical resistance. It was also pointed out that the higher fiber content caused a more significant reduction in the electrical resistivity of concrete. Typically, an addition of 1% steel fiber into 0.46 and 0.36 water-binder ratios specimens led to a reduction up to 79% and 78% in the 28-day electrical resistance of concrete, respectively. In another report [246] it has been shown that the presence of 60 kg/m$^3$ steel fiber (L=35 mm and D=0.5 mm) in concrete resulted in a reduction in the electrical resistivity of self-consolidating concrete up to 65%, 63%, and 60% at 7, 28, and 91 days, respectively as compared to that of the plain concrete.

Kakooei et al. [247] studied the effect of polypropylene fiber on the electrical resistance of FRC. Polypropylene (PP) fiber (L=19 mm and D=0.02 mm) was used at the content of 0.5, 1.0, 1.5, and 2.0 kg/m$^3$. Additionally, the influence of coral and siliceous aggregates on the behavior of concrete was considered. It was pointed out that the sample fabricated with 1.5 kg/m$^3$ PP fiber showed better results in comparison with other fiber contents. This resulted in an increase up to 26% in the electrical resistivity of concrete when compared to that of the control concrete. They also indicated that the sample made using coral aggregate had the least electrical resistivity, which indicated the lower resistivity of concrete against the current. The reduction in the resistivity was due to the presence of chloride in the coral aggregate. However, Nili and Afroughsabet [248] reported that the addition of PP fiber caused a reduction in the electrical resistance of concrete. It has been shown that a slight decrease in the electrical resistance was observed as the fiber volume fraction increased from 0.2% to 0.5%. This was explained by the fact that the inclusion of PP fiber in concrete caused an increase in the porosity of the mixture. The connectivity and size of pores have a significant influence on transport properties in concrete. Hence, in concrete with a higher porosity

it is much easier for electrical current to be carried by ions through concrete's pore network, which consequently leads to a lower electrical resistance. As can be seen in Table 2.3 [249], the electrical resistivity of FRC is lower than that of the control concrete at both w/c ratios. This can be explained by the fact that the addition of fibers led to an increase in the porosity of concrete, and subsequently reduced the electrical resistivity of concrete.

Table 2.3 Typical electrical resistivity (kΩ cm) of fiber-reinforced concretes with various fiber types (Note: CC indicates control concrete, and SFC, PFC, and GFC indicate concrete reinforced with steel fiber, polypropylene fiber, and glass fiber, respectively) [249]

| | CC | SFC | PFC | GFC |
|---|---|---|---|---|
| w/c=0.65 | 21.3 | 11.3 | 18.1 | 17.6 |
| w/c=0.45 | 24.4 | 9.8 | 21.6 | 21.9 |

#### 2.4.4.4 Chloride penetration resistance

Durability is one of the most important aspects of the concrete due to its fundamental incidence on the serviceability working conditions of concrete structures [250]. For the durability of concrete, permeability is believed to be the most important characteristic [251, 252], which is related to its microstructural properties such as the size, distribution, and interconnection of pores and micro-cracks [253-256]. The rapid chloride-ion test indicates that a reduction in the water-binder ratio leads to a reduction in the connectivity of the pore system, which consequently makes the migration of aggressive ions more difficult in HPC than that of the conventional concrete [257, 258]. There are some classifications of concrete based on the chloride permeability and chloride diffusivity results that are shown in Table 2.4 [259], and Table 2.5 [260], respectively. Various factors influencing chloride ingress and the corrosion processes in the reinforced concrete such as

water-binder ratio, admixtures, cement composition, construction process, and environmental conditions [232].

Table 2.4 Classification of the concrete based on the chloride permeability [259]

| Charge passed (Coulombs) | Chloride permeability | Typical of concrete |
|---|---|---|
| >4000 | High | High w/c ratio (>0.60) conventional PCC. |
| 2000–4000 | Moderate | Moderate w/c ratio (0.40–0.50) conventional PCC. |
| 1000–2000 | Low | Low w/c ratio (<0.40) conventional PCC. |
| 100–1000 | Very low | Latex-modified concrete or internally-sealed concrete. |
| <100 | Negligible | Polymer-impregnated concrete, polymer concrete. |

Table 2.5. Typical resistance to chloride penetration of various types of concrete based on the 28-day chloride diffusivity [260]

| Chloride diffusivity, $D_{28} \times 10^{-12}$ $m^2/s$ | Classification of resistance to chloride penetration |
|---|---|
| >15 | Low |
| 10–15 | Moderate |
| 5–10 | High |
| 2.5–5 | Very high |
| <2.5 | Extremely high |

In general, it has been reported that the addition of mineral admixtures in concrete led to an increase in durability properties of concrete [261, 262], by increasing the chloride binding [263], decreasing the chloride permeability [264], elevating the threshold of chloride content [265], and improving the distribution of pore size and shape of the concrete matrix [266]. Furthermore, reductions in the chloride permeability of concrete have been reported up to 50% with the addition of 5% silica fume [267], 60% with the addition of 20% fly ash [240], 90% with the inclusion of 60% slag [268], and 23% by introducing SRA [269]. The corrosion resistance of steel FRC is governed by the same factors that influence the corrosion resistance of the conventionally

reinforced concrete. Processes such as carbonation, penetration of chloride ions and sulphate attack are related to the permeability of the cement matrix. As long as the matrix retains its inherent alkalinity and remains uncracked, deterioration of steel FRC is not likely to occur [246]. The transport of chloride in concrete by means of permeation may occur in concretes with a large number of cracks and defects [270, 271]. Meanwhile, engineers attempt to increase the design load by using the strain-hardening property of high performance steel FRC, as it allows the appearance of multiple fine cracking and prevents the occurrence of large cracks [272, 273]. However, due to the increased danger of corrosion in the cracked area, the crack width should be limited at the Serviceability Limit State (SLS) [274]. According to the different codes and guidelines [275-278], the maximum allowable crack width at the tensile face of reinforced concrete structures for severe environments vary from 0.1 to 0.33 mm, with the strictest requirement specified by ACI 224 [275]. It was also noted that crack widths larger than 500 μm have a significant effect on the chloride diffusion of steel FRC, while crack widths less than 200 μm have almost no influence on the chloride intrusion [279, 280]. It is widely reported that in case of SFRC, steel fiber corrosion is much less severe than when compared with steel rebar reinforcement of concrete structures [281-286]. Abbas et al. [287] assessed the effect of steel fiber on the rapid chloride penetration test (RCPT) of ultra-high performance concrete (UHPC). Steel fiber with a constant diameter of 0.2 mm and different length of 8 mm, 12 mm, and 16 mm was used at the fiber content of 1%, 3%, and 6% by volume of concrete. It was reported that all UHPC specimens showed a very high resistance to chloride transport and exhibited coulomb values less than 100, indicating negligible chloride ion penetrability based on the classification of concrete in ASTM C1202 [259]. It has been shown that the fiber length had no significant effects on the RCPT results. However, the steel fiber dosage had a remarkable effect on the passed coulomb values. Frazão et al. [246] studied the

chloride diffusivity of the steel fiber-reinforced self-consolidating concrete (SFRSCC) by using rapid migration test (RMT). Hooked-end steel fiber (L=35 mm and D=0.5 mm) was used at the content of 60 kg/m$^3$. It has been reported that the resistance to chloride penetration was slightly higher in SFRSCC (11.61 × $10^{-12}$ m$^2$/s) as compared to that of the SCC (10.27 × $10^{-12}$ m$^2$/s).


(a) (b) (c)

Fig. 2.13 Typical rapid chloride migration test: (a) Schematic of test set-up, (b) cathode solution of SFRSCC after test, (c) surface of SFRSCC specimens sprayed by silver nitrate [246]

As shown in Fig. 2.13, the steel fiber was corroded in the cathode solution of the test of SFRSCC and it was increased with the duration of the test. According to Granju and Balouch [288], there was no corrosion in the part of the specimen with cracks thinner than approximately 0.1 mm. It was also reported that only the steel fibers crossing the crack within a 2 to 3-mm rim from the external faces of the specimens exhibited extensive corrosion, as shown in Fig. 2.14.

Fig. 2.14 Typical photograph of corroded steel fiber in the crack [288]

The choice of hybrid fiber-reinforced concrete can be very effective in reducing chloride permeability, whereby instead of the appearance of a few large cracks, a multitude of closely spaced micro-cracks form in the concrete [289]. Blunt et al. [290] pointed out that hybrid fiber-reinforced composites are effective in delaying the corrosion initiation and in reducing the corrosion rate due to their higher resistance to cracking. The hybrid specimen was manufactured with 1.5% total fiber content that included 0.2% PVA fiber, 0.5% hooked-end steel fiber with a length of 30-mm and 0.8% hooked-end steel fiber with a length of 60-mm. As it is shown in Fig. 2.15, the control specimens exhibited a higher corrosion rate after being subjected to the salt solution ponding and same cyclic flexural loading, due to the formation of flexural and splitting cracks in concrete.

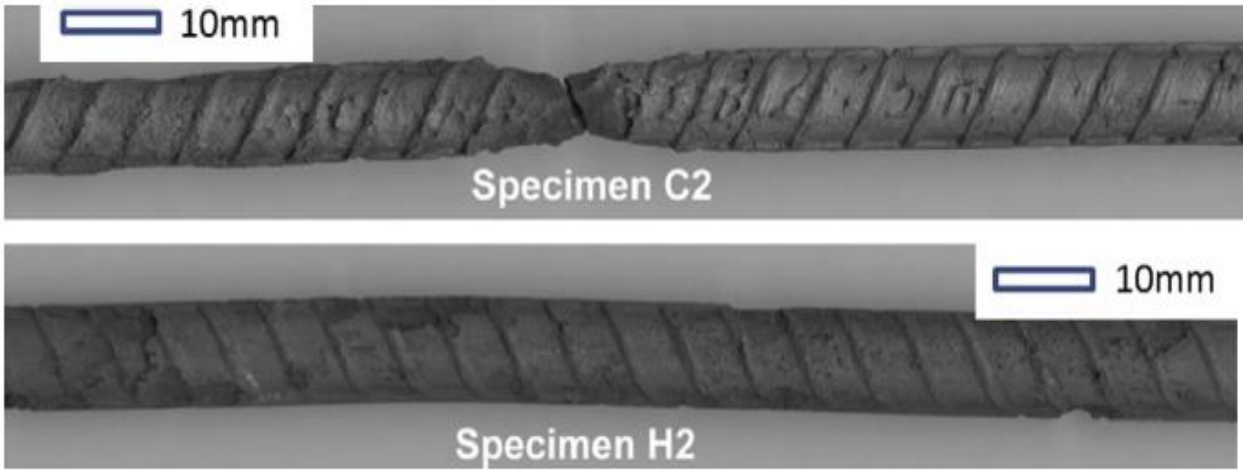


Fig. 2.15 Typical high resolution scans of the corrosion damaged region of rebar (Note: C2 and H2 are represent of plain specimens and hybrid fiber-reinforced specimens, respectively) [290]

# Chapter 3

# Materials and experimental program

## 3.1 Introduction

This chapter describes the materials properties were used in this study. Moreover, the mix design of different concretes developed in this study will be discussed. Finally, the experimental test methods including the compressive strength, splitting tensile strength, modulus of elasticity, flexural strength, single fiber pullout test, drying shrinkage, water absorption, electrical resistivity, electrochemical potential of fibers, scaning electron microscopy (SEM), and XRD are described. The study reported in this thesis is aimed at making a significant contribution towards the understanding of these important properties of high performance fiber-reinforced concrete. As a part of this research was carried out at the University of California, Berkeley, the materials and test methods were used there are also presented in this chapter.

## 3.2 Characteristics of materials

### 3.2.1 Cementitious materials

The binder materials used in this study were ASTM Type 1 Portland cement, and a commercial CSA cement. Additionally ground granulated blast-furnace slag (GGBS) was used in some mixes to study the properties of blend-cement concretes. Moreover, ASTM Type II/V Portland cement and Type K expansive cement with specific gravity of 3.15 and 3.1 were used in conventional concrete (CC) and shrinkage-compensating concrete (SHCC), respectively at the study was performed in UC, Berkeley. Their chemical compositions and physical properties are given in

Table 3.1. Unfortunately, the chemical composition of Type II/V and Type K cements were not provided by the producer.

Table 3.1 Chemical composition and physical properties of cementitious materials

| Item | Cementitious materials (%) | | | | |
|---|---|---|---|---|---|
| | ASTM Type I | ASTM Type II/V | ASTM Type K | CSA | Slag |
| $SiO_2$ | 19.8 | - | - | 7.6 | 36.0 |
| $Al_2O_3$ | 4.1 | - | - | 25.1 | 9.0 |
| $Fe_2O_3$ | 2.7 | - | - | 1.0 | 1.0 |
| MgO | 3.8 | - | - | 3.1 | 8.0 |
| $SO_3$ | 3.4 | - | - | 18.1 | - |
| $Na_2O$ | 0.4 | - | - | - | - |
| $K_2O$ | 0.9 | - | - | - | - |
| CaO | 61.9 | - | - | 41.0 | 44.0 |
| | Compounds | | | | |
| $C_3S$ | 62.1 | - | - | - | - |
| $C_2S$ | 16.7 | - | - | 12.4 | - |
| $C_3A$ | 2.7 | - | - | - | - |
| $C_4AF$ | 10.0 | - | - | - | - |
| $C_4A_3\$$ | - | - | - | 50.1 | - |
| $C_{11}A_7F$ | - | - | - | 2.3 | - |
| $CaSO_4$ | - | - | - | 15.6 | - |
| Others | 8.5 | - | - | 16.5 | - |
| | Physical properties | | | | |
| Specific gravity ($kg/m^3$) | 3,168 | 3,150 | 3,100 | 3,100 | 2,720 |
| Specific surface ($m^2/kg$) | 360 | - | - | 450 | 461 |

### 3.2.2 Aggregates

Both natural sand, with a 2.9 fineness modulus, and crushed gravel, with a nominal maximum size of 19 mm, were used as the aggregates at a volume fraction of 50%. The water absorption, specific gravity and other relevant data for the aggregates are given in Table 3.2. The grading curves of the aggregates are shown in Fig. 3.1.

Table 3.2 Physical properties of the aggregates

| Aggregate type | Maximum size aggregate (mm) | Water absorption (%) | Specific gravity | Fineness modulus |
|---|---|---|---|---|
| Fine aggregate | 4.75 | 1.1 | 2.65 | 2.9 |
| Coarse aggregate | 19.0 | 0.96 | 2.74 | - |

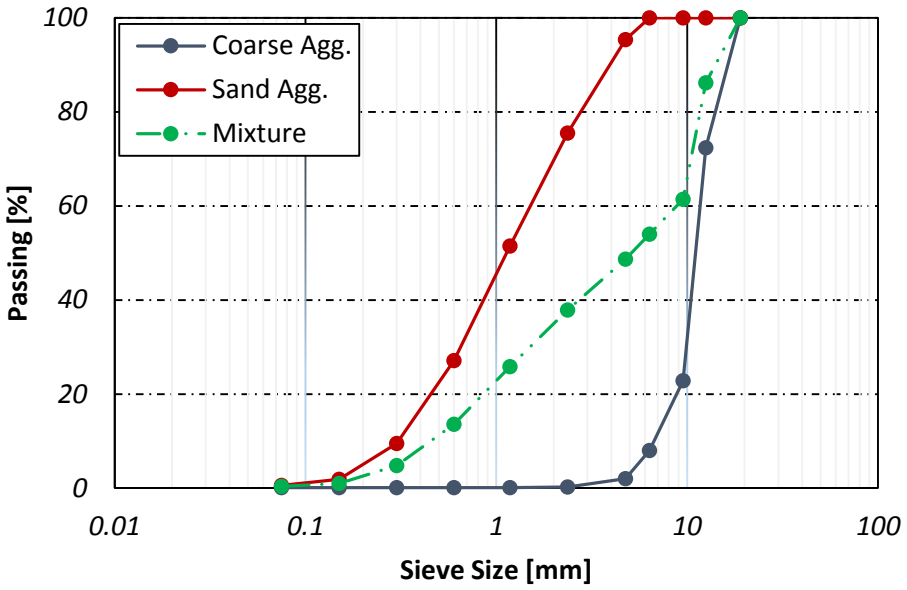


Fig. 3.1 Grading curves of aggregates

### 3.2.3 Water

Tap water was used as mixing water for this study.

### 3.2.4 Fibers

Double hooked-end (DHE) steel fibers with a 60-mm length and an aspect ratio of 65, hooked-end (HE) steel fibers with a 35-mm length and an aspect ratio of 65 were employed in this study. Also, two different types of polyvinyl alcohol (PVA) fibers were used in some mixes. The geometry and the properties of fibers are provided in Fig. 3.2 and Table 3.3, respectively.

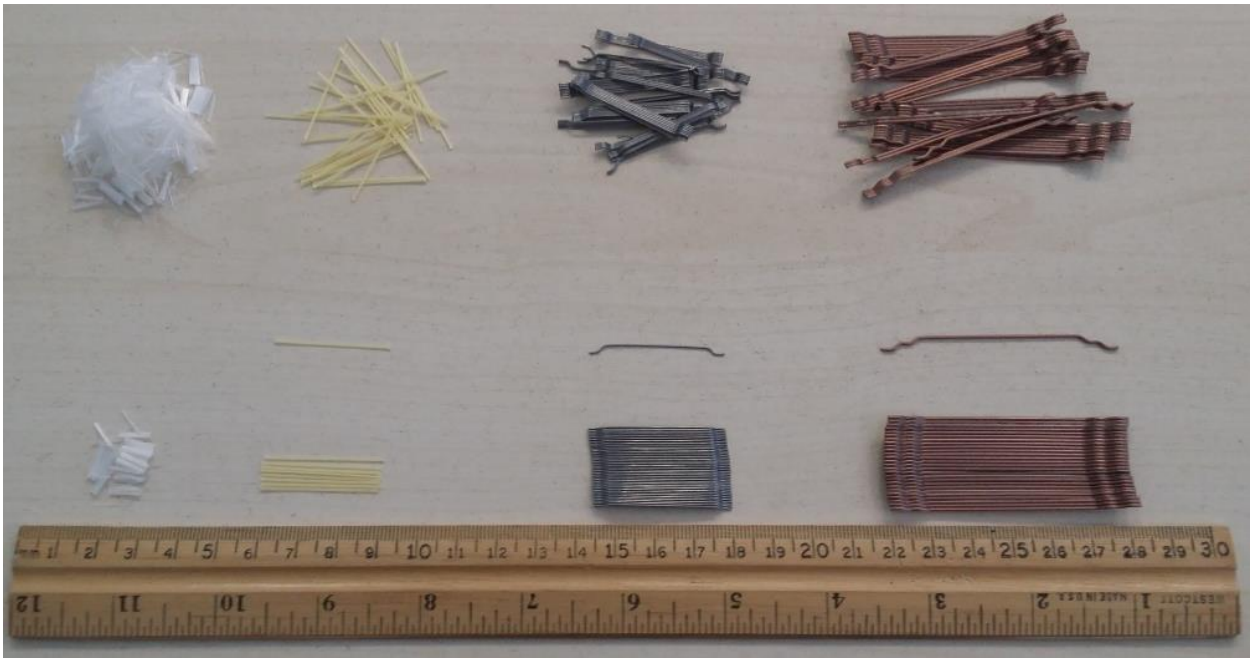

Fig. 3.2 Shape and dimension of steel and polyvinyl alcohol fibers

Table 3.3 Properties of hooked-end steel and PVA fibers

| Type and shape of fiber | Length $l$ (mm) | Diameter $d$ (mm) | Aspect ratio $l/d$ | Density (g/cm$^3$) | Tensile strength (N/mm$^2$) |
|---|---|---|---|---|---|
| Double hooked-end steel (DHE) | 60 | 0.9 | 65 | 7.8 | 2300 |
| Hooked-end steel (HE) | 35 | 0.55 | 65 | 7.8 | 1050 |
| Polyvinyl alcohol (PVA) | 12 | 0.039 | 300 | 1.3 | 1600 |
| Polyvinyl alcohol (PVA) | 30 | 0.4 | 75 | 1.3 | 900 |

### 3.2.5 Superplasticizer

To achieve the desired workability in different concrete mixtures, a MasterGlenium 7500 produced by the BASF factory, was used as a superplasticizer in conventional concretes. In concrete mixes were fabricated with Type K cement, a RECOVER hydration stabilizer was used to delay the setting time of those concretes. To manufacture different concrete mixes that contains CSA cement, Driver Care 10, and Tartaric acid were used.

## 3.3 Concrete mixtures and mixing procedure

All the concrete mixes prepared at Berkeley were produced at an effective water-binder ratio of 0.35, and a total binder content of 450 kg/m$^3$. Five different mixes containing expansive Type K cement and with hybridization of fibers were developed and details of their mix proportions are summarized in Table 3.4. Moreover, 19 different concrete mixes were produced in Politecnico di Milano to study the effects of CSA cement-based mixes, the addition of different type of fibers, the hybridization of fibers, and the influence of w/c ratio on the properties of concrete. A pan mixer was used for the preparation of all the mixes. Prior to adding the raw materials, the surface of the pan mixer was cleaned with a wet towel to avoid the absorption of aggregates moisture by the mixer. To fabricate uniform HPFRC, several mixing procedures have been tried and the following one was chosen. Initially, the fine aggregate and cementitious materials were mixed for one min. Then, approximately half of the water, including superplasticizer, was introduced into the mixer; the ingredients were further mixed for two min. The saturated surface dry (SSD) coarse aggregates and remaining mixing water were then introduced, and the mixing was carried on for another 5 min. In the last step, fibers were added gradually to the rotating mixer and were mixed for an additional 5 min to obtain a homogenous mixture. Details of mix proportions and the results of a slump test are summarized in Table 3.5 and Table 3.6. To simplify the presentation of the results, the mix proportions of the first 8 concrete mixes that are CSA-blend cement mixes are listed in Table 3.5, while the mix proportions of concretes containing different types of fibers and w/c ratios are listed in Table 3.6. The content of superplasticizer in those tables is given as a percentage of the total mass of the binder. To determine the workability of fresh concrete, slump tests were performed as per ASTM C143 [291] during the preparation of the concrete mixes.

Table 3.4 Mix proportions of concrete mixes were developed in University of California, Berkeley

| Mix No. | Mixture ID | W/B | Water | Cement | | Fine Agg. | Coarse Agg. | Fiber volume fraction (%) | | | SP (%) | HS (%) | Slump (cm) |
|---|---|---|---|---|---|---|---|---|---|---|---|---|---|
| | | | | OPC | Type K | | | DHE | HE | PVA | | | |
| | | | (kg/m$^3$) | | | | | | | | | | |
| 1 | CC | 0.35 | 157.5 | 450 | - | 901 | 936 | - | - | - | 1.0 | - | 22 |
| 2 | SHCC | | 157.5 | - | 450 | 898 | 933 | - | - | - | 1.2 | 0.2 | 24 |
| 3 | DHE1 | | 157.5 | - | 450 | 884 | 919 | 1.0 | - | - | 1.5 | 0.2 | 25 |
| 4 | DHE0.5+PVA0.5 | | 157.5 | - | 450 | 884 | 919 | 0.5 | - | 0.5 | 1.8 | 0.2 | 14 |
| 5 | DHE0.5+HE0.3+PVA0.2 | | 157.5 | - | 450 | 884 | 919 | 0.5 | 0.3 | 0.2 | 1.8 | 0.2 | 18 |

*Note: OPC (Type II/V), DHE, HE, PVA, SP, and HS represent ordinary Portland cement, double hooked-end steel fiber with the length of 60 mm, hooked-end steel fiber with the length of 35 mm, polyvinyl alcohol fiber with the length of 12 mm, superplasticizer (MasterGlenium 7500), and hydration stabilizer, respectively.

Table 3.5 Mix proportions of CSA-blend cement mixes were developed in Politecnico di Milano University

| Mix No. | Mixture ID | W/B | Water | Binder | | | Fine Agg. | Coarse Agg. | Fiber volume fraction (%) | | | SP (%) | | Slump (cm) |
|---|---|---|---|---|---|---|---|---|---|---|---|---|---|---|
| | | | | OPC | CSA | Slag | | | DHE | HE | PVA | DC10 | Tartaric | |
| | | | (kg/m$^3$) | | | | | | | | | | | |
| 1 | OPC | 0.35 | 157.5 | 450 | - | - | 905 | 895 | - | - | - | 1.0 | - | 21 |
| 2 | OPC-DHE1 | | | 450 | - | - | 892 | 882 | 1 | - | - | 1.2 | - | 21 |
| 3 | CSA | | | - | 450 | - | 901 | 891 | - | - | - | 1.2 | 0.2 | 20 |
| 4 | CSA-DHE1 | | | - | 450 | - | 888 | 878 | 1 | - | - | 1.4 | 0.2 | 19 |
| 5 | OPC50-CSA50 | | | 225 | 225 | - | 903 | 893 | - | - | - | 1.3 | 0.2 | 22 |
| 6 | OPC50-CSA50-DHE1 | | | 225 | 225 | - | 890 | 880 | 1 | - | - | 1.5 | 0.2 | 20 |
| 7 | OPC25-CSA50-SL25 | | | 112 | 225 | 112 | 895 | 885 | - | - | - | 1.5 | 0.2 | 23 |
| 8 | OPC25-CSA50-SL25-DHE1 | | | 112 | 225 | 112 | 881 | 872 | 1 | - | - | 1.7 | 0.2 | 23 |

*Note: OPC (Type I), CSA, Slag, DHE, HE, and PVA represent ordinary Portland cement, calcium sulfoaluminate cement, ground granulated blast-furnace slag, double hooked-end steel fiber with the length of 60 mm, hooked-end steel fiber with the length of 35 mm, and polyvinyl alcohol fiber with the length of 30 mm, respectively. Moreover, in mixes that were manufactured with CSA cement, tartaric acid was used as a retarder to adjust the setting time of concrete mixes.

Table 3.6 Mix proportions of fiber-reinforced concrete mixes were developed in Politecnico di Milano University

| Mix No. | Mixture ID | W/B | Water | Binder | | | Fine Agg. | Coarse Agg. | Fiber volume fraction (%) | | | SP (%) | | Slump (cm) |
|---|---|---|---|---|---|---|---|---|---|---|---|---|---|---|
| | | | | OPC | CSA | Slag | | | DHE | HE | PVA | DC10 | Tartaric | |
| | | | | ($kg/m^3$) | | | | | | | | | | |
| 1 | OPC | | | 450 | - | - | 905 | 895 | - | - | - | 1.0 | - | 21 |
| 2 | CSA | | | - | 450 | - | 901 | 891 | - | - | - | 1.2 | 0.2 | 20 |
| 3 | CSA-DHE1 | | | - | 450 | - | 888 | 878 | 1 | - | - | 1.4 | 0.2 | 19 |
| 4 | CSA-HE1 | 0.35 | 157.5 | - | 450 | - | 888 | 878 | - | 1 | - | 1.4 | 0.2 | 18 |
| 5 | CSA-PVA1 | | | - | 450 | - | 888 | 878 | - | - | 1 | 1.4 | 0.2 | 15 |
| 6 | CSA-DHE0.5-HE0.5 | | | - | 450 | - | 888 | 878 | 0.5 | 0.5 | - | 1.4 | 0.2 | 15 |
| 7 | CSA-DHE0.5-PVA0.5 | | | - | 450 | - | 888 | 878 | 0.5 | - | 0.5 | 1.4 | 0.2 | 16 |
| 8 | OPC | | | 550 | - | - | 868 | 858 | - | - | - | 1.3 | - | 19 |
| 9 | CSA | | | - | 550 | - | 863 | 853 | - | - | - | 1.5 | 0.2 | 18 |
| 10 | CSA-DHE1 | | | - | 550 | - | 849 | 840 | 1 | - | - | 1.7 | 0.2 | 20 |
| 11 | CSA-HE1 | 0.28 | 154.0 | - | 550 | - | 849 | 840 | - | 1 | - | 1.7 | 0.2 | 18 |
| 12 | CSA-PVA1 | | | - | 550 | - | 849 | 840 | - | - | 1 | 1.7 | 0.2 | 16 |
| 13 | CSA-DHE0.5-HE0.5 | | | - | 550 | - | 849 | 840 | 0.5 | 0.5 | - | 1.7 | 0.2 | 17 |
| 14 | CSA-DHE0.5-PVA0.5 | | | - | 550 | - | 849 | 840 | 0.5 | - | 0.5 | 1.7 | 0.2 | 17 |

*Note: OPC (Type I), CSA, Slag, DHE, HE, and PVA represent ordinary Portland cement, calcium sulfoaluminate cement, ground granulated blast-furnace slag, double hooked-end steel fiber with the length of 60 mm, hooked-end steel fiber with the length of 35 mm, and polyvinyl alcohol fiber with the length of 30 mm, respectively. Moreover, in mixes that were manufactured with CSA cement, tartaric acid was used as a retarder to adjust the setting time of concrete mixes.

## 3.4 Specimens molding and curing

Details of specimens casting and testing method were employed in this study are given in Table 3.7. The specimens were molded with different dimensions that matched the requirements of their standards test and were compacted on a vibration table. The samples were covered with a wet plastic sheet to prevent them from dripping water in the first 24 h of curing. Then, the concrete specimens were demolded and immersed in lime-saturated water at 23°C until reaching their testing ages. For each test, three samples were prepared, and the average value was demonstrated as the final result.

Table 3.7 Details of the specimens and test methods utilized to determine properties of HPC

| Property | Test standard | Specimen size | Age at test |
|---|---|---|---|
| Compressive strength | ASTM C39 | 100 mm cube | 1, 7, 28, and 56 days |
| Splitting tensile strength | ASTM C496 | 100 × 200 mm cylinder | 7, 28, and 56 days |
| Modulus of elasticity | ASTM C469 | 100 × 200 mm cylinder | 28 days |
| Flexural strength | BS EN 14651 | 150 × 150 × 600 mm prism | 7, 28, and 56 days |
| Water absorption | ASTM C642 | 100 mm cube | 28 days |
| Drying shrinkage | ASTM C157 | 75 × 75 × 285 mm prism | 28 days |
| Electrical resistivity | ---------- | 100 mm cube | 1, 3, 7, 14, and 28 days |
| Potential of steel fibers | ASTM C876 | 100 mm cube | 1, 3, 7, 14, and 28 days |
| Potential-static test | BS EN 480 | 100 mm cube | 28 days |
| Single fiber pull-out | ---------- | 37.5 × 37.5 mm cylinder | 28 days |
| SEM | ---------- | ----- | 28 days |
| XRD | ---------- | ----- | 7, 28, and 56 days |

## 3.5 Testing methods

### 3.5.1 Compressive, splitting tensile and flexural strengths

Compressive strength and modulus of elasticity were conducted on the cubic and cylindrical specimens, with dimensions of 100 mm and 100×200 mm using a 3000-KN universal compression

machine in accordance with ASTM C39 [292] and ASTM C469 [293], respectively. The splitting tensile strength also performed on the cylindrical specimens with dimensions of 100×200 mm as per ASTM C496 [294]. The flexural strength test was also carried out on beam specimens with dimensions of 150×150×600 mm as per BS EN 1465 [295]. The tests setup for aforementioned experiments are shown in Fig. 3.3.

(a) (b) (c)

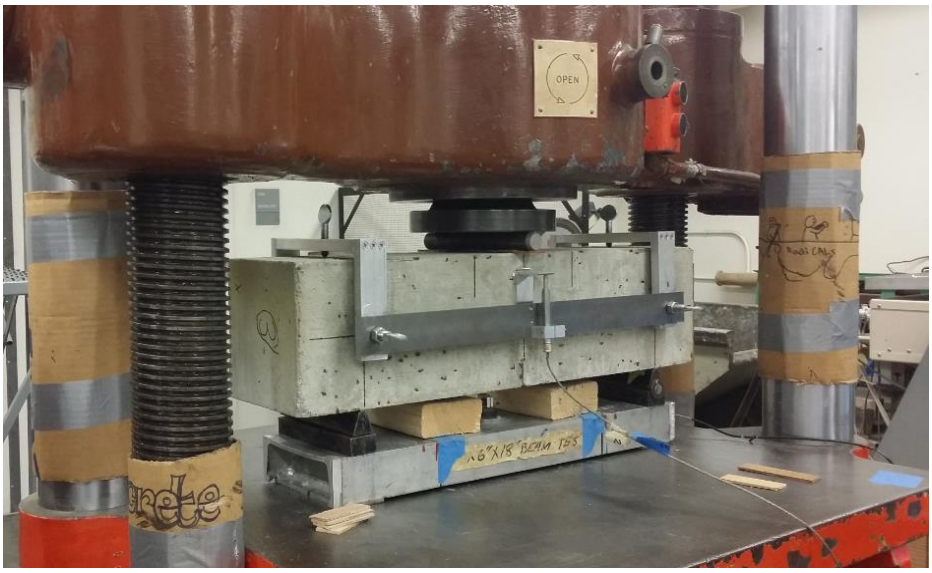


(d)

Fig. 3.3 The test setup for: (a) compressive strength, (b) splitting tensile, (c) modulus of elasticity, (d) bending tests

### 3.5.2 Water absorption

The water absorption tests were performed on cubic specimens in accordance with ASTM C642 [296]. The specimens were cured in water (23°C ) for 27 days. Subsequently, the specimens were dried in an oven at 45°C for at least 14 days. In the case where the difference between values obtained from two successive measurements of mass exceeded 0.5 % of the lesser value, the specimens were returned to the oven for an additional 24-hour drying period. Weights of the specimens were then measured at additional days until the difference between any two successive measurements was less than 0.5 %. The cured specimens were then immersed in the water tank for 0.5 and 168 hours and they were weighed on a 0.01 g balance after being wiped with a dry paper towel. In the present study, water absorptions at 0.5 h and 7 days are referred to as the initial and ultimate water absorption, respectively.

### 3.5.3 Drying shrinkage

The free drying shrinkage test was performed on prismatic specimens in accordance with ASTM C 157 [297]. Upon removal of specimens from the molds, the samples were maintained in lime-saturated water for 30 min to minimize variation in length due to variation in temperature. Then the specimens removed from water storage, wiped with a damp cloth and the initial comparator reading was measured immediately. After the initial comparator reading, the specimens were stored in lime-saturated water at 23°C until they reached the age of 28 days. The drying shrinkage was performed on the air stored specimens at a room with a relative humidity of 50% and temperature of 23°C, and consecutive reading were carried out after curing of 4, 7, 14, 28, and 56 days. During each measurement, first the reference bar was placed in the comparator, and the

comparator dial was set to zero. Next, the specimen was placed in the comparator and reading was taken. Using the comparator readings, the shrinkage strain was calculated as:

$$\varepsilon_{sh}(t) = \left(\frac{l_2 - l_1}{l_g}\right) \quad (3\text{-}1)$$

where $\varepsilon_{sh}(t)$ is the drying shrinkage strain of the specimen at time t, $l_1$ is the initial comparator reading, $l_2$ is the comparator reading at time t, and $l_g$ is the effective gage length between the steel studs were fixed at the opposite ends of specimens. The test setup for shrinkage test is shown in Fig. 3.4.

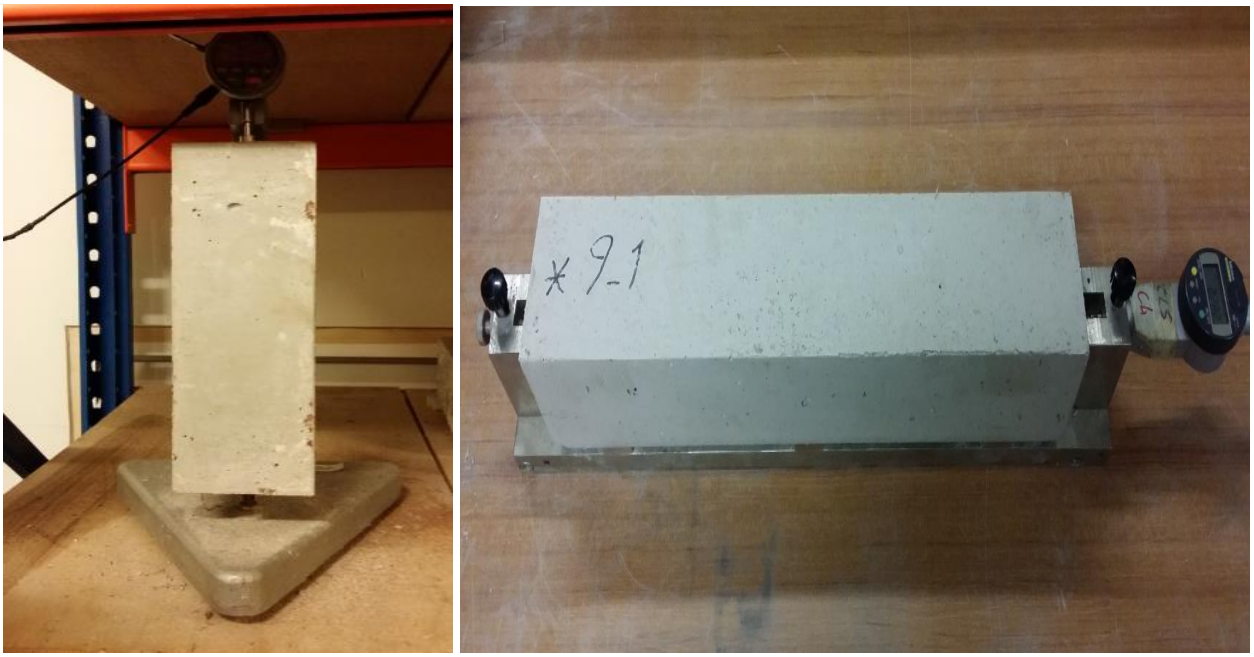


(a) (b)

Fig. 3.4 Test set up for measuring the drying shrinkage of prismatic specimens: (a) as per ASTM C157, (b) as per Europe standard

It worth nothing that the shrinkage of specimens fabricated in Politecnco di Milano was measured on prismatic beams with dimensions of 100×100×500 mm based on the Europe standard. In addition, the shrinkage measurements was started after demolding of specimens and continued at the ages of 1, 2, 3, 7, 14, 28, and 56 days.

### 3.5.4 Electrical resistivity

The electrical resistivity of the specimens was measured via a conductometer equipment. As can be seen in Fig. 3.5, the concrete specimens were placed between two copper plates at the bottom and top surface of cubic specimen. To make sure that the current is passing through the specimens, two wet sponges were placed between the surface of concrete and copper plates. Then, the conductivity of specimens were measured by using two wires that connected to copper plates. Afterward, the electrical resistivity of each specimens was calculated as:

$$R = \frac{1}{C} \qquad (3-2)$$

$$\rho = R\frac{A}{l} \qquad (3-3)$$

where $R$ is electrical resistance, $C$ is the conductivity, ρ is the electrical resistivity of the concrete, $A$ is the surface area of the concrete, and $l$ is the height of the concrete specimen.

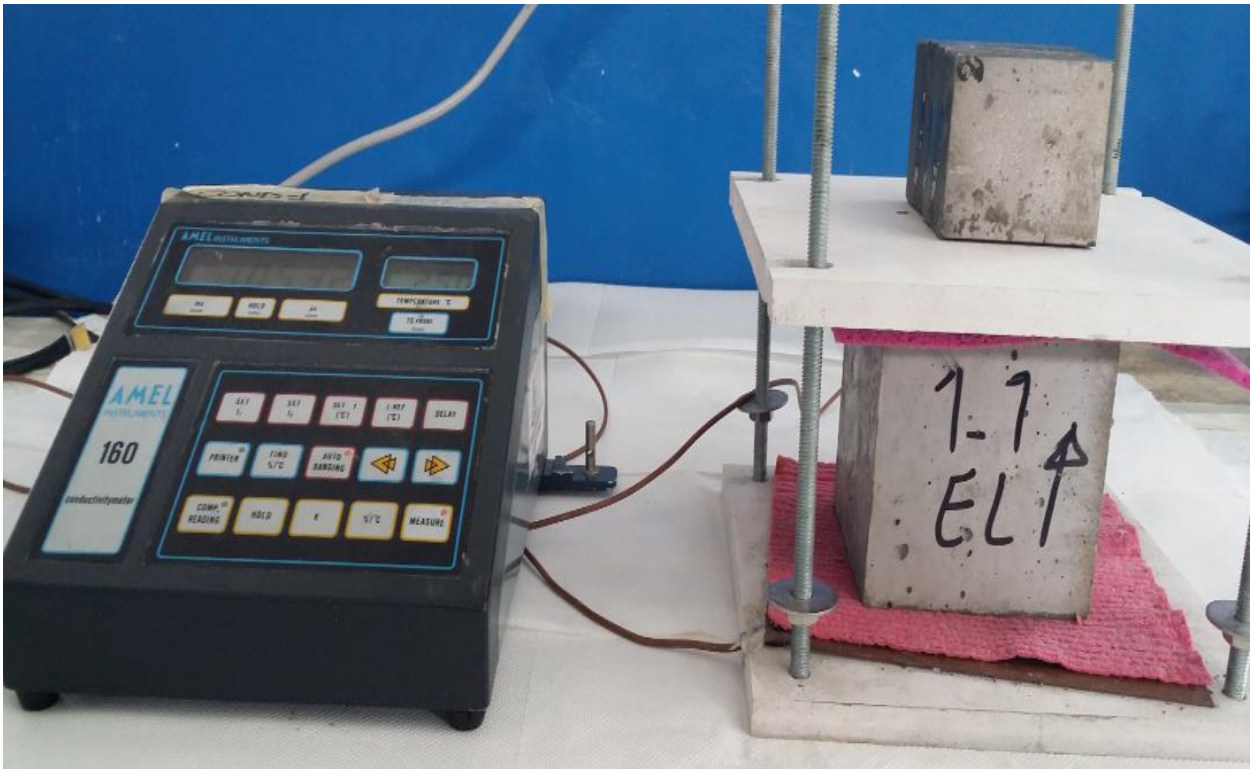


Fig. 3.5 Test set up to measure the electrical resistivity of concrete specimens

### 3.5.5 Electrical half-cell potential of steel fiber in concrete

The electrical half-cell potentials of steel fibers embedded in concretes was measured via a voltmeter equipment as per ASTM C876 [298]. To measure the potential of steel fibers, they have embedded in the body of concrete when it was at its fresh state. Then, a wire was connected to the calomel cell (instead of copper-copper cell) that was placed on the surface of concrete specimen. As recommended in ASTM C876, a wet sponge was used to ensure the connection of calomel cell and concrete surface. Another wire that connected to the positive terminal of voltmeter was then used to measure the potential of steel fibers as is shown in Fig. 3.6. It is worth noting that concrete samples were cured at 23°C and relative humidity of higher than 90%.

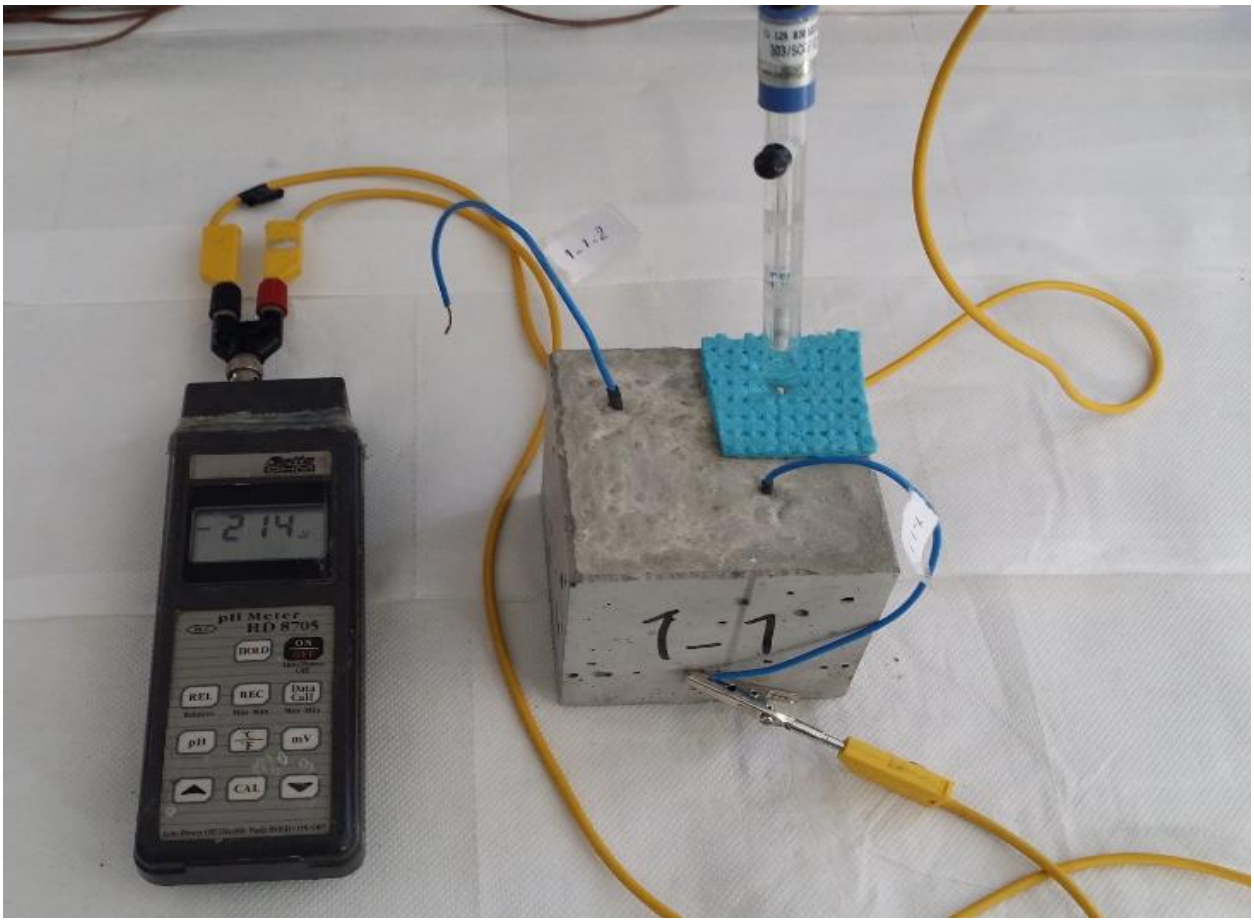


Fig. 3.6 Test set up to measure the electrical half-cell potential of steel fiber in concrete

### 3.5.6 Potential-static electro-chemical test

To determine the corrosion susceptibility of steel fiber in concrete, the potential-static electro-chemical technique was used as per BS EN 480-14 [299]. During the test, the concrete specimens containing two embedded steel fibers were maintained at a constant potential of 200 mV with respect to the saturated calomel electrode (SCE) for 24 hours. The electrolyte of the cell was a tap water at a temperature of 23°C. An ammeter with an accuracy $\leq$ 0.1 μA was used to measure changes in the current between the steel fibers and SCE immediately after polarization, 10, 30, and 60 minutes and 24 hours. The potential-static test set up is shown in Fig. 3.7. After 24 hours, the applied constant potential of 200 mV was canceled and the potentials of fibers were measured by using a voltmeter up to 2 hours.

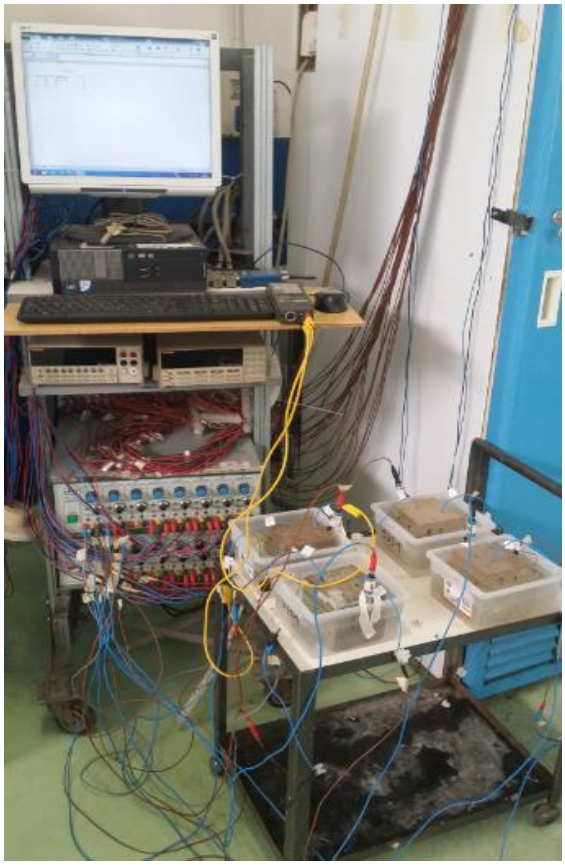

Fig. 3.7 Test set up for potential-static electro-chemical test

### 3.5.7 Single fiber pullout test

The fiber pullout test was conducted on cylindrical samples with diameter and height of 37.5 mm. The embedment length of steel fiber was 19±0.5 mm. The single fiber pullout test set up is shown in Fig. 3.8. To observe the micro-cracking process of pullout samples by a microscope, the following technique was used. First, the samples were kept in a vacuum impregnation for the period of 24 hours to ensure that voids have been sucked out from the mortar. Then, an epoxy was poured on the top surface of samples and leaved it for a while to allow epoxy be penetrated inside the free spaces of mortar. After 2 days that epoxy got hardened enough, the samples were cut along their fiber axis. Afterwards, the side of cut sample including the injected epoxy was selected to be polished carefully and reach the right position where the steel fiber was in the mortar. The polishing of samples stopped as soon as a clear appearance of fiber channel filled with hardened epoxy was seen. The prepared samples for microscopic observation are shown in Fig. 3.9.

Fig. 3.8 Test setup for single fiber pullout test

(a)

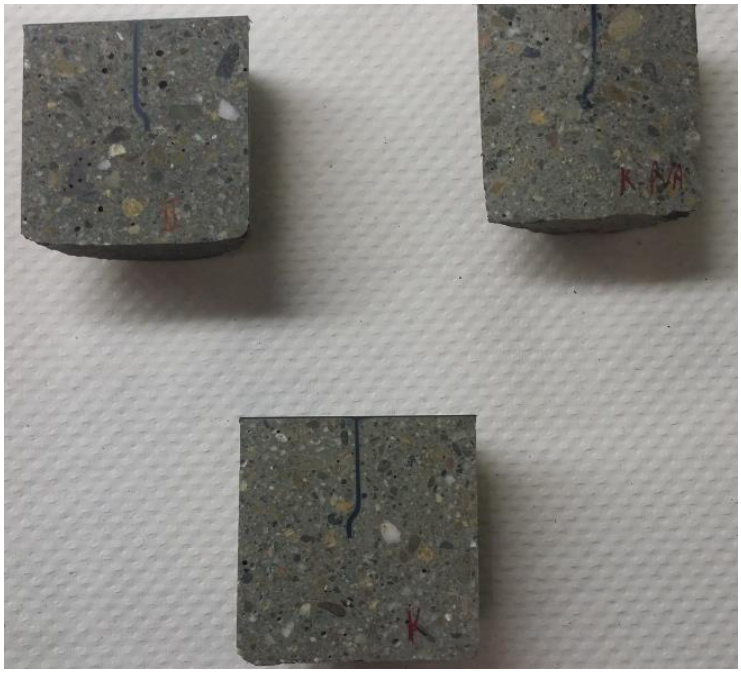

(b)

Fig. 3.9 Prepared specimens for microscopic observation: (a) specimens were filled with epoxy, (b) polished specimens

### 3.5.8 Scanning electron microscopy (SEM)

The SEM technique is used to investigate the morphology and surface characterization of materials by capturing images at the micro or nano scale. In this technique, a focused beam of electrons strikes the surface of the material. The surface interactions result in the emission of secondary and backscattered electrons as well as X-rays and other responses. The electrons are collected and converted to an image of the surface. Any compound, as long as it is electrically conductive, can be examined by this technique. The contrast formed by the collected electrons originates from the difference in surface topography and composition. Both secondary electrons (SE) and backscattered electrons (BSE) modes provide imaging facility. The SE mode is dominated by topographic contrast, whereas the BSE mode mainly detects atomic density which helps differentiate regions rich in a specific atom. It is also possible to collect the X-rays emitted from the surface. This technique which is referred to as energy dispersive X-ray spectroscopy (EDX) enables elemental analysis and the detection of different atoms in the compound. EDX imaging facilitates estimation of the distribution of various elements in the compound. In this study, a ZEISS EVO®MA10 SEM was used to collect microscale morphology of the samples. The SE mode was used to study a fracture surface, and the BSE mode was used to image a well-polished surface. The samples were carbon-coated prior to the SEM experiment, to avoid charging problem. The preparation of the thin section followed the protocol described by Kjellsen et al. [300]. The scanning electron microscopy devise is shown in Fig. 3.10.

Fig. 3.10 Scanning electron microscopy device

### 3.5.9 X-ray diffraction

The X-ray diffraction (XRD) technique is one of the most commonly used methods in cement chemistry. As each crystal has a unique X-ray pattern, the XRD technique is an effective tool for the characterization of crystalline materials. In a crystalline structure, various atoms are located in a repeating order which results in the formation of similar atomic planes. The distance between these planes is referred to as d-spacing. X-ray beams give constructive interference when they hit different parallel layers. The diffracted beams can be detected if they are in phase. This occurs according to Bragg's law:

$$n\lambda = 2d\ sin\ (\theta) \qquad (3-4)$$

in which $\lambda$ is the wavelength of the X-ray (e.g. about 0.15 nm for copper), d is the distance between the atomic planes, $\theta$ is the angle between the incidence beam and the normal to the reflecting lattice plane, and *n* is an integer called order of reflection (Fig. 3.11) [301].

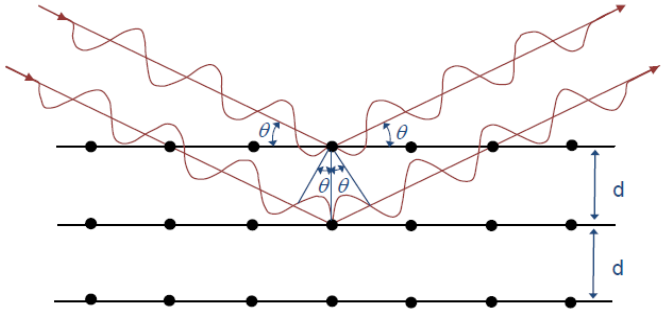


Fig. 3.11 Diffraction of X-rays expressed by Bragg's law [301]

The unreacted cement powders, as well as hydrated pastes of selected ages (7, 28, and 56 days), were measured by XRD. The hydrated paste were hand-grinded using a ceramic mortar and pestle. The sample were immediately sent to XRD measurements and therefore no special care was taken to stop the hydration. A PANalytical X'Pert Pro diffractometer as shown in Fig. 3.12, was used for the XRD measurement, operating at 40 keV and 40 mA with a Cobalt anode. The 2-theta scanning range was between 5° and 80°, with a step width of 0.0167° and total collection time of 1 hour. Software HighScore (Plus) was used to identify the peak positions.


Fig. 3.12 The test setup for X-rays diffraction test

# Chapter 4

# The influence of expansive cement on the mechanical, physical, and microstructural properties of hybrid-fiber-reinforced concrete

## 4.1 Introduction

This chapter investigates the properties of concrete fabricated by replacement of ordinary Portland cement (OPC) with Type K expansive cement. New hybrid-fiber-reinforced concrete (HyFRC) containing expansive cement and with combinations of metallic and non-metallic fibers at total fiber volume fraction of 1% were also developed. The effectiveness of double hooked-end (DHE) steel fibers in concrete is also investigated. The compressive strength, splitting tensile strength, modulus of elasticity, flexural behavior, drying shrinkage and water absorption were evaluated. The microstructure and compositions of concrete matrix were studied using Scanning Electron Microscopy and X-ray diffraction, respectively. The fiber pullout test was also performed to investigate the effectiveness of Type K cement in improving the fiber-matrix interfacial bond.

## 4.2 Compressive strength

The compressive strength results of different mixes at curing ages of 7, 28, and 56 days is shown in Fig. 4.1. The results indicate that the replacement of OPC with Type K cement has no significant influence on the compressive strength of concrete, and a slight reduction up to 3% has been occurred by cement substitution. It may be attributed to the formation of higher ettringite in concrete with expansive cement which is the source of volume expansion and can create some micro-cracks in the body of concrete that subsequently reduce the strength compared to conventional concrete. A slight reduction in the strength of concrete fabricated by expansive

cement has been observed by other researchers [302, 303] as a result of aforementioned phenomena. It can be seen that the inclusion of 1% DHE steel fibers led to an increase in the compressive strength of SHCC. For instance, the compressive strength of concrete reinforced with 1% DHE steel fibers were 8%, 4%, and 5% higher than those of CC at 7, 28, and 56 days, respectively. DHE steel fibers, owing to their high elastic modulus and particular shape that restricts the propagation of cracks, alters the tendency of cracks, and subsequently improves the compressive strength of concrete [304]. However, the substitution of 0.5% DHE steel fibers volume content with PVA fibers led to a slight reduction in the compressive strength of concrete. There are several factors including the fiber content, fiber type, fiber size, and porosity of cement matrix that affect the compressive strength of FRC. The reduction attained in the strength of DHE0.5+PVA0.5 mix can be attributed to the higher porosity of this mix compared to that of SHCC that becomes the dominant factor in this mix. The results demonstrate that the strength of DHE0.5+HE0.3+PVA0.2 mix is slightly higher than that of the corresponding mix without fibers.

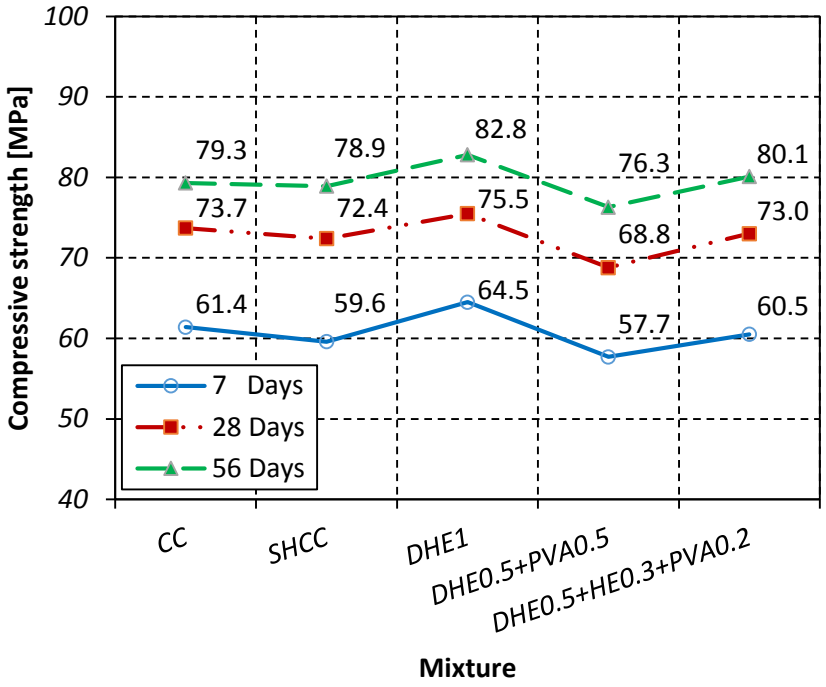


Fig. 4.1 Compressive strength of different concrete mixes

## 4.3 Splitting tensile strength

The splitting tensile strength of the different mixes prepared in this study is shown in Fig. 4.2. Similarly, the splitting tensile strength of concrete produced with Type K cement is reduced by only 3% compared to that of CC. The results indicate that the incorporation of fibers significantly improves the splitting tensile strength of concrete due to the restraining the extension of cracks. Among different mixes that considered in this study, the highest strength was achieved by the mix containing 1% DHE steel fibers. The splitting tensile strength of this mix were 99%, 94%, and 133% higher than those of CC at 7, 28, and 56 days, respectively. Even though hybridization of fibers resulted in a reduction in the splitting tensile strength of concrete compared to DHE1 mix; however, the strength of HyFRC mixes is still significantly higher than that of the plain concrete. For instance, the splitting tensile strength of DHE0.5+PVA0.5 and DHE0.5+HE0.3+PVA0.2 mixes increased by 22% and 49% at 28 days compared to that of SHCC, respectively. As can be seen in Fig. 4.2, the effect of curing age on the improvement of splitting tensile strength is relatively higher in FRC compared to plain concrete. As FRC mixes manufactured with expansive cement, this result suggests that the bond between fibers and cement matrix has been improved due to the self-stressing that resulted from the expansive behavior of Type K cement. For instance, the splitting tensile strength of SHCC mix was increased by 14% and 19% at 28 and 56 days compared to its 7 days strength, respectively, while the average increase in FRC mixes was 13% and 35%, respectively. This result has been verified by the results of single fiber pullout test and SEM images that show the effectiveness of Type K cement in improvement of bond between fibers and cement matrix that will be discussed in sections 4.8.2 and 4.9.2.

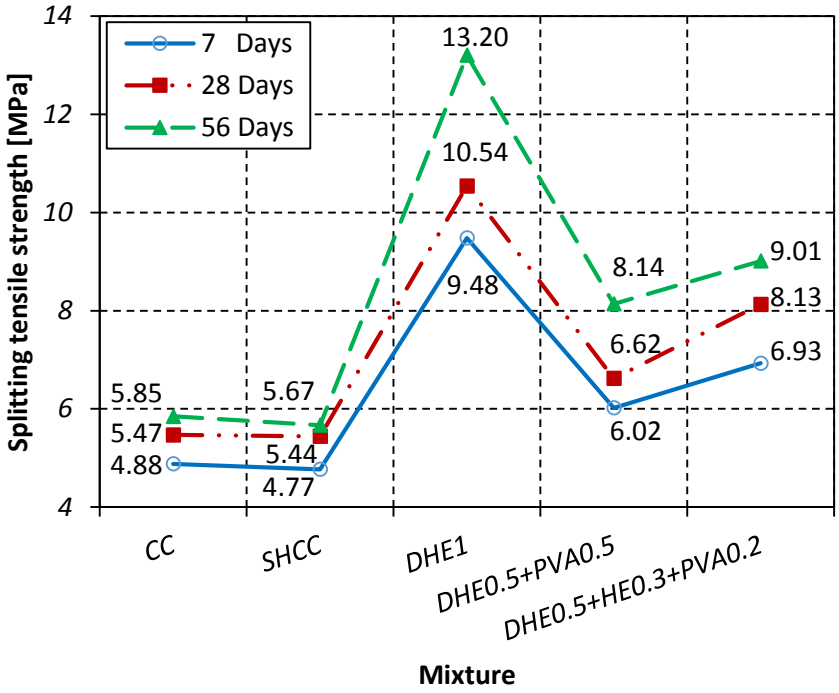


Fig. 4.2 Splitting tensile strength of different concrete mixes

## 4.4 Modulus of elasticity

There is a direct correlation between density and modulus of elasticity in homogeneous materials. However, in heterogeneous, multiphase materials, such as concrete, the density, the modulus of elasticity of the principal constituents, and the characteristics of the transition zone determine the elastic modulus behavior of the composite [142, 305]. The 28-days modulus of elasticity of different mixes is shown in Fig. 4.3, and the percentage of modulus of elasticity over that of SHCC has been shown on top of each bar. The results indicate that cement type has no important effect on the modulus of elasticity of concretes considered in this study. It was also observed that the addition of fibers of any type and hybridization resulted in an increase in the static modulus of the concrete when compared to that of the SHCC. This improvement can be attributed to the presence of steel fibers with higher elastic modulus compared to cement matrix that consequently improves

the modulus of elasticity of concrete. Moreover, the hybridization of steel with PVA fibers was effective to restrict the propagation of micro-cracks that led to a better performance in HyFRC.

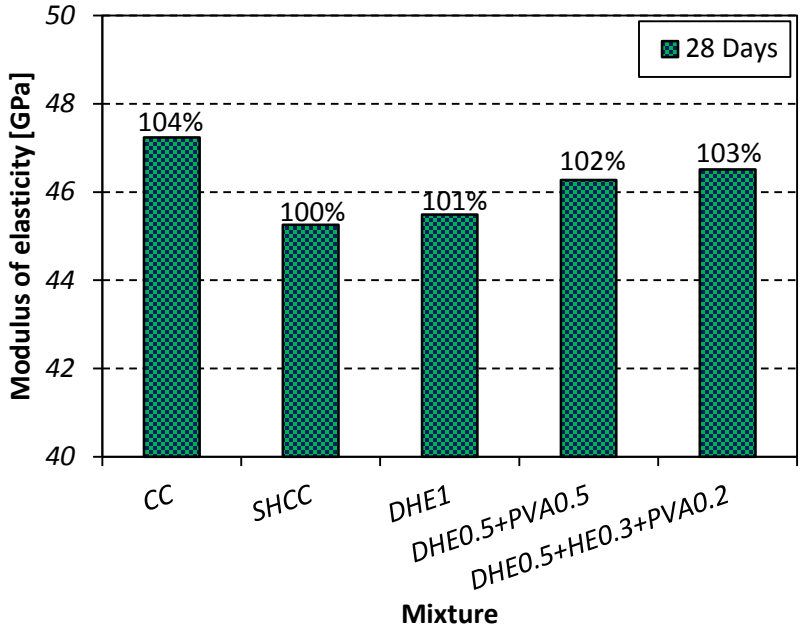


Fig. 4.3 28-days modulus of elasticity of different concrete mixes (Note: xx% indicates the percentages of modulus of elasticity based on SHCC-28 Days)

## 4.5 Flexural performance

### 4.5.1 Flexural strength-CMOD curve

The diagram of 28-day flexural strength-CMOD for different concrete mixes is shown in Fig. 4.4, and flexural test results are presented in Table 4.1. As can be seen in Fig. 4.4, the behavior of concretes without fibers was almost linear up to the maximum load, followed by a sharped descending branch up to failure point, then the beam specimens split into two separated parts. The results indicate that substitution of OPC with Type K cement slightly increased the flexural strength. It has been reported that the addition of expansive agent in concrete led to an almost similar flexural strength compared to ordinary concrete [306]. On the other hand, the results of

fiber-reinforced concretes illustrate that the addition of fibers remarkably improved the post-cracking behavior of FRC with an extensive cracking process between first crack load and peak load. Once the first crack was occurred, the fibers bridging the crack resisted the load and prevented further crack propagation. This resulted in an increase in the load that could be resisted to loads beyond the first cracking load. Basically, improvement of flexural strength-CMOD characteristic is dependent on the fiber type, fiber content, fiber orientation, and the bond between fiber and cement matrix. Fig. 4.4 shows that the best performance has been achieved by incorporation of 1% DHE steel fibers in concrete. The inclusion of 1% DHE steel fibers in concrete led to an increase in the load bearing capacity after first crack and the flexural strength increased up to CMOD equal to 1.5 mm. Then, a relatively big crack occurred in the beam and the flexural load gradually decreased. The excellent performance of this mix can be attributed to the ability of DHE steel fibers to carry the load after matrix cracks until further creation of cracks. The flexural load would be reduced due to the failure of fiber anchorage or debonding of fibers and the matrix [189, 190]. However, the replacement of 0.5% DHE steel fibers content with PVA fibers adversely affected the flexural performance of concrete compared to DHE1 mix, while its behavior was significantly better over that of plain concrete. The flexural strength of this mix was increased by only 4% compared to that of SHCC, and a drop in the flexural strength of concrete was observed after appearance of first crack. Then, a relatively flat behavior was seen in the load bearing capacity up to CMOD equal to 3.5 mm. When the flexural stress at the fiber-matrix interface has surpassed the bond developed by the matrix, the fibers are either slipping or being unbounded. As a result, the only mechanism that contribute to improve the strength of cracked section is through mechanical anchorage. Since, PVA fibers are straight and have lower length compared to steel fibers, they can bridge mainly the micro-cracks and have minor influence on the flexural strength.

The results demonstrate that hybridization of three different kind of fibers increased the flexural strength by 60% compared to that of the SHCC. Similar to DHE1 mix, combination of fibers in DHE0.5+HE0.3+PVA0.2 mix led to a load-deflection hardening behavior. As can be observed from Table 4.1, the $CMOD_{MOR}$ corresponding to the peak load for plain concretes and DHE0.5+PVA0.5 mix was similar to $CMOD_{LOP}$. However, the $CMOD_{MOR}$ for DHE1 and DHE0.5+HE0.3+PVA0.2 mixes were 1.5 and 1.6 mm, respectively that were 15 and 26.6 times of their $CMOD_{LOP}$. For these mixes, the $f_{MOR}$ increased by 52% and 50% compared to their $f_{LOP}$, respectively. An increase of up to 46% was also observed in the $f_{LOP}$ of FRC compared to that of SHCC. The research finding of this study demonstrate that all the HyFRC considered in this work show a deflection hardening behavior and conventional steel bar can be replaced by randomly distributed fiber according to fib Model Code 2010 [307]. Therefore, HyFRC were developed in this study can be of high interest for design of structural member that subjected to bending load.

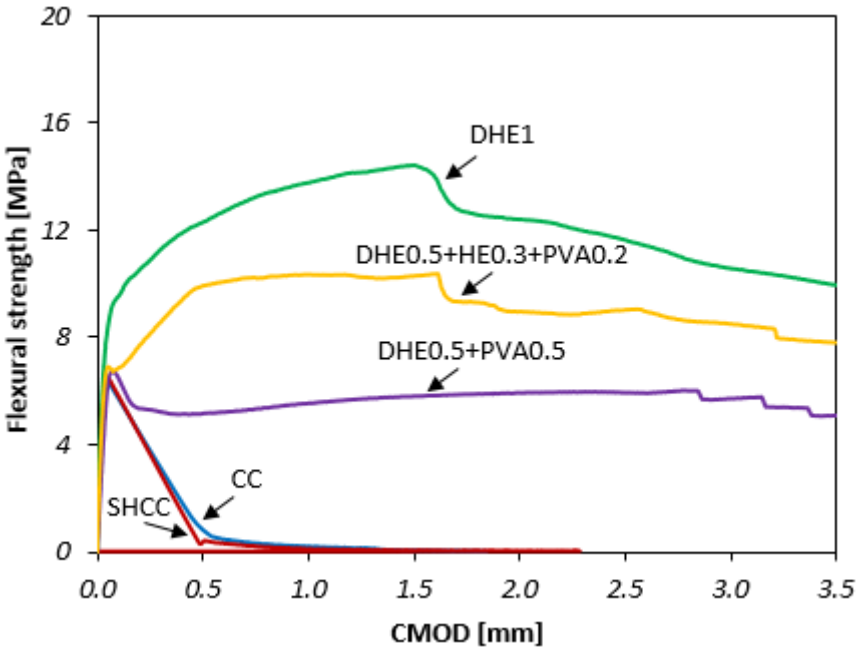


Fig. 4.4 28-days flexural strength-CMOD curves of different concrete mixes

Table 4.1 Flexural test results

| Mix No. | Mixture ID | First crack | | Peak load | | Residual flexural strength (MPa) | | | | Toughness |
|---|---|---|---|---|---|---|---|---|---|---|
| | | Strength, $f_{LOP}$ (MPa) | $CMOD_{LOP}$ (mm) | Strength, $f_{MOR}$ (MPa) | $CMOD_{MOR}$ (mm) | $CMOD_{0.5}$ | $CMOD_{1.5}$ | $CMOD_{2.5}$ | $CMOD_{3.5}$ | |
| 1 | CC | 6.25 | 0.06 | 6.25 | 0.06 | 0.63 | 0.09 | - | - | 6.4 |
| 2 | SCC | 6.49 | 0.05 | 6.49 | 0.05 | 0.40 | 0.04 | - | - | 5.8 |
| 3 | DHE1 | 9.48 | 0.10 | 14.39 | 1.50 | 12.26 | 14.39 | 11.61 | 9.93 | 131.5 |
| 4 | DHE0.5+PVA0.5 | 6.74 | 0.08 | 6.74 | 0.08 | 5.18 | 5.82 | 5.96 | 5.10 | 61.8 |
| 5 | DHE0.5+HE0.3+PVA0.2 | 6.91 | 0.06 | 10.39 | 1.60 | 9.95 | 10.31 | 9.05 | 7.82 | 112.8 |

### 4.5.2 Residual flexural tensile strength and flexural toughness

The residual flexural tensile strength for different concrete mixes is shown in Fig. 4.5, and the flexural toughness results are listed in Table 4.1. As it can be seen in Fig. 4.5, the residual flexural strength of plain concretes are quite similar and since these samples split in two separated parts, the results beyond CMOD of 0.5 mm were not provided. The results indicate that the inclusion of fibers and specifically DHE steel fibers significantly improves the residual flexural strength of concrete. The results also show that the hybridization of fibers resulted in a reduction in the residual flexural strength compared to that of the mix containing 1% DHE steel fibers. For example, the residual flexural strength of DHE0.5+PVA0.5 mix reduced by 58%, 60%, 49%, and 49% at CMOD of 0.5, 1.5, 2.5, and 3.5 mm, respectively compared to those of DHE1 mix. DHE steel fibers due to their particular shape resist significantly against the propagation of cracks, absorbed more energy, and caused an increase in the load carrying capacity.

However, the inclusion of PVA fibers in mixes that reinforced with steel fibers was very effective in order to improve the post-cracking behavior of concrete and avoid the propagation of micro-cracks. For instance, the residual flexural strength of DHE0.5+PVA0.5 mix at CMOD of 0.5, 1.5, 2.5, and 3.5 were 5.18, 5.82, 5.96, and 5.10 MPa, respectively. This result show that the main influence of micro fibers like PVA is to enhance the toughness of concrete instead of increasing the peak flexural load. As it can be observed in Table 4.1, the replacement of OPC with Type K cement slightly reduced the toughness of concrete. On the other hand, the introducing of fibers of any type and combination has a remarkable effect on the improvement of toughness. The highest toughness was attained by the mix containing 1% DHE steel fibers that its toughness was 22.7 times compared to SHCC. This is followed by DHE0.5+HE0.3+PVA0.2 and DHE0.5+PVA0.5 mixes that their toughness were 10.7 and 19.5 times, respectively over that of SHCC.

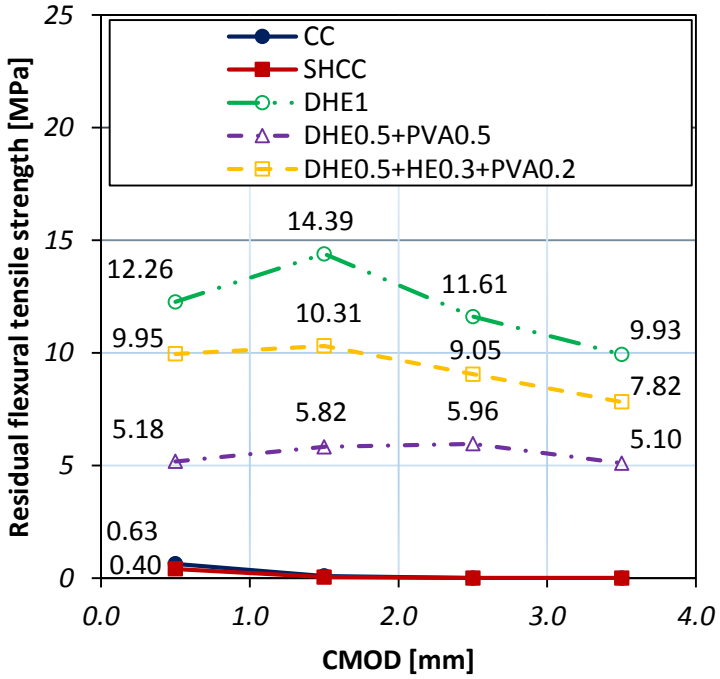


Fig. 4.5 Residual flexural tensile strength of different concrete mixes

## 4.6 Drying shrinkage

The result of drying shrinkage for different concrete mixes is shown in Fig. 4.6. The results indicate that the replacement of OPC with Type K cement led to an expansion, while samples prepared with OPC experienced shrinkage over testing time. Fig. 4.6 shows a great expansion (369 μm/m) that occurred in SHCC after 1 day, whereas the shrinkage of CC samples was 27 μm/m. This high value of early volume expansion in SHCC mix can be attributed to the high amount formation of ettringite. The results also demonstrate that the addition of Type K cement can compensate the shrinkage of concrete and the length change remained almost unchanged after 56 days. It was also observed that highest shrinkage among all mixes considered in this study was attained by CC that a shrinkage strain of 475 μm/m was happened at 56 days. As it can be seen in Fig. 4.6, the inclusion of fibers of any type and fiber combination resulted in a reduction in the expansion of FRC made with Type K cement. However, an expansion strain up to 85 μm/m was observed in FRC at 1 day due to the presence of expansive cement. Thereafter, the expansion of concrete samples has been fully cancelled due to the restraining effect of fibers. The effectiveness of steel fibers in restraining the expansion of shrinkage-compensating concrete has been also shown by Paul et al. [204]. In another study, He et al. [308] studied the expansive deformation of self-stressing concrete reinforced with steel fibers. They pointed out that the inclusion of fibers can fully eliminate the swelling of concrete resulted from the introducing of expansive agent. They hypothesized that this phenomenon would create a mutual interfacial stress between matrix and fibers and consequently leads to an internal homogeneous compressive prestress. Moreover, the improved chemical bond between fibers and cement matrix and subsequently enhanced flexural performance of FRC can be attributed to the self-prestress effect. The results of present study in the sections of splitting tensile strength and single fiber pullout test verified the abovementioned hypothesis. The results

of FRC indicate that hybridization of fibers is a promising way to reduce the shrinkage deformation of concrete. Among different FRC considered in this study, the lowest drying shrinkage was attained by DHE0.5+HE0.3+PVA0.2 mix. As cracks are initiated with small size and later propagated with different sizes in a body of concrete, hybridization of fibers with various features, such as different lengths and modulus of elasticity, plays an important role in resisting cracking at different scales and causes lower shrinkage. It was also reported by Sun et al. [217] that combined use of PVA fibers and steel fibers can significantly inhibit the shrinkage of concrete compared to using monotype of steel fibers. The results also indicate that the shrinkage of all samples tends to stabilize after 14 days.

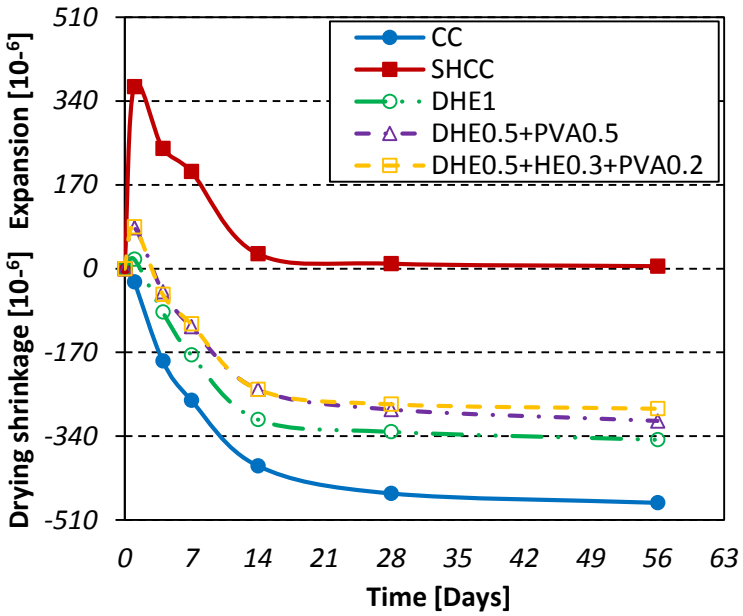


Fig. 4.6 Drying shrinkage of different concrete mixes

## 4.7 Water absorption

The ingress of destructive ions like chloride and sulfate into the concrete adversely affects the durability of concrete. The water absorption test is known as an indirect way to determine the

porosity of concrete, in which also provide information about the permeable pore volume and their connectivity inside the concrete. Fig. 4.7 shows early (30 min) and ultimate (7 day) water absorption of different concrete mixes. As can be seen, SHCC indicates lower water absorption compared to that of the CC. The reduction were 24% and 22% for early and ultimate water absorption, respectively. This reduction can be attributed to the formation of higher amount of ettringite in mix containing Type K cement that fills the voids, leads to the discontinuity of pore network, and also improves the characteristics of cement matrix [309]. The finding of this research in microstructural observation confirmed the improved properties of cement matrix in SHCC mix.

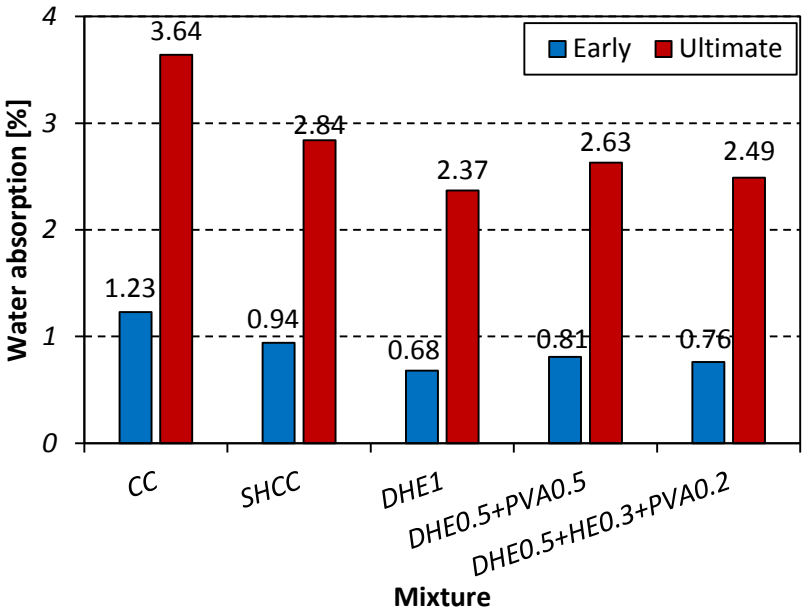


Fig. 4.7 Early and ultimate water absorption of different concrete mixes

The results show that irrespective of the fiber type and combination, the addition of fibers reduced the water absorption of concrete with respect to SHCC. It was observed that the lowest water absorption was attained by the mix reinforced with 1% DHE steel fibers that its ultimate water absorption was 17% lower than that of SHCC. This reduction can be attributed to the ability of fibers to restrict the creation and propagation of cracks in the body of concrete that resulting in a

reduced permeability [245]. The results illustrate that the substitution of DHE steel fibers with PVA and HE steel fibers slightly increased the water absorption of concrete, while these concretes reached lower absorption compared to SHCC. This result suggests that the addition of PVA fiber content results in a relatively higher porosity compared to one reinforced by only steel fibers. The results of water absorption demonstrate a good correlation with the compressive strength test results, in which higher PVA fiber content led to a reduction in the strength of concrete.

## 4.8 Compressive, splitting tensile, and pullout test results of mortars

### 4.8.1 Compressive and splitting tensile strength

The mechanical test results of different mortar mixes are listed in Table 4.2. As it can be seen in that table, the mixes that prepared with Type K cement showed slightly lower compressive and splitting tensile strength compared to that of mixes manufactured with OPC. These results are in good agreement with our finding for concrete mixes that has been already discussed.

Table 4.2 Mechanical and fiber pullout test results of mortar mixes

| Mix No. | Mixture ID | Compressive strength (MPa) | Splitting tensile strength (MPa) | Pullout | |
|---|---|---|---|---|---|
| | | | | Pmax (N) | Δpeak (mm) |
| 1 | Type II/V-Plain | 63.5 | 5.9 | 418.1 | 0.75 |
| 2 | Type K-Plain | 59.4 | 5.6 | 525.9 | 0.65 |
| 3 | Type II/V-1%PVA | 64.4 | 7.4 | 366.0 | 0.60 |
| 4 | Type K-1%PVA | 61.0 | 6.9 | 427.7 | 1.33 |

It was also observed that the addition of 1% PVA fibers in both plain mortars led to an increase in the mechanical properties and particularly the splitting tensile strength. For instance, the compressive and splitting tensile strength of Type II/V-1%PVA mix increased by 2% and 25%,

respectively compared to those of corresponding mix without fibers, while these increase for mortars with Type K cement were 3% and 23%, respectively. This improvement can be related to the ability of fibers to restrict the formation and propagation of cracks in the body of concrete.

### 4.8.2 Single fiber pullout test

The load versus displacement curve of different mortar mixes is depicted in Fig. 4.8 and pullout test results are presented in Table 4.2. As it can be seen in Fig. 4.8, a relatively similar appearance observed in all fiber pullout curves. The load versus displacement curves can be divided to three distinctive parts, in which each of them represent a specific behavior of fiber inside the mortar [310]. The hooked-end of steel fiber including a straight part at end that followed by an inclined part connected to the long straight steel fiber. Part a, represents a linear ascending branch that resulted from the plastic deformation of both parts of hooked-end. Afterwards, a descending branch was observed that followed by a second peak with a relatively lower pullout force (part b). This peak corresponds to the bending of straight part of hooked-end at the position where inclined part was in the beginning. Finally, fiber pullout curve shows a relatively flat behavior with a gradual reduction in the pullout force that corresponds to the movement of steel fiber through the original channel of mortar after complete straightening of hooked-end (part c). The results indicate that the replacement of OPC with Type K cement has a positive influence on the pullout force of mortar. It was observed that the pullout force increased by 26% as a result of cement substitution. This improvement can be attributed to the better bond that took place between the steel fibers and cement matrix as a result of cement expansion and formation of self-prestress effect [308].

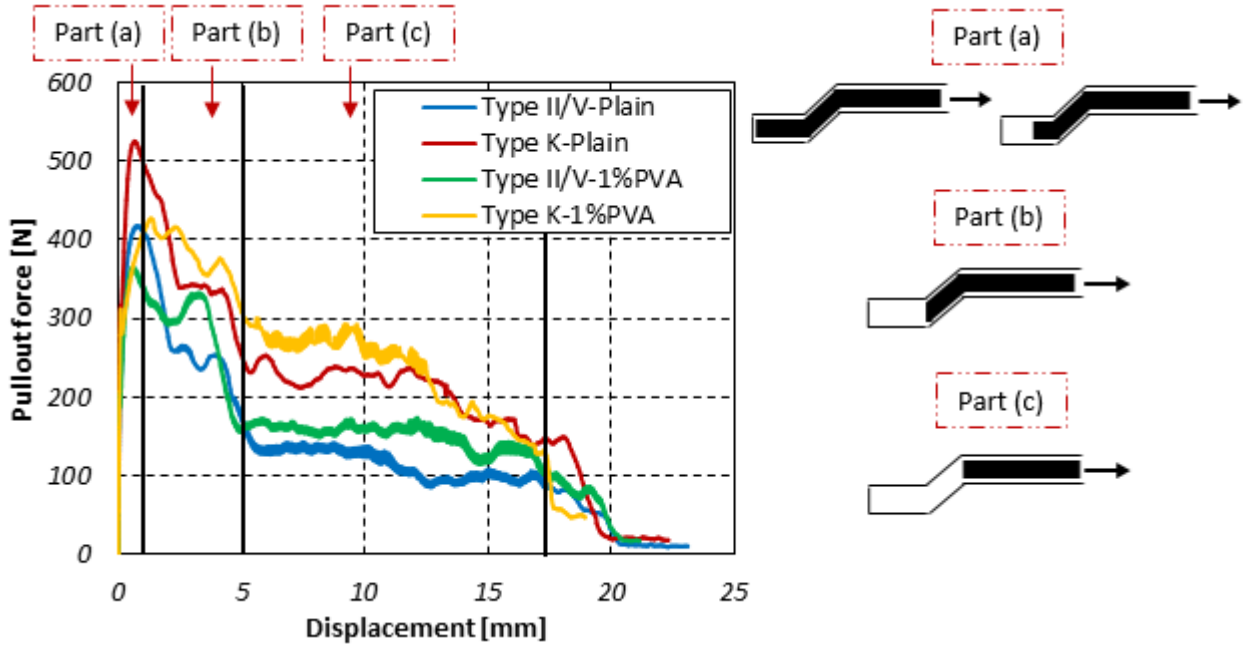


Fig. 4.8 Fiber pullout curves versus displacement of different fiber-reinforced mortars

The results of FRC indicate that the reinforcement of plain mortars with 1% PVA fibers led to a reduction in the peak load of pullout force. It was observed that pullout force of Type II/V-1%PVA and Type K-1%PVA mixes were 12% and 19% lower when compared to that of the corresponding plain mortar mixes. In fact, introducing microfibers in concrete either resulting in higher pullout resistance due to the restriction of micro-cracks or reducing the pullout resistance because of the lower shrinkage that is not favorable for the bond between fiber and matrix [311]. The results of this study suggests that the pullout resistance was reduced as a result of the lower shrinkage in cement matrix that weakened the fiber-matrix bonding. This reduction can also be explained by the higher porosity of mixes containing PVA fibers compared to plain mortars. Indeed, the appearance of large voids around the hook counteracts the positive effect of PVA fibers to restrict the initiation of micro-cracks. This result has been confirmed by microscopic observation of cut surface that will be discussed in next section. As it can be seen in Fig. 4.8, the second peak reached

a value almost similar to the first peak in case of mortars reinforced with PVA fibers, while there was a big drop in the pullout force of plain mortars after the first peak. Comparing the pullout behavior of different mortars in part c indicate that the addition of PVA fibers resulted in an increase in the frictional stress between steel fibers and surrounding matrix.

### 4.8.3 Microscopic observation of pullout samples

Fig. 4.9 shows the microscopic observation of different samples after the fiber was pulled out. As it can be seen, the plastic deformation of hook and slipping of fiber inside the channel led to the formation of micro-cracking around the fiber and particularly at the area closed to the hook in plain samples. There was no clear difference between the number and width of cracks in two different plain mortars. On the other hand, the addition of 1% PVA fibers in mortar increased the porosity of mortar and two big voids were observed very close to the hook in Type K-1%PVA sample. As shown in previous section, the pullout force of reinforced mortars was lower compared to that of plain mortars and it can be contributed to the appearance of these voids due to the less workability of mixes.

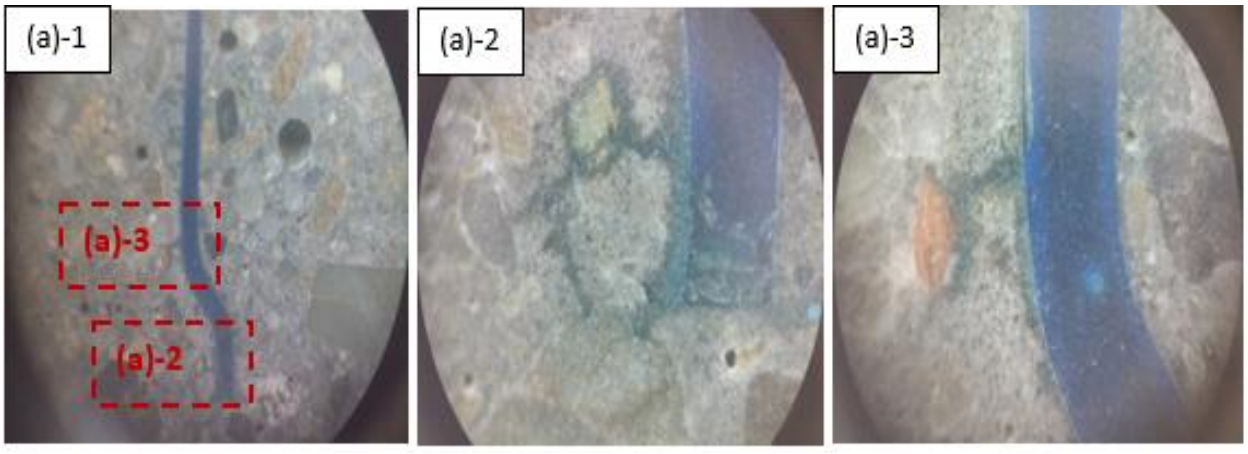


(a)

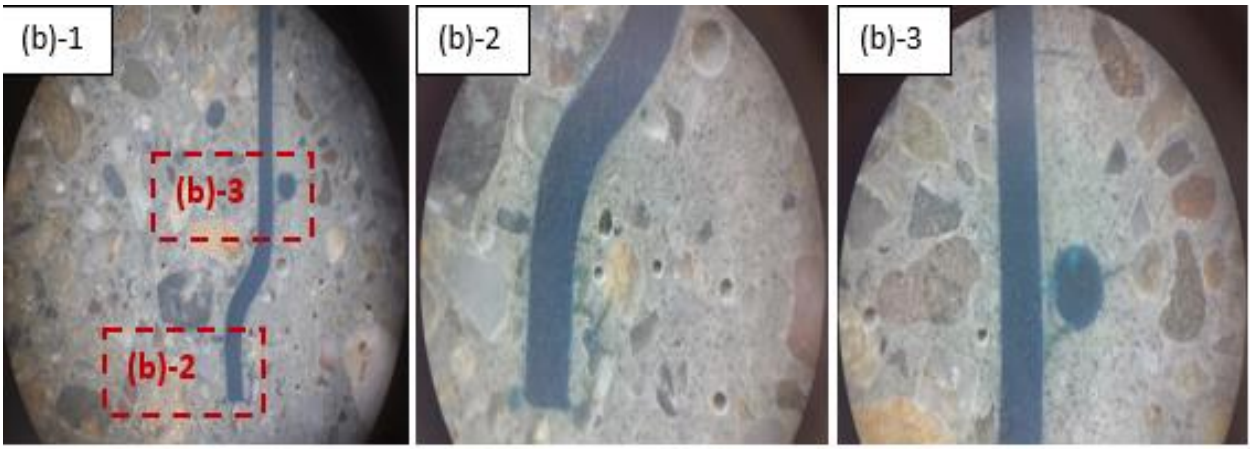


(b)

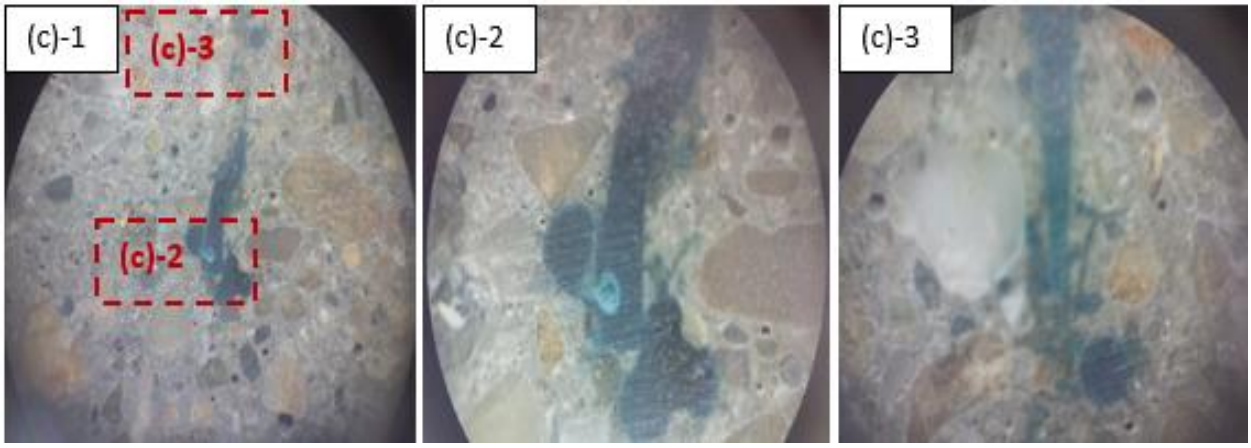


(c)

Fig. 4.9 Microscopic observation of micro-cracking process around the fiber hook of different fiber-reinforced mortars: (a) sample with Type II cement, (b) sample with Type K cement, (c) sample with Type K cement and reinforced with 1.0% PVA fiber

## 4.9 Evidence from the microstructure

### 4.9.1 Components analysis from XRD measurements

To track the phase change of at the microscale during hydration process, XRD was conducted to both types of paste at different hydration ages. As shown in Fig. 4.10(a), the anhydrous Type K cement contains significant amount of ye'elimite and $CaSO_4$, apart from the $C_3S$. As a result, the

7 days hydration product contains significant amount of ettringite, which contributes to the volume expansion of the paste. Another major crystalline phase in the hydration product is portlandite, which is from the hydration of $C_3S$. It should be noted that, the intensity of $C_3S$ peaks decreases rapidly in the first week, but the decrease clearly slows down thereafter. However the major peak of ye'elimite (~27.8°) exhibits a continuous attenuating until complete absence in 28 days.

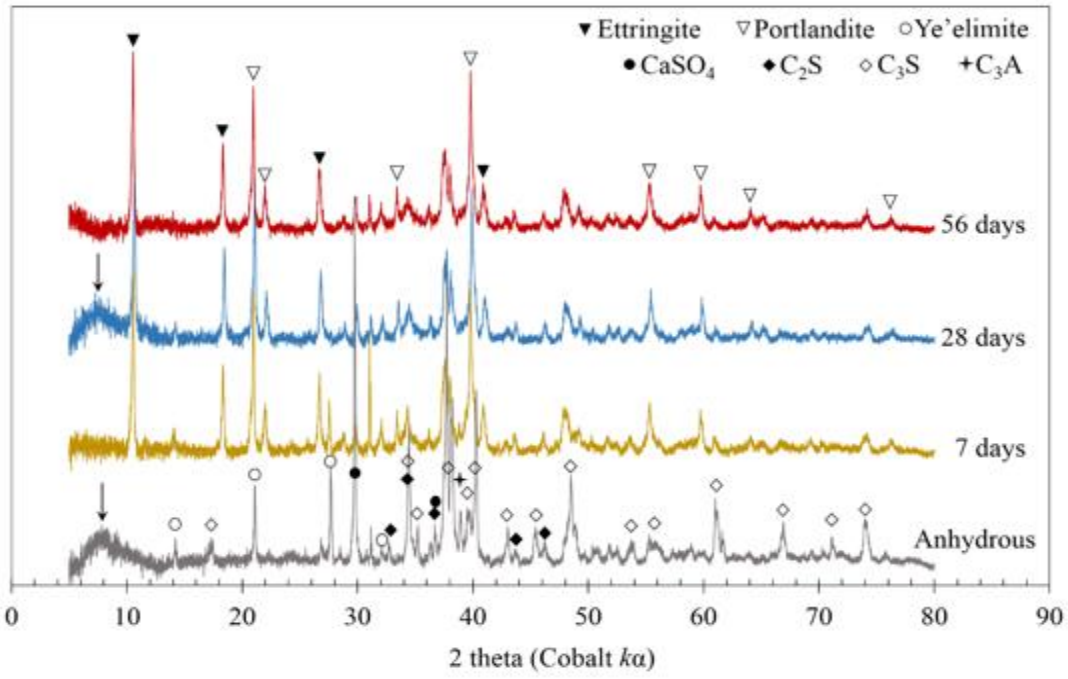


(a)

As shown in Fig. 4.10(b), the Type II/V cement composed mainly of $C_3S$, and minor contents of $C_2S$, $C_3A$, $C_4AF$ and gypsum. Its hydration products contains significant amount of portlandite, and minor content of ettringite. Similar to the behavior of $C_3S$ in Type K, hydration of Type II/V cement is rapid in the first week, but significantly slows down after that.

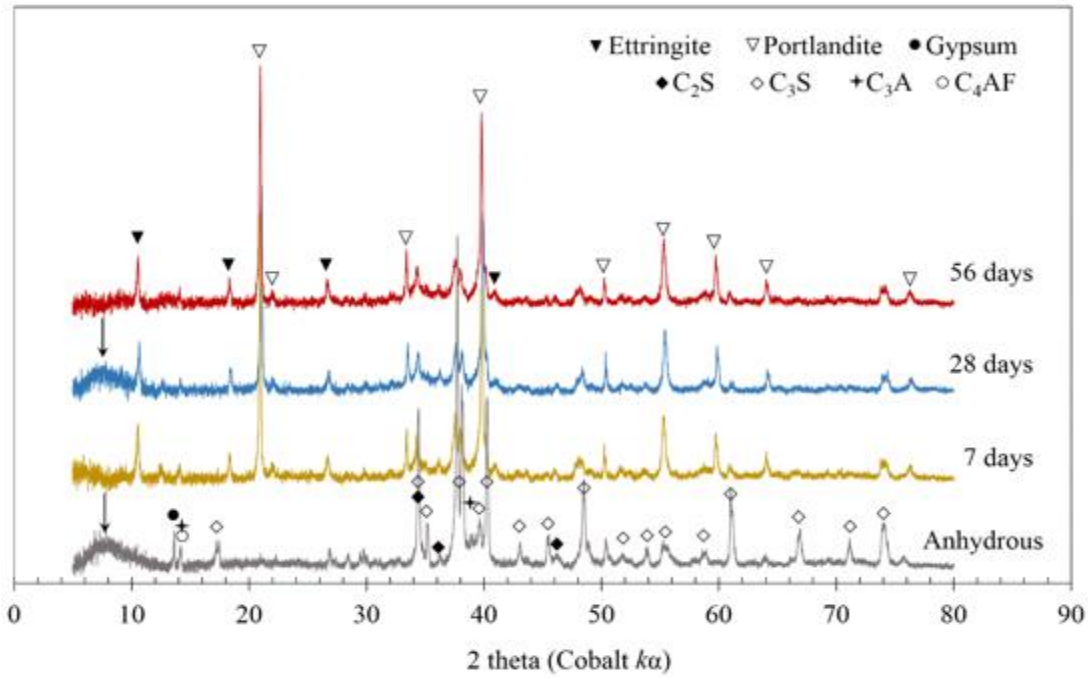


(b)

Fig. 4.10 XRD pattern of anhydrous cements and hydration products of both types of cement at different ages: (a) Type K cement, (b) Type II/V cement. The black arrows in the small 2-theta domain is the background peak from certain sample holders

### 4.9.2 SEM observations

To provide microscale morphology for the tested samples, SEM were conducted on the flexural-test samples, at both SE and BSE modes. To have a reliable knowledge about the microstructure, large numbers of images were collected and analysed. Here, representative images are shown in Fig. 4.11 for concision. As shown in Fig. 4.11(a), the hydrated matrix is composed of featureless paste and crystals embedded within. The crystals with large size and smooth cleavage (white arrow in Fig. 4.11(a)) are assigned to Portlandite, due to its unique morphology and abundance in XRD results. Some fibrillar products are observed within the paste and are assigned to ettringite needles, which exhibit small quantity of signals in the XRD results. The featureless paste is the anhydrous

cement and the hydration product C-S-H gel. In general, hardened Type II/V paste resembles the microstructure of a typical hydrated matrix of OPC. As shown in Fig. 4.11(b), fibrillar crystals dominate the microscale morphology of Type K cement paste. This is consistent with XRD result that hydration product of expansive cement contains large quantity of ettringite. Ettringite in Type K cement paste grows to much larger size (length 15-30 μm, and diameter 1-1.5 μm), compared with the ettringite needles in OPC paste (length 3-5 μm, and diameter 0.3-0.4 μm). The rapid formation of ettringite in expansive cement contributes to its volumetric expansion that was seen in drying shrinkage test results.

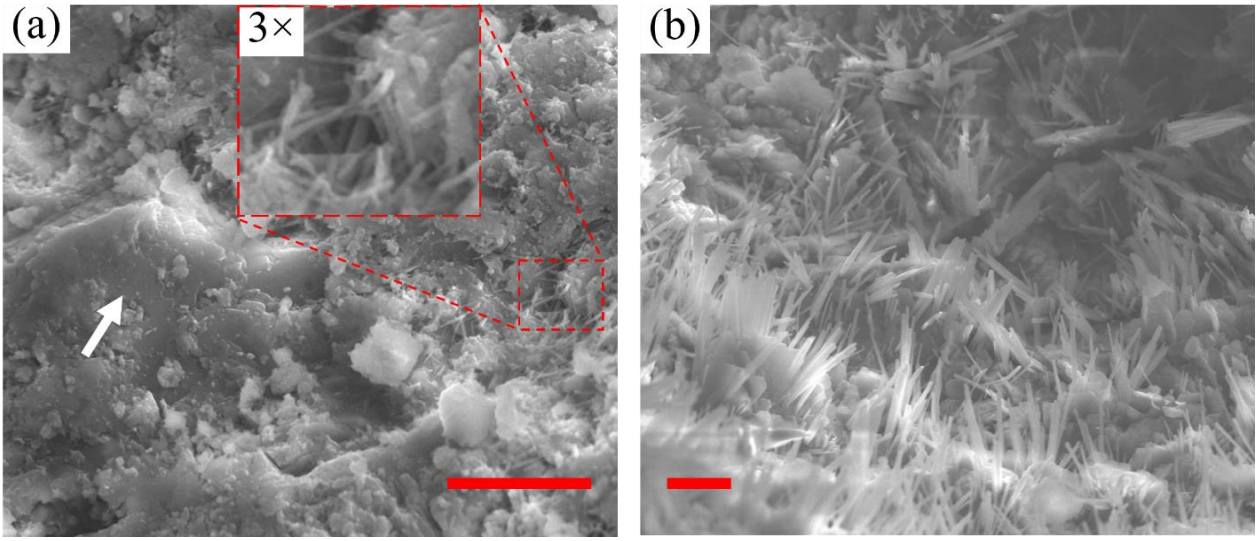


Fig. 4.11 Microscale morphology of: (a) Type II/V cement paste and (b) Type K cement paste after 28-day curing. Scale bars are 10 μm. White arrow in (a) indicates the large and smooth cleavage of Portlandite crystals. A fibrillar morphology (red-dashed square) in (a) is magnified

The microscale morphology of fiber embedment in Type K cement paste is also investigated. As shown in Fig. 4.12(a), on a fracture surface of mix containing 0.5% PVA fibers, a PVA fiber is half-embedded in the paste (red solid square). However the other end of the fiber (red dashed square) exhibits a large deformation, which could possibly be a fracture too. This indicates that

the PVA fiber is very well embedded in the matrix, and therefore increases the resistance against cracking-opening. In Fig. 4.12(b), a tight bond between the paste and steel fiber is also observed even after fracture, and the paste is still closely attached to the surface of the steel fiber. The microstructure evidence therefore confirm that the mechanical bonding between two types of fiber and the paste is solid, and should significantly increase the fracture toughness of the composite. This can also contribute to the better performance of fiber pullout resistance in mixes containing expansive cement.

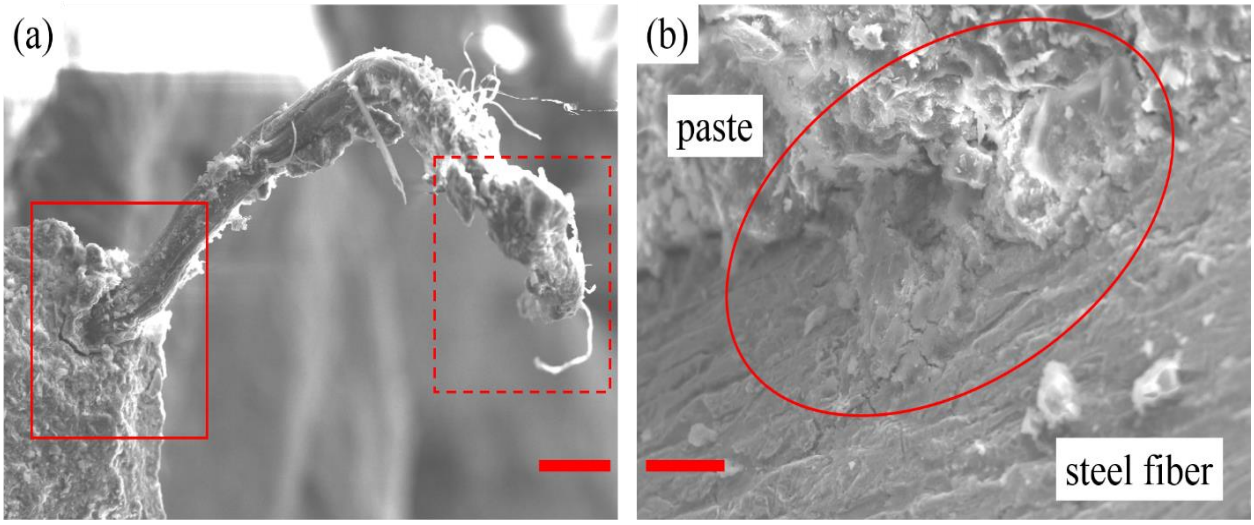


Fig. 4.12 Microscale morphology of: (a) DHE0.5+PVA0.5 paste and (b) DHE0.5+HE0.3+PVA0.2 paste after 28-day curing. Scale bars are 20 μm. Red squares and circles indicate details of PVA fiber and steel fiber, respectively

To obtain a better estimation of the pore structure, BSE mode was applied to finely-polished surfaces of pastes, as shown in Fig. 4.13. In each image, there exist gaps between aggregates and paste, which is most likely generated during the polishing process and will not be discussed. In Fig. 4.13(a), pores of a several micron are universally observed in the paste of Mix 1 (Type II/V), whereas in (b) the paste of Mix 2 (Type K) cement appears much less porous. The matrix of Mix 3 also exhibit no visible pores. This can be attributed to the large volume of the Type K cement

hydrates which efficiently fill the pore space. However, in the hardened paste of Mix 4 and 5 that contains PVA fibers, large pores are observed. There pores exhibit spherical shape, with diameter in the range of 10-100 μm. In Table 3.4, it is shown that the workability of Mix 4 and 5 are worse than the other three mixes, even the additions of superplasticizer in these mixes are the highest. Therefore the observed pores in Mix 4 and 5 can probably be attributed to two reasons: 1) the honeycomb due to the low workability, and 2) the PVA fiber itself is black under SEM, and is accounted as pores. Mix 3 has the best workability and an intermediate dosage of superplastisizer, and it turns out that the paste of Mix 3 does not contain as many large pores as in Mix 4 and 5. Using software Image J, Figs. 4.13(a), (d) and (e) are converted to binary images with pores being highlighted and solids as background. The binary images are then processed with a 'particle analysis' plugin for size distribution analysis. The results are shown in Fig. 4.13(f). Most pores in Mix 1 have diameter smaller than 10 μm, with average value ~3 μm. However in Mix 4 and 5, the major contribution to porosity is from pores with diameter larger than 40-50 μm. The average pore diameters of Mix 4 and 5 are ~60 and ~67 μm, respectively. As already discussed, the substitution a part of steel fibers with PVA fibers resulted in a reduction in the mechanical properties of concrete. Also, among different HyFRC considered in this study, the highest water absorption was attained by the mix containing higher amount of PVA fibers (i.e. Mix 4). The microstructural analysis show that the appearance of voids with larger size can also contribute to the abovementioned results.

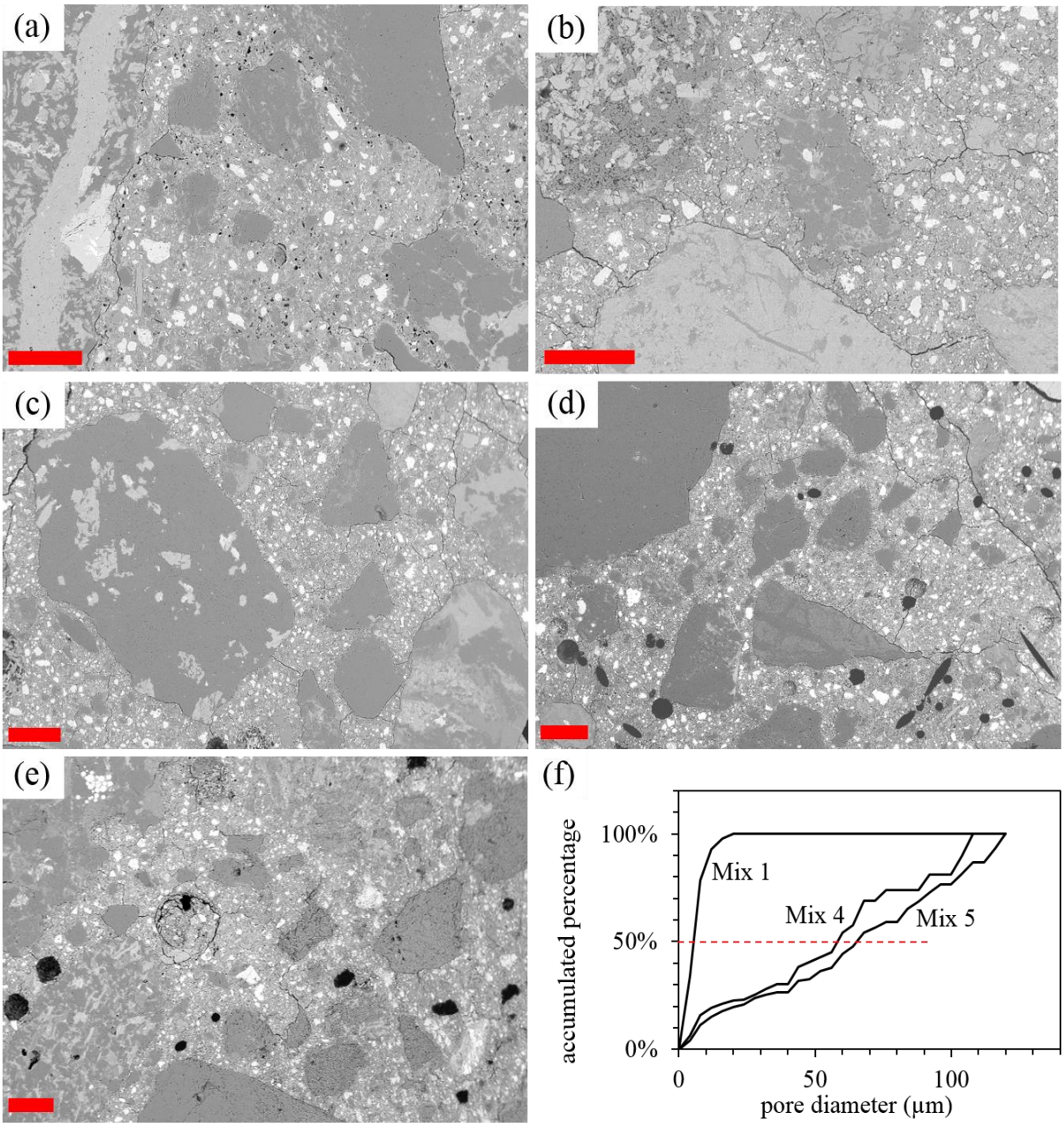


Fig. 4.13 Back-scattered electron mode images of hardened paste of Mix 1 to Mix 5, in the order of (a) to (d). Scale bars are 200 μm. The accumulated volume percentage of pores as a function of their pore diameter is shown (f), as calculated from (a), (d) and (e)

# Chapter 5

# Mechanical, durability, and microstructural properties of high performance CSA-based composites

## 5.1 Introduction

This chapter investigates the properties of concrete fabricated with blended cementitious materials. Additionally, the effect of 1% DHE steel fibers on the mechanical, durability, and microstructural properties of those concrete were studied. Eight different concrete mixes were developed as is shown in Table 3.5. The compressive strength, splitting tensile strength, modulus of elasticity, flexural behavior, drying shrinkage, water absorption, electrical resistivity, and electrochemical potential of steel fibers were evaluated. To study the morphology and microstructure of concretes, SEM method was used. As it is well documented, the setting time of CSA cement is quite lower compared to that of OPC, which subsequently it results in a difficulty to prepare the concrete specimens. Therefore, the addition of retarder or hydration stabilizer is inevitable to produce concrete containing CSA cement, particularly at low w/c ratio. However, to evaluate the workability and compressive strength evolution of CSA cement-based mixes without retarder, four plain concrete including OPC, CSA, OPC50-CSA50, and OPC25-CSA50-SL25 were produced. It is worth noting that in concretes that a portion of OPC was replaced with CSA cement, the setting of concrete was occurred in less than 10 minutes. Therefore, the molding of specimens was done very fast due to the limited setting time of those mixes. In other words, it is not practical to produce CSA-blend mixes without the addition of retarder. The results of their compressive strength at different curing ages are shown in Table 5.1. As it can be seen, the replacement of OPC with CSA resulted in an increase in the compressive strength of concrete at all curing ages considered in this

study. It can be explained by the fast formation of ettringite that consequently improved the strength of concrete. Moreover, the results further indicate that combination of OPC with CSA, and even substitution a portion of OPC with slag resulted in compressive strengths comparable to those of plain OPC concrete. However, due to the limited working time of those concretes, a retarder was used in all mixes containing CSA cement as is shown in Table 3.5. Thereafter, the results presented in this study belong to the mixes listed in Table 3.5.

Table 5.1 Compressive strength of different CSA cement-based concretes fabricated without retarder

| Mix No. | Mixture ID | Compressive strength (MPa) | | | |
|---|---|---|---|---|---|
| | | 1 Days | 7 Days | 28 Days | 91 Days |
| 1 | OPC | 51.2 | 65.2 | 72.3 | 75.9 |
| 2 | CSA | 60.6 | 76.2 | 83.4 | 87.7 |
| 3 | OPC50-CSA50 | 39.2 | 57.1 | 65.4 | 71.9 |
| 4 | OPC25-CSA50-SL25 | 39.7 | 59.3 | 67.3 | 74.3 |

## 5.2 Consistency

The consistency of the different mixes developed in this study was evaluated by a slump test, and the results are shown in Table 3.5. The slump values of the concretes varied between 19 and 23 cm. It was observed that a minimum of 1% superplacticizer was required to adjust the consistency of concrete. As it can be seen, higher content of superplacticizer was used in CSA-based concretes compared to that of the OPC to obtain an almost similar slump value. This can be explained by the fineness of CSA particle size that is lower compared to that of the OPC. Furthermore, the fast rate of CSA cement hydration and its high demand of water to generate ettringite are other reasons that necessitate the addition of higher amount of superplacticizer. The results also show that higher content of superplacticizer was used in the binary and ternary mixes to develop concretes with the

same slump value. The results indicate that the incorporation of steel fibers had a negative influence on the properties of fresh concrete. The long steel fibers and aggregates interlock in the body of concrete and lead to a reduction in the slump value. To attain the same consistency in the concretes with and without fibers, the content of superplacticizer was slightly increased. Fig. 5.1 shows the appearance of fresh concrete during the slump test for the concretes without fibers and concrete reinforced with 1% DHE steel fibers.


Fig. 5.1 Appearance of fresh concretes in slump test: (a) OPC mix, (b) OPC25-CSA50-SL25 mix, (c) CSA-DHE1 mix

## 5.3 Compressive strength

The compressive strength results of different mixes at curing ages of 1, 7, 28, and 56 days are shown in Fig. 5.2 and Table 5.2. The relative compressive strength of different CSA-based concretes compared to that of the reference OPC mix is also shown in Fig. 5.3. As it can be seen, the compressive strength of concretes containing CSA cement is significantly lower at 1 days compared to that of the OPC mix. This reduction at the early age can be explained by the presence of retarder in the CSA concrete that postponed the formation of ettringite, and subsequently reduced the strength of concrete. The results indicate that the full replacement of OPC with CSA cement led to a reduction of 55% at 1 day compressive strength, while its strength at 7 days is slightly higher than that of the OPC concrete. It was also observed that the compressive strength of CSA mix was increased by 10% and 12% at 28 days and 56 days, respectively, compared to that of the OPC concrete. Fig. 5.2 shows that the compressive strength of the concrete containing 50% OPC and 50% CSA cement was lower than that of the reference OPC concrete at all the curing ages considered in this study. For instance, the compressive strength of OPC50-CSA50 mix reduced by 42%, 32%, 21%, and 13% at 1, 7, 28, and 56 days of curing, respectively compared to those of the OPC concrete. Similar to CSA concrete mix, the significant amount of strength reduction at 1 day is attributed to the presence of retarder. However, the compressive strength has been increased at later ages as a result of ettringite formation (ye'elimite hydration) and also the hydration of alite and belite that are the main component of OPC. On the basis of results reported in Fig. 5.2, it was noticed that with respect to the reference OPC concrete, the lowest compressive strength at 1 day was attained by the CSA-blend mix containing three type of binders (i.e. OPC25-CSA50-SL25 mix). However, the results indicate that the compressive strengths of this mix at 28, and 56 days are only slightly lower than those of the OPC concrete.

Table 5.2 Compressive strength of different blend-cement concretes

| Mix No. | Mixture ID | Compressive strength (MPa) | | | | Strength gain over that of 7 days (%) | | | |
|---|---|---|---|---|---|---|---|---|---|
| | | 1 Days | 7 Days | 28 Days | 56 Days | 1 Days | 7 Days | 28 Days | 56 Days |
| 1 | OPC | 56.0 (-) | 69.9 (-) | 75.9 (-) | 78.8 (-) | 80 | 100 | 109 | 113 |
| 2 | OPC-DHE1 | 57.3 (+2%) | 72.2 (+3%) | 79.7 (+5%) | 83.7 (+6%) | 79 | 100 | 110 | 116 |
| 3 | CSA | 25.4 (-55%) | 70.9 (+1%) | 83.7 (+10%) | 88.2 (+12%) | 36 | 100 | 118 | 124 |
| 4 | CSA-DHE1 | 28.3 (-49%) | 74.1 (+6%) | 87.8 (+16%) | 91.5 (+16%) | 38 | 100 | 118 | 123 |
| 5 | OPC50-CSA50 | 32.6 (-42%) | 47.4 (-32%) | 60.1 (-21%) | 68.5 (-13%) | 69 | 100 | 127 | 145 |
| 6 | OPC50-CSA50-DHE1 | 38.3 (-32%) | 51.8 (-26%) | 65.4 (-14%) | 74.1 (-6%) | 74 | 100 | 126 | 143 |
| 7 | OPC25-CSA50-SL25 | 11.1 (-80%) | 50.4 (-28%) | 64.8 (-15%) | 72.1 (-9%) | 22 | 100 | 129 | 143 |
| 8 | OPC25-CSA50-SL25-DHE1 | 13.2 (-76%) | 55.7 (-20%) | 66.1 (-13%) | 73.3 (-7%) | 24 | 100 | 119 | 132 |

Note: The number in the () shows the percentage of strength increase or decrease over that of the plain OPC concrete.

As it can be seen in Fig. 5.3, the compressive strength of OPC25-CSA50-SL25 mix reduced by 80%, 28%, 15%, and 9% at 1, 7, 28, and 56 days of curing, respectively compared to those of the OPC concrete. Comparing to the results of OPC50-CSA50 mix, it can be noticed that the presence of slag in CSA-blend mix resulted in a reduction in the compressive strength at 1 day of curing. However, the compressive strengths of the mix containing slag were higher at later ages of curing compared to those of the OPC50-CSA50 mix. Introducing GGBS can result in an increase in the cohesiveness of the cementitious matrix, which reduces the induction of micro-cracks leading to an increased strength of concrete [312]. Moreover, GGBS fills the capillary pores of cement matrix and consequently improves the properties of the interfacial transition zone (ITZ) [313].

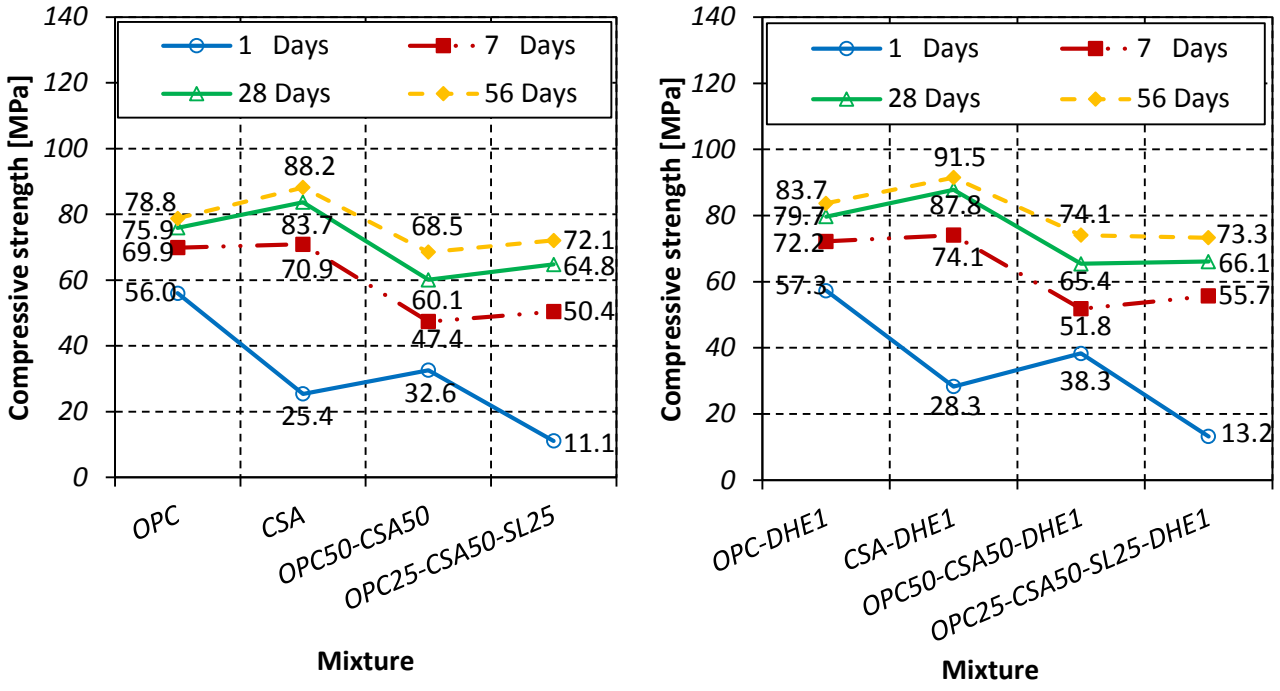


(a) (b)

Fig. 5.2 Compressive strengths of different blend-mix concretes containing: (a) 0% fiber volume fraction, (b) 1% DHE steel fiber volume fraction

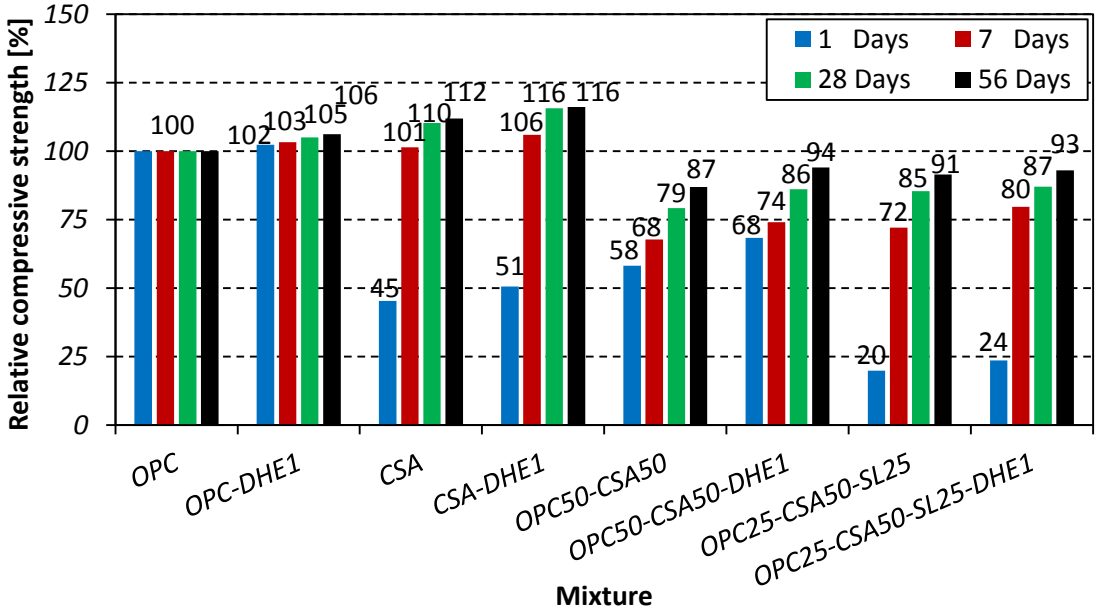


Fig. 5.3 Relative compressive strengths of different blend-mix concretes

In a study conducted by Sharma and Pandey [314], the XRD pattern of 90-day hydrated sample of OPC mix blended with GGBS indicated higher reactivity of GGBS at this age compared to those of early ages. Therefore, reduction in the early age (1 day) strength was observed in the present study can be attributed to the lower hydration rate of concretes incorporating GGBS, which has been well documented in the literature [314, 315]. The strength evolutions of different concrete mixes compared to their 7 days strength are presented in Table 5.2. As it can be observed, the 28 and 56 days compressive strength of OPC concrete were 9% and 13% higher than its 7 days strength, while the compressive strength of CSA concrete were 18% and 24% higher than its 7 days strength. The higher rate of strength improvement in CSA concrete compared to that of OPC concrete can be explained by the development of a significant amount of ettringite. The presence of ettringite leads to an enhancement in the microstructure of the concrete that consequently increased the compressive strength of concrete. The results further indicate that the highest rate of strength development was attained by the CSA-blend concretes. For instance, the 28 days compressive strengths of OPC50-CSA50, and OPC25-CSA50-SL25 mixes were 27%, and 29% higher than their 7 days strength, while their 56 days strengths were 45%, and 43% higher than their 7 days strength, respectively. The higher strength gain of these mixes at a prolonged curing time can be attributed to the continued ettringite formation due to the hydration of alite and belite, and higher hydration rate of slag at later ages that led to an increased strength.

Fig. 5.2 shows that similar trend to concrete without fibers was occurred in concrete mixes reinforced with 1% DHE steel fibers. The best performing mix was the CSA mix with 1% steel fiber, which attained a 56-days compressive strength of 91.5 MPa. It was also observed that introducing 1% DHE steel fibers into concrete led to an enhancement in the compressive strength

of concrete mixes at all ages. For instance, the compressive strength of OPC, CSA, OPC50-CSA50, and OPC25-CSA50-SL25 concretes containing 1% DHE steel fibers increased by 5%, 5%, 9%, and 2% at 1, 7, 28, and 56 days of curing, respectively compared to those of the corresponding mixes without fibers. DHE steel fibers, owing to their high elastic modulus and particular shape that restricts the propagation of cracks, alters the tendency of cracks, and subsequently improves the compressive strength of concrete [304].

## 5.4 Splitting tensile strength

The splitting tensile strength results of different concrete mixes at curing ages of 7, 28, and 56 days are shown in Fig. 5.4 and listed in Table 5.3. The relative splitting tensile strength of different CSA-based concretes compared to that of the reference OPC mix is also shown in Fig. 5.5. The results show that the full replacement of OPC with CSA cement resulted in a slight reduction in 7 days tensile strength, while its 28 and 56 days splitting tensile strength were increased compared to those of the OPC. As it can be seen in Table 5.3, the splitting tensile strength of CSA concrete was 11% higher at both curing ages of 28 and 56 days compared to those of OPC concrete. The strength reduction at 7 days can be attributed to the presence of retarder that delayed the ettringite formation. However, at later ages of curing, a rich amount of ettringite has been formed as a result of ye'elimite hydration, which consequently caused an improvement in the strength of concrete. The results further indicate that combination of OPC and CSA cements at equal percentage of 50% led to a reduction in the splitting tensile strength of concrete at all curing ages considered in this study. For instance, the splitting tensile strength of the OPC50-CSA50 concrete reduced by 18%, 22%, and 19% at 7, 28, and 56 days, respectively, compared to those of the OPC.

Table 5.3 Splitting tensile strength of different blend-cement concretes

| Mix No. | Mixture ID | Compressive strength (MPa) | | | Strength gain over that of 7 days (%) | | |
|---|---|---|---|---|---|---|---|
| | | 7 Days | 28 Days | 56 Days | 7 Days | 28 Days | 56 Days |
| 1 | OPC | 3.41 (-) | 3.88 (-) | 4.30 (-) | 100 | 114 | 126 |
| 2 | OPC-DHE1 | 5.70 (+67%) | 6.60 (+70%) | 7.63 (+77%) | 100 | 116 | 134 |
| 3 | CSA | 3.35 (-2%) | 4.29 (+11%) | 4.77 (+11%) | 100 | 128 | 142 |
| 4 | CSA-DHE1 | 5.31 (+56%) | 7.55 (+95%) | 8.48 (+97%) | 100 | 142 | 160 |
| 5 | OPC50-CSA50 | 2.81 (-18%) | 3.04 (-22%) | 3.47 (-19%) | 100 | 108 | 123 |
| 6 | OPC50-CSA50-DHE1 | 4.60 (+35%) | 5.16 (+33%) | 6.34 (+47%) | 100 | 112 | 138 |
| 7 | OPC25-CSA50-SL25 | 2.92 (-14%) | 3.45 (-11%) | 3.79 (-12%) | 100 | 118 | 130 |
| 8 | OPC25-CSA50-SL25-DHE1 | 5.06 (+48%) | 5.80 (+49%) | 6.62 (+54%) | 100 | 115 | 131 |

Note: The number in the () shows the percentage of strength increase or decrease over that of the plain OPC concrete.

Fig. 5.4 shows that the incorporation of slag in OPC-CSA concrete led to an improvement in the splitting tensile strength, while its strength is lower compared to that of the reference OPC concrete. This increased strength can be attributed to the formation of additional C-S-H gel, particularly at later ages which is the main strength contributing compound. Moreover, slag also fills in the capillary pores and improve the features of ITZ and microstructures of cement matrix [316, 317]. It was noticed that the best performing mix was the CSA concrete that was attained a 56-days splitting tensile strength of 4.77 MPa, while the lowest strength was gained by the OPC50-CSA50 concrete with the strength of 3.47 MPa.

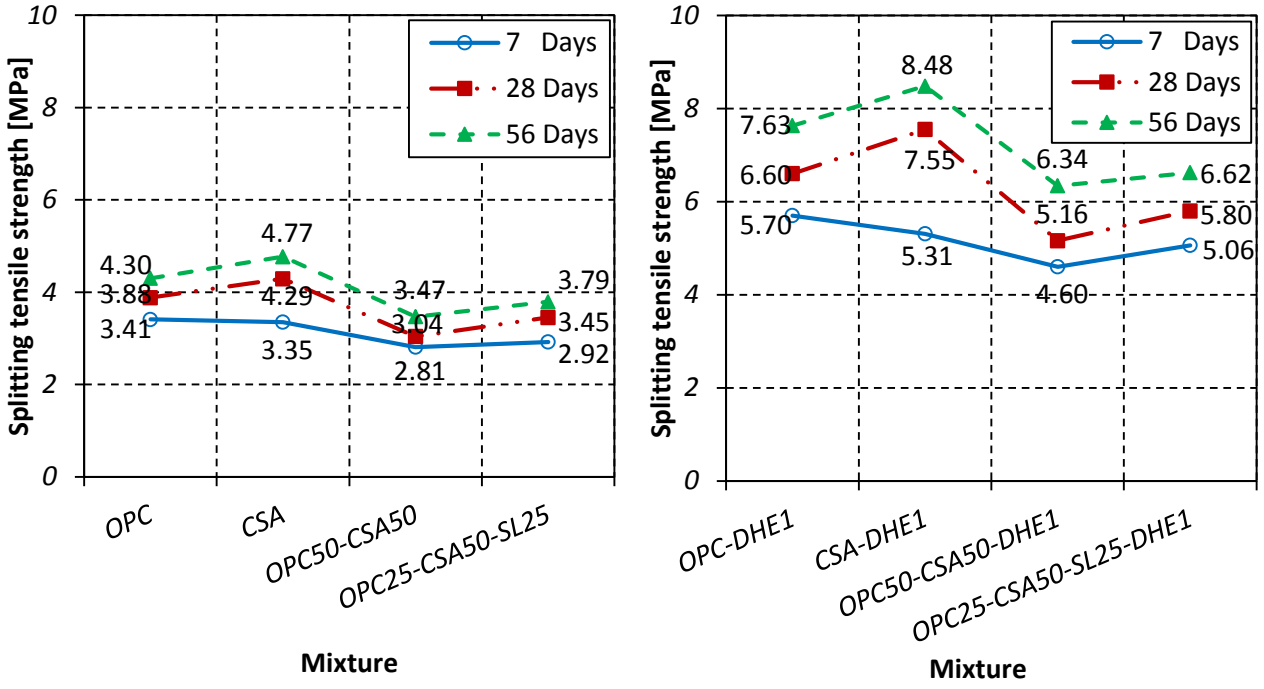


Fig. 5.4 Splitting tensile strengths of different blend-mix concretes containing: (a) 0% fiber volume fraction, (b) 1% DHE steel fiber volume fraction

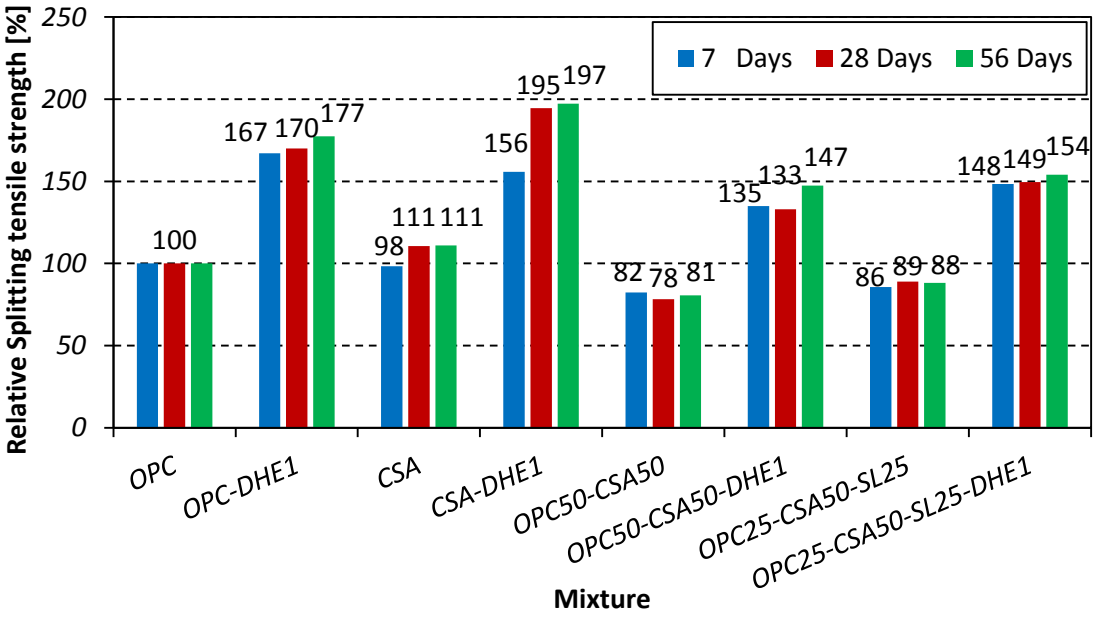


Fig. 5.5 Relative splitting tensile strengths of different blend-mix concretes

The rate of splitting tensile strength development for different concrete mixes compared to their 7 days strength are presented in Table 5.3. In general, the rate of strength evolution in concrete that OPC was fully or partially replaced with CSA cement was higher compared to that of the reference OPC concrete. For instance, the 56 days splitting tensile strength of OPC, CSA, OPC50-CSA50, and OPC25-CSA50-SL25 concretes mixes were 26%, 42%, 23%, and 30% higher than their 7 days strength, respectively. This higher rate of strength development in CSA concrete can be explained by the appearance of higher amount of ettringite compared to OPC concrete that is a source of strength. As can be seen, the rate of strength evolution in concrete that contains slag is also slightly higher than OPC. This increase can be attributed to the improvement in the bond between the hydrated cement matrix and the aggregate. This improved bond is due to the alteration of calcium hydroxide, which tends to form on the surface of aggregate particles, into C-S-H in the presence of pozzolanic materials like slag [318].

The results of fiber-reinforced concretes indicate that the addition of 1% DHE steel fibers can significantly increase the splitting tensile strength of concrete. For instance, the splitting tensile strength of OPC-DHE1 concrete mix increased by 67%, 70%, and 77% at 7, 28, and 56 days of curing, respectively compared to those of the OPC concrete. This improvement is attributed to the high tensile strength, elastic modulus, and effective anchoring mechanism of DHE steel fibers, which restrained the extension of macro-cracks in concrete. Similarly, Yoo et al. [319] reported that the inclusion of hooked-end steel fibers at a volume fraction of 1% or higher leads to significant improvement in tensile strength of high-strength concrete. DHE steel fibers used in the present study exhibited significantly higher maximum pullout forces compared to those of hooked-end steel fibers [320]. As a result, greater improvements in the splitting tensile strength of concrete

mixes were attained in this study compared to those reported in previous studies, in which conventional hooked-end steel fibers were used. It was also observed that the simultaneous using of CSA cement and steel fibers was very effective to enhance the splitting tensile strength of concrete, and the best performing mix was attained in CSA-DHE1 concrete mix. As it can be seen in Fig. 5.5, the splitting tensile strength of aforementioned mix was increased by 57%, 95%, and 97% at 7, 28, and 56 days of curing, respectively compared to those of the OPC concrete. This improvement can be attributed to the better bond between the steel fibers and CSA cement matrix due to self-stressing that resulted from the expansive behavior of CSA cement. As it can be noticed in Fig. 5.4, the effect of curing age on the improvement of splitting tensile strength is relatively higher in FRC compared to the plain concrete. For instance, the splitting tensile strength of CSA-DHE1 mix was increased by 42% and 60% at 28 and 56 days compared to its 7 days strength, respectively, while these increase were 28% and 42% for CSA concrete, respectively.

## 5.5 Modulus of elasticity

In homogeneous materials, a direct relationship exists between density and modulus of elasticity. In heterogeneous, multiphase materials such as concrete, the density, the modulus of elasticity of the principal constituents, and the characteristics of the transition zone determine the elastic modulus behavior of the composite [142]. The 28-days modulus of elasticity of different mixes is shown in Fig. 5.6, and the relative modulus of elasticity of different concretes compared to that of the reference OPC mix is also shown in Fig. 5.7. The results indicate that the cement type had a significant influence on the modulus of elasticity of the concrete. As it can be seen in Fig. 5.7, the full replacement of OPC with CSA cement caused an increase of 24% in the 28-days modulus of elasticity. This increase can be explained by the ability of CSA cement to densify the

microstructure of cement matrix and improving the characteristics of ITZ, which those consequently lead to an enhancement in the modulus of elasticity of concrete. The results further demonstrate that combination of OPC and CSA cements at equal percentage of 50% led to a slight increase in the modulus of elasticity. Additionally, the substitution a portion of OPC with slag in CSA-blend concrete mix resulted in an increase of 7% compared to that of the OPC. Fig. 5.6 shows that the lowest modulus of elasticity was attained by the mix containing 100% of OPC, while the best performing mix was the CSA mix, which attained a modulus of elasticity of 38.8 GPa.

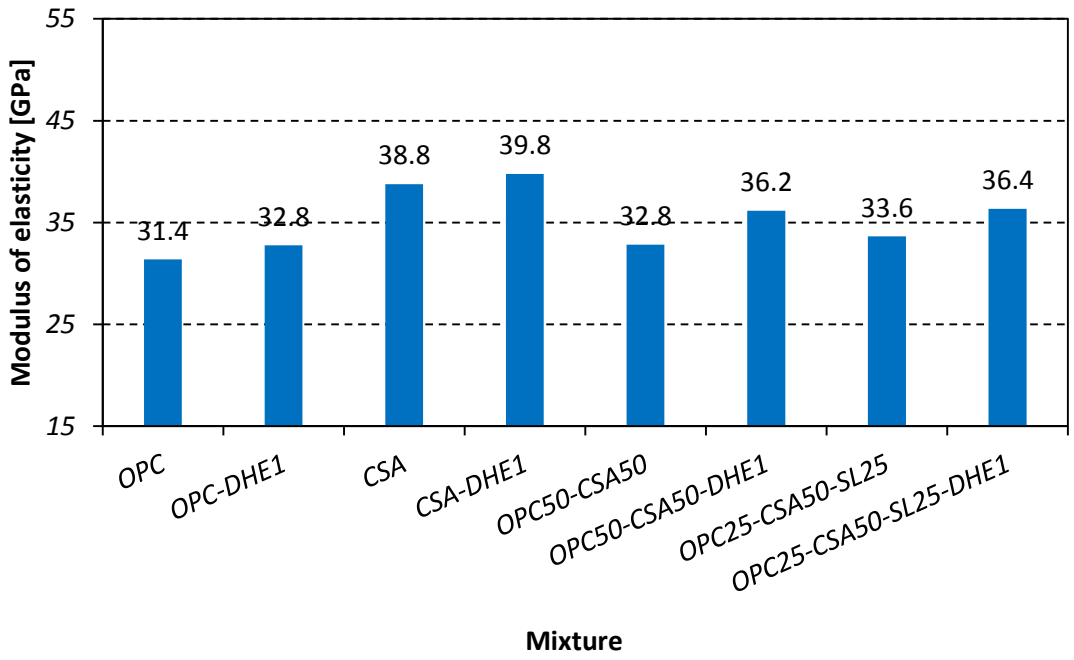


Fig. 5.6 Modulus of elasticity of different blend-mix concretes at curing age of 28 days

As it can be noticed in Figs. 5.6 and 5.7, the inclusion of 1% DHE steel fibers led to an increase in the modulus of elasticity of all concretes studied in this research. For instance, the modulus of elasticity of OPC, CSA, OPC50-CSA50, and OPC25-CSA50-SL25 concretes mixes containing 1% DHE steel fibers were 4%, 3%, 10%, and 8% higher than those of the corresponding mixes

without fibers, respectively. This result suggest that the addition of steel fibers with higher elastic modulus compared to that of the cement matrix can improve the modulus of elasticity of concrete.

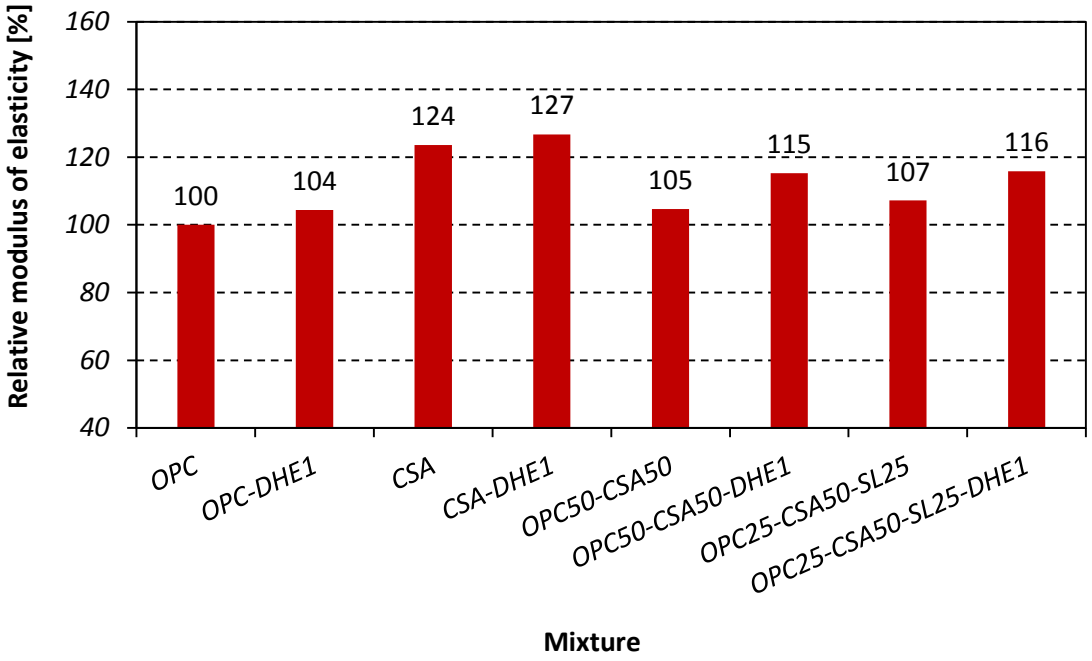


Fig. 5.7 Relative modulus of elasticity of different blend-mix concretes at curing age of 28 days

## 5.6 Flexural Load-CMOD curve and residual flexural tensile strength

The diagram of 28-day Load-CMOD for different concrete mixes is shown in Fig. 5.8. As it can be seen in Fig. 5.8, the behavior of concretes without fibers was almost linear up to the maximum load, followed by a sharped descending branch up to failure point, then the beam specimens split into two separated parts. The results indicate that the full replacement of OPC with CSA cement resulted in an increase of 20% in the maximum flexural load of concrete. Similar to the splitting tensile strength results, the rich amount of ettringite in this mix that was produced by hydration of ye'elimite that is the main component of CSA cement is the main reason for this improvement. It was also observed that the flexural strength of CSA-blend mixes was lower compared to that of the OPC mix. For instance, the flexural strength of OPC50-CSA50 and OPC25-CSA50-SL25

mixes were 44% and 35% lower than that of the reference OPC mix. As can be seen, the substitution of OPC with 25% of slag caused an improvement in the flexural strength compared to that of the OPC50-CSA50 concrete. This improvement can be attributed to the formation of additional C-S-H gel which is the main strength contributing compound as a result of reaction between slag and calcium hydroxide. Moreover, slag may fill in the capillary pores and improve the features of transition zone and microstructures of cement matrix [316, 317].

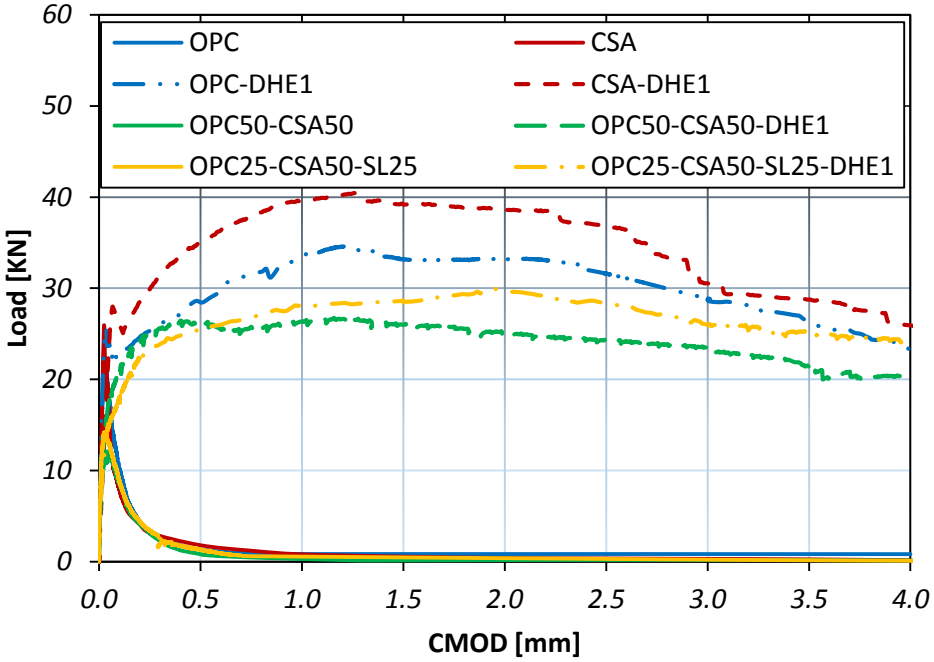


Fig. 5.8 Load-CMOD curves of different blend-mix concretes at curing age of 28 days

On the other hand, the results of fiber-reinforced concretes illustrate that the addition of fibers remarkably improved the post-cracking behavior of FRC with an extensive cracking process between first crack load and peak load. It was noticed that the addition of 1% DHE steel fibers changed the behavior of concrete and a deflection-hardening performance was occurred in all mixes reinforced with steel fibers. In these concrete mixes, once the first crack was occurred, the fibers bridging the crack resisted the load and prevented further crack propagation. The excellent

performance of these mixes can be attributed to the ability of DHE steel fibers to carry the load after matrix cracks until further creation of cracks. The flexural load would be reduced due to the failure of fiber anchorage or debonding of fibers and the matrix [189, 190]. Fig. 5.8 shows that the best performing was by the mix that OPC was fully replaced with CSA cement and reinforced with 1% steel fiber (i.e. CSA-DHE1). The flexural strength of this mix increased by 87% and 55% as compared to that of the OPC and CSA concrete, respectively. The expansion behavior of CSA cement can lead to a better bond between the cement matrix and steel fibers, which subsequently led to an increase in the flexural strength of concrete. The results further show that the flexural strength of OPC, CSA, OPC50-CSA50, and OPC25-CSA50-SL25 mixes containing 1% DHE steel fibers was increased by 60%, 55%, 120%, and 113%, respectively as compared to that of their corresponding mixes without fibers. As it can be seen, the inclusion of steel fibers had the most influence on the flexural strength of concrete that CSA cement was used in blend mixes. As already mentioned, the expansion behavior of CSA-blend mixes may lead to a better bond between the cement matrix and steel fibers as a result of self-stressing, which subsequently led to an increase in the flexural strength of concrete.

The residual flexural tensile strength for different concrete mixes is shown in Fig. 5.9. The residual flexural strengths corresponding to CMOD at 0.5 mm, 1.5 mm, 2.5 mm, and 3.5 mm are defined as $Fr_1$, $Fr_2$, $Fr_3$, and $Fr_4$, respectively. As the concrete mixes produced without fibers were split after maximum peak load, the result of residual flexural tensile strength was not presented for these mixes. The results show that an almost similar trend was observed in all mixes reinforced with 1% DHE steel fibers. As it can be noticed in Fig. 5.9, the maximum residual flexural tensile strength in all mixes was occurred at CMOD equal to 1.5 mm (i.e. $Fr_2$). For instance, the $Fr_2$ of OPC, CSA,

OPC50-CSA50, and OPC25-CSA50-SL25 mixes containing 1% DHE steel fibers was 12.5, 10.6, 9.2, and 8.3 MPa, respectively that was increased by 12%, 16%, 10%, and 2%, respectively as compared to their $Fr_1$. It was observed that residual flexural tensile strength gradually reduced after CMOD equal to 1.5 mm and the lowest strength was attained at CMOD equal to 3.5 mm. The results indicate that $Fr_4$ of OPC, CSA, OPC50-CSA50, and OPC25-CSA50-SL25 mixes containing 1% DHE steel fibers was reduced by 18%, 8%, 5%, and 16%, respectively as compared to their $Fr_1$. The research finding of this study demonstrate that all the FRC considered in this work show a deflection-hardening behavior and conventional steel bar can be partially replaced by randomly distributed fiber according to fib Model Code 2010 [307]. Therefore, FRC were developed in this study can be of high interest for design of structural member that subjected to bending load.

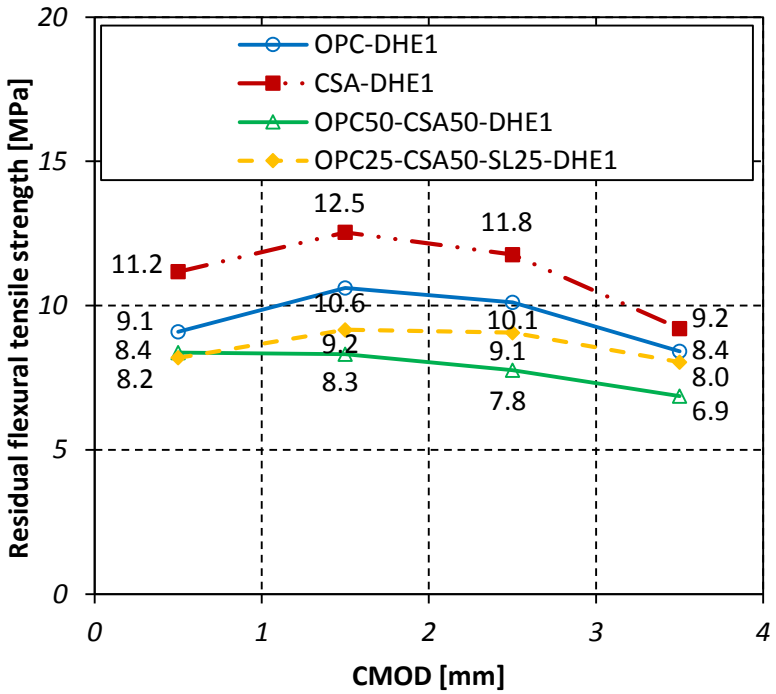


Fig. 5.9 Residual flexural tensile strength of different blend-mix concretes at curing age of 28 days

## 5.7 Shrinkage under drying condition

The results of the shrinkage tests under drying condition for different concrete mixes are shown in Fig. 5.10. Additionally, the shrinkage deformations of different specimens at 1 and 56 days are shown in Fig. 5.11. The drying shrinkage strain of concrete has a direct relationship with the amount of free water and the porosity of concrete. Generally, the drying shrinkage occurs when the free water stored in the capillary pores evaporates due to a low relative-humidity environment. This circumstance leads to a humidity gradient which induces the transport of water particles from the C-S-H to the capillary pores after which it evaporates [321]. The results indicate that the behavior of concretes were produced with OPC or CSA cement is significantly different with those concretes that binary or ternary systems were used. As it can be seen in Fig. 5.10, the highest shrinkage strain was attained by the mix that OPC cement was added. It was observed that the full replacement of OPC with CSA cement led to an expansion in 1 day, and reduced the shrinkage strain of concrete at later ages. As it can be noticed in Fig. 5.11, the shrinkage strain of CSA mix was reduced by 38% over that of the reference OPC concrete at 56 days. The shrinkage of CSA mix at 56 days was 302 μm/m. This reduction in the shrinkage deformation can be attributed to the ettringite formation and its expansive nature that relatively compensate the shrinkage of concrete and resulted in a concrete with a volume stability properties. Moreover, ye'elimite that is the main source for ettringite formation in CSA cement requires much more molecule of water to be hydrated, which this subsequently reduces the amount of free water that can transport through the body of concrete. This reduction in the shrinkage strain of concretes were produced with CSA cement agrees with the finding of previous researchers [322]. Furthermore, the results illustrate that in OPC mix, the shrinkage occurred at a fast rate at early ages and continuously was increased over measuring time.

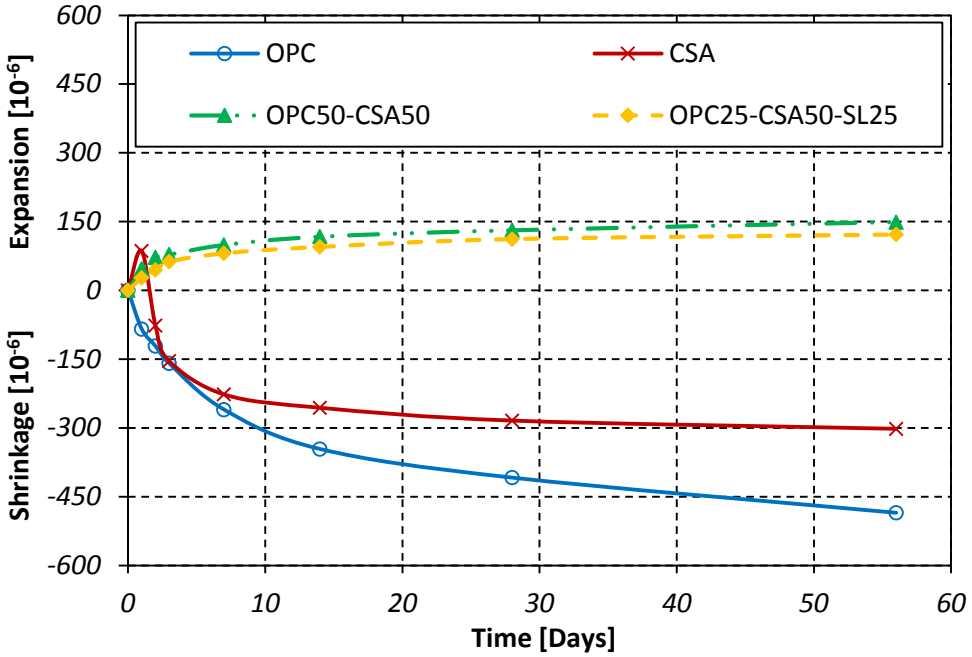


(a)

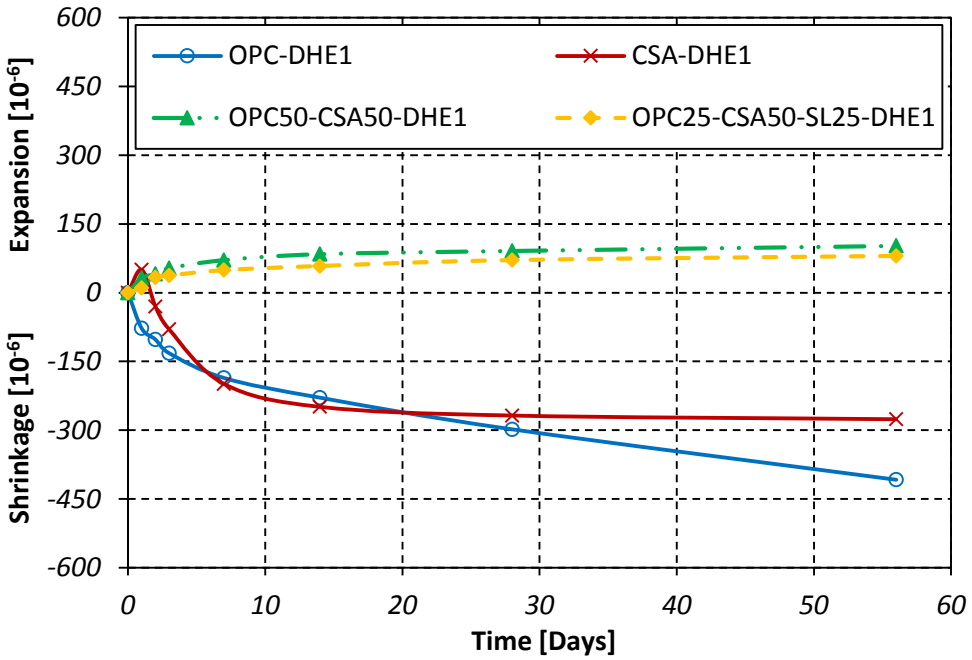


(b)

Fig. 5.10 Dimensional stability of different blend-mix concretes containing: (a) 0% fiber volume fraction, (b) 1% DHE steel fiber volume fraction

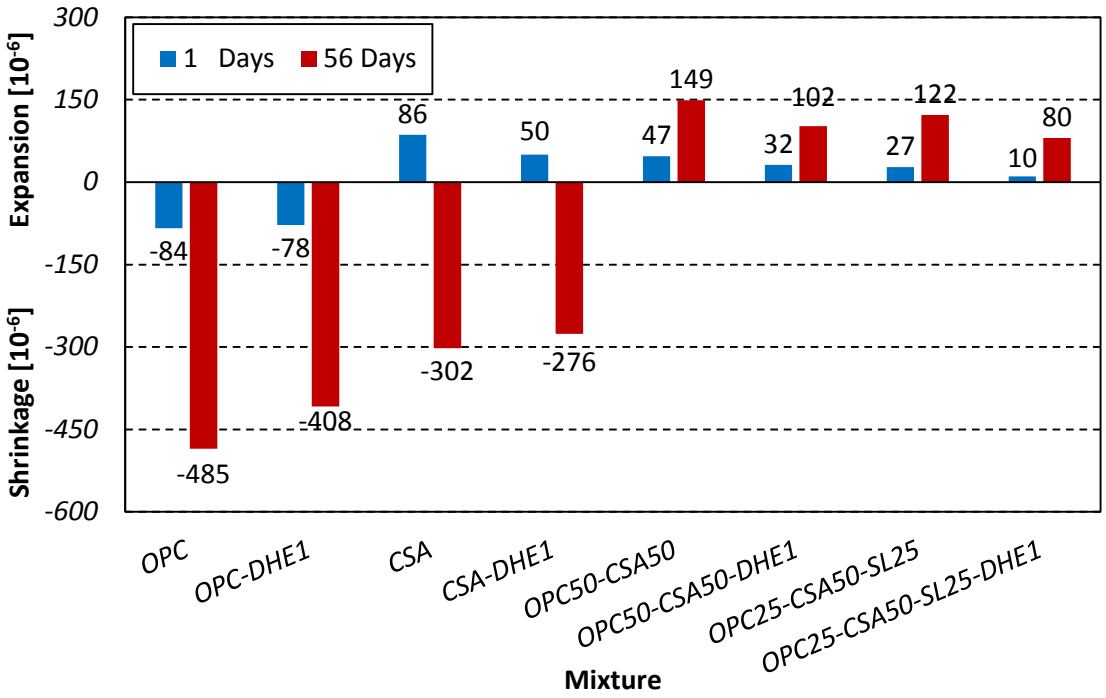


Fig. 5.11 Shrinkage deformation of different blend-mix concretes at 1 and 56 days

On the other hand, the addition of CSA cement led to an expansion at 1 day as a result of fast ettringite formation, and then it starts to shrink although the rate of shrinkage tends to stabilize after 14 days. The results of CSA-blend cement mixes shows that a stable expansion was happened in binary and ternary mixes. As it can be observed in Fig. 5.11, an expansion equal to 149 and 122 µm/m was happened at 56 days in the binary and ternary mixes, respectively. This can be explained by the generation of ettringite with expansive behavior as a result of ye'elimite hydration in the presence of lime and calcium sulfate [323]. The source of lime are free CaO derived from CSA clinker, or calcium hydroxide produced by the hydration of belite incorporated in CSA clinker, as well as alite, and belite available in OPC. Moreover, in the presence of belite that is another important component of CSA cement and aluminum hydroxide that is produced as a result of ye'elimite hydration, strätlingite can be generated. Furthermore, the available silica in the slag can

react and leads to the formation of stable strätlingite. The aforementioned hydration products are significantly different with those produced by the hydration of OPC. Therefore, the appearance of such crystals in the microstructures of binary and ternary cement mixes are responsible for their different performance.

Fig. 5.10 shows that a similar trend to concrete without fibers was occurred in concrete mixes reinforced with 1% DHE steel fibers. As expected the highest shrinkage strain was developed by the mix containing 100% of OPC. Similarly, the CSA-blend mixes manufacture with 1% DHE steel fibers show a stable expansion over measuring time. Generally, the results indicate that the addition of 1% DHE steel fibers resulted in a reduction in the shrinkage or expansion strain of all mixes considered in this study. For instance, the shrinkage or expansion strains of OPC, CSA, OPC50-CSA50, and OPC25-CSA50-SL25 concretes mixes containing 1% DHE steel fibers were 16%, 9%, 32%, and 34% lower than those of the corresponding mixes without fibers, respectively. This result is in good agreement with the findings of the previous research reported that the fibers can arrest propagation of cracking produced as a result of drying shrinkage [135, 215]. As it can be observed, the effectiveness of DHE steel fibers in restraining the volume change of concrete specimens was higher in CSA-blend mixes. This can be explained by the fact that a better bond between the steel fibers and binders was developed as a result of expansive behavior of those concretes.

### 5.8 Water absorption

The ingress of destructive ions like chloride and sulfate into the concrete adversely affects the durability of concrete. The water absorption test is known as an indirect way to determine the

porosity of concrete, in which also provide information about the permeable pore volume and their connectivity inside the concrete. Fig. 5.12 shows initial (30 min) and ultimate (7 day) water absorption of different concrete mixes. The relative water absorptions of different concrete mixes over that of the reference OPC mix are shown in Fig. 5.13. As it can be observed in Fig. 5.13, the full replacement of OPC with CSA cement led to an increase in both initial and ultimate water absorptions of concrete. The initial and ultimate water absorptions of CSA mix were 146% and 65% higher than those of the OPC mix, respectively. Obviously, the higher amount of ettringite has been generated in CSA concrete as compared to OPC concrete. This can affect the properties of concrete and particularly its water absorption in two different ways. The presence of rich amount of ettringite can fill the voids, lead to the discontinuity of pore network, and also improve the characteristics of cement matrix that subsequently resulted in a reduction in the permeability of concrete [309]. On the other hand, ettringite can adsorb the water and consequently increase the water absorption of concrete. These two phenomena counteract each other and the results of this study suggest that the adsorption of water by ettringite is the dominant factor that influencing the water absorption of concrete. The results further indicate that the water absorptions of CSA-blend mixes are also higher over that of the OPC concrete. For instance, the initial water absorption of OPC50-CSA50 and OPC25-CSA50-SL25 mixes were 191% and 59% higher than that of the OPC concrete, respectively, while their ultimate water absorptions were 76% and 56% higher. As it can be noticed, the presence of slag in ternary mix resulted in a reduction in the water absorption compared to that of the binary mix (i.e. OPC50-CSA50). This reduction can be attributed to the ability of slag to improve the microstructure of cement matrix, decreasing the pores size, and interrupting the connection of pores [324]. In addition to the pozzolanic activity of slag, its filler

effect might have also contributed to the reduction of water absorption owing to the small particle size of slag.

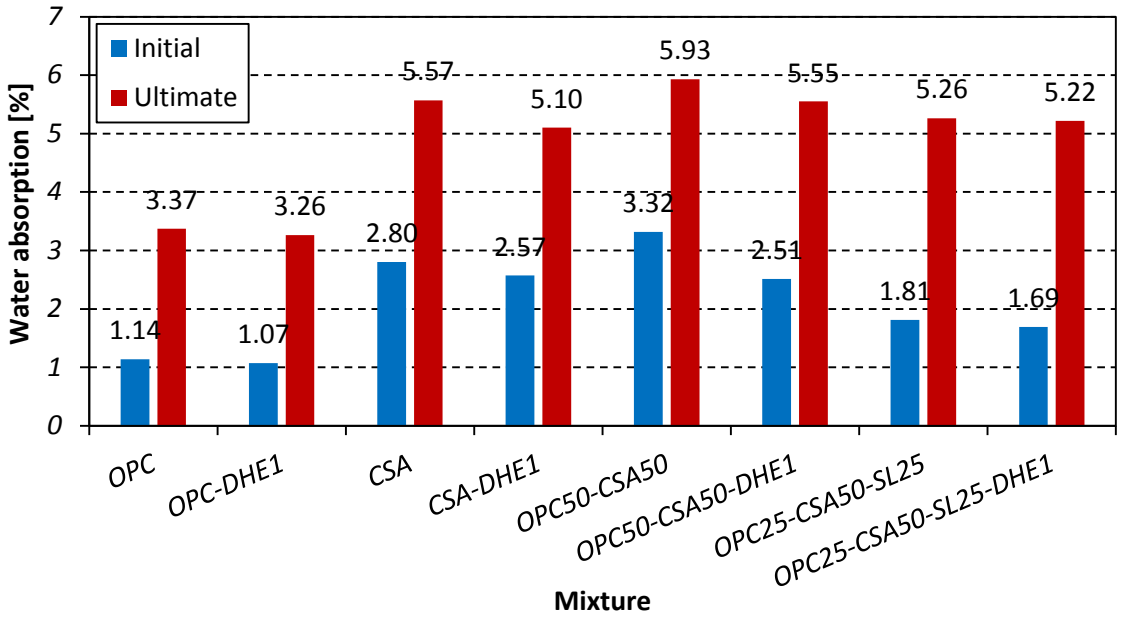


Fig. 5.12 Water absorption of different blend-mix concretes

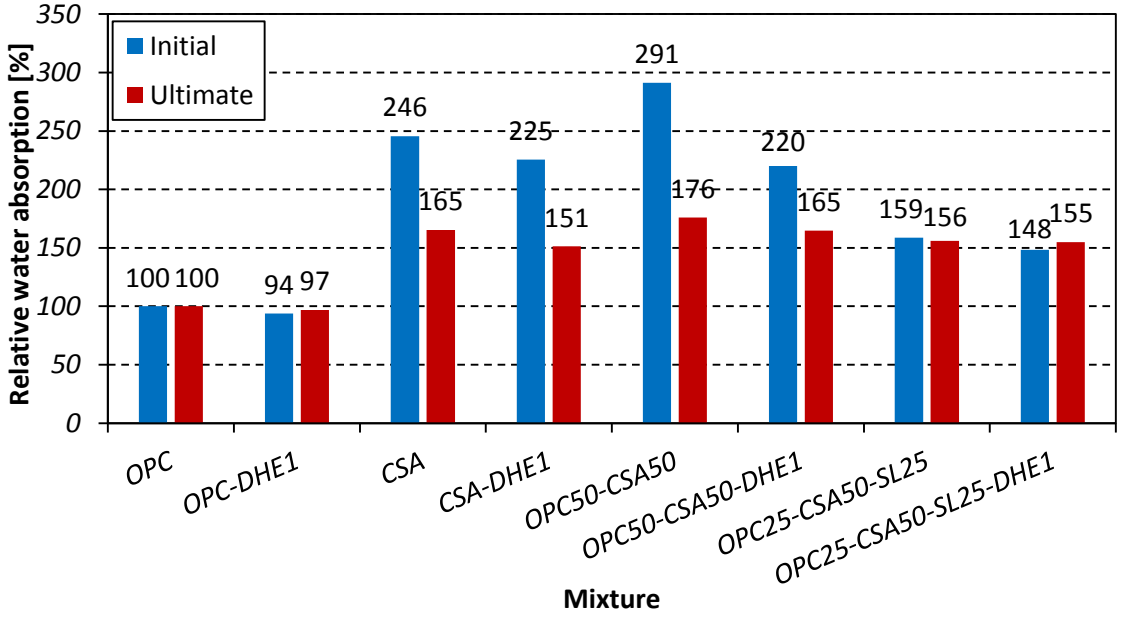


Fig. 5.13 Relative water absorption of different blend-mix concretes

The results of fiber-reinforced concretes show that irrespective to the type of binders, the addition of 1% DHE steel fibers in concrete led to a slight reduction in the water absorption of concretes. For instance, the initial water absorptions of OPC, CSA, OPC50-CSA50, and OPC25-CSA50-SL25 concretes mixes containing 1% DHE steel fibers were 6%, 8%, 24%, and 7% lower than those of the corresponding mixes without fibers, respectively. These reductions for the ultimate water absorption were 3%, 8%, 6%, and 1%, respectively. These results suggest that the inclusion of fibers restrict the formation and propagation of cracks in the body of concrete, leading to a reduced permeability [245]. As it can be seen in Fig. 5.12, the best performing mix was the OPC concrete that was attained an ultimate water absorption of 3.37%, while the highest water absorption was gained by the OPC50-CSA50 concrete with the water absorption 5.93%.

## 5.9 Electrical resistivity

Electrical resistivity is one of the most important features of concrete durability, as it is a significant factor affecting corrosion in reinforced concrete. It was shown previously that an electrical resistivity of 120 Ω m is the limit for corrosion propagation in internal steel reinforcing bars, above which corrosion of concrete reinforcement would not be probable [318]. The results of the electrical resistivity tests for the different concrete mixes are shown in Fig. 5.14. In general, it was observed that the electrical resistivity of all concretes considered in this study was higher than 120 Ω m at 28 days, which secures the bars from the corrosion. The results indicate that the full replacement of OPC with CSA cement resulted in a significant increase in the electrical resistivity of concrete. For instance, the 28-days electrical resistivity of CSA concrete mix was 20.69 times higher than that of the OPC concrete mix. This important improvement can be explained by the rich ettringite formation in the CSA mix that consequently improves the

microstructure of the cement matrix and hinders the movement of ions in the pore solution. It was also reported that the addition of CSA cement densifies the pore structures and its hydration developed pores with radius smaller than 25 nm [62], and formed an interconnected pore network [12, 62], which resulting in good performance in durability related properties. The results further show that even at 1 day of curing, the electrical resistivity of CSA mix was considerably higher with respect to that of the OPC mix. This result suggests that ettringite crystals were generated quickly at early age as a result of ye'elimite hydration.

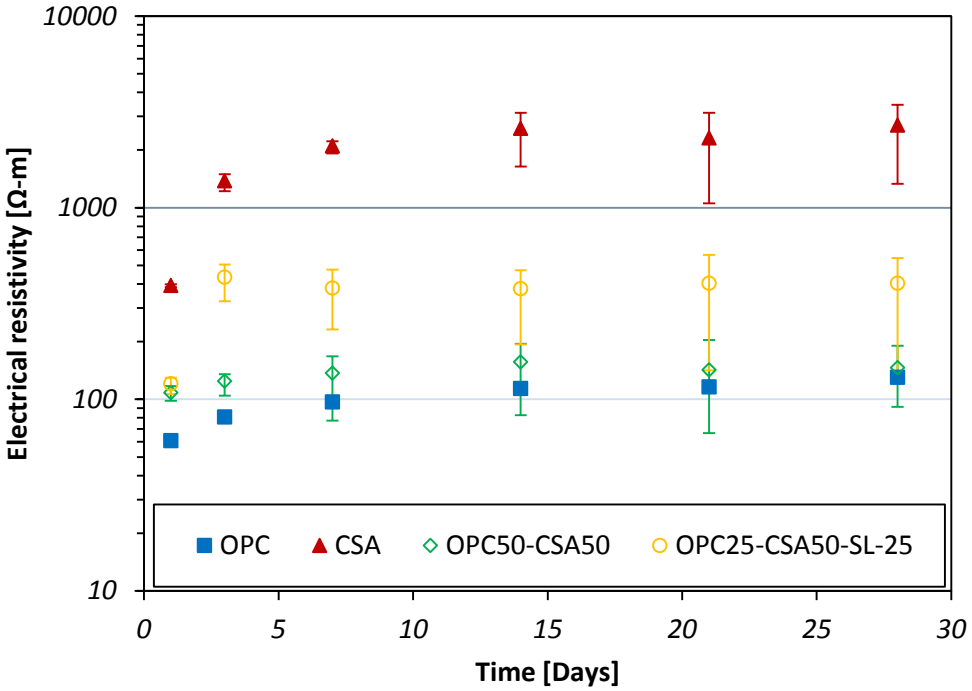


Fig. 5.14 Electrical resistivity of different concrete mixes

As it can be seen in Fig. 5.14, the electrical resistivity of binary mix was higher than that of the OPC at early ages, while its 28-days resistivity was almost similar to that of the OPC. Increased resistivity at early ages can be attributed to the hydration products of CSA cement that are mainly ettringite crystals. The results demonstrate that the electrical resistivity of ternary mix was also significantly improved by blending slag with OPC and CSA cement. For instance, the 28-days

electrical resistivity of OPC25-CSA50-SL25 mix was increased by 210% with respect to that of the OPC mix. The presence of slag densifies the microstructure of concrete, while its pozzolanic reaction causes the formation of secondary C-S-H. The C-S-H gel, which is known as a source of strength in concrete, increases the volume of solid phases and reduces the formation of capillary pore systems in concrete. These phenomena result in improvements in durability properties of concrete, such as concrete resistivity [325]. Additionally, it is expected that the presence of lime increases the content of ettringite crystals [326], which grow in the pores and interrupt the travel of ions in the concrete [327].

It is well documented that the compressive strength of concrete is significantly affected by the porosity and properties of cement matrix. Additionally, the porosity and the ions concentration in the pore solution have important impact on the electrical resistivity of concrete. Therefore, an attempt has been made to correlate the electrical resistivity results to the compressive strength of concretes. Fig. 5.15 shows the correlation for different concrete mixes were considered in this study. As it can be seen in Fig. 5.15, a strong linear relationship was obtained between the electrical resistivity and compressive strength for all mixes. Higher compressive strengths were attained by an increase in the magnitude of the electrical resistivity. The result of this research is in good agreement with the findings of Ramezanianpour et al. [328] that reported the existence of a linear correlation between the electrical resistivity and compressive strength of concrete. These results are highly promising and suggest that the electrical resistivity technique can be successfully used as a non-destructive test to predict the compressive strength of different concrete mixes in practice.

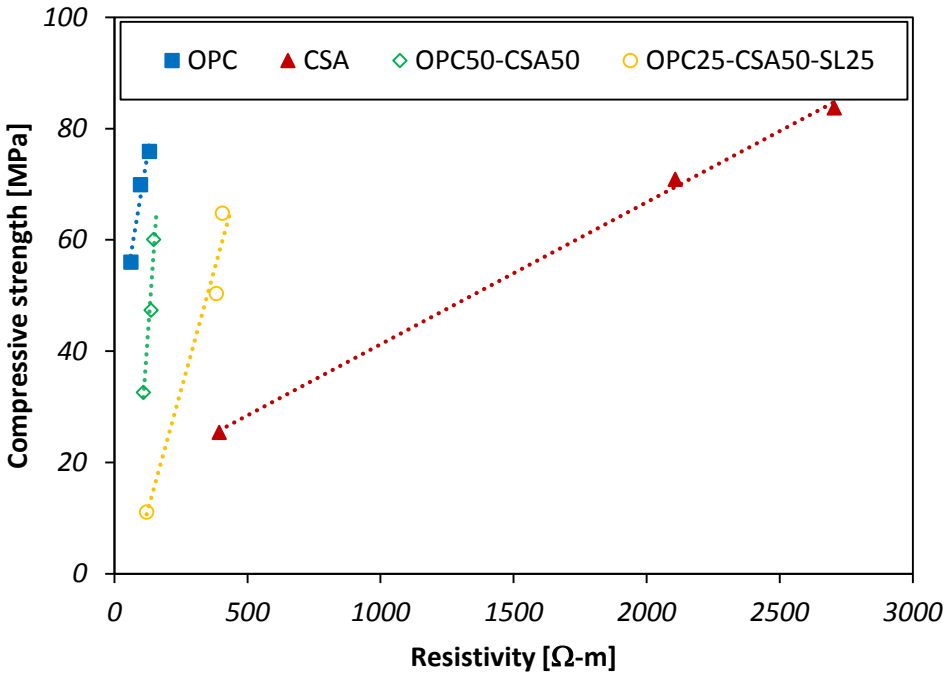


Fig. 5.15 Correlation between electrical resistivity and compressive strength of different concrete mixes

## 5.10 Electrical half-cell potential of steel fibers

Electrical half-cell potentials of steel fibers embedded in different concrete mixes are shown in Fig. 5.16. It was recommended [298] that a potential of more positive than -120 mV, between -120 and -270 mV, and more negative than -270 mV with respect to the saturated calomel electrode (SCE), could be used to respectively represent the following probabilities for steel bars corrosion: greater than 90% of no corrosion, uncertain corrosion area, and greater than 90% of corrosion. As it can be seen in Fig. 5.16, the potentials of OPC mix ranged from -294 mV to -205 mV, and more positive potentials were attained at later ages of curing. The results indicate that the full replacement of OPC with CSA cement resulted in more negative potentials at early ages, while their potentials were more positive than OPC after 7 days of curing. The potentials of fibers in CSA mix varied between -443 mV to -166 mV, depending on the testing ages. The better

performance of CSA mix rather than OPC can be explained by the fact that the hydration of CSA cement generate a rich amount of ettringite crystals that grow in the pore solutions, densify the microstructure of cement matrix, and consequently improve the potential of fibers in concrete. According to the classification recommended by ASTM C876 [298], the potentials of both OPC and CSA concrete mixes are in the range that the probability of steel bars corrosion is uncertain.

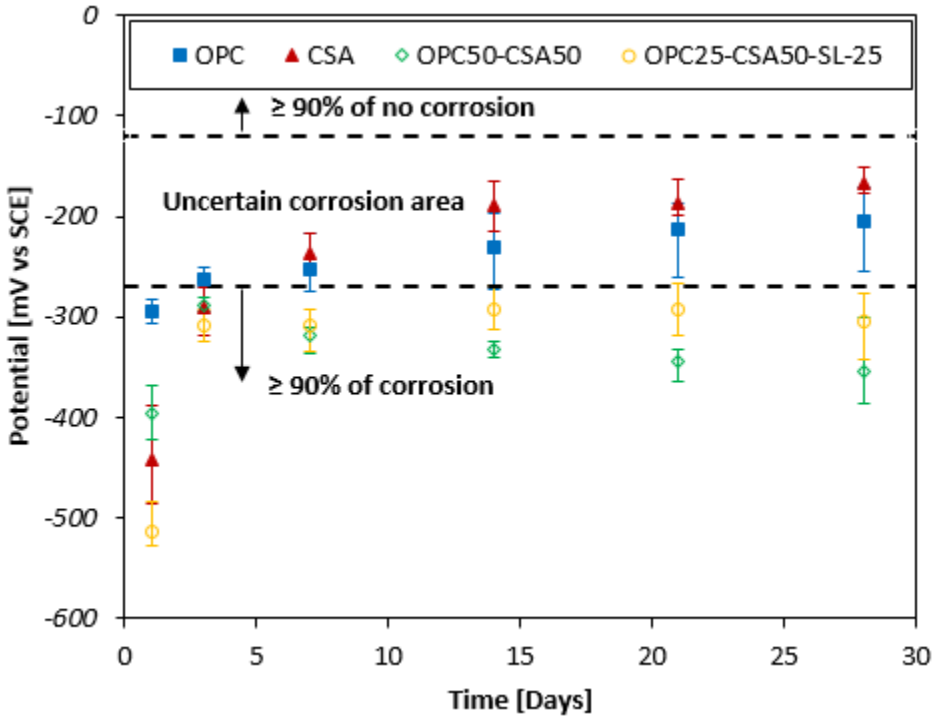


Fig. 5.16 Half-cell potential of fibers embedded in different concrete mixes

The results of the existing studies about the corrosion resistance of concrete fabricated with CSA cement are contradictory [12, 82]. For instance, Glasser and Zhang [12] pointed out that there was no evidence of corrosion on the surface of steel bars embedded in CSA concrete after 14 years, and they remained passivated. They reported that the good performance of concrete with CSA cement against the corrosion can be attributed to the lower permeability as well as the self-desiccation features that subsequently reduces the bleeding water in the vicinity of steel bars. On the contrary, Kalogridis et al. [82] observed that more negative potential was attained in concrete

with CSA cement compared to that of the OPC concrete in half-cell potential test. This can be explained by the less alkalinity of pore solution in concrete fabricated with CSA cement that subsequently increases the risk of bars corrosion.

As it can be seen in Fig. 5.16, the potentials of CSA-blend mixes were more negative than OPC mix. For instance, the potentials of OPC50-CSA50 mix varied between -397 mV to -354 mV, while the potentials of OPC25-CSA50-SL25 varied between -513 mV to -304 mV. These results suggest that there is a high probability of steel bars corrosion in both mixes as potentials more negative than -270 mV were attained at all curing ages considered in this study. This can be attributed to the lower alkalinity of pore solutions as well as higher permeability of these mixes as compared to the OPC mix, which resulting in deterioration of passive film and increasing the possibility of the fibers corrosion. The findings of this study are in conflict with the results of Janotka et al. [329] who reported blending 15% OPC with 85% CSA cement resulted in a desirable environment for steel rebar that protect them from the corrosion. The results further indicate that in CSA-blend mixes, the 3-days potentials were more positive than those of 1 day, while the trend of the potentials have been changed and more negative potentials were attained at later ages when compared to the 3-days potentials of corresponding mixes. This result suggest that the hydration products of CSA-blend mixes may have been altered after 3 days in which adversely affected the corrosion resistance of concretes. It is worth noting that after 7 days of curing there were some evidence of micro-cracks and detachment of the cement paste on the surface of binary and ternary blended concrete specimens. Hence, an optical microscopy was used to observe the surface of all specimens and the images of different specimens are shown in Fig. 5.17.

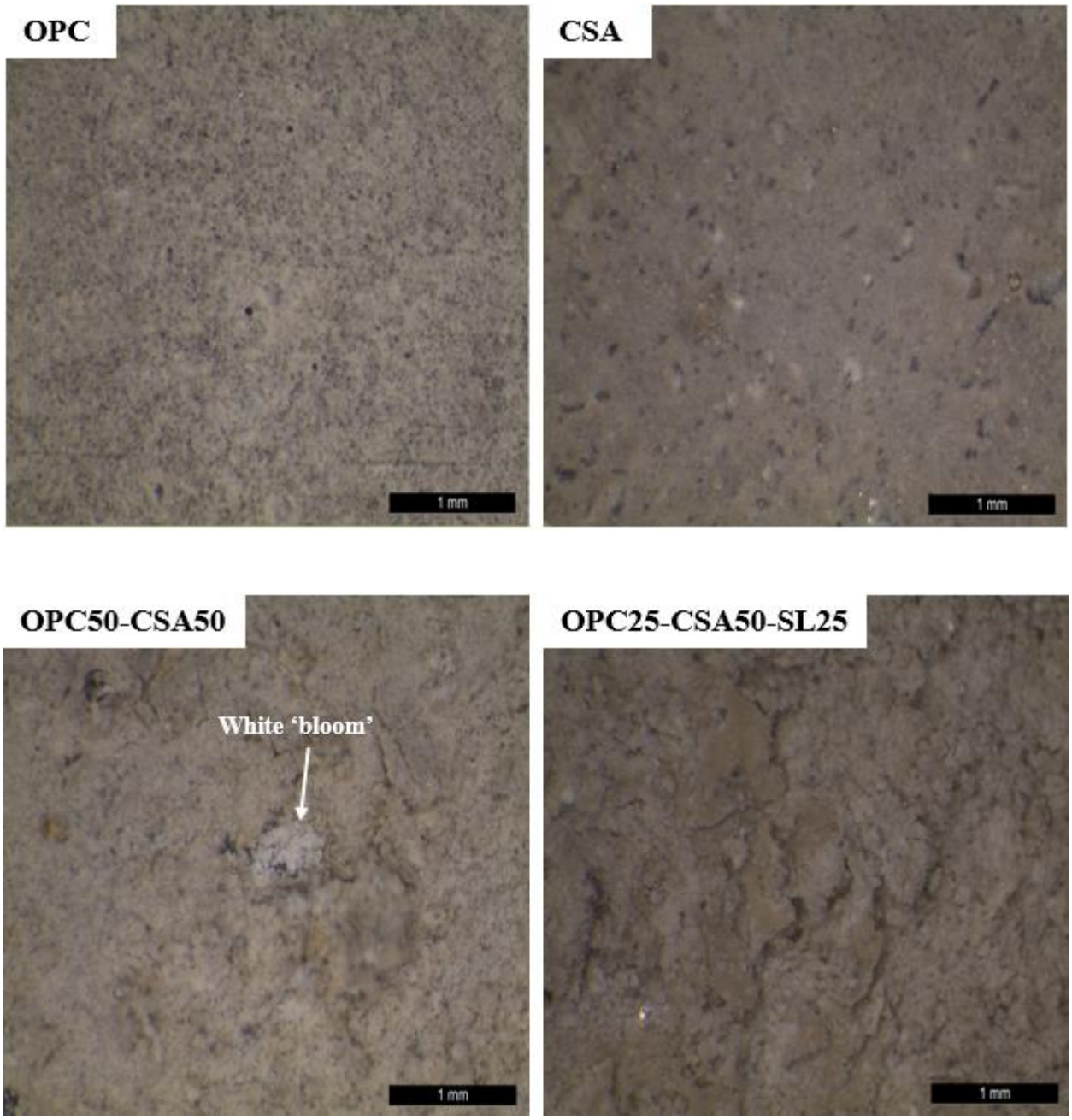


Fig. 5.17 Appearance of the surface of different concrete specimens cured at 23°C and higher than 95% humidity for half-cell potential test

As it can be seen, in OPC50-CSA50 mix some white crystals were also developed under the cement past layer. The XRD analysis of this powder is shown in Fig. 5.18. As it is shown in Fig. 5.18, the powder consists of significant amount of calcite followed by the gibbsite crystals. These

results suggest that the presence of micro-cracks may facilitate the diffusion of available $CO_2$ in the concrete that consequently resulted in the faster carbonation. The presence of white 'bloom' which has been formed on the surface of binary blended mix may be attributed to the carbonation of mobile alkalis from the pore solution due to the efflorescence phenomena. It is well documented that carbonation of concrete can lead to the decomposition of ettringite crystals as well as the reduction of the alkalinity in the pore solutions, which subsequently increases the risk of steel bars corrosion [330].

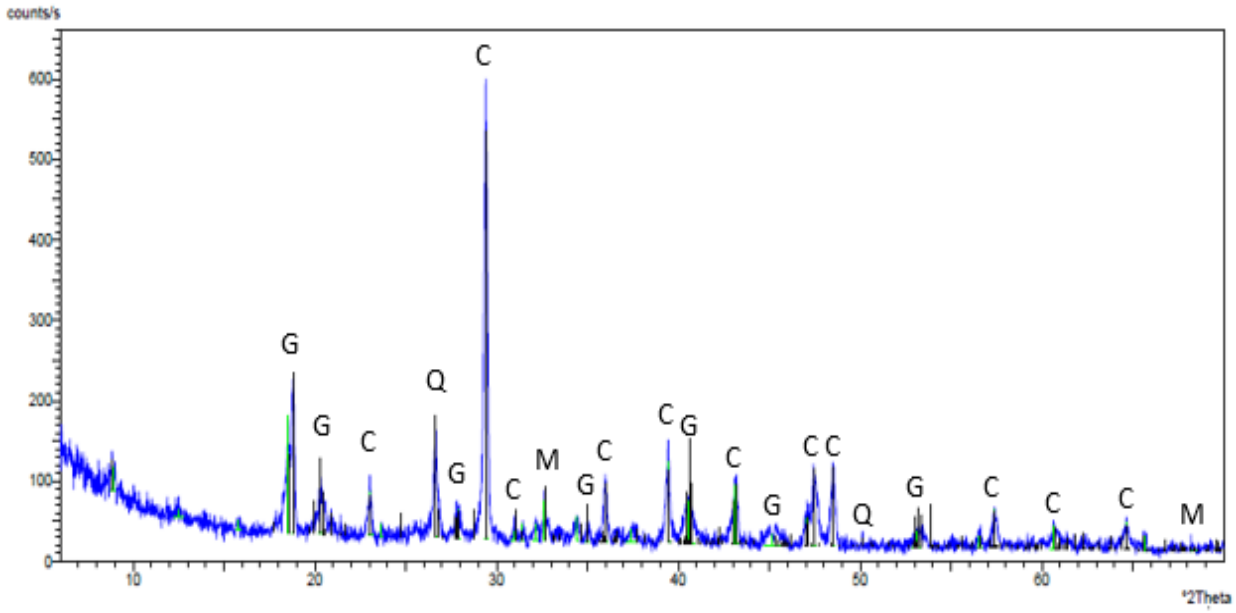


Fig. 5.18 XRD pattern of the powder grows on the surface of OPC50-CSA50 mix cured at 23°C and higher than 95% humidity (C: calcite, G: gibbsite, Q: quartz, M: magnesite)

Since the features of cement microstructures and pore solutions have an impact on the results of potentials and electrical resistivity, an attempt has been made to correlate the potentials of fibers to the electrical resistivity results of concretes. Fig. 5.19 shows the correlation for different concrete mixes were considered in this study. The results indicate that there is a strong linear correlation between these results. Higher potentials were attained by an increase in the magnitude

of the electrical resistivity. These results are highly promising and can contribute toward expanding the use of electrical resistivity method to monitor the potentials of steel reinforcement and probability of steel bars corrosion.

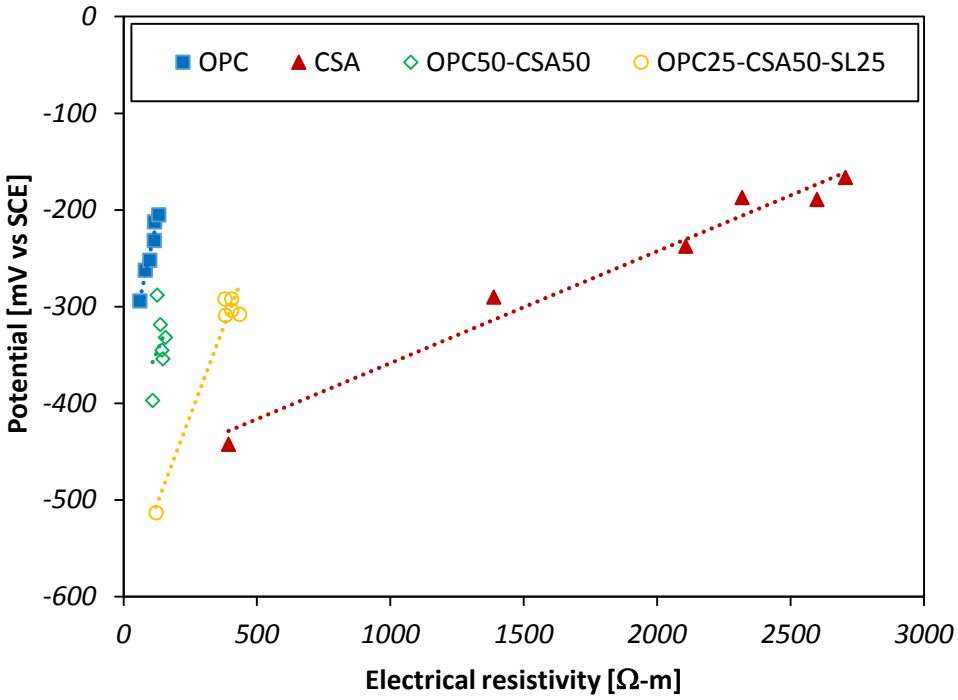


Fig. 5.19 Correlation between half-cell potential of fibers and electrical resistivity of different concrete mixes

## 5.11 Corrosion susceptibility of steel fibers by potential-static test

The current density of steel fibers embedded in different concrete mixes is depicted in Fig. 5.20. The results indicate that the current density of steel fibers in OPC mix ranged from 73.7 mA/m$^2$ to 0.74 mA/m$^2$. As it can be seen in Fig. 5.20, there was a continuous reduction in the current density, and the lowest current density was attained at 24 hours. The full replacement of OPC with CSA cement resulted in an increase in the current density of fibers, and the current density remained almost unchanged after 30 minutes of polarization. This result suggest that the susceptibility of steel fibers corrosion is higher in CSA mix with respect to the OPC mix. This can be attributed to

the less alkalinity of pore solutions in CSA mix that tend to destroy the protective passive film around the steel fibers and resulted in a higher risk of corrosion. The results further indicate that the current density of fibers has been significantly increased in the binary and ternary mixes. For instance, the current density of steel fibers in OPC50-CSA50 mix ranged from 1279.9 mA/m$^2$ (immediately after polarization) to 171.6 mA/m$^2$ (after 24 hours of polarization), while the current densities in OPC25-CSA50-SL25 mix immediately and after 24 hours of polarization were 1227.6 mA/m$^2$ and 852.1 mA/m$^2$, respectively. As it can be seen in Fig. 5.20, the presence of slag in concrete changed the performance of concrete and higher current density was attained at later ages compared to those at early ages. These result show that the passive film in the concretes containing blended CSA cement has been destroyed and steel fibers corrosion was occurred. The results of this study are in good agreement with the finding of Huang et al. [331] who reported that the tendency of steel bars corrosion was increased in the mixes containing slag as a replacement of the OPC.

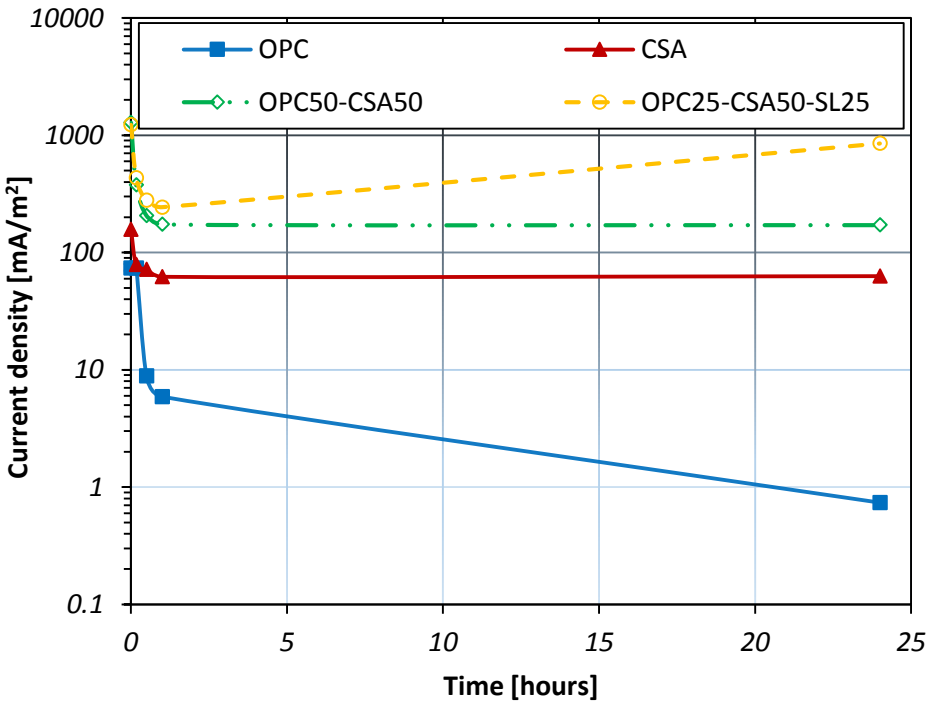


Fig. 5.20 Current density of different concrete mixes subjected to the polarization

The potentials of steel fibers embedded in different concrete mixes after depolarization are shown in Fig. 5.21. The results indicate that a great reduction in the potentials of steel fibers was occurred in all mixes, while the rate of reduction was significantly higher in concretes containing CSA cement. For instance, the potentials of steel fibers in OPC, CSA, OPC50-CSA50, and OPC25-CSA50-SL25 mixes were -13, -194, -399, and -432 mV, respectively 2 hours after depolarization. This result mean that the tendency of corrosion is significantly higher in concretes were fabricated with CSA cement compared to that of the OPC mix. The weak corrosion resistance of CSA cement blended mixes may also be attributed to the carbonation of those mixes that led to the decomposition of ettringite crystals as well as the reduction of the alkalinity in the pore solutions, which subsequently increased the risk of steel fibers corrosion [330].

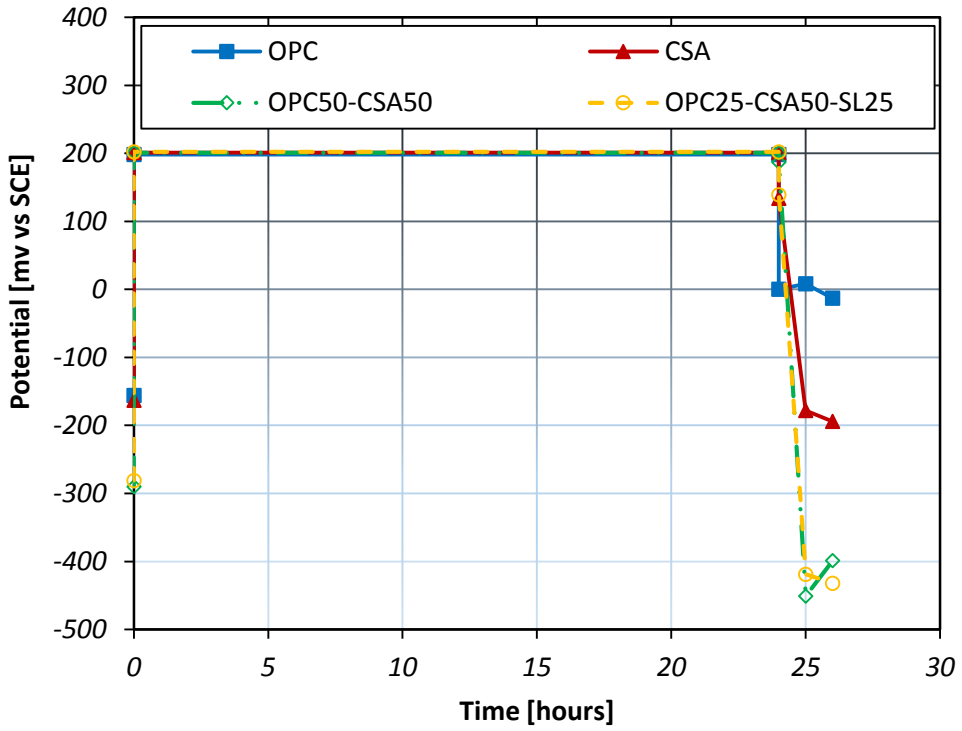


Fig. 5.21 Potential of fibers embedded in different concrete mixes after depolarization

To further study the corrosion performance of different concrete mixes, the concrete specimens were demolished after the test and an optical microscope was used to observe the surface of fibers as well as the concrete specimens. The images of steel fibers and concrete specimens are shown in Fig. 5.22. As it can be seen, there was no evidence of corrosion products in the surface of steel fibers and concrete containing OPC. On the other hand, it was observed that the passive film was destroyed in the mix containing CSA cement and both polarized and not polarized fibers were corroded. Additionally, the corrosion products can be seen on the surface of concrete specimen. Fig. 5.22 shows that the rate of corrosion was significantly higher in the CSA cement blended mixes with respect to the concrete that pure CSA cement was used. It was observed that strong black corrosion products were generated at the tip of steel fibers that resulted in a reduction of the cross-section in some areas. These results suggest that the electrical resistivity method can lead to misleading results as higher resistivity were attained in mixes containing CSA cement compared to that of the OPC. However, the potential-static test clearly show that the passive film protected the steel fibers against corrosion in OPC mix in spite of their lower resistivity over that of the concretes produced with CSA cement.

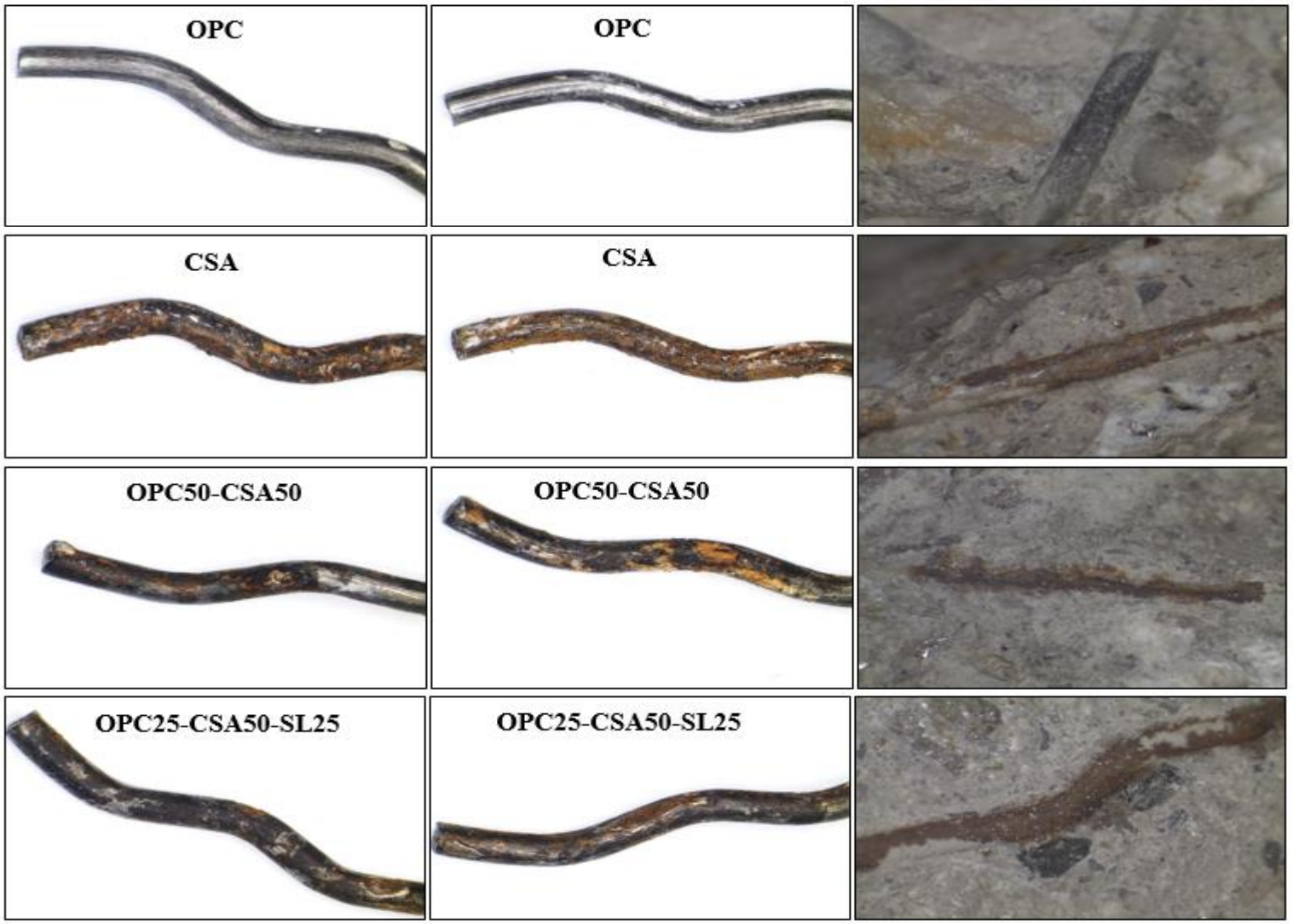


Fig. 5.22 Corrosion damaged of steel fibers and the corroded product on the surface of corresponding concrete

## 5.12 SEM observations

There is a strong correlation between the microstructural properties and physical-mechanical characteristics of concrete. It is well documented that the features of interfacial transition zone (ITZ) between the aggregate and cement past can significantly affects the mechanical properties of concrete. It was pointed that the ITZ is the most important interface in concrete, although it only consists a little portion in concrete [332], and subsequently it is able to substantially influence the physical and mechanical properties of hardened concrete [333]. SEM micrographs of ITZ between aggregate and cement paste of different concretes with w/c ratio of 0.35 are shown in Fig. 5.23. As it can be seen, in the OPC concrete, the aggregate was properly embedded in the cement matrix and a uniform C-S-H was developed around the aggregate. Fig. 5.23a shows the presence of a micro-crack at the interface of aggregate and cement matrix, which can result in a lower mechanical properties in this concrete. Cwirzen and Penttala [334] also reported that the weakest interface in the conventional concrete would be the ITZ between the cement matrix and aggregates.

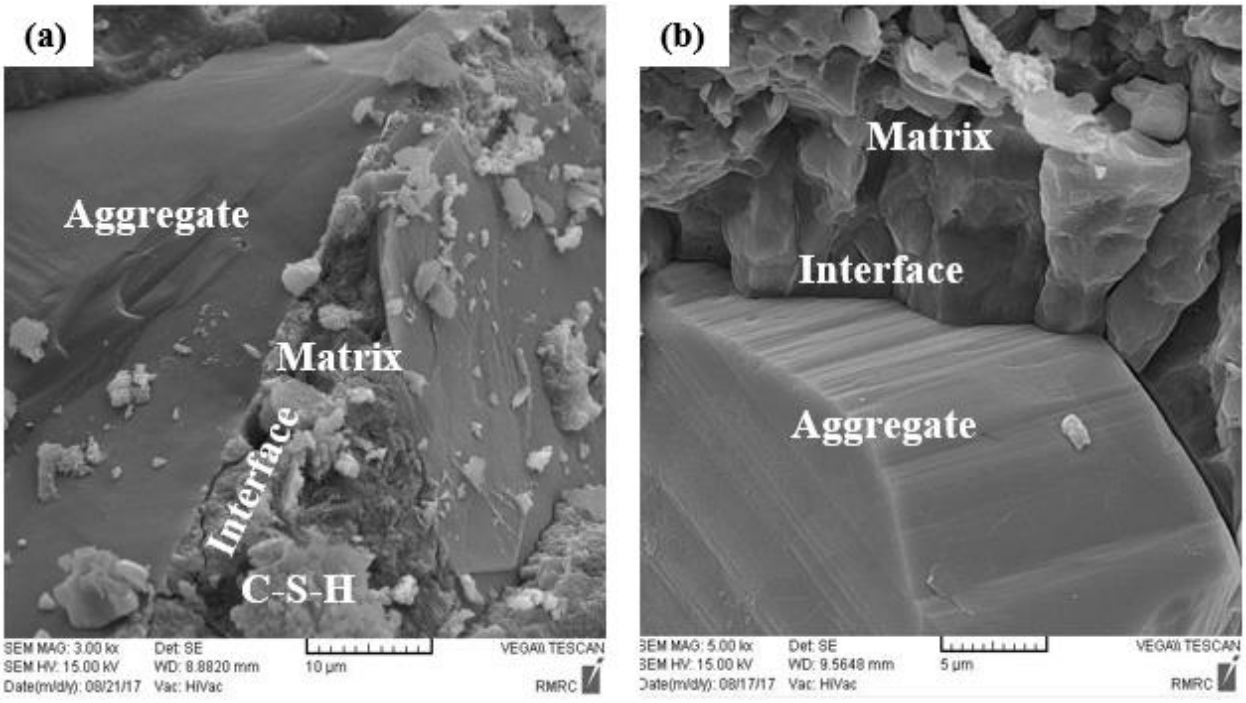

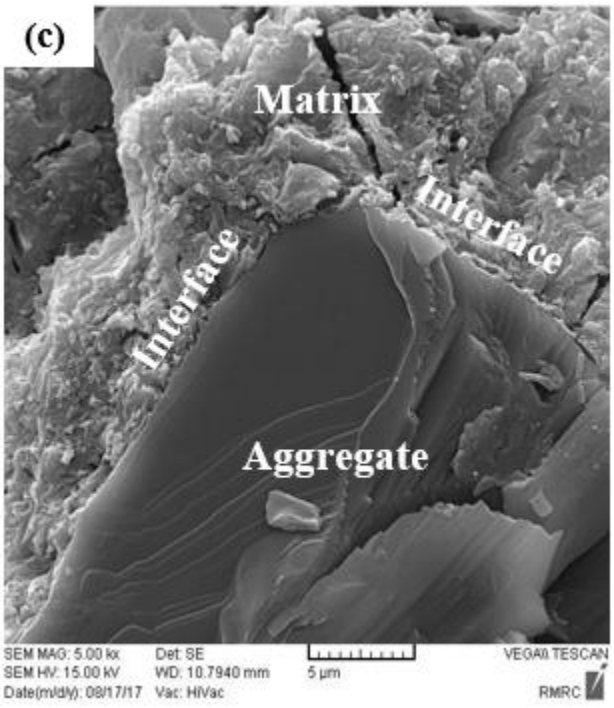


Fig. 5.23 SEM images of ITZ between aggregate and cement paste of different concretes with water-cement ratio of 0.35: (a) OPC concrete, (b) CSA concrete, (c) OPC25-CSA50-SL25 concrete

As it can be noticed in Fig. 5.23b, the full replacement of OPC with CSA cement resulted in a very dense microstructure around the interface of aggregate and matrix. The higher mechanical properties of CSA mix compared to the OPC mix can be attributed to the rich amount of ettringite as well as improved properties of ITZ. The results further indicate that in the ternary blended mix, the aggregate was surrounded by cement matrix consists of several micro-cracks. However, as can be seen in Fig. 5.23c, there is no evidence of any gap between the aggregate and cement matrix.

To study the microstructural properties of concretes produced with different cements as well as blended systems, several images were collected and the ones that are most representative are presented in Fig. 5.24. As it can be observed, the hydration products of OPC concrete consists of featureless gel of C-S-H, ettringite crystals with needle-like shape, and calcium hydroxide (CH)

crystals with plate shape. The results indicate that the content of calcium hydroxide is relatively higher over that of the ettringite. Additionally, it can be seen that the length of ettringite crystals developed in OPC concrete varied from 1 to 3 µm. The results also show the presence of pores with different sizes in the surface of hydrated cement, which can consequently influence the durability properties of concrete. Fig. 5.24b shows the morphology of hardened concrete containing CSA cement. As it can be seen, by hydration of ye'elimite that is the main component of CSA cement, a significant amount of ettringite crystals were generated. It is well documented by other researchers that ye'elimite can be hydrated in three different ways [335]. First, the hydration of ye'elimite with only water that can result in monosulfate and aluminum hydroxide. Second type of hydration is in the presence of calcium sulfate in addition to water to generate ettringite and aluminum hydroxide. The third type of hydration can be developed by the presence of lime, calcium sulfate and water, which subsequently resulted in the ettringite crystal alone.

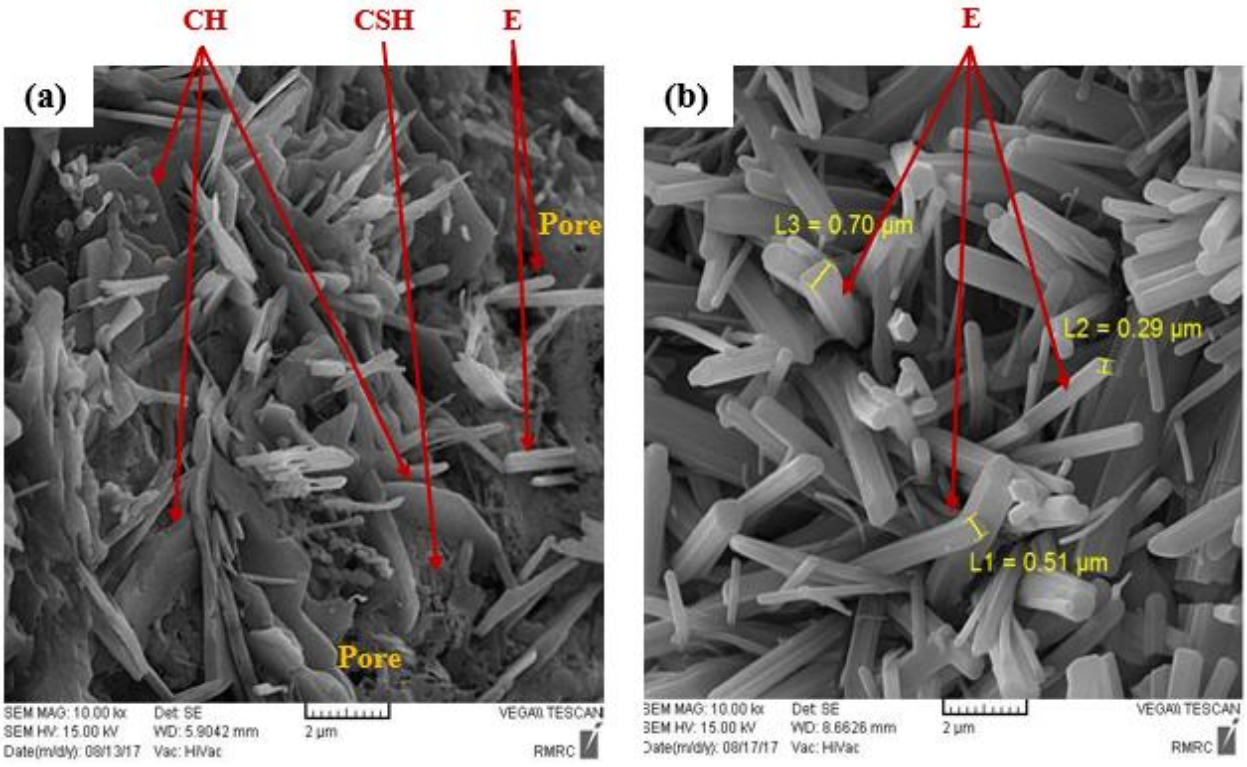

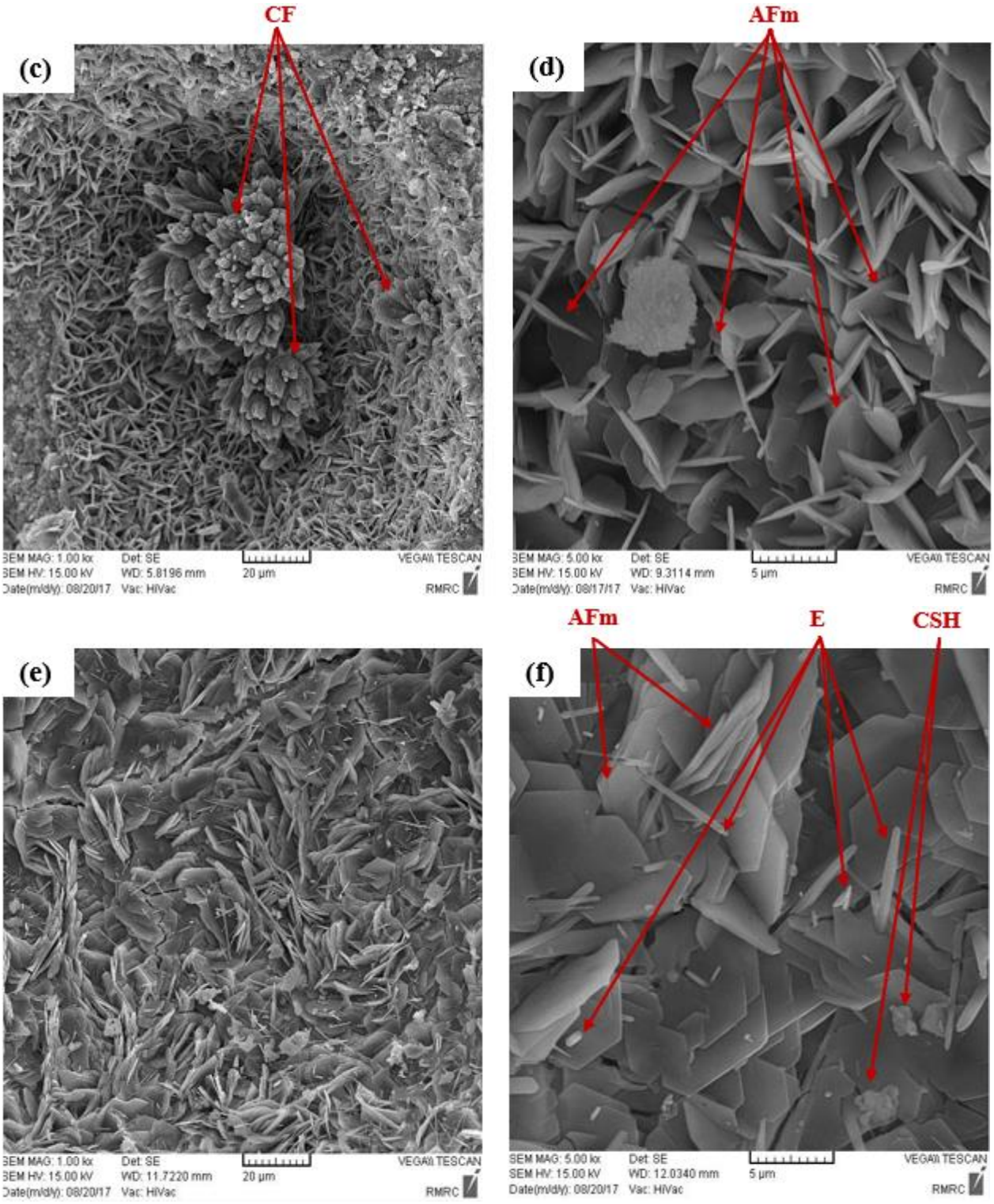


Fig. 5.24 SEM images of different concretes with water-cement ratio of 0.35: (a) OPC concrete, (b) CSA concrete, (c) OPC50-CSA50 concrete, (d) close-up of a section in fig. 5.24c, (e) OPC-25-CSA50-SL25 concrete, (f) close-up of a section in fig. 5.24e (E: ettringite, CH: portlandite, CSH: calcium silicate hydrate, CF: carbonated phase)

The results of this study show that the second hydration type was occurred. It was also observed that the size of prismatic ettringite crystals ranged from 0.29-0.7 μm wide, and 2-6 μm length. This type of ettringite crystals cause an improvement in the mechanical properties of concrete and also lead to the dimension stability of cement [336, 337]. The finding of this research in previous sections are in good agreement with the aforementioned explanation.

Fig. 5.24c shows the morphology of the binary blended system at low magnification, while Fig. 5.24d shows a close-up of a section with higher magnification. As it can be observed from those figures, the microstructure of hydrated cement was significantly changed by the combination of OPC with CSA cement at equal percentages of 50. As already mentioned, the presence of lime can notably influence the hydration products and result in three moles of ettringite instead of one, and subsequently increase the possibility of expansion [322]. It was also reported that this type of ettringite is characterized by high specific surface that accompanying with its negative charge are able to attract a great amount of water molecules. The expansion of the system can be attributed to the repulsion of those charged particles from each other [11]. The available lime in this system could be calcium hydroxide generated from the hydration of alite and belite coming from OPC, or the belite incorporated in the CSA clinker. Fig. 5.24c shows that some cluster crystal were formed in different areas of hydrated cement that may assign to the carbonated phase. It was noticed that these type of crystals had quite large size and their length were up to 30 μm. This may be related to the carbonation of mobile alkalis from the pore solution as a result of efflorescence phenomena. It is also well documented that carbonation of concrete can lead to the decomposition of ettringite crystals, which subsequently reduced the mechanical properties of concrete [330]. In addition to those crystals, some plate-like crystals with high specific surface were also generated as is shown

in Fig. 5.24d. The plate-like crystals that were generated in this study were about 5-7 μm wide and 3 μm long that most of them tend to be AFm phase.

The morphology of ternary mix containing OPC, CSA, and slag is shown in Figs. 5.24e, while a close-up of a section with higher magnification is shown in Fig. 5.24f. As it can be seen, differently from the binary mix, the inclusion of slag resulted in a disappearance of long cluster crystals. The ternary system consists of different type of crystals including needle-like ettringite, AFm phases and C-S-H gel. The appearance of C-S-H in this system can be explained by the fact that slag was reacted with the calcium hydroxide produced by OPC, and consequently led to the formation of secondary C-S-H gel. The higher mechanical properties and lower expansion of ternary system compared to those of the binary system can be attributed to the disappearance of cluster crystals with long size and also formation of additional C-S-H.

# Chapter 6

# The influences of different types of fibers and fiber hybridization on the engineering properties of concretes containing CSA cement

## 6.1 Introduction

This chapter studies the influence of different types of fibers and combination of fibers on the engineering properties of CSA-based concretes at different w/c ratios of 0.35 and 0.28. Double hooked-end (DHE) steel fibers, hooked-end (HE) steel fibers, and polyvinyl alcohol (PVA) fibers were used at fiber content of 1%. Some mixes were produced with the combination of metallic and synthetic fibers at a total fiber content of 1.0% to study the effect of fiber hybridization. All the fiber-reinforced concretes (FRC) were produced by using CSA cement. The mix proportions of fourteen different concrete mixes were developed in this study are shown in Table 3.6. The compressive strength, splitting tensile strength, modulus of elasticity, flexural behavior, and drying shrinkage of the concrete mixes were examined. Moreover, the morphology of the fractured specimens was studied by using SEM method.

## 6.2 Compressive strength

The compressive strength of different concrete mixes were studied at both water and air curing conditions to observe the effect of curing. The compressive strength results of different mixes with w/c ratio of 0.35 under water curing are shown in Fig. 6.1 and Table 6.1. The relative compressive strength of different FRC compared to that of the reference CSA mix is also shown in Fig. 6.2. The results indicate that the inclusion of CSA cement led to a reduction in the 1 day compressive strength of concrete, while its strength is higher compared to that of the OPC at later ages of curing.

This reduction at the early age can be explained by the fact that the addition of retarder delayed the ettringite formation in CSA cement. On the other hand, the increase in the strength of concrete at later ages can be attributed to the rich amount of ettringite in that mix that consequently improved the features of cement matrix and led to an increased strength.

As it can be noticed in Fig. 6.1, the use of fibers in any form and fiber hybridization resulted in an increase in the compressive strength compared to that of the reference CSA concrete. This increase in the compressive strength can be explained by the fibers ability to restrain the extension of cracks, reduce the extent of stress concentration at the tip of cracks, change the direction of cracks, and delay the growth rate of cracks [98]. The results shown in Table 6.1 indicate that compressive strength of concrete increases from 1% to 13% as a result of the addition of fibers to the CSA mix, depending on the fiber type and testing age. It can also be observed in the same table that the effect of steel fibers was more significant than that of the PVA fibers in the improvement of the compressive strength. This can be attributed to the higher strength and elastic modulus of steel fibers compared to those of PVA fibers, which resulting in their higher efficiency in bridging macro-cracks and consequently increasing the compressive strength. As it can be seen in Fig. 6.1, the best performing mix was the one with 1.0% HE steel fiber, which attained a 56-day compressive strength of 92.9 MPa. The failure mode of high performance concrete under compression load is shown in Fig. 6.3. As it can be seen, the plain CSA specimen was damaged significantly and its behavior was almost explosive. However, the addition of fibers significantly changed the failure pattern of concrete. It was noticed that the PVA fibers act better than DHE steel fibers to restrain the propagation of micro-cracks in the body of concrete due to their higher number of fibers per volume of concrete at a similar fiber content.

Table 6.1 Compressive strength of different fiber-reinforced concretes (water curing)

| Mix No. | Mixture ID | W/B | Compressive strength (MPa) | | | | Strength gain over that of 7 days (%) | | | |
|---|---|---|---|---|---|---|---|---|---|---|
| | | | 1 Days | 7 Days | 28 Days | 56 Days | 1 Days | 7 Days | 28 Days | 56 Days |
| 1 | OPC | 0.35 | 56.0 (+120%) | 69.9 (-1%) | 75.9 (-9%) | 78.8 (-11%) | 80 | 100 | 109 | 113 |
| 2 | CSA | | 25.4 (-) | 70.9 (-) | 83.7 (-) | 88.2 (-) | 36 | 100 | 118 | 124 |
| 3 | CSA-DHE1 | | 28.3 (+11%) | 74.1 (+5%) | 87.8 (+5%) | 91.5 (+4%) | 38 | 100 | 118 | 123 |
| 4 | CSA-HE1 | | 28.8 (+13%) | 73.2 (+3%) | 86.9 (+4%) | 92.9 (+5%) | 39 | 100 | 119 | 127 |
| 5 | CSA-PVA1 | | 25.7 (+1%) | 71.6 (+1%) | 85.0 (+2%) | 89.6 (+2%) | 36 | 100 | 119 | 125 |
| 6 | CSA-DHE0.5-HE0.5 | | 29.5 (+16%) | 74.6 (+5%) | 89.3 (+7%) | 93.1 (+6%) | 40 | 100 | 120 | 125 |
| 7 | CSA-DHE0.5-PVA0.5 | | 26.4 (+4%) | 74.2 (+5%) | 87.1 (+4%) | 91.8 (+4%) | 36 | 100 | 117 | 124 |
| 8 | OPC | 0.28 | 62.3 (+50%) | 70.1 (-3%) | 79.8 (-7%) | 81.5 (-10%) | 89 | 100 | 114 | 116 |
| 9 | CSA | | 41.5 (-) | 72.3 (-) | 85.4 (-) | 90.1 (-) | 57 | 100 | 118 | 125 |
| 10 | CSA-DHE1 | | 47.6 (+15%) | 82.2 (+14%) | 91.7 (+7%) | 95.6 (+6%) | 58 | 100 | 112 | 116 |
| 11 | CSA-HE1 | | 49.8 (+20%) | 84.7 (+17%) | 92.0 (+8%) | 97.7 (+8%) | 59 | 100 | 109 | 115 |
| 12 | CSA-PVA1 | | 45.9 (+11%) | 77.8 (+8%) | 89.1 (+4%) | 91.8 (+2%) | 59 | 100 | 115 | 118 |
| 13 | CSA-DHE0.5-HE0.5 | | 48.7 (+17%) | 84.4 (+17%) | 94.0 (+10%) | 96.5 (+7%) | 58 | 100 | 111 | 114 |
| 14 | CSA-DHE0.5-PVA0.5 | | 47.5 (+14%) | 80.2 (+11%) | 91.5 (+7%) | 92.9 (+3%) | 59 | 100 | 114 | 116 |

Note: The number in the () shows the percentage of strength increase or decrease over that of the plain CSA concrete.

Fig. 6.2 shows that the compressive strength of concretes manufactured with fibers hybridization were up to 16% higher than that of the plain CSA concrete, depending on the fibers combination, and testing age. The results of hybrid fiber-reinforced concretes (HyFRC) illustrate that the substitution of a portion of DHE steel fibers with HE steel fibers led to a slight increase in the compressive strength, while the combination of DHE steel fibers and PVA fibers caused a compressive strength similar to that of the CSA-DHE1 mix. Among the different fiber combinations considered in this study, the highest compressive strength was developed by the mix containing 0.5% DHE and 0.5% HE steel fibers that attained a 56-day compressive strength of 93.1 MPa.

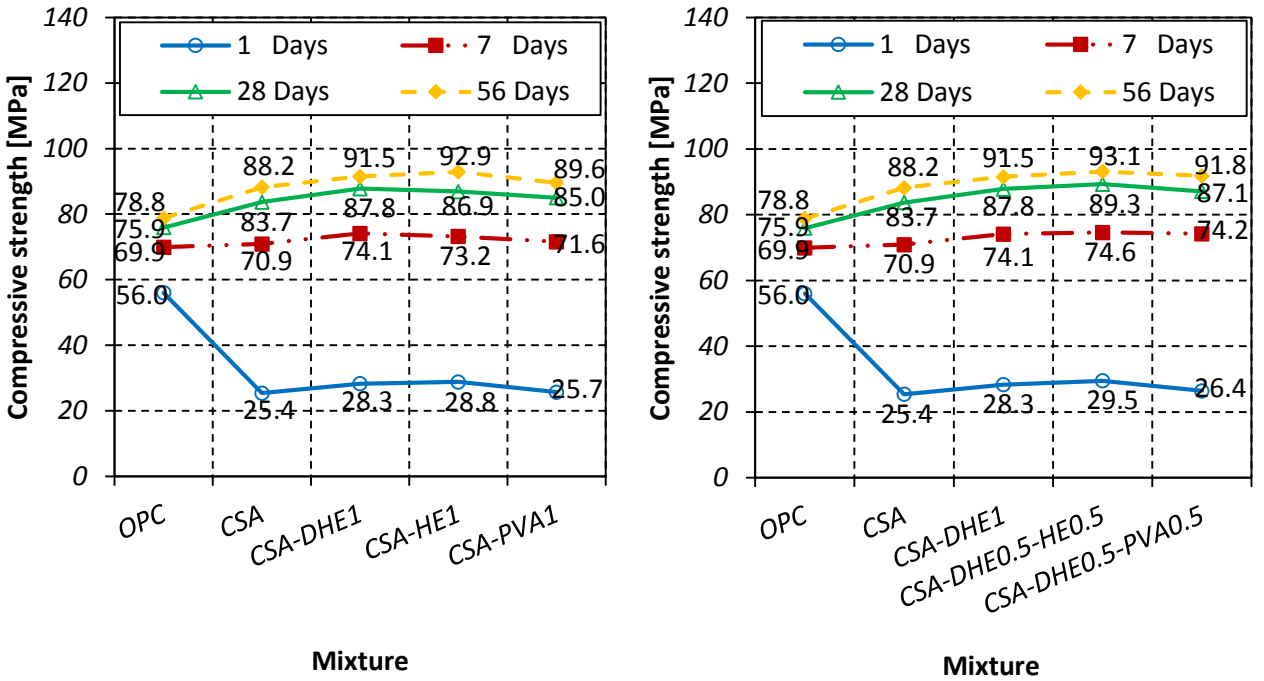


Fig. 6.1 Compressive strengths of different concretes with water-cement ratio of 0.35 under water curing: (a) fiber-reinforced concretes, (b) hybrid fiber-reinforced concretes

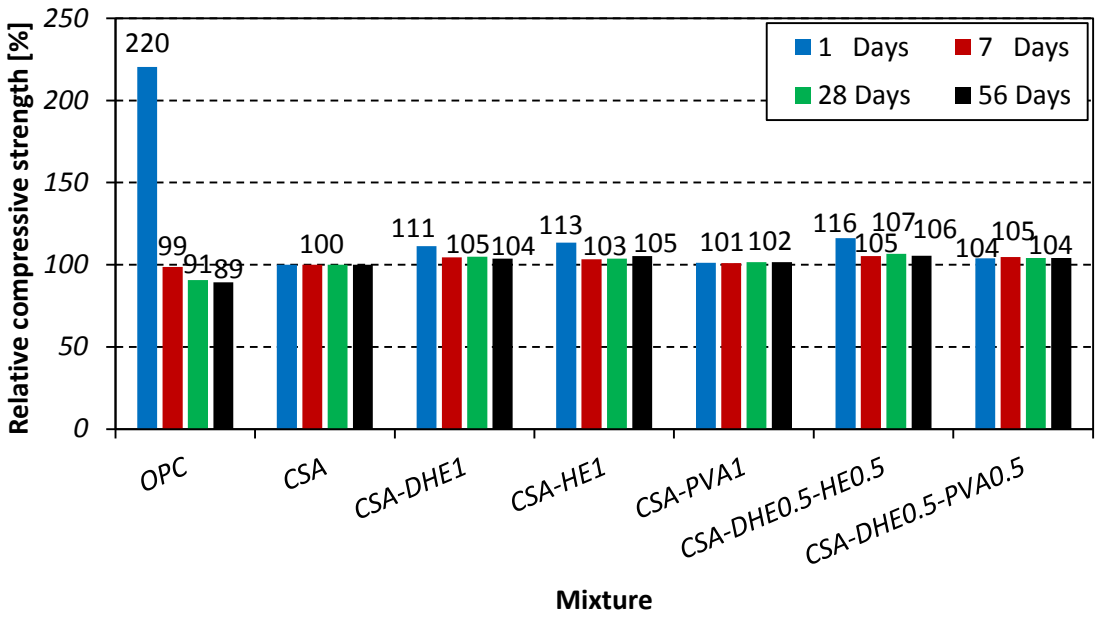


Fig. 6.2 Relative compressive strengths of different fiber-reinforced concretes with water-cement ratio of 0.35 under water curing

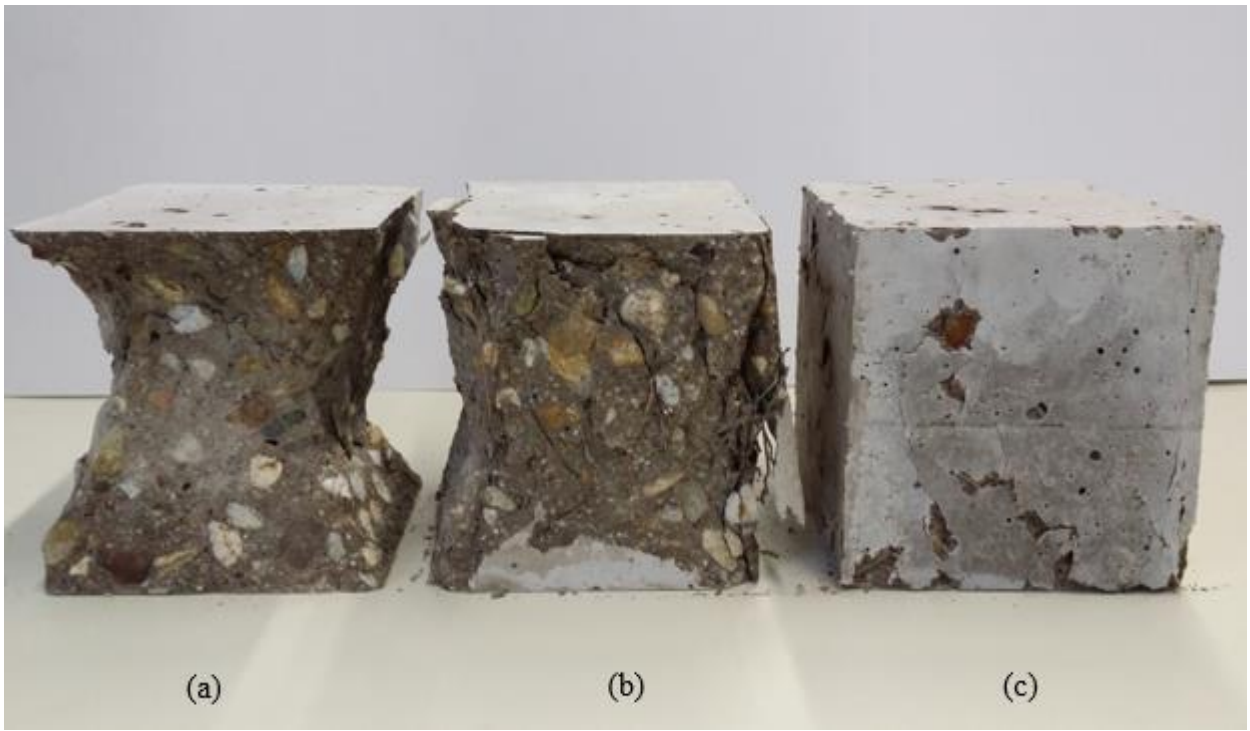


Fig. 6.3 Failure mode of high performance concrete under compression load: (a) 0% fiber, (b) 1% DHE steel fiber, (c) 1% PVA fiber

The compressive strength results of different mixes with w/c ratio of 0.35 under air curing are shown in Fig. 6.4, and the relative compressive strength is also shown in Fig. 6.5. As it can be seen in those figures, a similar trend to specimens that wet cured was occurred in the strength of concretes. The results indicate that the effectiveness of steel fibers was higher compared to that of the PVA fibers in improvement of the compressive strength. The results further indicate that the compressive strength improvement of FRC ranged from 1% to 16%, depending on the fiber type, fiber hybridization, and testing age.

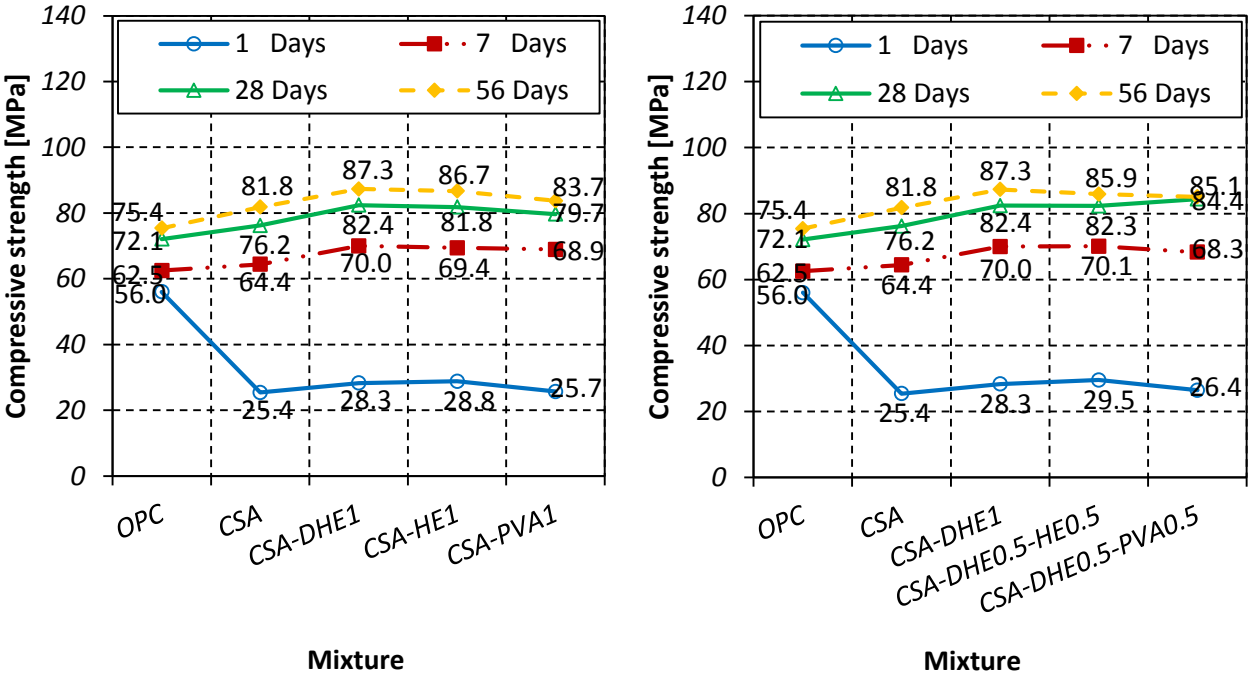


(a) (b)

Fig. 6.4 Compressive strengths of different concretes with water-cement ratio of 0.35 under air curing: (a) fiber-reinforced concretes, (b) hybrid fiber-reinforced concretes

The compressive strength ratio of water to air cured specimens of different fiber-reinforced concretes with w/c ratio of 0.35 is shown in Fig. 6.6. As it can be observed, the compressive strength of water cured specimens were slightly higher than that of the specimens subjected to air

curing. For instance, the increase in the compressive strength of water cured FRC over that of the air cured specimens varied from 3% to 9%, depending on the fiber type, fiber hybridization, and testing age. Obviously, the specimens that water cured can absorb water from surrounding environment to further generate the ettringite, which subsequently increased the strength of concrete.

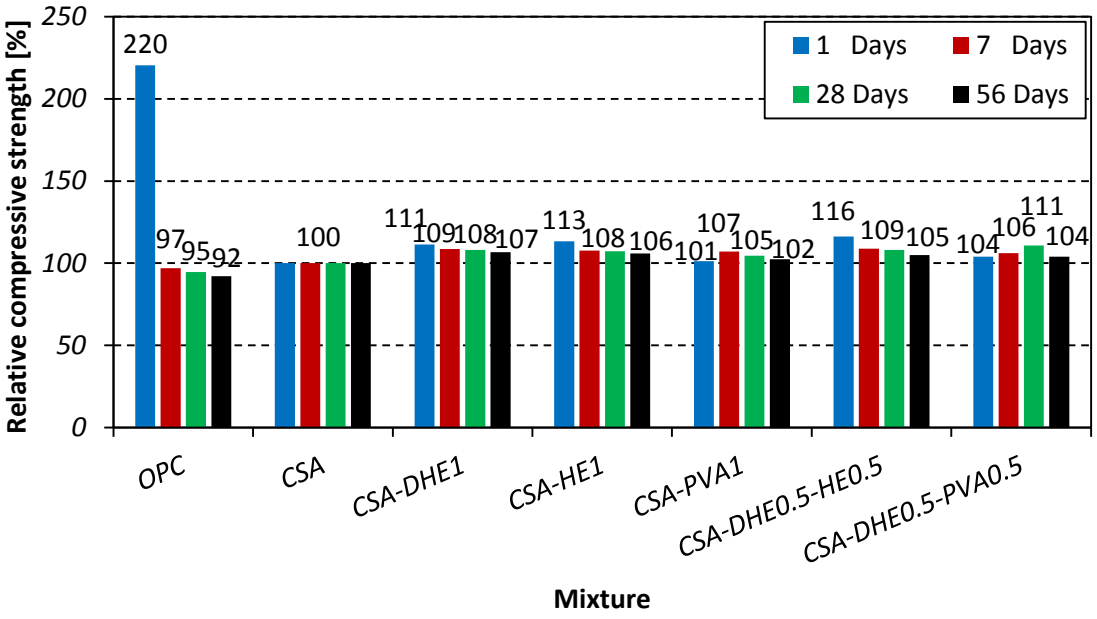


Fig. 6.5 Relative compressive strengths of different fiber-reinforced concretes with water-cement ratio of 0.35 under air curing

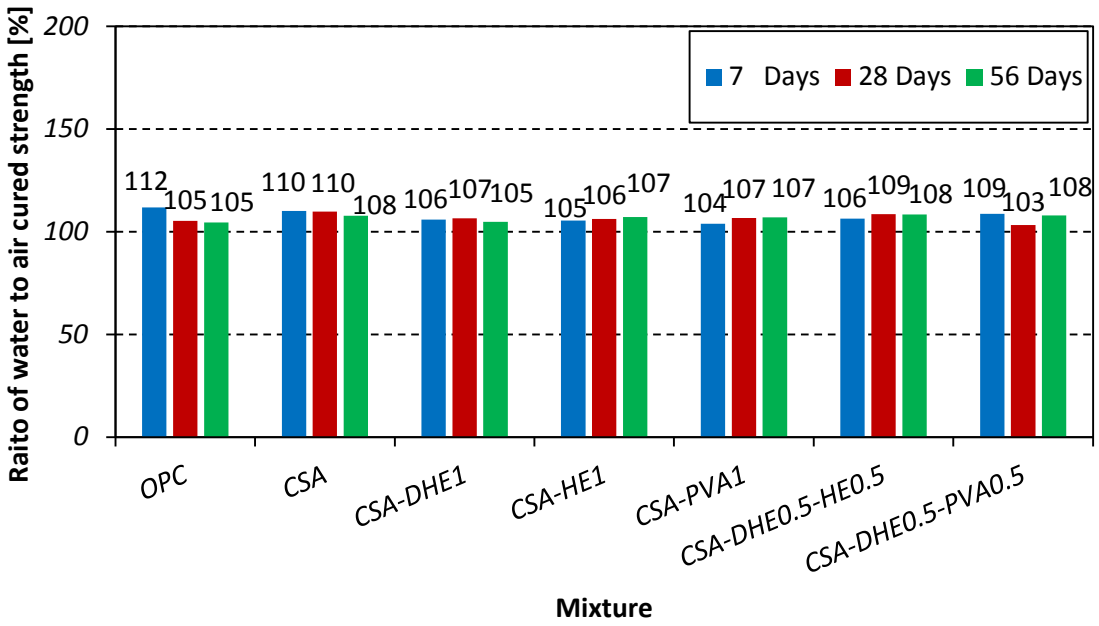


Fig. 6.6 Compressive strength ratios of water to air cured specimens of different fiber-reinforced concretes with water-cement ratio of 0.35

The compressive strength results of different mixes with w/c ratio of 0.28 under water curing are shown in Fig. 6.7 and Table 6.1. The relative compressive strength of different FRC compared to that of the reference CSA mix is also shown in Fig. 6.8. Similar to the concretes with w/c ratio of 0.35, the full replacement of OPC with CSA cement led to reduction of 33% at 1 day compressive strength, while the compressive strengths of CSA mix were 3%, 7%, and 10% higher over those of the OPC mix at 7, 28, and 56 days, respectively. The results indicate that the addition of fibers caused an increase in the compressive strength of concrete irrespective to the fiber types and fiber hybridization. As it can be seen in the Fig. 6.8, the compressive strength improvement of FRC ranged from 2% to 20%, depending on the fiber type, fiber hybridization, and testing age.

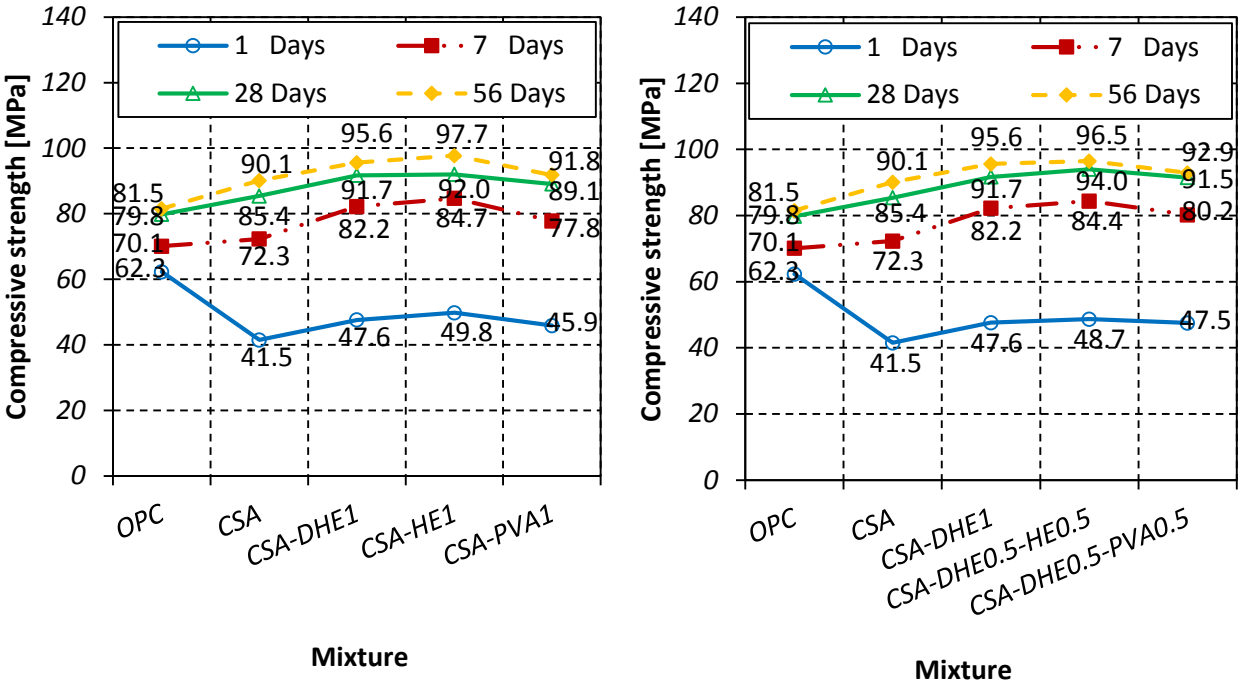


Fig. 6.7 Compressive strengths of different concretes with water-cement ratio of 0.28 under water curing: (a) fiber-reinforced concretes, (b) hybrid fiber-reinforced concretes

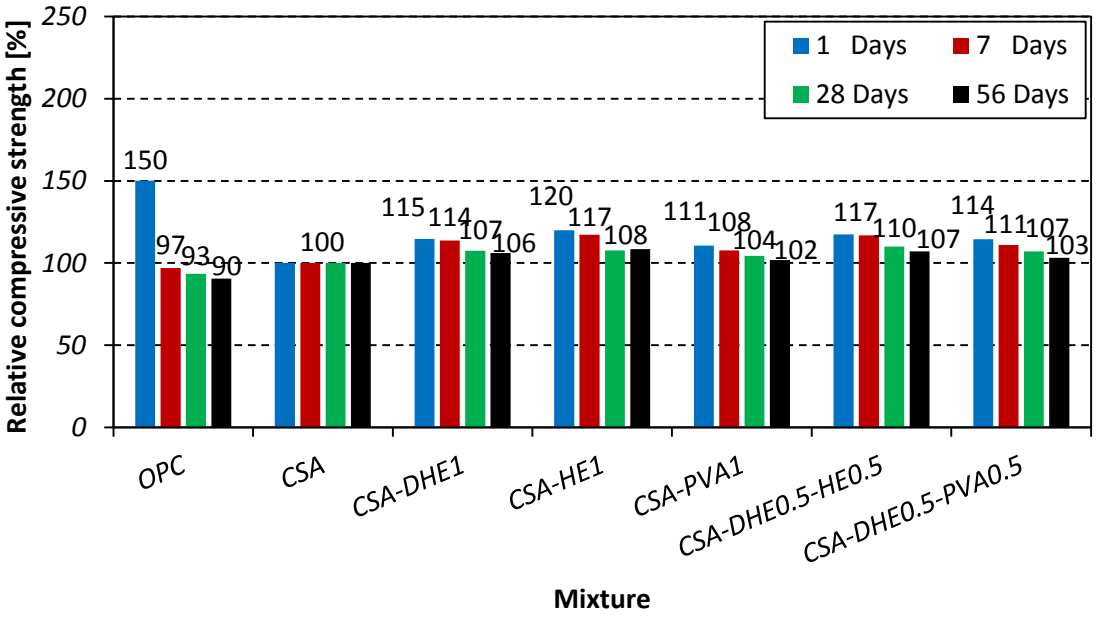


Fig. 6.8 Relative compressive strengths of different fiber-reinforced concretes with water-cement ratio of 0.28 under water curing

Fig. 6.7 shows that the best performing mix was the CSA-HE1 mix that attained a 56-day compressive strength of 97.7 MPa. The results of HyFRC indicate that the substitution of a portion of DHE steel fibers with HE steel fibers led to a slight increase in the compressive strength, while the combination of DHE steel fibers and PVA fibers caused a compressive strength similar to that of the CSA-DHE1 mix.

The compressive strength results of different mixes with water-cement ratio of 0.28 under air curing are shown in Fig. 6.9, and the relative compressive strength is also shown in Fig. 6.10. As it can be seen in those figures, the effectiveness of steel fibers in improvement of compressive strength was higher over that of the PVA fibers. The results demonstrate that an increase up to 27% was attained in the compressive strength of concrete through the addition of 1% HE steel fibers in the CSA concrete.

The compressive strength ratio of water to air cured specimens of different fiber-reinforced concretes with w/c ratio of 0.28 is shown in Fig. 6.11. The results show that the effect of water curing on the compressive strength of specimens were developed by w/c ratio of 0.28 was insignificant. For instance, the water cured compressive strengths of CSA mix at 7, 28, and 56 days were 9%, 3%, and 4% higher than those of the specimens subjected to air curing condition, respectively. This increase for FRC specimens was up to 4%. This result suggest that air curing can be used for CSA-based concretes to attain compressive strength matching those of concretes under water curing.

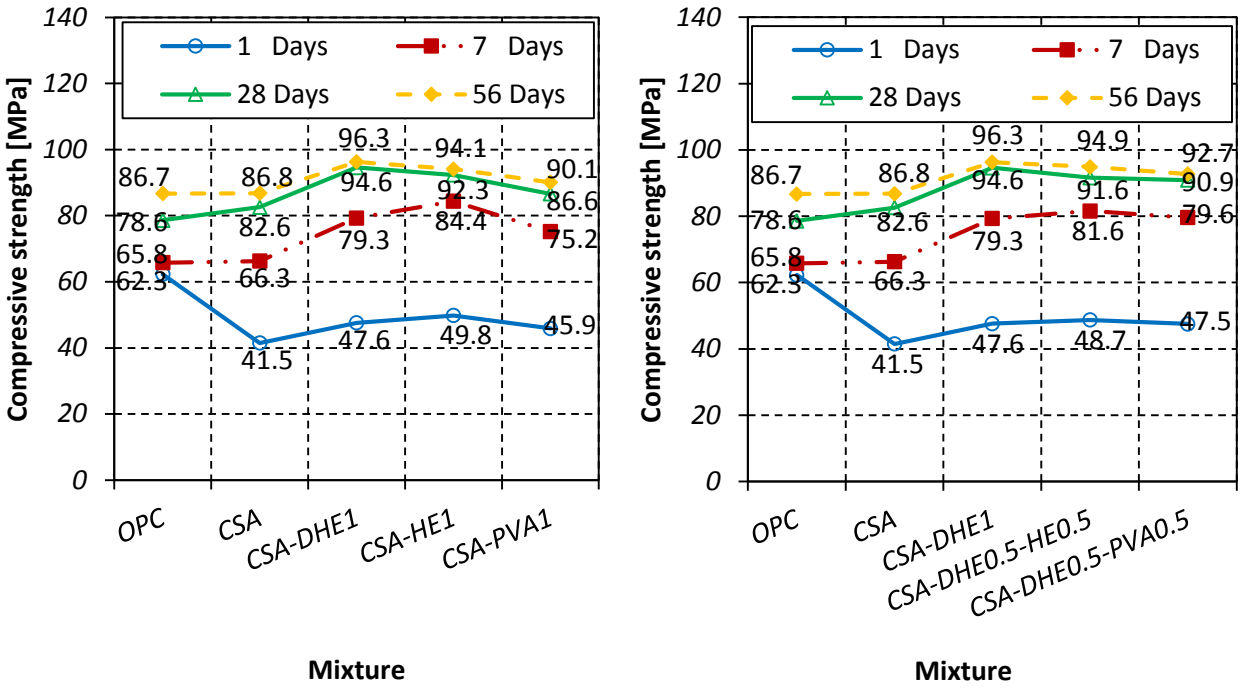


Fig. 6.9 Compressive strengths of different concretes with water-cement ratio of 0.28 under air curing: (a) fiber-reinforced concretes, (b) hybrid fiber-reinforced concretes

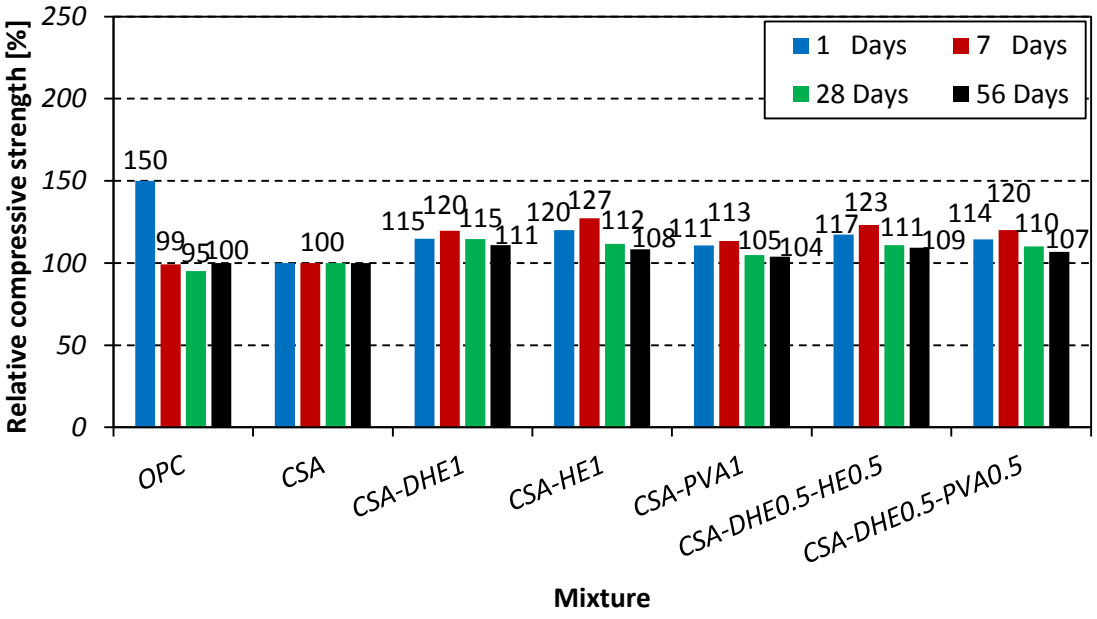


Fig. 6.10 Relative compressive strengths of different fiber-reinforced concretes with water-cement ratio of 0.28 under air curing

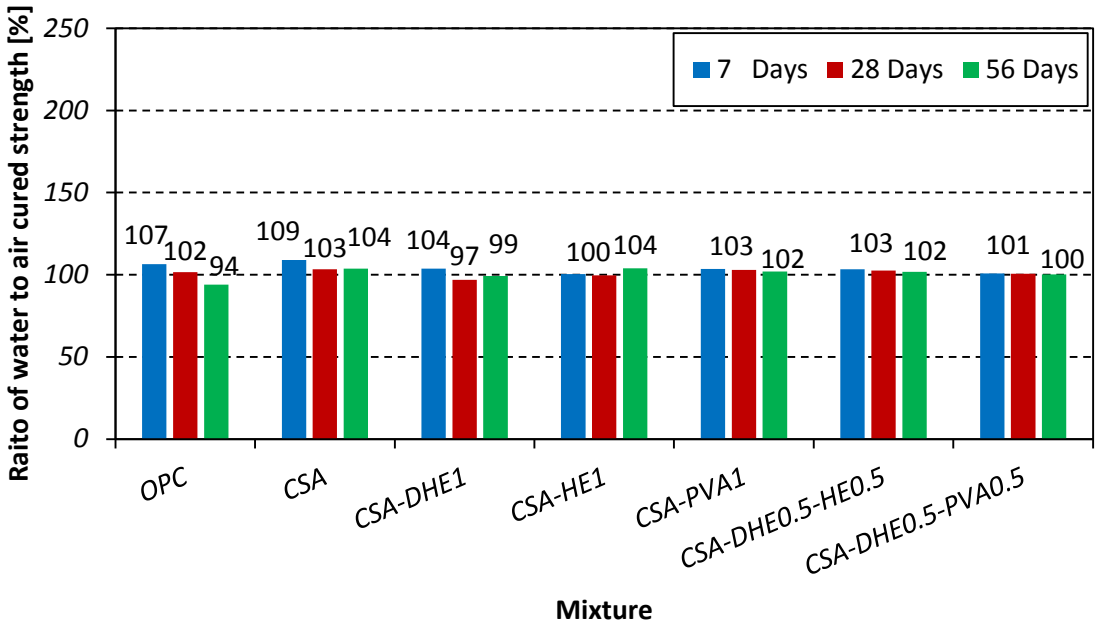


Fig. 6.11 Compressive strength ratios of water to air cured specimens of different fiber-reinforced concretes with water-cement ratio of 0.28

The strength evolutions of different FRC compared to their 7 days strength are presented in Table 6.1. It was observed that the strength development in concretes were produced at higher w/c ratio (i.e. 0.35) was higher compared to that of the concretes were manufactured at w/c ratio of 0.28. For instance, the average 28 and 56 days compressive strengths of FRC with w/c ratio of 0.35 were 19% and 25% higher than their 7 days strength, while these increase were 12% and 16% in FRC produced at w/c ratio of 0.28. This can be explained by the fact that the free water that was available in concretes with w/c ratio of 0.28 was consumed very fast by ye'elimite to generate ettringite, and less amount of water was available for its further hydration and strength gain. On the other hand, in concretes that were manufactured at w/c ratio of 0.35, further reaction was occurred at later ages that consequently developed higher strength growth.

The comparison between the compressive strength results of concrete were produced at different water-cement ratios shows that the reduction in the water-cement ratio of CSA-based concretes has a significant effect on the 1 day strength, while it has negligible influence on their strength at later ages of curing. Ac it can be seen in Table 6.1, the compressive strength of CSA concrete at water cement ratio of 0.28 increased by 63%, 2%, 2%, and 2% at 1, 7, 28, and 56 days, respectively compared to those of the CSA concrete with water-cement ratio of 0.35. This may be due to the fact that at very low water-cement ratios like 0.28, the ye'elimite hydration was occurred very fast and as a consequence notably increased the 1 day strength.

### 6.3 Splitting tensile strength

The splitting tensile strength results of different FRC mixes with w/c ratio of 0.35 are shown in Fig. 6.12 and listed in Table 6.2. The relative splitting tensile strength of different FRC mixes with w/c ratio of 0.35 compared to that of the reference CSA mix is also shown in Fig. 6.13. The results indicate that the replacement of OPC with CSA cement led to a slight reduction in the 7 day splitting tensile strength, while increased the 28 and 56 days strengths of concrete. This increase can be due to the fact that the addition of CSA cement caused an improvement in the properties of cement matrix as a result of higher ettringite formation.

The results of fiber-reinforced concretes show that incorporation of fibers, especially DHE steel fibers, had a significant influence on the splitting tensile strength of the concrete. For example, the splitting tensile strength of the mixes containing 1% DHE steel fibers increased by 59%, 76%, and 78% at 7, 28, and 56 days, respectively compared to those of the reference CSA concrete. As it can be seen in Table 6.2, the increase in the splitting tensile strength of CSA-HE1 mix ranged from

28% to 52%, while this increase for CSA-PVA1 mix varied from 25% to 28% as compared to those of the CSA mix, depending on the testing age. Since, PVA fibers are short and have lower tensile strength and elastic modulus compared to those of steel fibers, they bridged mainly micro-cracks and have lower effect on the splitting tensile strength as compared to steel fibers. On the other hand, owing to their higher tensile strength and modulus of elasticity, steel fibers had a remarkable influence on the splitting tensile strength of concrete. Furthermore, DHE steel fibers used in the present study, due to the anchoring mechanism created by their hooked ends were able to develop considerably higher maximum pullout forces compared to those developed by HE steel and straight PVA fibers. The results of HyFRC point to the higher efficiency of DHE steel fibers compared to HE and PVA fibers in enhancing the concrete strength. However, it was observed that specimens containing any combination of fibers additives exhibited a better performance compared to that of CSA mix without fibers. As it can be seen in Table 6.2, the splitting tensile strength improvement of HyFRC ranged from 41% to 76%, depending on the fiber combination, and testing age.

The failure mode of high performance concrete under splitting tensile load is shown in Fig. 6.14. As can be seen, the plain CSA concrete was split into two parts, whereas this was prevented in the sample containing 1% DHE steel fibers, in which the fibers restrained the propagation of macro-cracks, and a longitudinal crack occurred only on the surface of concrete. It was also observed that the addition of 1% PVA fibers although increased the splitting tensile strength of concrete, it was not able to significantly restrain the extension of macro-cracks. As a result of that, the CSA-PVA1 mix was also split into two parts.

Table 6.2 Splitting tensile strength of different fiber-reinforced concretes

| Mix No. | Mixture ID | W/B | Compressive strength (MPa) | | | Strength gain over that of 7 days (%) | | |
|---|---|---|---|---|---|---|---|---|
| | | | 7 Days | 28 Days | 56 Days | 7 Days | 28 Days | 56 Days |
| 1 | OPC | 0.35 | 3.41 (+2%) | 3.88 (-10%) | 4.30 (-10%) | 100 | 114 | 126 |
| 2 | CSA | | 3.35 (-) | 4.29 (-) | 4.77 (-) | 100 | 128 | 142 |
| 3 | CSA-DHE1 | | 5.31 (+59%) | 7.55 (+76%) | 8.48 (+78%) | 100 | 142 | 160 |
| 4 | CSA-HE1 | | 4.29 (+28%) | 6.53 (+52%) | 7.07 (+48%) | 100 | 152 | 165 |
| 5 | CSA-PVA1 | | 4.20 (+25%) | 5.46 (+27%) | 6.12 (+28%) | 100 | 130 | 146 |
| 6 | CSA-DHE0.5-HE0.5 | | 4.92 (+47%) | 6.94 (+62%) | 8.38 (+76%) | 100 | 141 | 170 |
| 7 | CSA-DHE0.5-PVA0.5 | | 4.71 (+41%) | 6.75 (+57%) | 7.62 (+60%) | 100 | 143 | 162 |
| 8 | OPC | 0.28 | 3.77 (-1%) | 4.43 (-5%) | 4.87 (-6%) | 100 | 118 | 129 |
| 9 | CSA | | 3.82 (-) | 4.64 (-) | 5.18 (-) | 100 | 121 | 136 |
| 10 | CSA-DHE1 | | 6.32 (+65%) | 8.72 (+88%) | 9.37 (+81%) | 100 | 138 | 148 |
| 11 | CSA-HE1 | | 5.75 (+51%) | 7.48 (+61%) | 8.43 (+63%) | 100 | 130 | 147 |
| 12 | CSA-PVA1 | | 4.72 (+24%) | 5.70 (+23%) | 6.17 (+19%) | 100 | 121 | 131 |
| 13 | CSA-DHE0.5-HE0.5 | | 6.08 (+59%) | 8.14 (+75%) | 8.71 (+68%) | 100 | 134 | 143 |
| 14 | CSA-DHE0.5-PVA0.5 | | 5.98 (+57%) | 7.83 (+69%) | 8.52 (+64%) | 100 | 131 | 142 |

Note: The number in the () shows the percentage of strength increase or decrease over that of the plain CSA concrete.

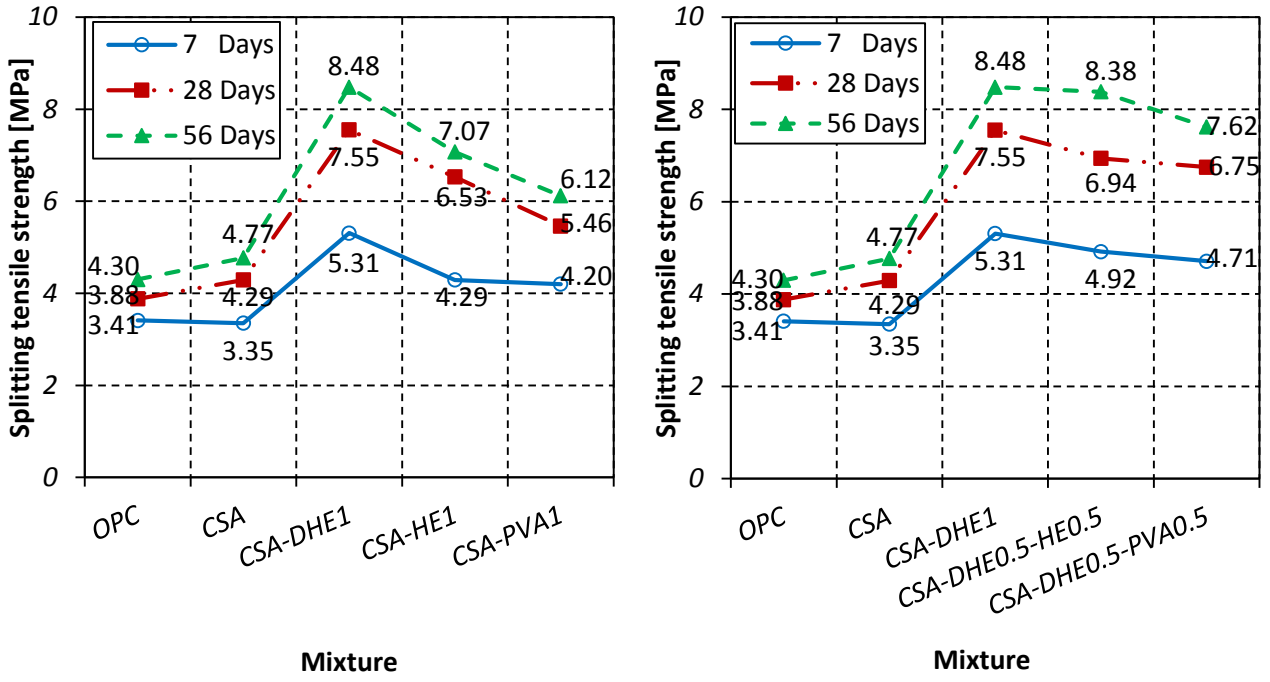


(a) (b)

Fig. 6.12 Splitting tensile strengths of different concretes with water-cement ratio of 0.35: (a) fiber-reinforced concretes, (b) hybrid fiber-reinforced concretes

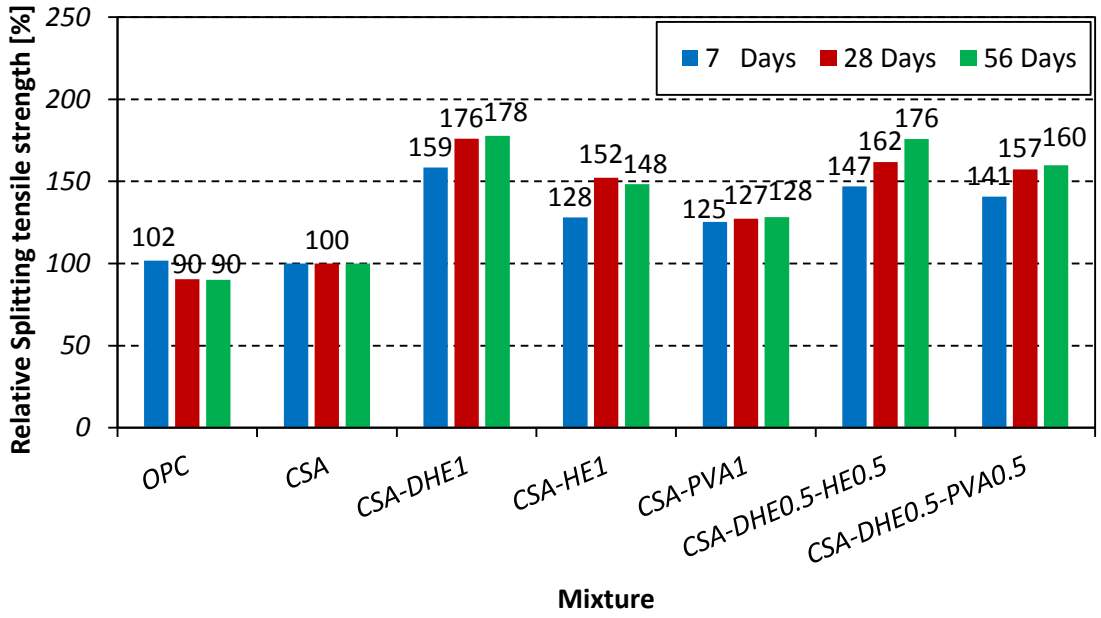


Fig. 6.13 Relative splitting tensile strengths of different fiber-reinforced concretes with water-cement ratio of 0.35

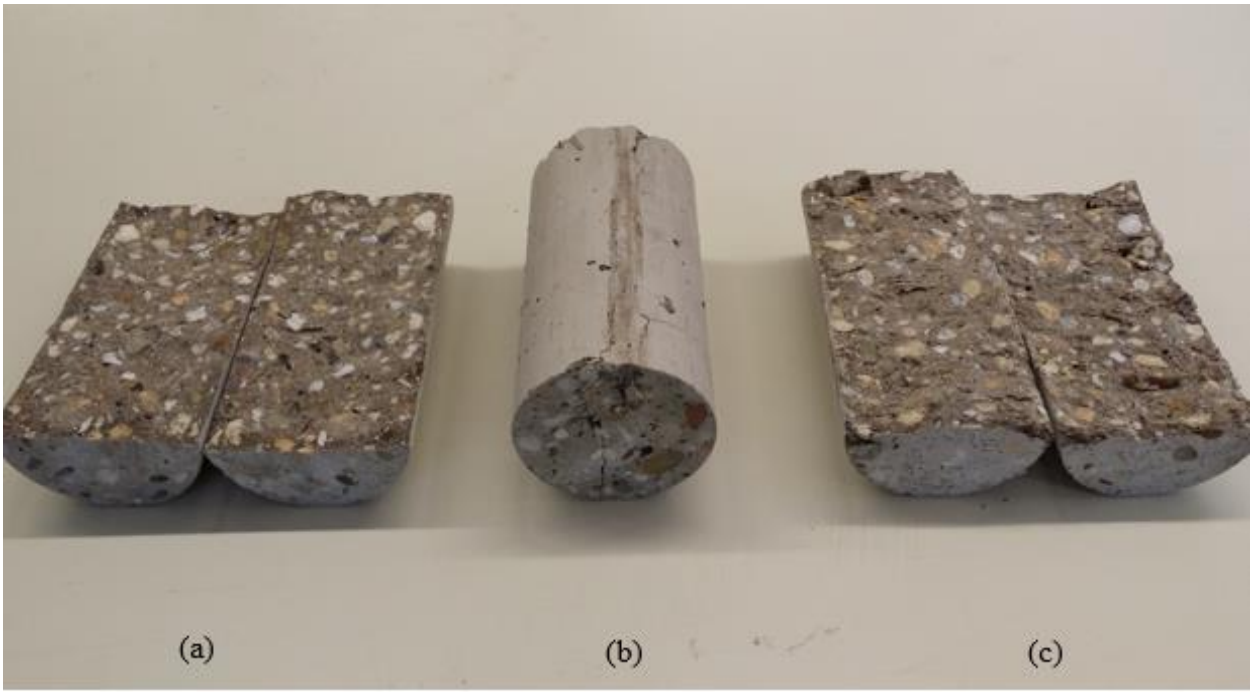


Fig. 6.14 Failure mode of high performance concrete under splitting tensile load: (a) 0% fiber, (b) 1% DHE steel fiber, (c) 1% PVA fiber

The splitting tensile strength results of different FRC mixes with w/c ratio of 0.28 are shown in Fig. 6.15 and listed in Table 6.2. The relative splitting tensile strength of different FRC mixes with w/c ratio of 0.28 compared to that of the reference CSA mix is also shown in Fig. 6.16. The results indicate that by substitution of OPC with CSA cement, the splitting tensile strength increased by 1%, 5%, and 6% at 7, 28, and 56 days, respectively. This slight increase can be attributed to the enhancement of cement matrix properties due to the higher content of ettringite.

For FRC were developed at w/c ratio of 0.28, a similar trend to higher w/c ratio was observed. The addition of fibers in concrete led to an increase in the splitting tensile strength irrespective to the type of the fibers. As it can be seen in Fig. 6.15, the best performing was by the mix containing 1% DHE steel fibers. For instance, the splitting tensile strength of this mix increased by 65%, 88%,

and 81% at 7, 28, and 56 days, respectively over that of the reference CSA concrete. As it can be seen in Fig. 6.16, the increase in the splitting tensile strength of CSA-HE1 mix ranged from 51% to 63%, while this increase for CSA-PVA1 mix varied from 19% to 24% as compared to those of the CSA mix, depending on the testing age. The results of HyFRC show that the substitution a portion of DHE steel fibers with HE steel or PVA fibers led to a reduction in the splitting tensile strength compared to that of the CSA-DHE1, while their strengths were significantly higher than the reference CSA concrete. It was noticed that the combination of DHE steel fibers with HE steel or PVA fibers resulted in an almost similar performance in the splitting tensile strength test. For instance, the splitting tensile strength improvement of CSA-DHE0.5-HE0.5 mix ranged from 59% to 75%, while this improvement for CSA-DHE0.5-PVA0.5 mix varied from 57% to 69% as compared to that of the CSA mix, depending on the testing age.

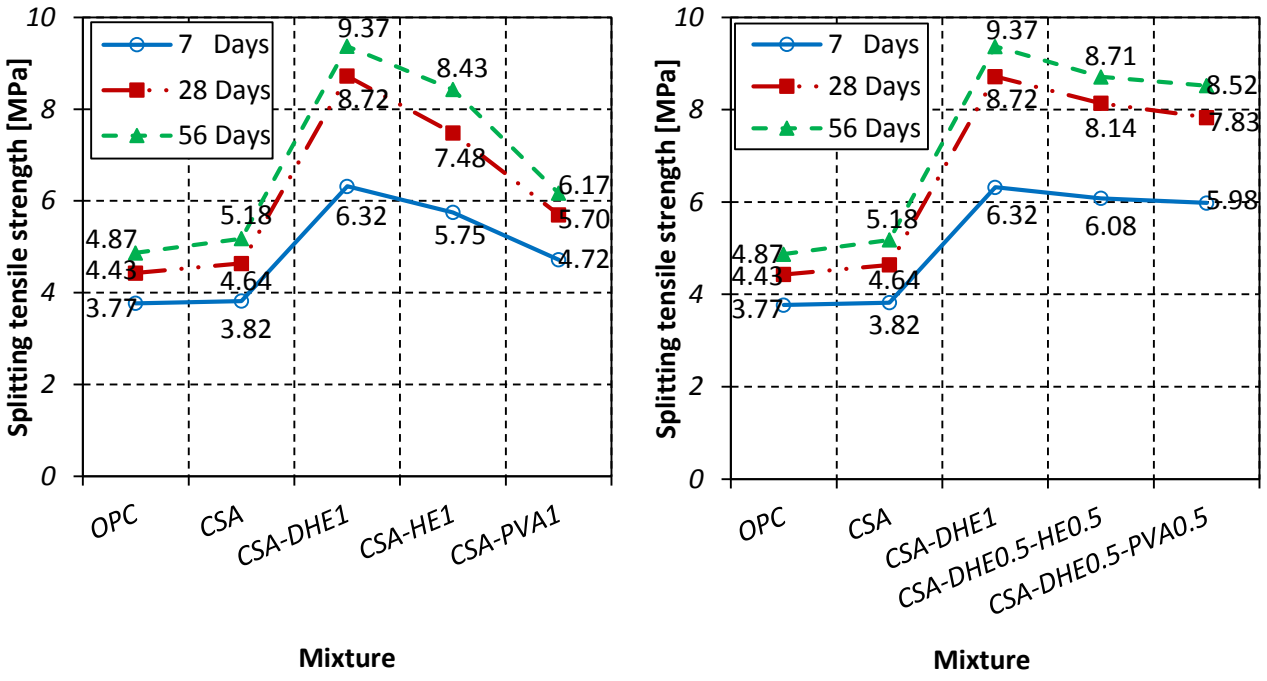


Fig. 6.15 Splitting tensile strengths of different concretes with water-cement ratio of 0.28: (a) fiber-reinforced concretes, (b) hybrid fiber-reinforced concretes

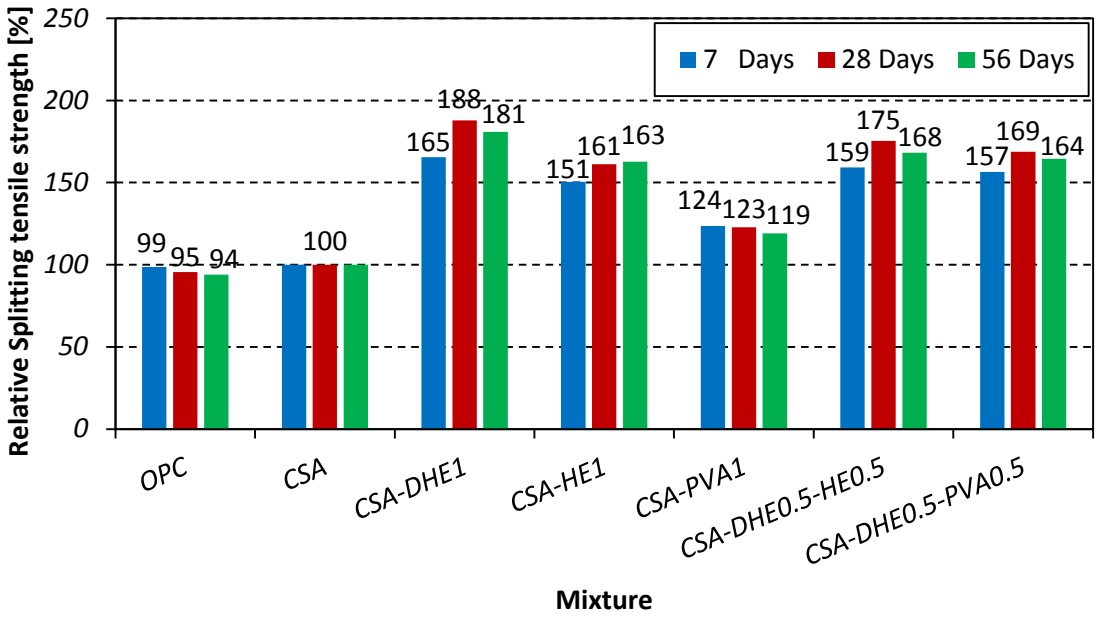


Fig. 6.16 Relative splitting tensile strengths of different fiber-reinforced concretes with water-cement ratio of 0.28

The splitting tensile strength evolution of different concretes compared to their 7 days strength are presented in Table 6.2. As it can be noticed, the improvement in the concrete strength was higher at later ages of curing in all mixes considered in this study. For instance, the 28 and 56 days splitting tensile strengths of OPC mix with w/c ratio of 0.35 were 14% and 26% higher than its 7 days strength, while these increase were 28% and 42% in CSA mix, respectively. The results show that the rate of strength gain in CSA-based concrete was higher over that of the OPC-based concrete. It can be explained by the fact that the CSA cement was hydrated over time and developed a rich amount of ettringite in concrete. As a consequence of that, the properties of cement matrix was improved at later ages and led to an enhancement in the splitting tensile strength. As it can be seen in Table 6.2, the curing age had higher impact on the improvement of FRC strength as compared to that of the concretes without fibers. For example, the average 28 and 56 days splitting tensile strengths of FRC with w/c ratio of 0.35 were 42% and 61% higher than

their 7 days strength. This result suggest that the bond between fibers and cement matrix has been increased over time as a result of cement expansion, and consequently increased the splitting tensile strength of concrete. As it can be noticed in the same table, the effect of curing age on the improvement of splitting tensile strength of concrete was reduced by decreasing the w/c ratio. For example, the average 28 and 56 days splitting tensile strengths of FRC with w/c ratio of 0.28 were 31% and 42% higher than their 7 days strength. This can be explained by the fact that in concretes with low w/c ratio (i.e. 0.28), the free water was consumed significantly at early ages and developed higher strength at 7 days. Therefore, there is a lack of free water inside the concrete for further cement hydration at later ages (i.e. 28 and 56 days).

## 6.4 Modulus of elasticity

The 28-days modulus of elasticity of different FRC mixes with w/c ratio of 0.35 and 0.28 are shown in Figs. 6.17 and 6.18, and their relative modulus of elasticity compared to that of the reference CSA mix are also shown in Figs. 6.19 and 6.20. The results indicate that the full replacement of OPC with CSA cement at both w/c ratios led to an increase in the modulus of elasticity of concrete. These increase were 24% and 19% at w/c ratios of 0.35 and 0.28, respectively as compared to that of the corresponding OPC mixes. This improvement can be attributed to the enhanced properties of the cement matrix by formation of high content of ettringite. As it can be seen in Figs. 6.17 and 6.18, the addition of metallic fibers resulted in negligible increase in the elastic modulus of concrete, while introducing PVA fibers in concrete slightly reduced its modulus of elasticity.

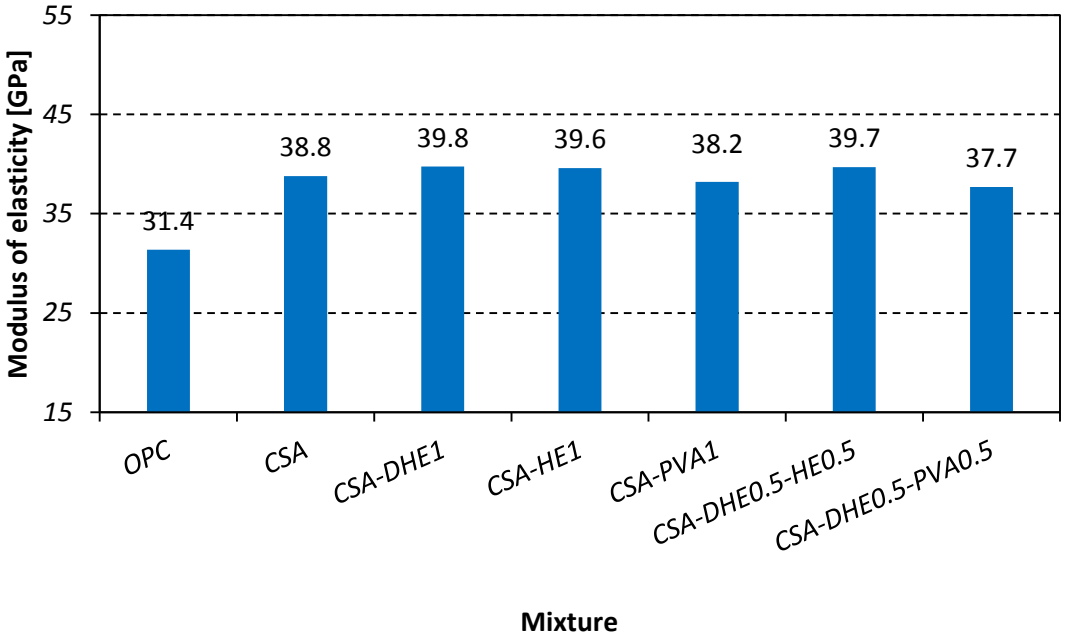


Fig. 6.17 Modulus of elasticity of different fiber-reinforced concretes with water-cement ratio of 0.35

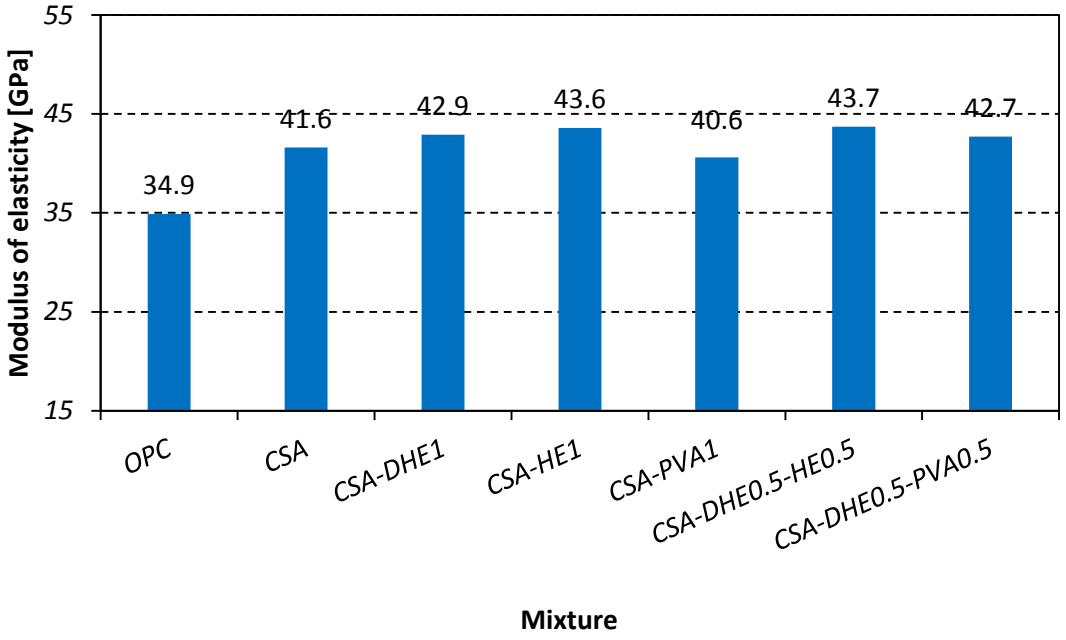


Fig. 6.18 Modulus of elasticity of different fiber-reinforced concretes with water-cement ratio of 0.28

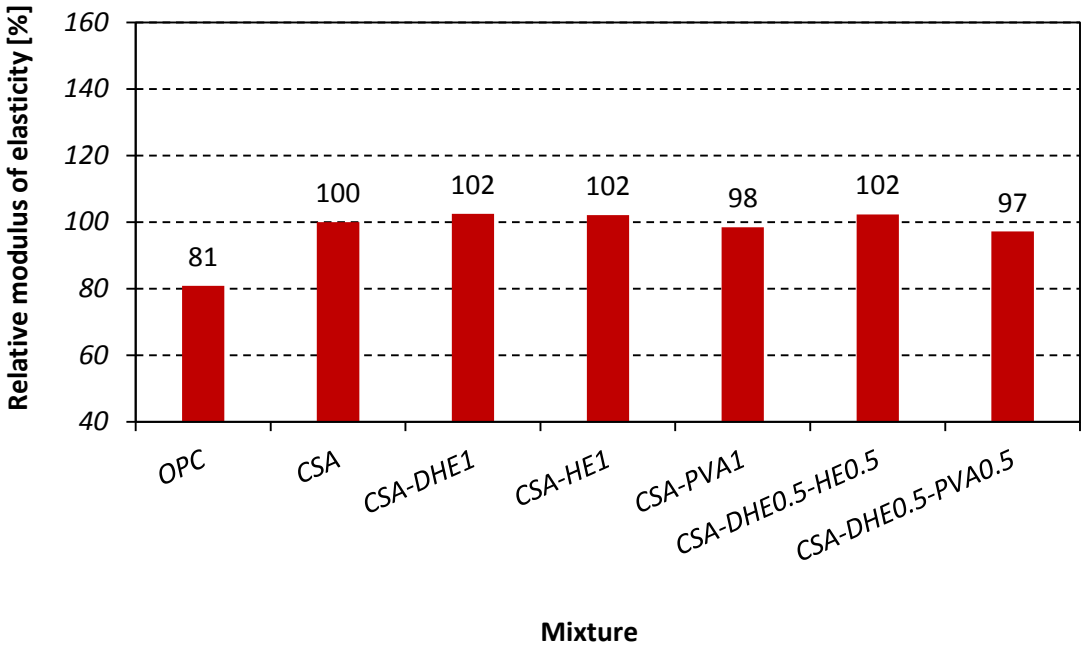


Fig. 6.19 Relative modulus of elasticity of different fiber-reinforced concretes with water-cement ratio of 0.35

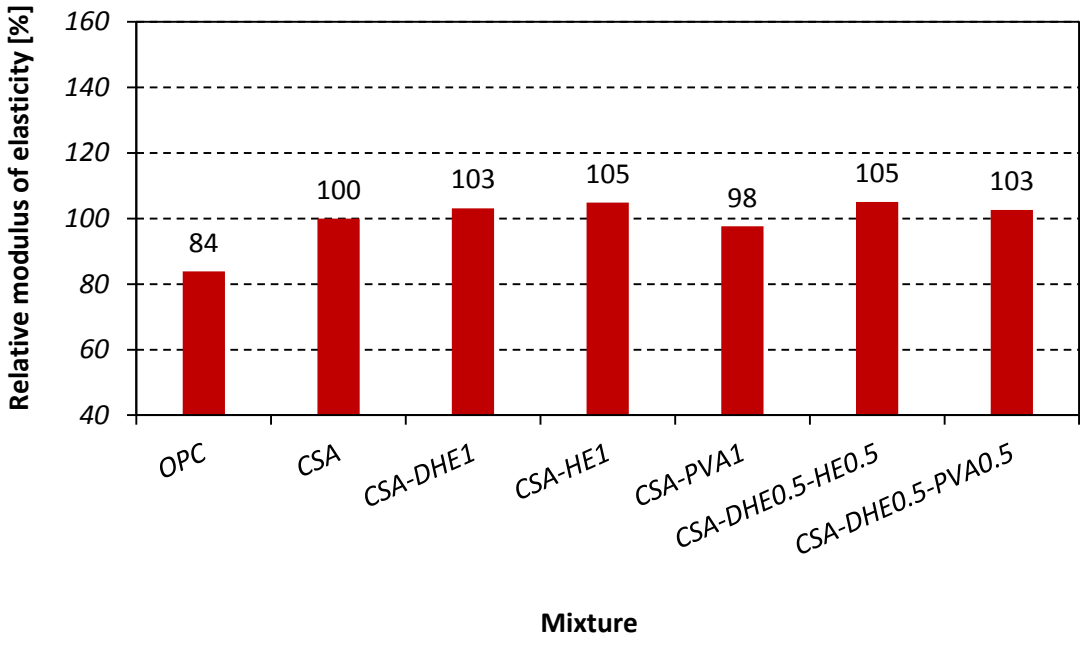


Fig. 6.20 Relative modulus of elasticity of different fiber-reinforced concretes with water-cement ratio of 0.28

The performance of steel fibers was better than that of the PVA fibers due to their higher strength and modulus of elasticity, which subsequently improved the static modulus of the concrete. The results of HyFRC indicate that the substitution a portion of DHE steel fibers with other types of fibers had insignificant influence on the modulus of elasticity of concrete. As it can be noticed in Figs. 6.19 and 6.20, the maximum increases in the elastic modulus of concrete as a result of fiber reinforcement were 2 % and 5% at w/c ratios of 0.35 and 0.28, respectively.

## 6.5 Flexural performance

### 6.5.1 Load-CMOD curve

The diagram of Load-CMOD for different fiber-reinforced concretes with w/c ratio of 0.35 at the ages of 7, 28, and 56 days are shown in Figs. 6.21-6.23. The results indicate that the addition of fibers resulted in an increase in the maximum flexural load of concrete at all curing ages irrespective to the fiber type. For instance, the flexural strength improvement of CSA-DHE1, CSA-HE1, and CSA-PVA1 mixes ranged from 55% to 73%, 37% to 42%, and 7% to 15%, respectively, depending on the testing age. As it can be noticed, the concretes containing 1% DHE steel fibers exhibited the best performance compared to other FRC considered in this study. The significant influence of DHE steel fibers on the flexural strength of concrete is attributed to its high tensile strength, elastic modulus, and effective anchoring mechanism, which restrained the extension of macro-cracks in concrete. The results further indicate that the Load-CMOD behavior of concretes is significantly different, depending on the fiber type was used. As can be observed in Figs. 6.21-6.23, introducing 1% DHE steel fibers in CSA concrete resulted in a deflection-hardening behavior in concrete, while concretes reinforced with 1% HE steel fibers exhibited a deflection-softening performance.

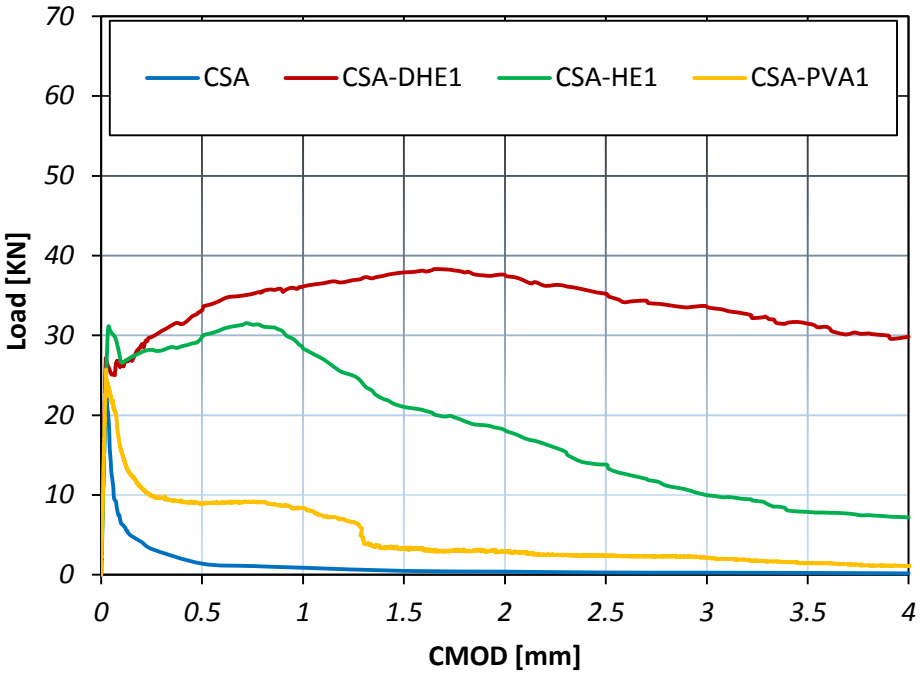


(a)

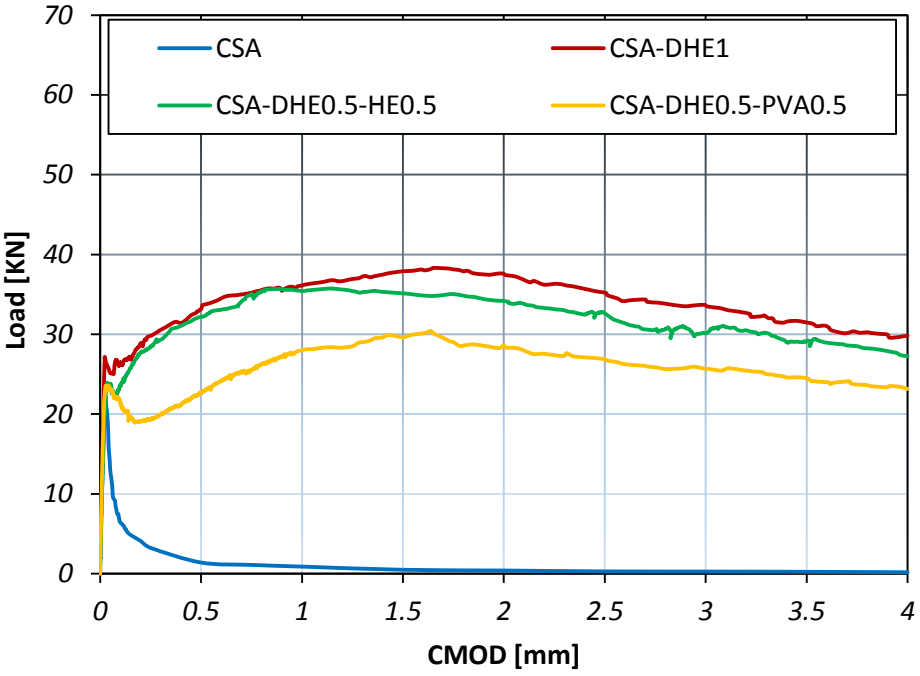


(b)

Fig. 6.21 Load-CMOD curves of different concretes with water-cement ratio of 0.35 at curing age of 7 days: (a) fiber-reinforced concretes, (b) hybrid fiber-reinforced concretes

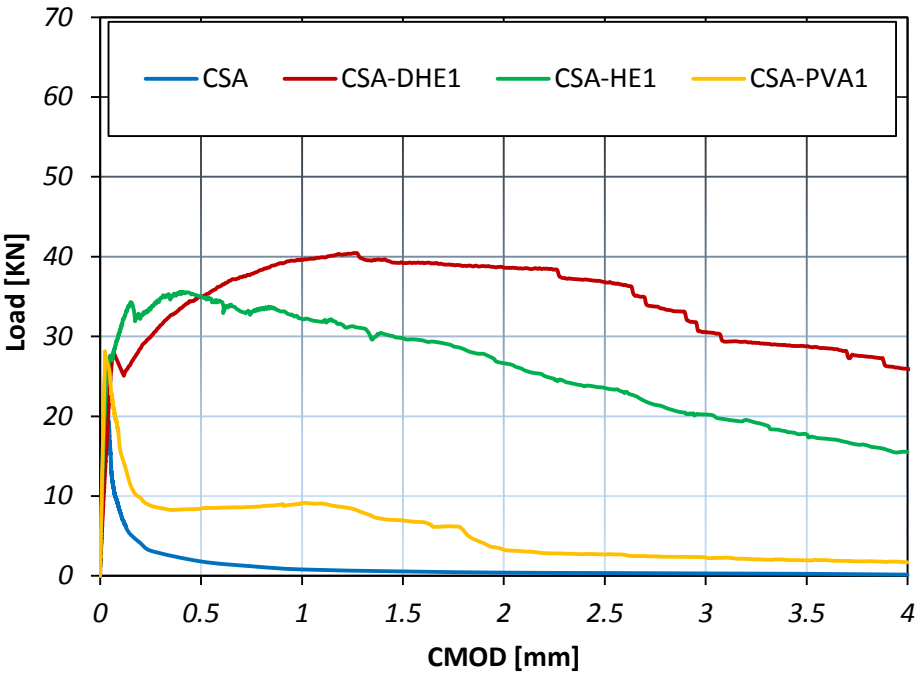


(a)

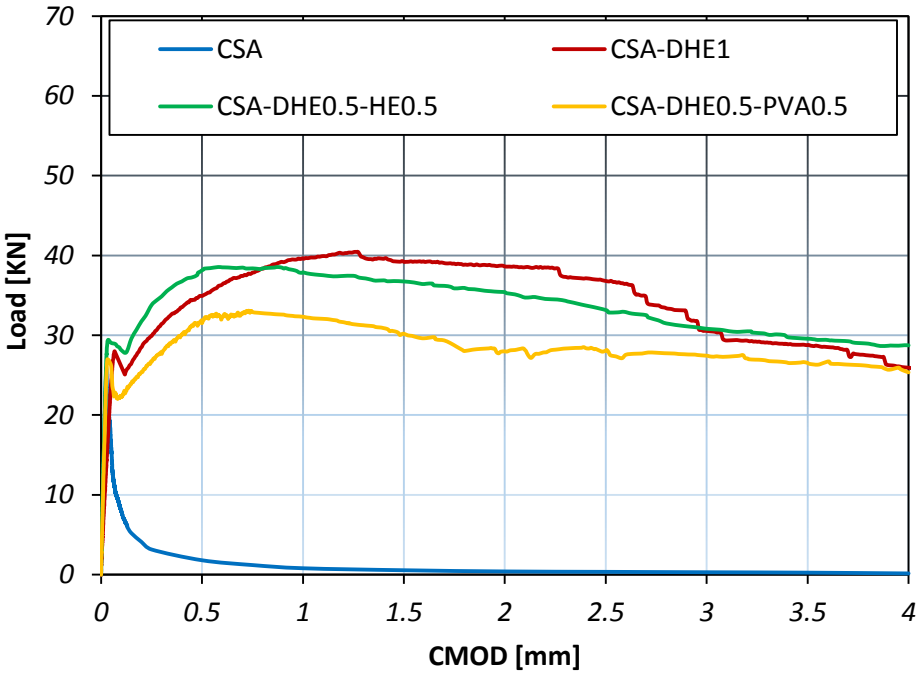


(b)

Fig. 6.22 Load-CMOD curves of different concretes with water-cement ratio of 0.35 at curing age of 28 days: (a) fiber-reinforced concretes, (b) hybrid fiber-reinforced concretes

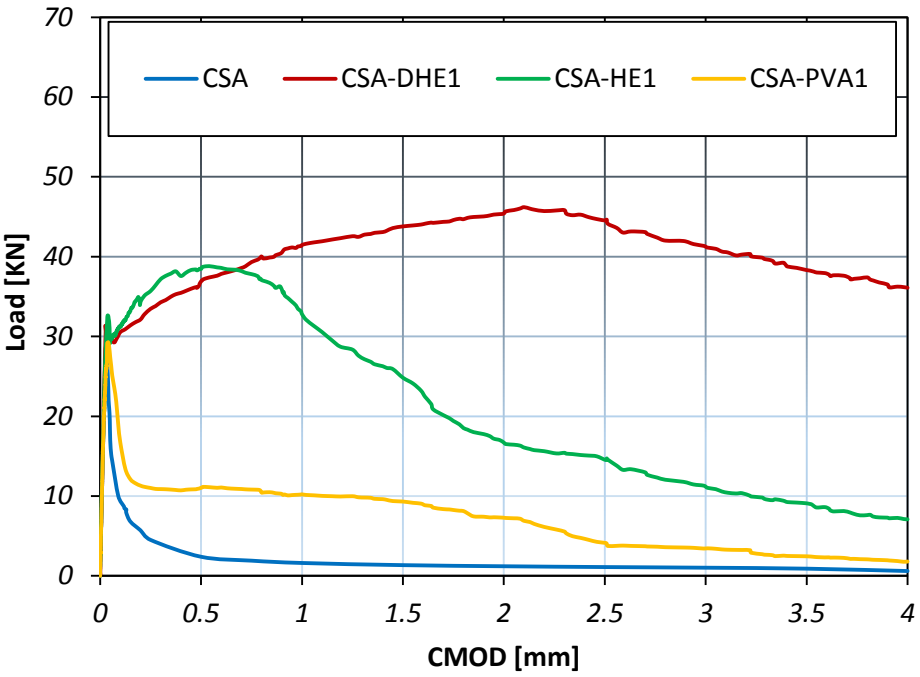


(a)

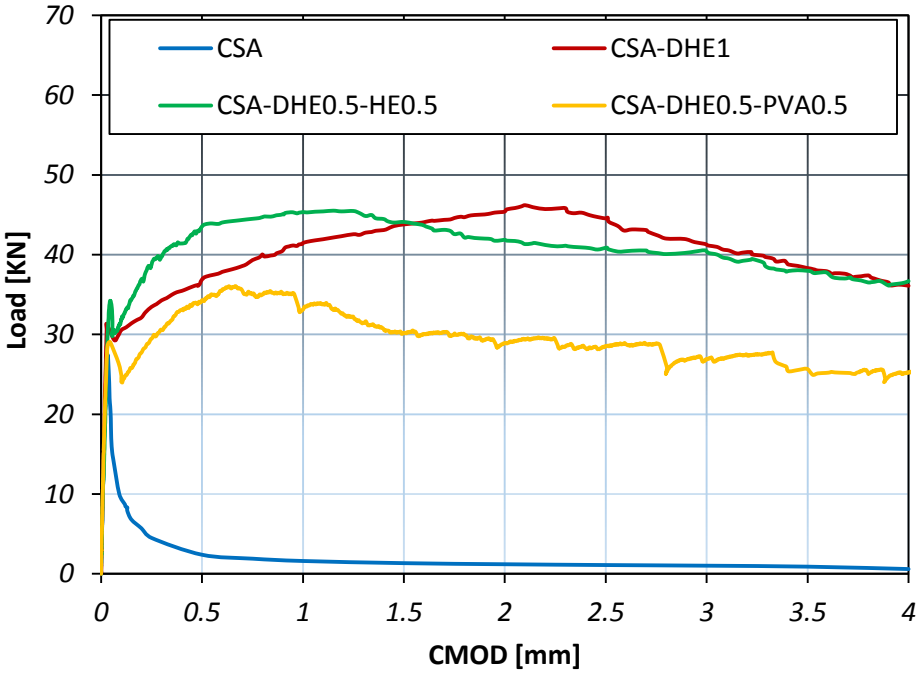


(b)

Fig. 6.23 Load-CMOD curves of different concretes with water-cement ratio of 0.35 at curing age of 56 days: (a) fiber-reinforced concretes, (b) hybrid fiber-reinforced concretes

The results also indicate that the CMOD corresponding to the maximum flexural load varied from 1.26 to 2.11 mm for CSA-DHE1 mix, while this varied from 0.39 to 0.72 mm for CSA-HE1 mix, depending on the testing age. This can be explained by the ability of DHE steel fibers to restrain the propagation of macro-cracks in concrete as a result of its higher length, tensile strength, and anchoring mechanism. On the other hand, HE steel fibers due to their lower tensile strength and length improved the flexural load carrying capacity of concrete beyond the appearance of first crack up to the CMOD equal to 0.72, and caused a deflection-softening behavior due to the extensive cracks creation. Moreover, the results indicate that the addition of PVA fibers in concrete slightly increased the flexural load and after the appearance of first crack, PVA fibers are not able to bridge the macro-cracks and prevent further cracks propagation. As a consequence of that, the flexural load significantly reduced and an almost flat behavior in load carrying capacity of CSA-PVA1 mix was seen.

The results of HyFRC indicate that the substitution a portion of DHE steel fibers with HE steel or PVA fibers led to a reduction in the flexural strength of concrete, while their strength was significantly better over that of the reference CSA concrete. It was observed that the flexural strength improvement of CSA-DHE0.5-HE0.5 and CSA-DHE0.5-PVA0.5 mixes over that of the CSA mix ranged from 48% to 66% and 28% to 37%, respectively, depending on the testing age. When the flexural stress at the fiber-matrix interface has surpassed the bond developed by the matrix, the fibers are either slipping or being unbounded. As a result, the only mechanism that contribute to improve the strength of cracked section is through mechanical anchorage. Therefore, DHE steel fibers used in the present study were able to develop considerably higher maximum pull-out forces compared to those pullout forces that could be developed by HE steel fibers or

straight PVA fibers. As it can be seen in Figs. 6.21-6.23, in general, the load-CMOD curves of all HyFRC developed in this study exhibited a deflection-hardening behavior. The flexural load was reduced after the appearance of first crack, and then the combination of fibers with different sizes or types prevent the formation of macro-cracks in the concrete and the load was increased gradually. This result suggest that the presence of 0.5% DHE steel fibers in HyFRC is very effective to develop concretes with deflection-hardening behavior.

The diagram of Load-CMOD for different fiber-reinforced concretes with w/c ratio of 0.28 at the ages of 7, 28, and 56 days are shown in Figs. 6.24-6.26. In general, a similar trend to the flexural behavior of concretes were developed at w/c ratio of 0.35 was occurred for these mixes. The addition of fibers resulted in an increase in the flexural strength of concrete irrespective to the fiber type. For instance, the flexural strength improvement of CSA-DHE1, CSA-HE1, and CSA-PVA1 mixes ranged from 86% to 92%, 47% to 56%, and 10% to 20%, respectively, depending on the testing age. Similarly, it was observed that introducing 1% DHE steel fibers significantly affect the flexural performance of concrete and resulted in a deflection-hardening behavior, while the addition of other type of fibers caused a deflection-softening behavior. The results indicate that the highest flexural strength was attained by the CSA-DHE1 mix that its flexural strength at 56 days was 16.9 MPa. The results of HyFRC show that the replacement of DHE steel fibers with HE steel or PVA fibers led to a reduction in the flexural strength of concrete. It was observed that the flexural strength improvement of CSA-DHE0.5-HE0.5 and CSA-DHE0.5-PVA0.5 mixes over that of the CSA mix ranged from 61% to 78% and 36% to 56%, respectively, depending on the testing age. However, all the HyFRC were developed in this study show a deflection-hardening behavior due to the prevention of macro-cracks in concrete.

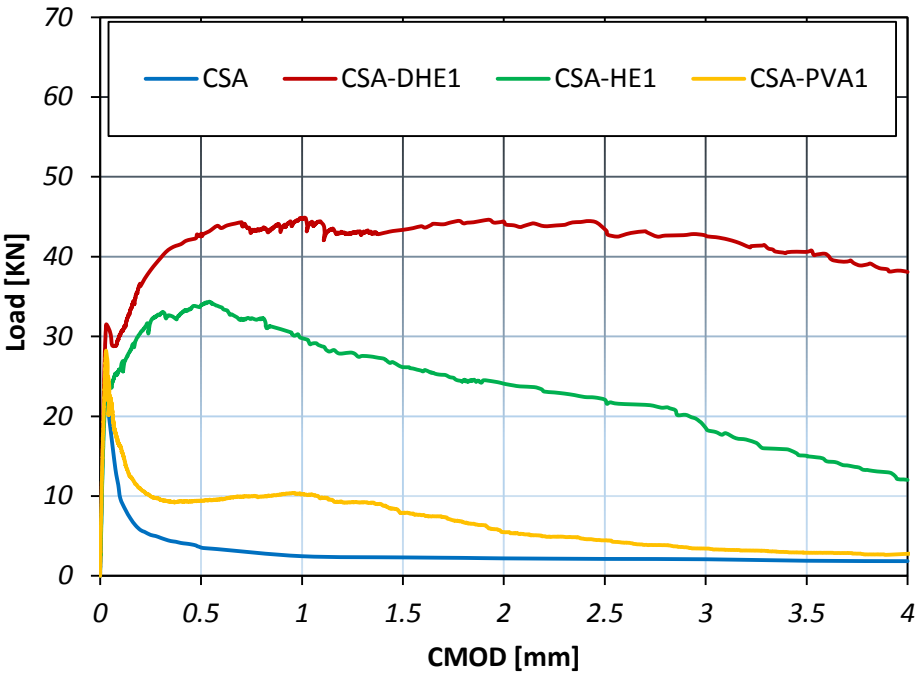


(a)

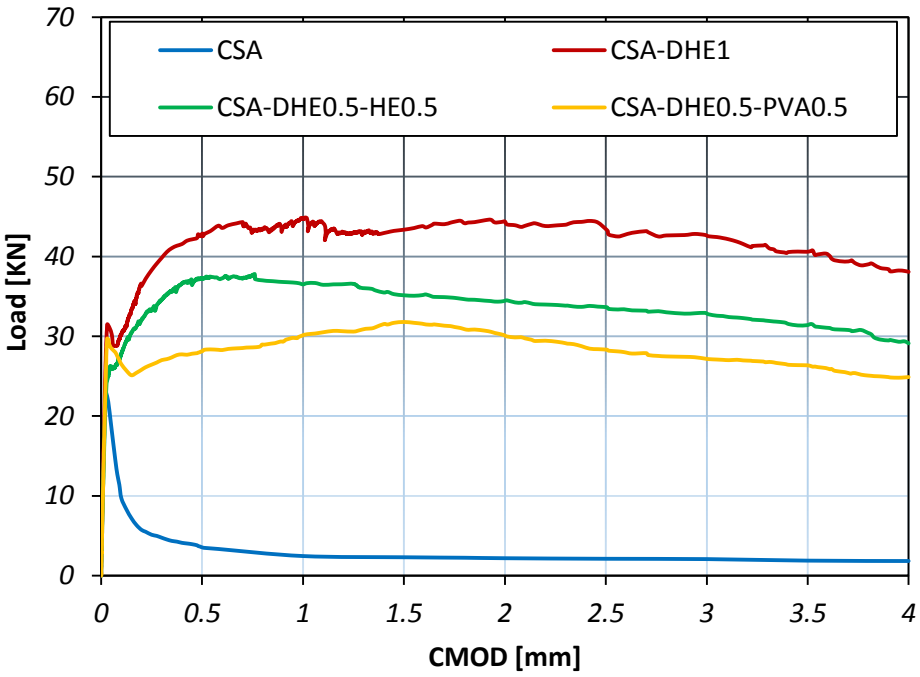


(b)

Fig. 6.24 Load-CMOD curves of different concretes with water-cement ratio of 0.28 at curing age of 7 days: (a) fiber-reinforced concretes, (b) hybrid fiber-reinforced concretes

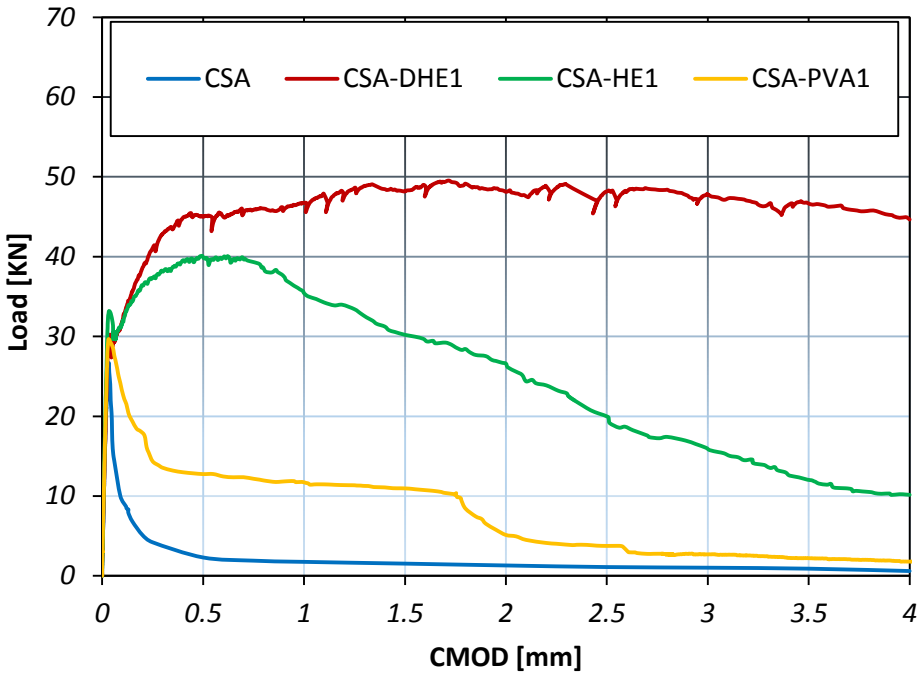


(a)

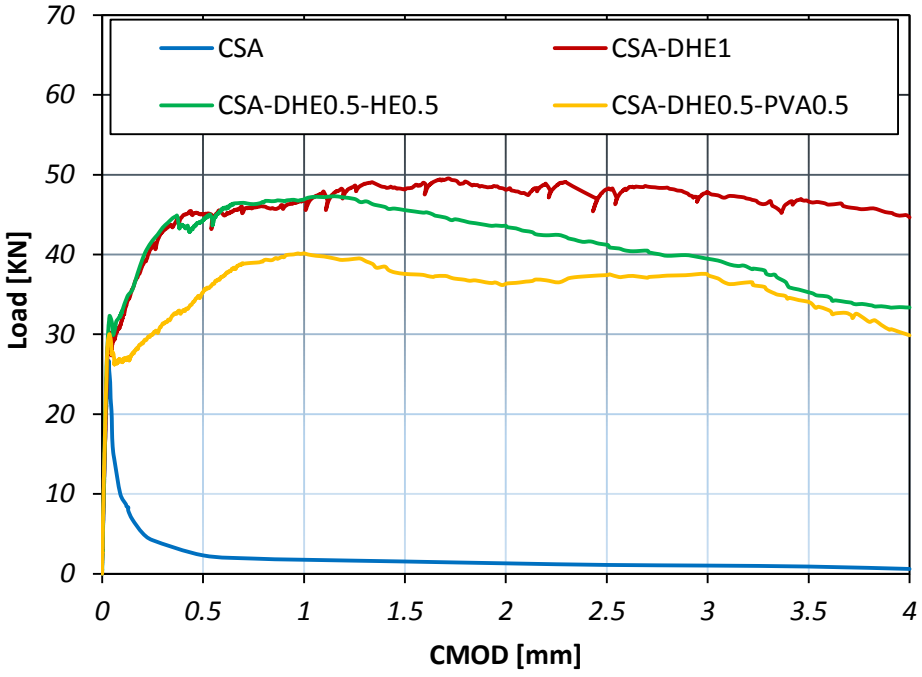


(b)

Fig. 6.25 Load-CMOD curves of different concretes with water-cement ratio of 0.28 at curing age of 28 days: (a) fiber-reinforced concretes, (b) hybrid fiber-reinforced concretes

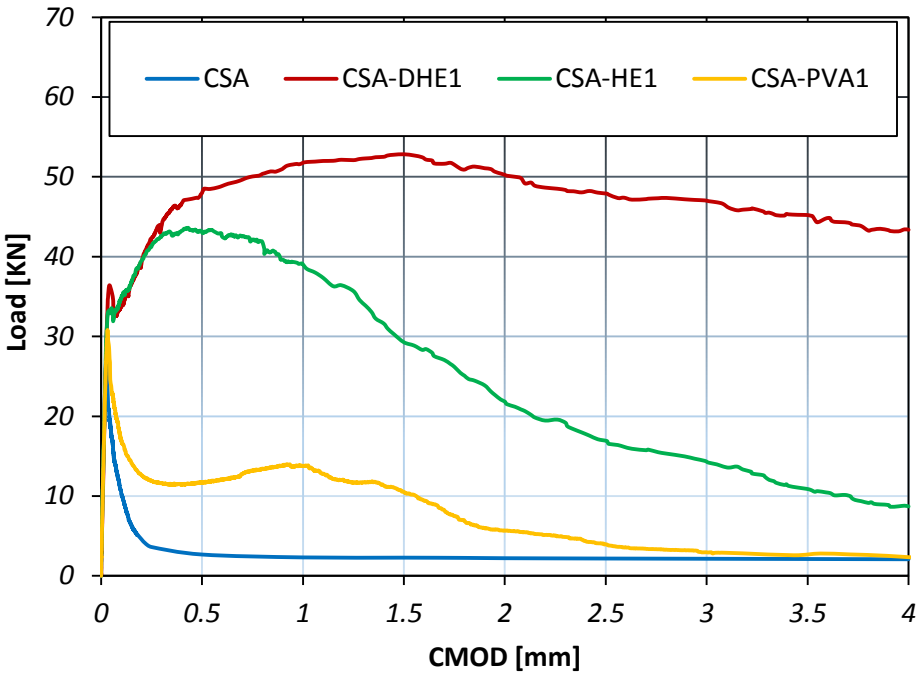


(a)

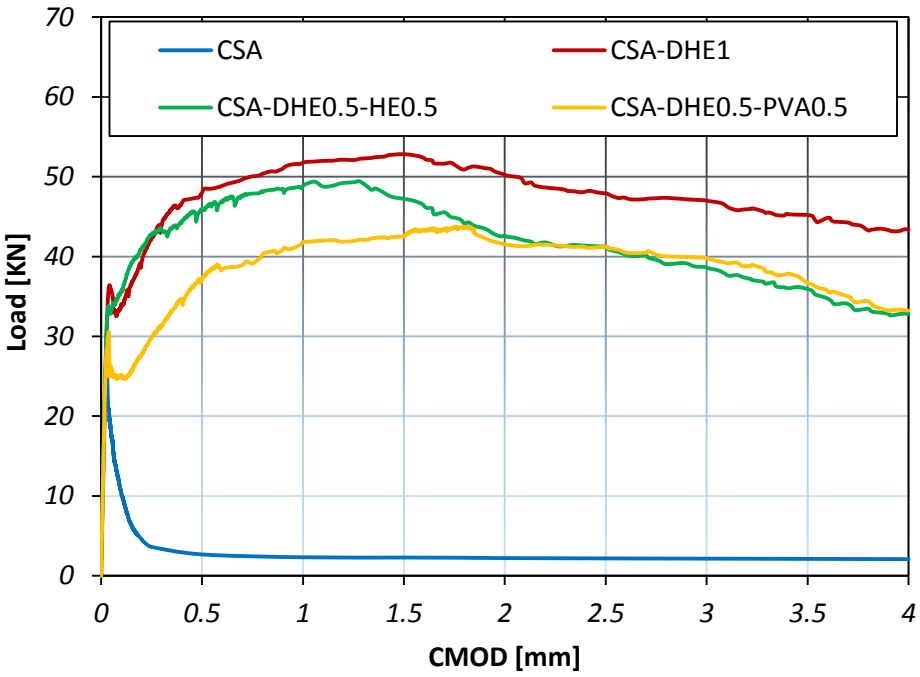


(b)

Fig. 6.26 Load-CMOD curves of different concretes with water-cement ratio of 0.28 at curing age of 56 days: (a) fiber-reinforced concretes, (b) hybrid fiber-reinforced concretes

The comparison of the flexural behavior of CSA-DHE0.5-HE0.5 with CSA-HE1 mixes indicate the better performance of hybrid mix. Since cracks occur at different stages and sizes in concrete, the use of carefully selected fibers with different lengths is a good way to address this problem. The results exhibit that there is a beneficial interaction between the steel fibers with different lengths and shapes, which in turn results in a better performance of the hybrid system than that of the mono type HE steel fiber composite. In other words, it should be taken into account that increasing the maximum flexural load of concretes through the addition of fibers is not enough, and developing FRC that exhibit ductile behavior is of interest to structural engineers.

### 6.5.2 Residual flexural tensile strength

The residual flexural tensile strength for different FRC with w/c ratio of 0.35 at the ages of 7, 28, and 56 days are shown in Figs. 6.27-6.29. The residual flexural strengths corresponding to CMOD at 0.5 mm, 1.5 mm, 2.5 mm, and 3.5 mm are defined as $Fr_1$, $Fr_2$, $Fr_3$, and $Fr_4$, respectively. These values were used to describe the post-cracking behavior of the fiber-reinforced concretes. Generally, it can be seen that the residual flexural tensile strengths reduce by increasing displacement (CMOD) of the specimens and minimum strengths were attained at the CMOD equal to 3.5 mm. However, the mix containing 1% DHE steel fibers shows a distinctive deflection-hardening behavior and its residual flexural strength increases until CMOD of 1.5 mm and gradually reduces at CMOD equal to 2.5 mm. For instance, the $Fr_2$ and $Fr_3$ of CSA-DHE1 mix cured for 28 days increased by 12% and 5% as compared to its $Fr_1$, while the $Fr_4$ reduced by 18% as compared to its $Fr_1$. The results of CSA-HE1 mix at 28 days indicate that the $Fr_2$, $Fr_3$, and $Fr_4$ reduced by 15%, 33%, and 49%, respectively as compared to its $Fr_1$. These results confirm the significant influence of DHE steel fibers in improving the flexural response of concrete and it can

certainly have a major positive contribution in designing concrete structure in resisting bending load.

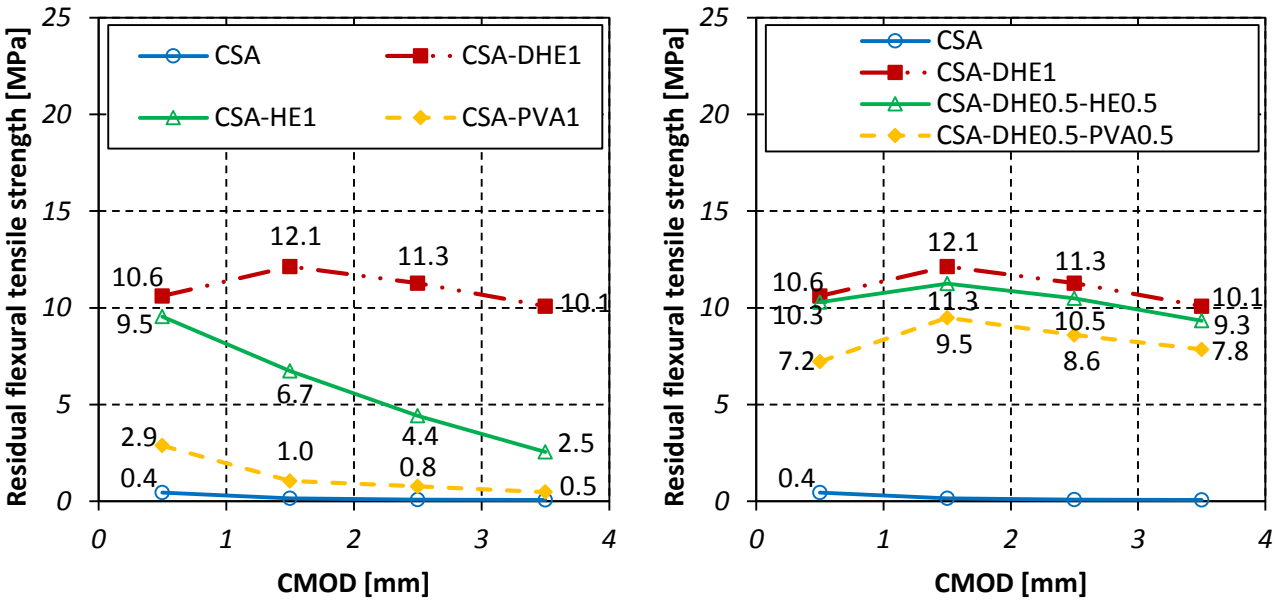


(a) (b)

Fig. 6.27 Residual flexural tensile strength of different concretes with water-cement ratio of 0.35 at curing age of 7 days: (a) fiber-reinforced concretes, (b) hybrid fiber-reinforced concretes

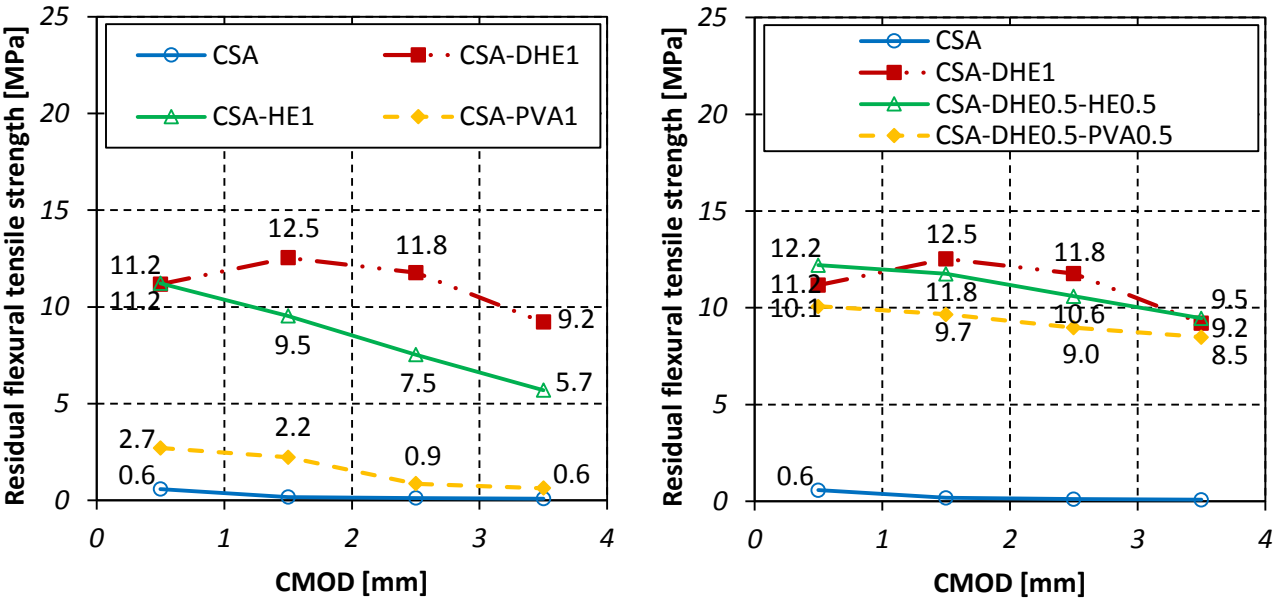


(a) (b)

Fig. 6.28 Residual flexural tensile strength of different concretes with water-cement ratio of 0.35 at curing age of 28 days: (a) fiber-reinforced concretes, (b) hybrid fiber-reinforced concretes

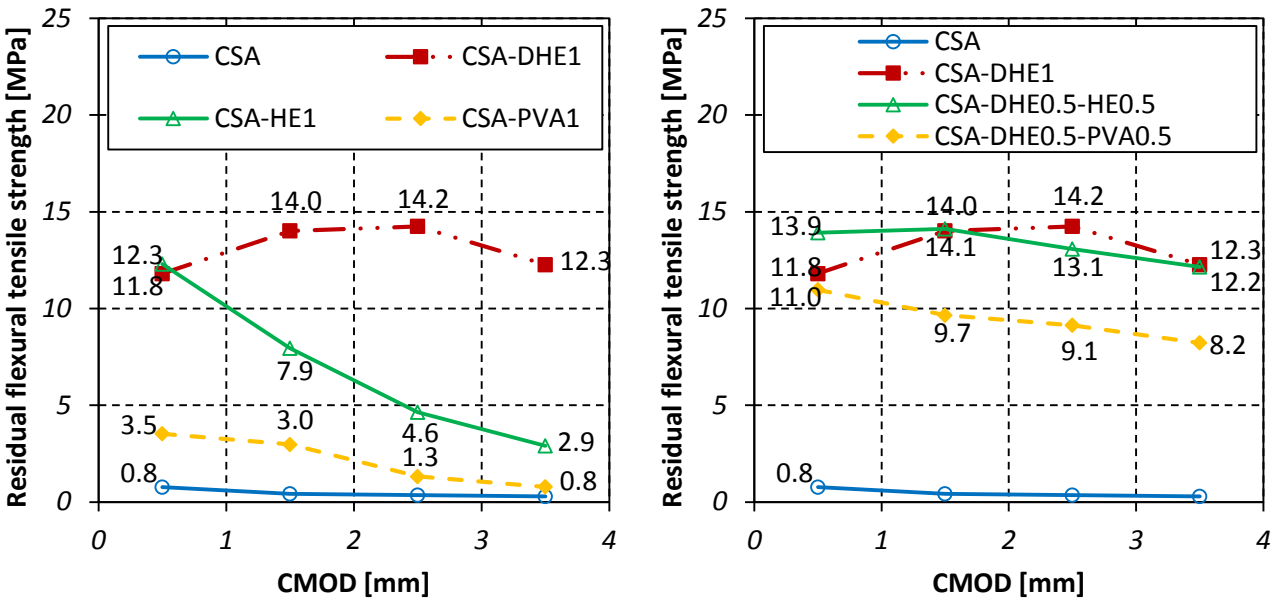


Fig. 6.29 Residual flexural tensile strength of different concretes with water-cement ratio of 0.35 at curing age of 56 days: (a) fiber-reinforced concretes, (b) hybrid fiber-reinforced concretes

The residual flexural tensile strength for different FRC with w/c ratio of 0.28 at the ages of 7, 28, and 56 days are shown in Figs. 6.30-6.32. The results indicate that the residual flexural tensile strengths of concrete reinforced with 1% DHE steel fibers were significantly higher compared to those of the concretes containing 1% HE steel or PVA fibers, particularly at greater CMOD. For instance, the $Fr_3$ of CSA-DHE1, CSA-HE1, and CSA-PVA1 mixes at 28 days were 15.4, 6.4, and 1.2 MPa, respectively. As it can be noticed in Figs. 6.30-6.32, concretes that were manufactured with the addition of 1% DHE steel fiber were the only specimens that carried the flexural load until 3.5-mm CMOD without a major reduction in the load. The reason is that after matrix cracks, the fibers would carry the load that the concrete sustained until further cracking due to failure of fiber anchorage or interfacial bond between the fibers and the matrix [189, 304]. Therefore, DHE steel fibers due to their particular shape can resist the propagation of cracks, absorb more energy,

and increase the load carrying capacity. The results of HyFRC show that the hybridization of fibers is an effective way to produce concretes with deflection-hardening properties. It was observed that the residual flexural strength of HyFRC reduced by replacement a portion of DHE steel fibers with other type of fibers. However, the presence of 0.5% DHE steel fibers in hybrid mixes were enough to develop concretes that can successfully carry the flexural load after the appearance of first crack and prevent the extension of macro-cracks. For example, the $Fr_4$ of CSA-DHE0.5-HE0.5, and CSA-DHE0.5-PVA0.5 mixes at 28 days reduced by 20%, and 4%, respectively as compared to their $Fr_4$.

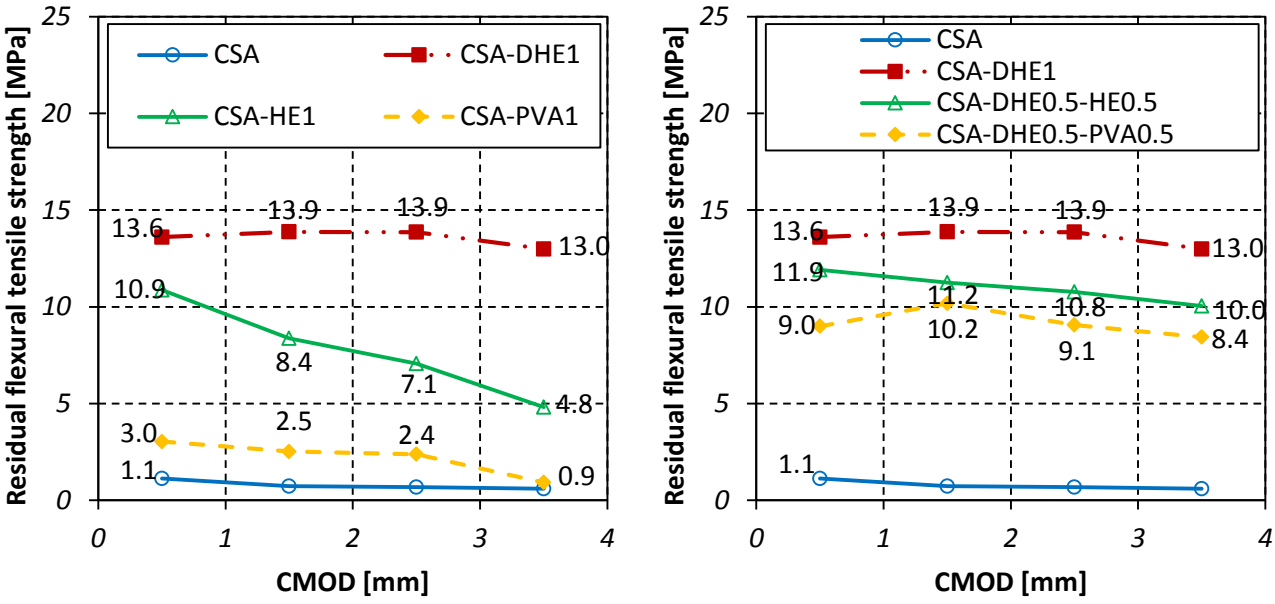


(a) (b)

Fig. 6.30 Residual flexural tensile strength of different concretes with water-cement ratio of 0.28 at curing age of 7 days: (a) fiber-reinforced concretes, (b) hybrid fiber-reinforced concretes

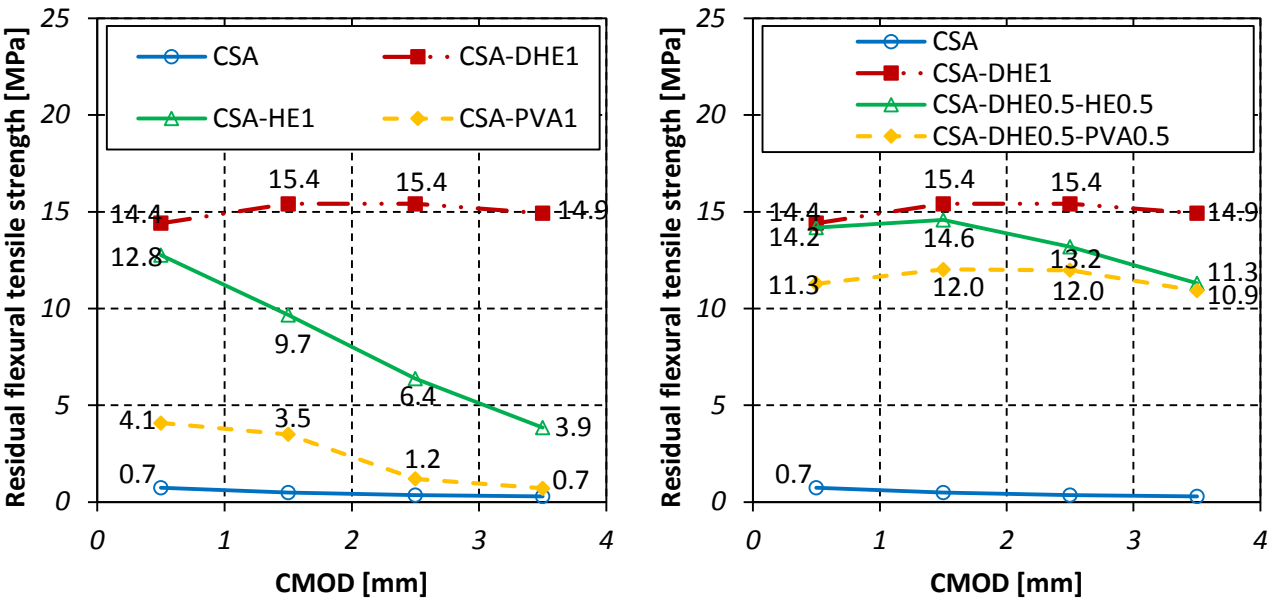


(a) (b)

Fig. 6.31 Residual flexural tensile strength of different concretes with water-cement ratio of 0.28 at curing age of 28 days: (a) fiber-reinforced concretes, (b) hybrid fiber-reinforced concretes

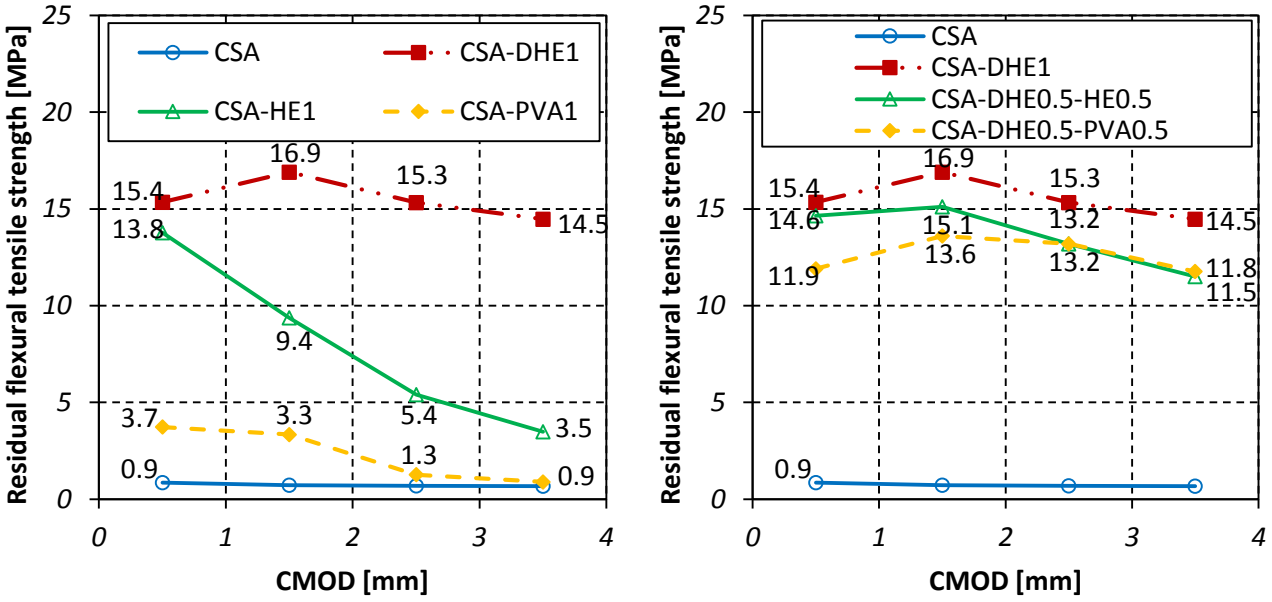


(a) (b)

Fig. 6.32 Residual flexural tensile strength of different concretes with water-cement ratio of 0.28 at curing age of 56 days: (a) fiber-reinforced concretes, (b) hybrid fiber-reinforced concretes

Cracks propagation on the surface of concrete beams reinforced with different type and hybridization of fibers are shown in Fig. 6.33. Also, close-up of cracks propagation are shown in right side of each beams in the same figure. As it can be observed, the plain concrete without any kind of fibers was split into two parts as a result of exceeding the flexural load over the flexural strength of concrete. The results of fiber-reinforced concretes illustrate that the addition of metallic fibers and particularly DHE steel fibers led to the appearance of multiple micro-cracks around a single big crack along the notch. Fig. 6.33 shows that the addition of 1% PVA fibers although improved the flexural strength of concrete by restraining micro-cracks, it was not able to further prevent the extension of macro-cracks and a single big crack was occurred in this mix. It was also observed that the hybridization of fibers with different lengths and types was an effective way to restrain the propagation of cracks with different sizes, and consequently multiple micro-cracks were happened around the main big crack.

Fig. 6.33 Cracks propagation on the surface of concrete beams reinforced with different type and hybridization of fibers (close-up of cracks propagation are shown in right side of each beams)

It should be noted that the orientation of fibers and their distribution in the concrete beams has a significant influence on the flexural performance of concrete. The cross section of fracture concrete beams reinforced with different type and hybridization of fibers and the distribution of fibers on their surface are shown in Fig. 6.34. As it can be seen, DHE steel fibers were dispersed evenly in the cross section of concrete and majority of fibers were aligned perpendicular to the fracture surface. This can result in a good flexural performance as it is already shown in Load-CMOD curves. The Fig. 6.34 further shows that the HE steel fibers were not dispersed uniformly at the cross section of the concrete beams, and some area remained uncovered with the fibers. This may result in the variation of flexural behavior and adversely affect the post-cracking behavior of the specimens. The fractured surface of CSA-PVA1 mix shows that the PVA fibers were ruptured or debonded from the cement matrix. As PVA fibers are straight and have lower length and tensile strength compared to those of the metallic fibers, they are not able to significantly increase the flexural strength of concrete and caused an improvement in the flexural toughness of concrete. It was also observed that steel fibers were distributed uniformly in the cross section of CSA-DHE0.5-HE0.5 mix that consequently resulted in an increase in the maximum flexural load and post-cracking performance of concrete.

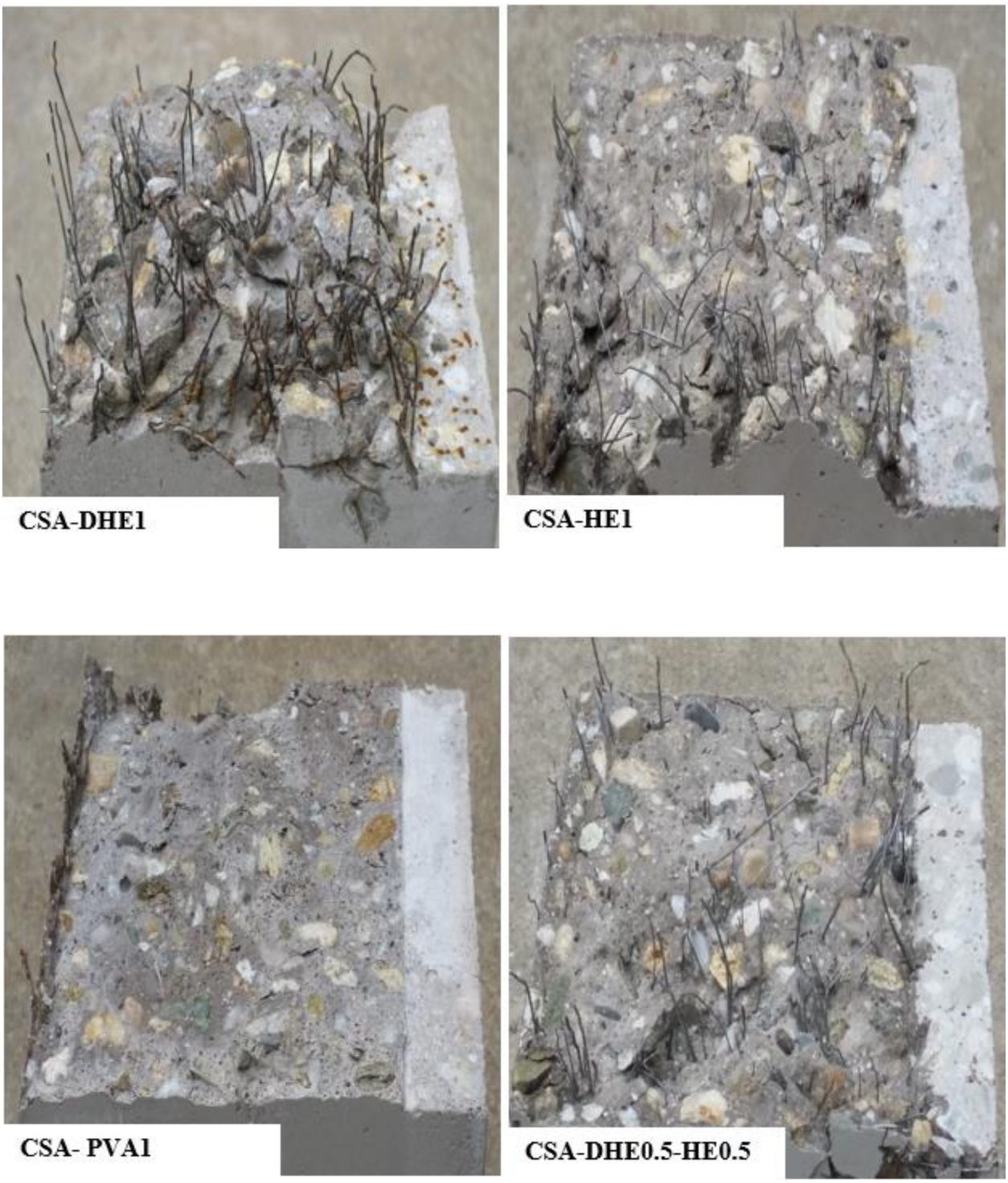


Fig. 6.34 Cross section of fracture concrete beams reinforced with different type and hybridization of fibers and the distribution of fibers on their surface

## 6.6 Dimensional stability under drying condition

The results of the dimensional stability test under drying condition for different fiber-reinforced concretes with w/c ratio of 0.35 are shown in Fig. 6.35. Additionally, the shrinkage deformations of different specimens at 1 and 56 days are shown in Fig. 6.36. Drying shrinkage has a serious impact on the structural and durability performance of the concrete. Shrinkage cracking in concrete structures may accelerate other forms of damage in concrete such as corrosion, freeze/thaw damage, and subsequently shorten the service life of structures [195, 196]. Shrinkage of concrete due to loss of water is closely linked to the properties of cement paste, in which pore structure, specifically pore size is principal factor. The shrinkage of concrete is also affected by many different parameters such as composition of the concrete, method of curing, ambient temperature, and humidity condition [197]. The results indicate that the concrete was produced by using OPC exhibited the highest shrinkage strain among all mixes considered in this study. As it can be seen in Fig. 6.35, the full replacement of OPC with CSA cement resulted in an expansion in the 1 day, and caused lower shrinkage strain at later ages as compared to that of the OPC mix. It was observed that the shrinkage strain of CSA mix was reduced by 38% over that of the OPC mix at 56 days. The lower shrinkage of CSA concrete can be attributed to the ettringite formation as a result of ye'elimite hydration, which reduces the shrinkage of concrete and results in volume stability. The results further indicate that the shrinkage of OPC mix was not tended to stabilize even after 56 days, while the CSA mix was dimensionally stabilized after 14 days.

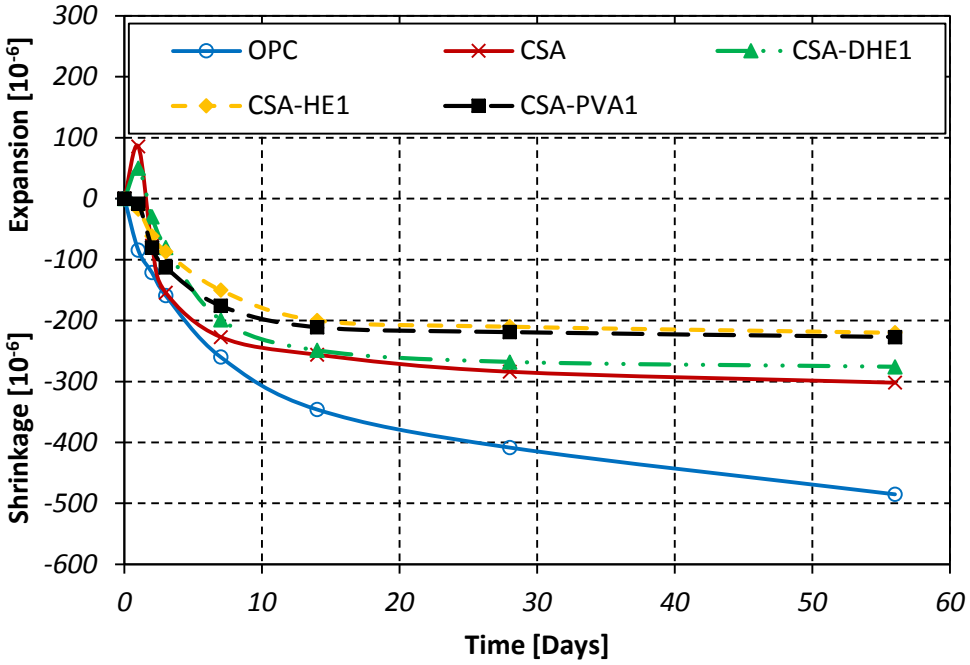


(a)

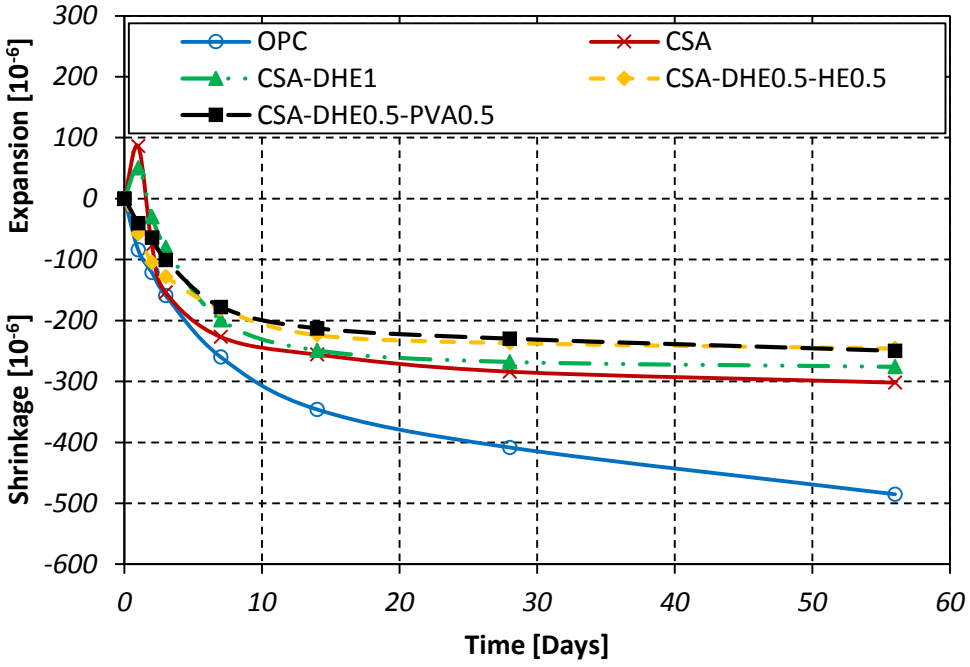


(b)

Fig. 6.35 Dimensional stability of different concretes with water-cement ratio of 0.35: (a) fiber-reinforced concretes, (b) hybrid fiber-reinforced concretes

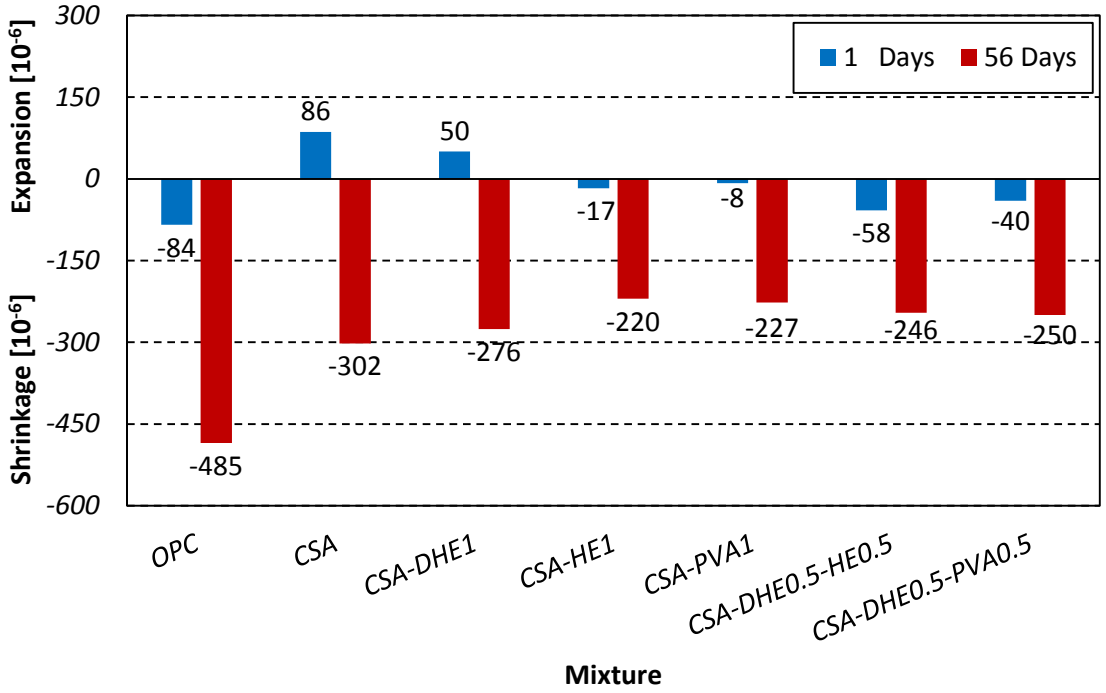


Fig. 6.36 Shrinkage or expansion deformation of different concretes with water-cement ratio of 0.35 at 1 and 56 days

The results also indicate that the addition of fibers in CSA concrete caused a reduction in the shrinkage stain irrespective to the fiber type. It was observed that the HE steel and PVA fibers also fully canceled the expansion of concrete at 1 day, while an expansion equal to 50 µm/m was occurred in the mix containing 1% DHE steel fibers. As it can be noticed in Fig. 6.36, the shrinkage strains of CSA-DHE1, CSA-HE1, and CSA-PVA1 mixes at 56 days were 276, 220, and 227 µm/m, respectively that reduced by 9%, 27%, and 25% as compared to that of the CSA mix. The higher efficiency of HE steel and PVA fibers in restraining the shrinkage of concrete can be explained by the fact the higher number of fibers were available in cement composites, which resulted in volume stability of those concretes. The results of HyFRC show that concretes were manufactured by hybridization of fibers exhibited lower shrinkage strain as compared to mono type use of DHE steel fibers. The drying shrinkage strains of CSA-DHE0.5-HE0.5 and CSA-DHE0.5-PVA0.5

mixes at 56 days were 246 and 250 μm/m, respectively that reduced by 19%, and 17% as compared to that of the CSA mix. The significant effect of the combined use of steel fibers and PVA fibers on the inhibiting shrinkage of concrete has been also reported by Sun et al. [217].

The results of the dimensional stability test under drying condition for different fiber-reinforced concretes with w/c ratio of 0.28 are shown in Fig. 6.37. Additionally, the shrinkage deformations of different specimens at 1 and 56 days are shown in Fig. 6.38. The results indicate that similar to the concretes with w/c ratio of 0.35, the highest shrinkage strain was attained by the OPC mix. It was observed that the full replacement of OPC with CSA cement led to a reduction of 43% on the shrinkage strain of concrete at 56 days. This is in agreement with the finding of other researchers that show the inclusion of CSA cement in concrete causes lower shrinkage over that of the OPC mix [330]. The results further indicate that on the contrary of concretes were manufactured at higher w/c ratio (i.e. 0.35), no evidence of expansion was occurred in CSA-based mixes at w/c ratio of 0.28. In other words, the expansion of concrete at 1 day has been fully canceled and a greater amount of shrinkage was happened at early ages as compared to concretes with w/c ratio of 0.35. This can be explained by the appearance of autogenous shrinkage that was occurred at these concretes as a result of higher cement content and lower w/c ratio were used. However, the shrinkage strain of concretes at later ages (i.e. 56 days) was lower as compared to concrete with higher w/c ratio. Cheung and Leung [198] have also studied the autogenous and drying shrinkage of concrete were produced at different water-binder ratios of 0.19, 0.3, and 0.4. They reported that the autogenous shrinkage represented a significant proportion of the total shrinkage in the concrete with a water-binder ratio of 0.19, whereas this was much reduced in concretes with higher water-binder ratios of 0.3 and 0.4.

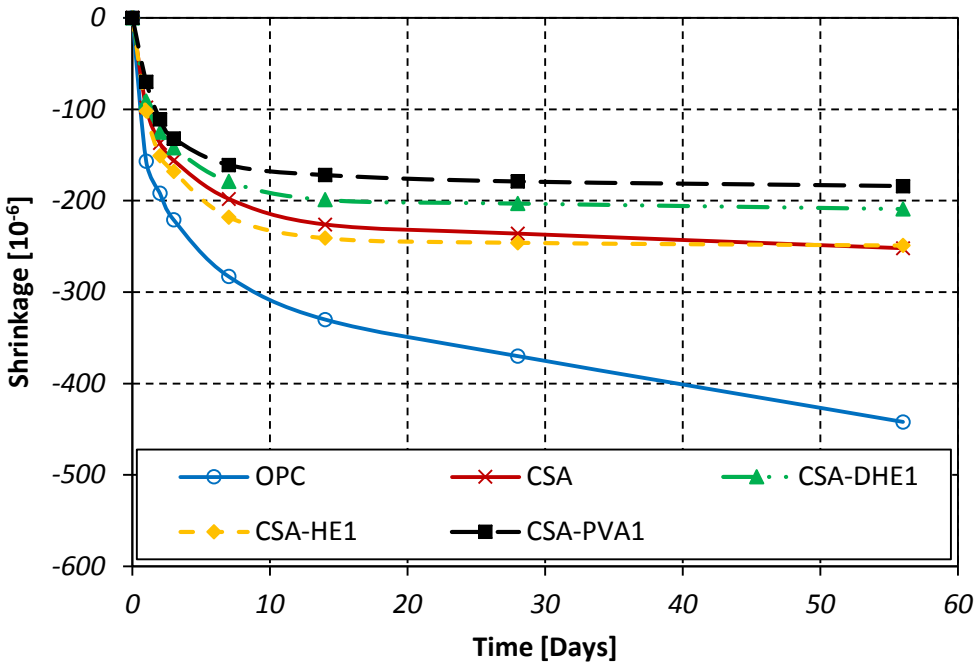


(a)

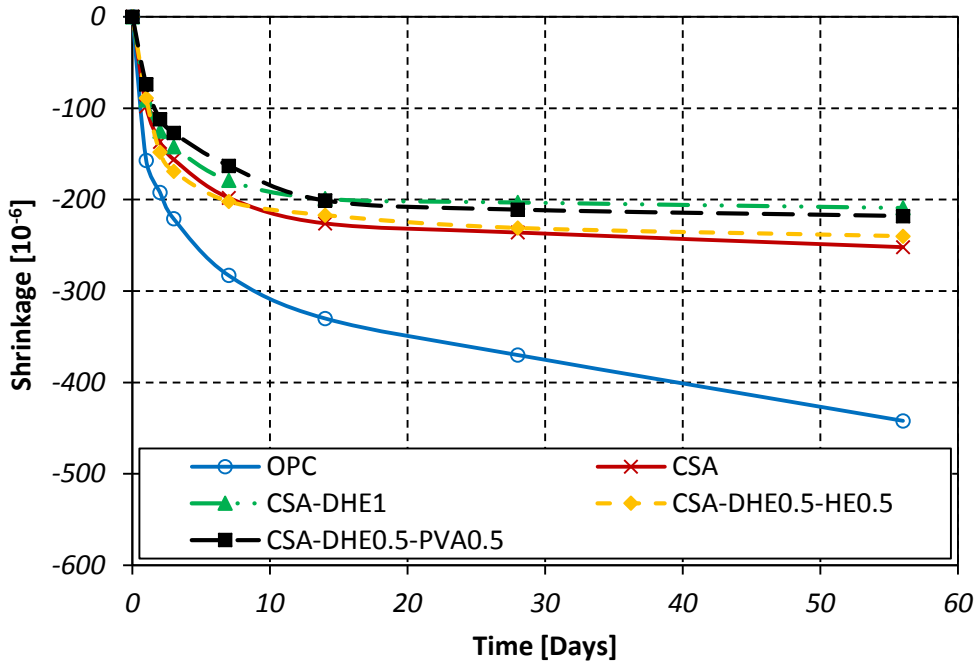


(b)

Fig. 6.37 Dimensional stability of different concretes with water-cement ratio of 0.28: (a) fiber-reinforced concretes, (b) hybrid fiber-reinforced concretes

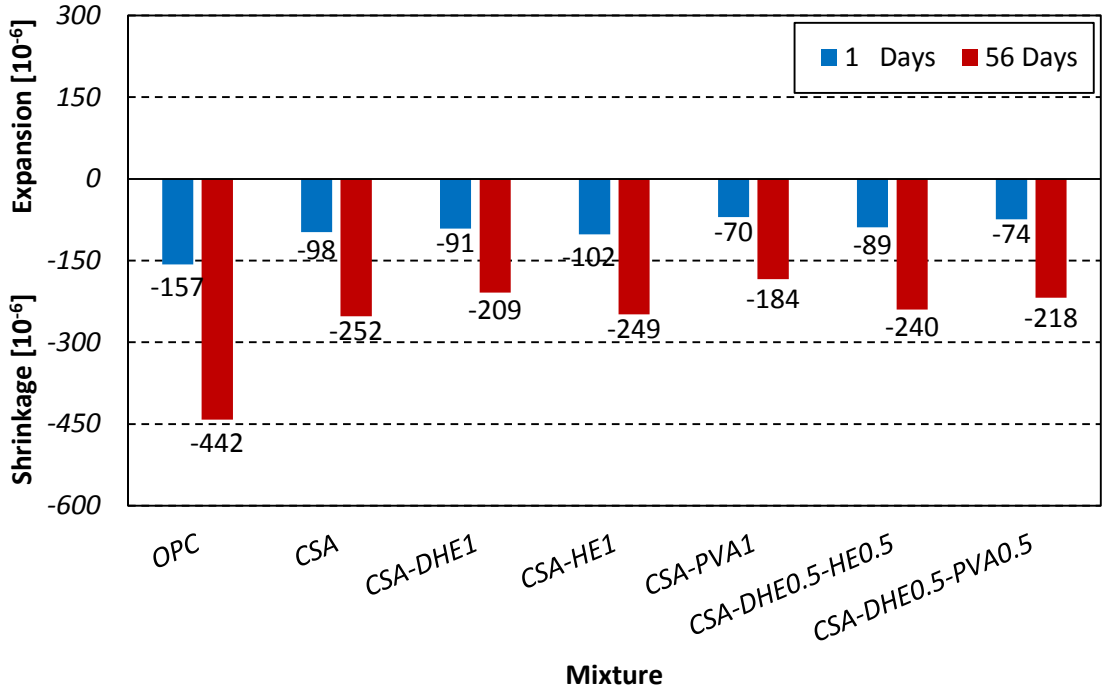


Fig. 6.38 Shrinkage deformation of different concretes with water-cement ratio of 0.28 at 1 and 56 days

The results of fiber-reinforced concretes show that the addition of fibers in concrete resulted in a reduction in the shrinkage strain irrespective to the type of fibers. As it can be seen in Figs. 6.37 and 6.38, the lowest shrinkage strain was developed by the mix containing 1% PVA fibers that reduced by 27% as compared to that of the reference CSA mix. It was followed by the CSA-DHE1 and CSA-HE1 mixes that attained a shrinkage strain of 209 and 249 µm/m, respectively, while the shrinkage of reference CSA mix was 252 µm/m. This result is in good agreement with previous research that showed that the fibers can arrest propagation of cracking produced as a result of drying shrinkage [135, 215]. The results of HyFRC indicate that the hybridization of fibers had an insignificant influence on the shrinkage strain of concretes, while these mixes exhibited lower shrinkage strain as compared to that of the reference CSA mix. The comparison between the results of concretes produced with different w/c ratios illustrate that reducing the w/c ratio resulted in a

lower final shrinkage, while the shrinkage of concrete was increased at early ages as a result of higher autogenous shrinkage.

## 6.7 SEM observations

To provide microscale morphology for the tested samples, SEM were conducted on the flexural-test samples at secondary electron (SE) modes. To have a reliable knowledge about the microstructure, large numbers of images were collected and analyzed. Here, representative images are shown in Fig. 6.39. As it can be seen in Fig. 6.39, the hydrated matrix of OPC concrete covered by its main hydration product that is C-S-H, followed by some crystals of ettringite and portlandite. The featureless paste is the anhydrous cement and the hydration product C-S-H gel. Obviously, needles crystal with hexagonal cross section are assigned to ettringite crystal. Fig. 6.39 shows that the ettringite needles formed in the OPC concrete have small size; 0.05-0.3 μm wide, and up to 3 μm length. Additionally, the plate crystals are assigned to calcium hydroxide (portlandite) crystals. It was also observed that some micro-cracks and pores were generated in the surface of hydrated cement matrix. In general, hardened type I cement paste resembles the microstructure of a typical hydrated matrix of OPC. Fig. 6.39b shows the formation a rich amount of ettringite in the CSA cement based concrete as a result of ye'elimite hydration. It can be seen that the size of prismatic ettringite crystals varied between 0.1-0.5 μm wide, and 2-6 μm length. The presence of high amount prismatic ettringite crystals in CSA concrete can be responsible for its higher mechanical properties strength compared to those of the OPC concrete. As expected, the lower shrinkage strain was occurred in CSA concrete can also be attributed to the ettringite formation with expansive

features. The SEM observation shows that there is a good correlation between the mechanical, physical, and microstructural properties of concretes developed in this study.

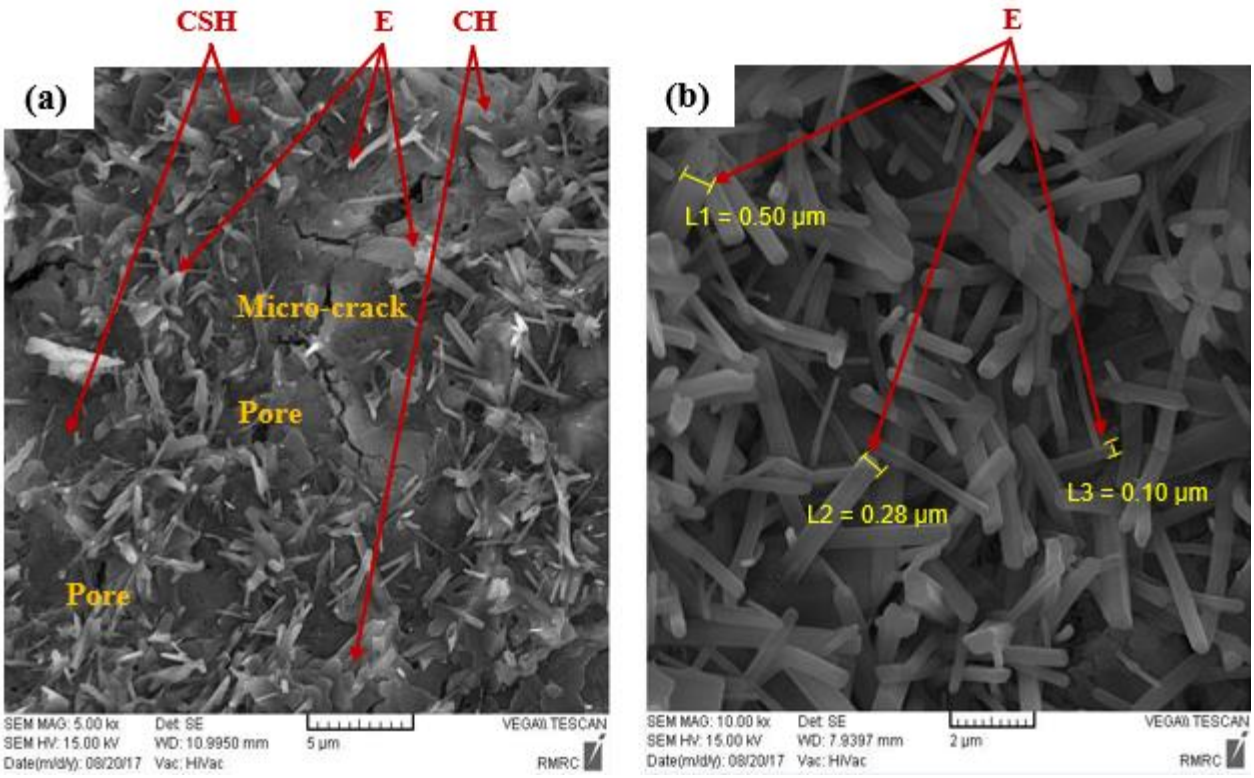


Fig. 6.39 SEM images of different concretes with water-cement ratio of 0.28: (a) OPC concrete, (b) CSA concrete (E: ettringite, CH: portlandite, CSA: calcium silicate hydrate)

Fig. 6.40 shows the SEM observation performed on the fiber-reinforced concretes to investigate the bond between the fibers and cement matrix. As it can be seen in Fig. 6.40a, there is a good bond between the metallic fiber and cement matrix, and a significant amount of hydrated cement adhered on the surface of steel fiber. Similarly, Fig. 6.40b shows that a great amount of cement past covered the surface of PVA fibers. This result confirm that the inclusion of CSA cement in concrete improves the chemical bond between fibers and cement matrix due to the expansion nature of this cement.

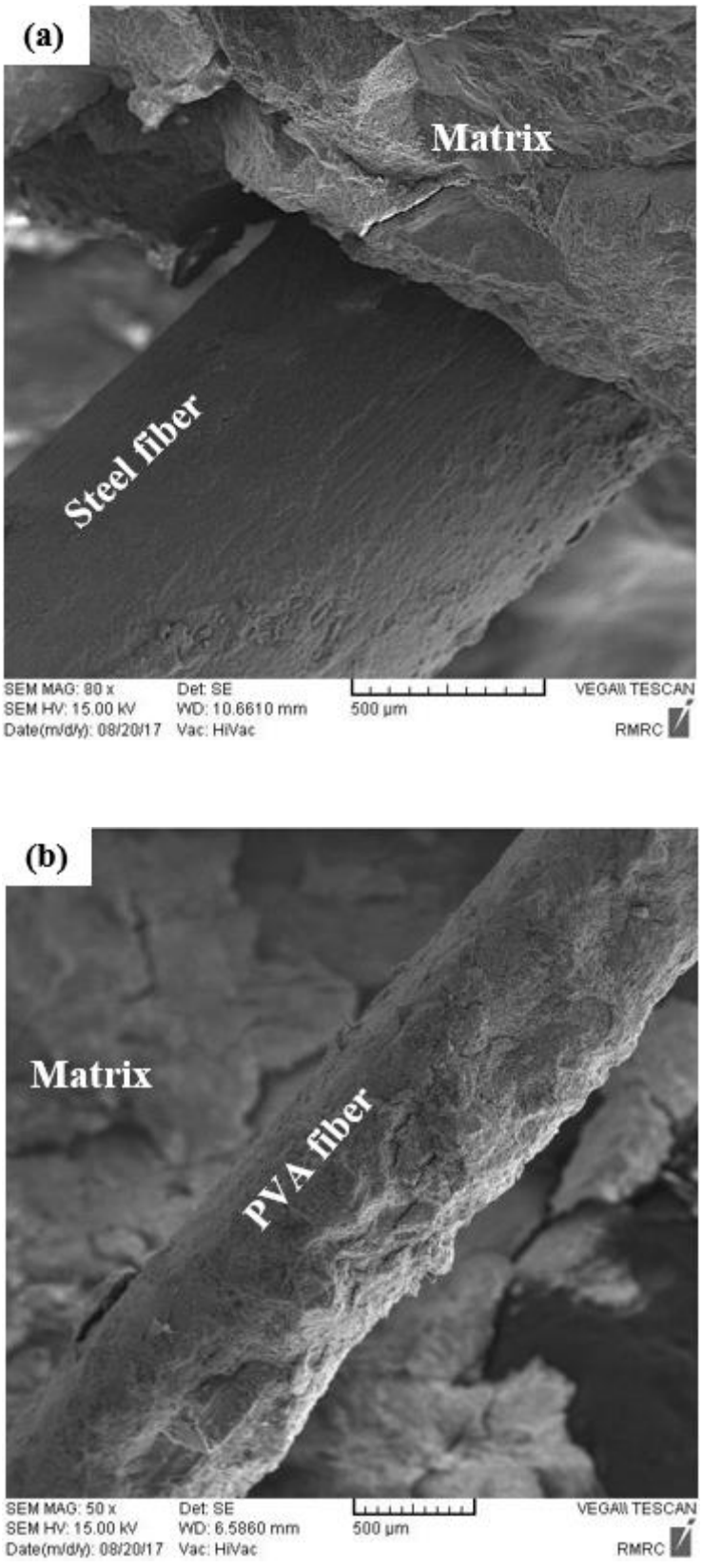


Fig. 6.40 SEM images of different fibers in cement paste: (a) steel fibers, (b) PVA fibers

# Chapter 7

# Conclusions and recommendation for future research

## 7.1 Thesis summary

The research summarized in this dissertation was aimed at understanding the engineering properties of high performance fiber-reinforced concretes made with innovative binders. This study focused on three different main subjects including the effect of Type K cement, calcium sulfoaluminate (CSA) cement, and different types of fibers on the mechanical, durability, and microstructural properties of HPC. In total, twenty four different concrete mixes were developed. The results show that the Type K cement has insignificant influence on the mechanical properties of HPC, while it is able to significantly compensate the shrinkage of concrete. Moreover, the presence of Type K cement in concrete leads to an enhancement in the bond between fibers and cement matrix that subsequently resulting in improved mechanical properties. This is the first study comprehensively investigating the effect of a commercial CSA cement on the properties of HPC. It was observed that the mechanical properties of CSA cement-based concretes were reduced at early ages, while higher strengths were attained at later ages compared to the OPC concrete. Additionally, the shrinkage of concretes made with CSA cement was significantly reduced. The properties of CSA cement-based concretes in the binary and ternary systems were found to be changed with respect to the concrete that pure CSA cement was used due to the variation in the hydration products of binders. For the first time, the effect of different fibers on the properties CSA cement-based concretes was studied. It was observed that the addition of fibers irrespective to the type of fibers resulted in an increase in the mechanical properties of concrete. The best performance was attained by introducing 1% DHE steel fibers. The findings of this research are

highly promising and have the potential to significantly contribute toward expanding the use of HPFRC made with CSA cement to different structural applications.

## 7.2 General conclusions

This study was aimed at understanding the properties of HPFRC made with innovative binders such as CSA cement and Type K cement. Different concrete mixes were developed in this research and their mechanical, durability, and microstructural properties were assessed. From the extensive experimental program conducted in this study, the following conclusions were obtained:

1- The replacement of OPC with Type K cement has insignificant influence on the mechanical strength of concrete and it leads to almost similar compressive, splitting tensile and flexural strength.

2- Using Type K cement in concrete leads to an expansion at early age, while it results in a dimensional stability after 56 days. This can be attributed to the formation of rich content of ettringite crystals with expansive behavior in the concrete, which subsequently compensates the shrinkage of concrete.

3- Using Type K cement in mortars led to an increase of 26% in the pullout resistance of steel fibers. This can be explained by the fact that the presence of expansive Type K cement leads to a better chemical adhesion between the fibers and cement matrix as a result of cement expansion and formation of self-prestress effect.

4- The microstructural analysis by means of XRD method show that the main hydration product of cement paste made with OPC and Type K cement is portlandite and ettringite, respectively. The SEM observation also demonstrate that the addition of Type K cement

improves the properties of cement matrix and leads to the appearance of ettringite needles with larger size compared to that of OPC.

5- The full replacement of OPC with CSA cement results in a reduction in the strengths of concretes at early ages, while higher strengths are obtained at later ages of curing (i.e. 28 and 56 days). The reduction of the strength can be attributed to the presence of retarder that was used to adjust the setting time of concrete and causes a delay in the formation of ettringite crystals. The increased strength of concrete at later ages can be explained by the fact the presence of ye'elimite phase in the CSA cement results in the generation of prismatic ettringite crystals, which interlocking and bonding between ettringite crystals consequently cause enhanced strengths.

6- Using CSA cement in concrete significantly reduces the shrinkage of concrete. The results indicate that the shrinkage deformation of concrete made with CSA cement was reduced by 38% over that of the OPC mix at 56 days.

7- Replacing OPC with CSA cement results in a significant increase in the electrical resistivity of concrete, which means lower risk of steel bars corrosion. However, the electrochemical test results indicate that electrical resistivity technique is not a reliable method to predict the probability of steel bars corrosion in the CSA-based concretes. The optical microscopy observation of fibers after the potential-static test show that the steel fibers embedded in CSA-based mixes are corroded as a result of lower pH in these mixes that destroys the passive layer around the fibers.

8- A strong correlation between the electrical resistivity and compressive strength test results is established. Higher compressive strengths are attained by an increase in the magnitude of the electrical resistivity.

9- The results of the binary and ternary CSA cement-based mixes show that their properties have been altered with respect to the mix that pure CSA cement was used. The mechanical strengths are reduced in the mixes that OPC is mixed with CSA cement with or without slag. Additionally, the results show that blending of CSA cement with OPC adversely affects the durability properties of concrete, such as water absorption, electrical resistivity and resistance against the steel rebar corrosion. The reduction in the mechanical and durability properties of concrete can be explained by the variation in the hydration products of the binder compared to that of the CSA mix. Carbonated phase and AFm are the main hydration products in the binary mix, while AFm, needle-like ettringite and C-S-H gel are developed in the ternary mix. The main hydration products of pure CSA cement are prismatic ettringite crystals that cause an increase in the strengths of concrete.

10- The electrochemical test results demonstrate that the probability of steel bars corrosion has been increased in the OPC50-CSA50 and OPC25-CSA50-SL25 concrete mixes. The weak corrosion resistance of CSA-blend mixes may be attributed to the carbonation of mobile alkalis from the pore solution due to the efflorescence phenomena that leads to the decomposition of ettringite crystals as well as the reduction of the alkalinity in the pore solutions, which subsequently increases the risk of steel fibers corrosion.

11- The inclusion of 1% DHE steel fibers in all the CSA cement-based mixes results in an increase in the mechanical properties, particularly the flexural strength of HPFRC. As evidenced by the splitting and flexural test results, the efficiency of DHE steel fibers in improvement of the flexural strength is higher in CSA-blend mixes. The expansion behavior of CSA-blend mixes leads to a better bond between the cement matrix and steel

fibers as a result of self-stressing, which subsequently causes an increase in the flexural strength of concrete.

12- The full hydration of CSA cement requires higher content of water with respect to the OPC. The findings of this study demonstrate that reducing the w/c ratio of CSA cement-based concretes from 0.35 to 0.28 results in a slight increase in the strengths of concrete due to the lack of enough water for the complete hydration of CSA cement.

13- Introducing of fibers irrespective to the type of fibers results in an increase in the mechanical properties of CSA cement-based concretes. The addition of 1% DHE steel fibers significantly affects the flexural performance of concrete and results in a deflection-hardening behavior, while HE steel fibers and PVA fibers are not able to restrict the propagation of macro-cracks and cause a deflection-softening behavior. DHE steel fibers used in the present study, due to their higher tensile strength, modulus of elasticity, and the anchoring mechanism created by their hooked ends are able to develop considerably higher maximum pullout forces compared to those develop by HE steel and straight PVA fibers.

14- The results of HyFRC show that the substitution a portion of DHE steel fibers with HE steel or PVA fibers leads to a reduction in the splitting tensile and flexural strength of concretes compared to those of the CSA-DHE1, while their strengths are significantly higher than the plain CSA concrete. The results show that a deflection-hardening behavior is achieved in all the HyFRC considered in this study. Since cracks occur at different stages and sizes in concrete, the use of various fibers with different lengths and types is a good way to address this problem, and produce concretes with enhanced properties.

15- The shrinkage test results show that the addition of any types of fibers results in a reduction in the shrinkage deformation of CSA cement-based concretes. For instance, the shrinkage

strains of CSA-DHE1, CSA-HE1, and CSA-PVA1 mixes at 56 days were 276, 220, and 227 μm/m, respectively that reduced by 9%, 27%, and 25% as compared to that of the CSA mix at w/c ratio of 0.35. The higher efficiency of HE steel and PVA fibers in restraining the shrinkage of concrete can be explained by the fact the higher number of fibers uniformly dispersed in the cement composites can restrict the initiation of cracks, which resulting in a reduced shrinkage deformation. The results of HyFRC show that concretes were manufactured by hybridization of fibers exhibit lower shrinkage strain as compared to mono type use of DHE steel fibers.

16- The SEM observation verifies the good bond between the fibers and cement matrix due to the expansion of CSA cement.

## 7.3 Recommendations for future work

1- In this study, the effect of the replacing of OPC with slag in the ternary system including CSA cement was assessed. It is recommended that the effect of supplementary cementitious materials such as fly ash, silica fume, and slag at a wide range of replacement in the binary and ternary systems to be investigated.

2- The finding of this study show that the risk of steel bars corrosion is increased in CSA cement-based mixes due to the lower pH of the pore solutions as well as the possibility of ettringite decomposition. Since the corrosion of steel bars in concrete can seriously damage the concrete structures, which resulting in a lower serviceability, it is recommended that further research to be conducted to study the long term durability properties of concrete, particularly its corrosion resistance. Additionally, the fire resistance, freeze/thaw

resistance, and resistance against the sulfate attack of CSA cement-based concretes needed to be explored.

3- Replacing natural aggregates with recycled concrete aggregates derived from the demolished concretes can result in the development of concretes with reduced environmental impact. Additionally, these aggregates with higher porosity and consequently higher water absorption compared to the natural aggregates may act better at the prolonged time to improve the properties of CSA cement-based concrete as a result of internal curing. Therefore, it is worth considering the influence of fine and course recycled concrete aggregates at different replacement ratios on the engineering properties of HPC.

4- The influence of different fibers on the properties of CSA cement-based concretes was studied in this research. The results show that HPFRC with enhanced flexural performance can be developed through the addition of DHE steel fibers in concrete. It is recommended that to explore the effect of partial replacement of steel bars with discrete DHE steel fibers in large scale concrete structures. The results of aforementioned study may have the potential to significantly contribute toward expanding the use of HPFRC to different structural applications.

# Chapter 8

# References


[1] Celik, K., Meral, C., Mancio, M., Mehta, P. K., & Monteiro, P. J. (2014). A comparative study of self-consolidating concretes incorporating high-volume natural pozzolan or high-volume fly ash. *Construction and Building Materials*, *67*, 14-19.

[2] Mehta, P.K., Monteiro, P.J.M., Concrete in the Era of Global Warming and Sustainability; *in Concrete Microstructure, Properties, and Materials*, 4th ed., McGraw-Hill, New York, in press.

[3] U.S. Geological Survey, Mineral Commodity Summaries, 2014. 39.

[4] International Energy Agency World Business Council for Sustainable Development, Cement Technology Roadmap 2009: Carbon Emissions Reductions up to 2050, 2009.

[5] Mehta, K. P. (2001). Reducing the environmental impact of concrete. *Concrete international*, *23(10)*, 61-66.

[6] Gartner, E., & Hirao, H. (2015). A review of alternative approaches to the reduction of CO 2 emissions associated with the manufacture of the binder phase in concrete. *Cement and Concrete research*, *78*, 126-142.

[7] Juenger, M. C. G., Winnefeld, F., Provis, J. L., & Ideker, J. H. (2011). Advances in alternative cementitious binders. *Cement and concrete research*, *41*(12), 1232-1243.

[8] Gartner, E. (2004). Industrially interesting approaches to "low-$CO_2$" cements. *Cement and Concrete research*, *34*(9), 1489-1498.

[9] Berger, S., Aouad, G., Coumes, C. C. D., Le Bescop, P., & Damidot, D. (2013). Leaching of calcium sulfoaluminate cement pastes by water at regulated pH and temperature: experimental investigation and modeling. *Cement and Concrete Research*, *53*, 211-220.

[10] Tang, S. W., Zhu, H. G., Li, Z. J., Chen, E., & Shao, H. Y. (2015). Hydration stage identification and phase transformation of calcium sulfoaluminate cement at early age. *Construction and Building Materials*, *75*, 11-18.

[11] Mehta, P. K. (1973). Mechanism of expansion associated with ettringite formation. *Cement and Concrete Research*, *3*(1), 1-6.

[12] Glasser, F. P., & Zhang, L. (2001). High-performance cement matrices based on calcium sulfoaluminate–belite compositions. *Cement and Concrete Research*, *31*(12), 1881-1886.

[13] Mehta, P. K. (1980). Investigations on energy-saving cements. *World cement technology*, *11*(5), 166-177.

[14] Bye, G. C. (1999). *Portland cement: composition, production and properties*. Thomas Telford, p 206.

[15] Zhang, L., Su, M., & Wang, Y. (1999). Development of the use of sulfo-and ferroaluminate cements in China. *Advances in cement research*, *11*(1), 15-21.

[16] Péra, J., & Ambroise, J. (2004). New applications of calcium sulfoaluminate cement. *Cement and concrete research*, *34*(4), 671-676.

[17] Zhang, L., & Glasser, F. P. (2005). Investigation of the microstructure and carbonation of CS A-based concretes removed from service. *Cement and concrete Research*, *35*(12), 2252-2260.

[18] Damtoft, J. S., Lukasik, J., Herfort, D., Sorrentino, D., & Gartner, E. M. (2008). Sustainable development and climate change initiatives. *Cement and concrete research*, *38*(2), 115-127.

[19] Sherman, N., Beretka, J., Santoro, L., & Valenti, G. L. (1995). Long-term behaviour of hydraulic binders based on calcium sulfoaluminate and calcium sulfosilicate. *Cement and concrete research*, *25*(1), 113-126.

[20] Winnefeld, F., & Barlag, S. (2009). Influence of calcium sulfate and calcium hydroxide on the hydration of calcium sulfoaluminate clinker. *Zkg Int*, *12*, 42-53.

[21] Han, J., Jia, D., & Yan, P. (2016). Understanding the shrinkage compensating ability of type K expansive agent in concrete. *Construction and Building Materials*, *116*, 36-44.

[22] Nagataki, S., & Gomi, H. (1998). Expansive admixtures (mainly ettringite). *Cement and concrete composites*, *20*(2-3), 163-170.

[23] ACI 223-98. (1998). Standard practice for the use of shrinkage-compensating concrete.

[24] Carballosa, P., Calvo, J. G., Revuelta, D., Sánchez, J. J., & Gutiérrez, J. P. (2015). Influence of cement and expansive additive types in the performance of self-stressing and self-compacting concretes for structural elements. *Construction and Building Materials*, *93*, 223-229.

[25] Hargis, C. W., Kirchheim, A. P., Monteiro, P. J., & Gartner, E. M. (2013). Early age hydration of calcium sulfoaluminate (synthetic ye'elimite,) in the presence of gypsum and varying amounts of calcium hydroxide. *Cement and Concrete Research*, *48*, 105-115.

[26] Purnell, P., Short, N. R., Page, C. L., Majumdar, A. J., & Walton, P. L. (1999). Accelerated ageing characteristics of glass-fibre reinforced cement made with new cementitious matrices. *Composites part A: applied science and manufacturing*, *30*(9), 1073-1080.

[27] Luz, C. A., Rocha, J. C., Cheriaf, M., & Pera, J. (2006). Use of sulfoaluminate cement and bottom ash in the solidification/stabilization of galvanic sludge. *Journal of Hazardous Materials*, *136*(3), 837-845.

[28] Peysson, S., Péra, J., & Chabannet, M. (2005). Immobilization of heavy metals by calcium sulfoaluminate cement. *Cement and Concrete Research*, *35*(12), 2261-2270.

[29] Zhou, Q., Milestone, N. B., & Hayes, M. (2006). An alternative to Portland cement for waste encapsulation—the calcium sulfoaluminate cement system. *Journal of hazardous materials*, *136*(1), 120-129.

[30] Su, M., Kurdowski, W., & Sorrentino, F. (1992). Development in non-Portland cements. In *9th International Congress on the Chemistry of Cements, New Delhi, India*, 1, 317-354.

[31] Lan, W., & Glasser, F. P. (1996). Hydration of calcium sulphoaluminate cements. *Advances in cement Research*, *8*(31), 127-134.

[32] Sharp, J. H., Lawrence, C. D., & Yang, R. (1999). Calcium sulfoaluminate cements—low-energy cements, special cements or what? *Advances in Cement Research*, *11*(1), 3-13.

[33] Paglia, C. S., Wombacher, F. J., & Bohni, H. K. (2001). Hydration, Strength, and Microstructural Development of High Early-Strength C4A3S Activated Burnt Oil Shale-Based Cement System. *Materials Journal*, *98*(5), 379-385.

[34] Trauchessec, R., Mechling, J. M., Lecomte, A., Roux, A., & Le Rolland, B. (2015). Hydration of ordinary Portland cement and calcium sulfoaluminate cement blends. *Cement and Concrete Composites*, *56*, 106-114.

[35] Pace, M. L., Telesca, A., Marroccoli, M., & Valenti, G. L. (2011). Use of industrial byproducts as alumina sources for the synthesis of calcium sulfoaluminate cements. *Environmental science & technology*, *45*(14), 6124-6128.

[36] Kurdowski, W., George, C. M., & Sorrentino, F. P. (1986). Special cements. *Proc. 8th Int. Congr. Chem. Cem., Rio de Janeiro, Brasil*, *1*, 293-318.

[37] Sui, T., & Yao, Y. (2003). Recent progress in special cements in China. *Proc. 11th Int. Congr. Chem. Cem., Durban, South Africa*, *4*, 2028-2032.

[38] Havlica, J., & Sahu, S. (1992). Mechanism of ettringite and monosulphate formation. *Cement and concrete research*, *22*(4), 671-677.

[39] Mehta, P. K., & Hu, F. (1978). Further evidence for expansion of ettringite by water adsorption. *Journal of the American ceramic Society*, *61*(3-4), 179-181.

[40] Wang, S. (1982). Expansion of ettringite by water absorption. *Cement and Concrete Research*, *12*, 121-122.

[41] Beretka, J., Sherman, N., Marroccoli, M., Pompo, A., & Valenti, G. L. (1997). Effect of composition on the hydration properties of rapid-hardening sulfoaluminate cements. In *Proceedings of the 10th International Congress on the Chemistry of Cement* (Vol. 2, p. 2ii029). SINTEF Civil & Environmental Engineering, Cement & Concrete: Norway.

[42] Marroccoli, M., Nobili, M., Telesca, A., & Valenti, G. L. (2007). Early hydration of calcium sulfoaluminate-based cements for structural applications. In *International Conference on sustainable construction materials and technologies, Coventry*, 389-395.

[43] Bernardo, G., Buzzi, L., Canonico, F., Paris, M., Telesca, A., & Valenti, G. L. (2007). Microstructural investigations on hydrated high-performance cements based on calcium sulfoaluminate. *Proc. 12th Int. Congr. Chem. Cem., Montreal, Canada*.

[44] Winnefeld, F., & Lothenbach, B. (2010). Hydration of calcium sulfoaluminate cements-experimental findings and thermodynamic modelling. *Cement and Concrete Research*, *40*(8), 1239-1247.

[45] Pelletier, L., Winnefeld, F., & Lothenbach, B. (2010). The ternary system Portland cement–calcium sulphoaluminate clinker–anhydrite: hydration mechanism and mortar properties. *Cement and Concrete Composites*, *32*(7), 497-507.

[46] Lura, P., Jensen, O. M., & van Breugel, K. (2003). Autogenous shrinkage in high-performance cement paste: An evaluation of basic mechanisms. *Cement and Concrete Research*, *33*(2), 223-232.

[47] Fu, Y., Gu, P., Xie, P., & Beaudoin, J. J. (1995). Effect of chemical admixtures on the expansion of shrinkage-compensating cement containing a pre-hydrated high alumina cement—based expansive additive. *Cement and concrete research*, *25*(1), 29-38.

[48] Wang, K., Jansen, D. C., Shah, S. P., & Karr, A. F. (1997). Permeability study of cracked concrete. *Cement and Concrete Research*, *27*(3), 381-393.

[49] Chen, I. A., Hargis, C. W., & Juenger, M. C. (2012). Understanding expansion in calcium sulfoaluminate–belite cements. *Cement and Concrete Research*, *42*(1), 51-60.

[50] Cohen, M. D., & Richards, C. W. (1982). Effects of the particle sizes of expansive clinker on strength-expansion characteristics of type K expansive cements. *Cement and Concrete Research*, *12*(6), 717-725.

[51] Beretka, J., Marroccoli, M., Sherman, N., & Valenti, G. L. (1996). The influence of C4A3S content and WS ratio on the performance of calcium sulfoaluminate-based cements. *Cement and Concrete Research*, *26*(11), 1673-1681.

[52] Ping, X., & Beaudoin, J. J. (1992). Mechanism of sulphate expansion I. Thermodynamic principle of crystallization pressure. *Cement and concrete research*, *22*(4), 631-640.

[53] Scherer, G. W. (2004). Stress from crystallization of salt. *Cement and concrete research*, *34*(9), 1613-1624.

[54] Bizzozero, J. (2014). Hydration and dimensional stability of calcium aluminate cement based systems, PhD Thesis. École Polytechnique Fédérale de Lausanne. Switzerland.

[55] Taber, S. (1916). The growth of crystals under external pressure. *American Journal of Science*, (246), 532-556.

[56] Mehta, P. K. (1976). Scanning electron micrographic studies of ettringite formation. *Cement and Concrete Research*, *6*(2), 169-182.

[57] Mehta, P. K. (1973). Effect of lime on hydration of pastes containing gypsum and calcium aluminates or calcium sulfoaluminate. *Journal of the American Ceramic Society*, *56*(6), 315-319.

[58] Rossetti, V. A., Chiocchio, G., & Paolini, A. E. (1982). Expansive properties of the mixture C4ASH12− 2CS II. Effects of lime, porosity and liquid/solid ratio. *Cement and Concrete Research*, *12*(6), 667-676.

[59] Min, D., & Mingshu, T. (1994). Formation and expansion of ettringite crystals. *Cement and concrete research*, *24*(1), 119-126.

[60] Mather, B. (1984). A discussion of the paper "theories of expansion in sulfoaluminate-type expansive cements: Schools of thought," by MD Cohen. *Cement and Concrete Research*, *14*(4), 603-609.

[61] Taylor, H. F. W., Famy, C., & Scrivener, K. L. (2001). Delayed ettringite formation. *Cement and concrete research*, *31*(5), 683-693.

[62] Bernardo, G., Telesca, A., & Valenti, G. L. (2006). A porosimetric study of calcium sulfoaluminate cement pastes cured at early ages. *Cement and concrete research*, *36*(6), 1042-1047.

[63] Marchi, M., & Costa, U. (2011). Influence of the calcium sulphate and W/C ratio on the hydration of calcium sulphoaluminate cement. *Proceedings of the 13th ICCC, Madrid, Spain*.

[64] Hargis, C. W. (2013). *Advances in Sustainable Cements*. PhD Thesis. University of California, Berkeley.

[65] Živica, V. (2000). Properties of blended sulfoaluminate belite cement. *Construction and building Materials*, *14*(8), 433-437.

[66] ŽIVICA, V. (2001). Possibility of the modification of the properties of sulfoaluminate belite cement by its blending. *Ceramics− Silikáty*, *45*(1), 24-30.

[67] Fu, X., Yang, C., Liu, Z., Tao, W., Hou, W., & Wu, X. (2003). Studies on effects of activators on properties and mechanism of hydration of sulphoaluminate cement. *Cement and Concrete Research*, *33*(3), 317-324.

[68] Gastaldi, D., Boccaleri, E., Canonico, F., & Bianchi, M. (2007). The use of Raman spectroscopy as a versatile characterization tool for calcium sulphoaluminate cements: a compositional and hydration study. *Journal of Materials Science*, *42*(20), 8426-8432.

[69] Alesiani, M., Pirazzoli, I., Maraviglia, B., & Canonico, F. (2008). NMR and XRD study on calcium sulfoaluminate cement. *Applied Magnetic Resonance*, *35*(1), 33-41.

[70] Buzzi, L., Canonico, F., & Schaffel, P. (2011, July). Investigation on high-performance concrete based on calcium sulfoaluminate cement. In *Proceedings of the 13th international congress on the chemistry of cement, Madrid, Spain*.

[71] Winnefeld, F., Ben Haha, M., & Lothenbach, B. (2011). Hydration mechanisms of calcium sulfoaluminate cements assessed by scanning electron microscopy and thermodynamic modelling. In *Proceedings of the 13th International Congress on the Chemistry of Cement, Madrid, Spain*.

[72] Lura, P., Winnefeld, F., & Klemm, S. (2010). Simultaneous measurements of heat of hydration and chemical shrinkage on hardening cement pastes. *Journal of thermal analysis and calorimetry*, *101*(3), 925-932.

[73] Yanmou, W., Jun'an, D., & Muzen, S. (1986). An investigation into cement CaO-SiO2-Al2O3-Fe2O3-SO3 system. *Proc. 8th Int. Cong. Chem Cements*, *2*, 300-305.

[74] Winnefeld, F., & Barlag, S. (2010). Calorimetric and thermogravimetric study on the influence of calcium sulfate on the hydration of ye'elimite. *Journal of thermal analysis and calorimetry*, *101*(3), 949-957.

[75] Pelletier-Chaignat, L., Winnefeld, F., Lothenbach, B., Le Saout, G., Müller, C. J., & Famy, C. (2011). Influence of the calcium sulphate source on the hydration mechanism of Portland cement–calcium sulphoaluminate clinker–calcium sulphate binders. *Cement and Concrete Composites*, *33*(5), 551-561.

[76] Shi, X., Xie, N., Fortune, K., & Gong, J. (2012). Durability of steel reinforced concrete in chloride environments: An overview. *Construction and Building Materials*, *30*, 125-138.

[77] Zhang, L., & Glasser, F. P. (1999, September). New concretes based on calcium sulfoaluminate cement. In *Proceedings of the International Conference on Modern Concrete Materials: Binders, Additions and Admixtures* (pp. 261-274). London: Thomas Telford.

[78] García-Maté, M., Santacruz, I., Ángeles, G., León-Reina, L., & Aranda, M. A. (2012). Rheological and hydration characterization of calcium sulfoaluminate cement pastes. *Cement and Concrete Composites*, *34*(5), 684-691.

[79] Quillin, K. (2001). Performance of belite–sulfoaluminate cements. *Cement and Concrete Research*, *31*(9), 1341-1349.

[80] Beretka, J., Santoro, L., Sherman, N., & Valenti, G. L. (1992). Synthesis and properties of low energy cements based on C4A3S. In *Proc. 9th Int. Congr. Chem. Cement, New Delhi*, 3, 195-200.

[81] Mechling, J. M., Lecomte, A., Roux, A., & Le Rolland, B. (2014). Sulfoaluminate cement behaviours in carbon dioxide, warm and moist environments. *Advances in Cement Research*, *26*(1), 52-61.

[82] Kalogridis, D., Kostogloudis, G. C., Ftikos, C., & Malami, C. (2000). A quantitative study of the influence of non-expansive sulfoaluminate cement on the corrosion of steel reinforcement. *Cement and concrete research*, *30*(11), 1731-1740.

[83] Kwak, H. G., & Filippou, F. C. (1990). Finite element analysis of reinforced concrete structures under monotonic loads.

[84] Hearing, B. P. (1997). Fracture behavior of mortar-aggregate interfaces in concrete. *Doctoral dissertation, Massachusetts Institute of Technology*.

[85] Sicat, E., Gong, F., Ueda, T., & Zhang, D. (2014). Experimental investigation of the deformational behavior of the interfacial transition zone (ITZ) in concrete during freezing and thawing cycles. *Construction and Building Materials*, 65, 122-131.

[86] Nili, M., & Ehsani, A. (2015). Investigating the effect of the cement paste and transition zone on strength development of concrete containing nanosilica and silica fume. *Materials & Design*, 75, 174-183.

[87] Hameed, R., Turatsinze, A., Duprat, F., & Sellier, A. (2010). A study on the reinforced fibrous concrete elements subjected to uniaxial tensile loading. *KSCE Journal of Civil Engineering*, 14(4), 547-556.

[88] Kaufmann, W. (2013). Strength and deformations of structural concrete subjected to in-plane shear and normal forces. *Birkhäuser*.

[89] Shah, S. P. (1992). Do fibers increase the tensile strength of cement-based matrix? *ACI Materials Journal*, 88(6), 595-602.

[90] Paipetis, A., Galiotis, C., Liu, Y. C., & Nairn, J. A. (1999). Stress transfer from the matrix to the fibre in a fragmentation test: Raman experiments and analytical modeling. *Journal of composite materials*, 33(4), 377-399.

[91] Mindess, S. (1995). Fiber reinforced concrete: Challenges and prospects. Banthia, N. and Mindess, S., Second University-Industry Workshop on Fiber Reinforced Concrete and other Advanced Composites, Toronto, Canada.

[92] Li, V. C., & Maalej, M. (1996). Toughening in cement based composites. Part II: Fiber reinforced cementitious composites. *Cement and Concrete Composites*, 18(4), 239-249.

[93] Døssland, Å. L. (2008). Fibre reinforcement in load carrying concrete structures. Norwegian University of Science and Technology, Printed by NTNU Trykk.

[94] Ding, Y., & Kusterle, W. (2000). Compressive stress–strain relationship of steel fibre-reinforced concrete at early age. *Cement and Concrete Research*, 30(10), 1573-1579.

[95] Mo, K. H., Yap, K. K. Q., Alengaram, U. J., & Jumaat, M. Z. (2014). The effect of steel fibres on the enhancement of flexural and compressive toughness and fracture characteristics of oil palm shell concrete. *Construction and Building Materials*, 55, 20-28.

[96] Narwal, J., Goel, A., Sharma, D., Kapoor, D. R., & Singh, B. (2013). An Experimental Investigation on Structural Performance of Steel Fibre Reinforced Concrete Beam. *International Journal of Engineering and Advanced Technology*, 2(6), 301–304.

[97] Naaman, A. E. (2003). Engineered steel fibers with optimal properties for reinforcement of cement composites. *Journal of Advanced Concrete Technology*, 1(3), 241-252.

[98] Yan, H., Sun, W., & Chen, H. (1999). The effect of silica fume and steel fiber on the dynamic mechanical performance of high-strength concrete. *Cement and Concrete Research*, 29(3), 423-426.

[99] ACI Committee 544. (2002). State-of-the-Art Report on Fiber Reinforced Concrete Reported by ACI Committee 544.

[100] Banthia, N., & Nandakumar, N. (2003). Crack growth resistance of hybrid fiber reinforced cement composites. *Cement and Concrete Composites*, 25(1), 3-9.

[101] Löfgren, I. (2005). Fibre-reinforced Concrete for Industrial Construction-a fracture mechanics approach to material testing and structural analysis. *PhD Thesis, Chelmers University of Technology*.

[102] Wuest, J., Denarié, E., Brühwiler, E., Tamarit, L., Kocher, M., & Gallucci, E. (2009). Tomography analysis of fiber distribution and orientation in ultra high-performance fiber-reinforced composites with high-fiber dosages. *Experimental techniques*, 33(5), 50-55.

[103] Stähli, P., Custer, R., & van Mier, J. G. (2008). On flow properties, fibre distribution, fibre orientation and flexural behaviour of FRC. *Materials and Structures*, 41(1), 189-196.

[104] Tejchman, J., & Kozicki, J. (2010). Experimental and theoretical investigations of steel-fibrous concrete. *Springer series in geo-mechanics and geoengineering, 1st edn. Springer, Berlin.*

[105] Eik, M., Lõhmus, K., Tigasson, M., Listak, M., Puttonen, J., & Herrmann, H. (2013). DC-conductivity testing combined with photometry for measuring fibre orientations in SFRC. *Journal of Materials Science*, 48(10), 3745-3759.

[106] Laranjeira, F., Grünewald, S., Walraven, J., Blom, C., Molins, C., & Aguado, A. (2011). Characterization of the orientation profile of steel fiber reinforced concrete. *Materials and structures*, 44(6), 1093-1111.

[107] Barnett, S. J., Lataste, J. F., Parry, T., Millard, S. G., & Soutsos, M. N. (2010). Assessment of fibre orientation in ultra high performance fibre reinforced concrete and its effect on flexural strength. *Materials and Structures*, 43(7), 1009-1023.

[108] Suuronen, J. P., Kallonen, A., Eik, M., Puttonen, J., Serimaa, R., & Herrmann, H. (2013). Analysis of short fibres orientation in steel fibre-reinforced concrete (sfrc) by x-ray tomography. *Journal of Materials Science*, 48(3), 1358-1367.

[109] Ferrara, L., & Meda, A. (2006). Relationships between fibre distribution, workability and the mechanical properties of SFRC applied to precast roof elements. *Materials and Structures*, 39(4), 411-420.

[110] Kang, S. T., Lee, B. Y., Kim, J. K., & Kim, Y. Y. (2011). The effect of fibre distribution characteristics on the flexural strength of steel fibre-reinforced ultra high strength concrete. *Construction and Building Materials*, 25(5), 2450-2457.

[111] Laranjeira de Oliveira, F. (2010). Design-oriented constitutive model for steel fiber reinforced concrete. *PhD Thesis, University Politecnica de Catalunya*.

[112] Grünewald, S. (2012). Fibre reinforcement and the rheology of concrete. *in: Understanding the rheology of concrete, Editor: N. Roussel, Woodhead Publishing Limited*, 229-256.

[113] Ferrara, L., Ozyurt, N., & Di Prisco, M. (2011). High mechanical performance of fibre reinforced cementitious composites: the role of "casting-flow induced" fibre orientation. *Materials and Structures*, 44(1), 109-128.

[114] Orbe, A., Cuadrado, J., Losada, R., & Rojí, E. (2012). Framework for the design and analysis of steel fiber reinforced self-compacting concrete structures. *Construction and Building Materials*, 35, 676-686.

[115] Wille, K., Tue, N. V., & Parra-Montesinos, G. J. (2014). Fiber distribution and orientation in UHP-FRC beams and their effect on backward analysis. *Materials and Structures*, 47(11), 1825-1838.

[116] Ferrara, L., Park, Y. D., & Shah, S. P. (2008). Correlation among fresh state behavior, fiber dispersion, and toughness properties of SFRCs. *Journal of Materials in Civil Engineering*, 20(7), 493-501.

[117] Dupont, D., & Vandewalle, L. (2005). Distribution of steel fibres in rectangular sections. *Cement and Concrete Composites*, 27(3), 391-398.

[118] Gettu, R., Gardner, D. R., Saldivar, H., & Barragán, B. E. (2005). Study of the distribution and orientation of fibers in SFRC specimens. *Materials and Structures*, 38(1), 31-37.

[119] Soroushian, P., & Lee, C. D. (1990). Distribution and orientation of fibers in steel fiber reinforced concrete. ACI *Materials Journal*, 87(5), 433-439.

[120] Grünewald, S. (2004). Performance-based design of self-compacting fibre reinforced concrete. *TU Delft, Delft University of Technology*.

[121] Lappa, E. S. (2007). High strength fibre reinforced concrete: static and fatigue behaviour in bending. *TU Delft, Delft University of Technology*.

[122] Ozyurt, N., Mason, T. O., & Shah, S. P. (2006). Non-destructive monitoring of fiber dispersion in FRCS using AC-Impedance spectroscopy. In *Measuring, Monitoring and Modeling Concrete Properties, Springer Netherlands*, 285-290.

[123] Ozyurt, N., Mason, T. O., & Shah, S. P. (2006). "Non-destructive monitoring of fiber orientation using AC-IS: An industrial-scale application. *Cement and concrete research*, 36(9), 1653-1660.

[124] Torrents, J. M., Mason, T. O., Peled, A., Shah, S. P., & Garboczi, E. J. (2001). Analysis of the impedance spectra of short conductive fiber-reinforced composites. *Journal of Materials Science*, 36(16), 4003-4012.

[125] Martinie, L., Lataste, J. F., & Roussel, N. (2015). Fiber orientation during casting of UHPFRC: electrical resistivity measurements, image analysis and numerical simulations. *Materials and Structures*, 48(4), 947-957.

[126] Lataste, J. F., Behloul, M., & Breysse, D. (2008). Characterisation of fibres distribution in a steel fibre reinforced concrete with electrical resistivity measurements. *NDT & E International*, 41(8), 638-647.

[127] Vicente, M. A., González, D. C., & Mínguez, J. (2014). Determination of dominant fibre orientations in fibre-reinforced high-strength concrete elements based on computed tomography scans. *Nondestructive Testing and Evaluation*, 29(2), 164-182.

[128] Ponikiewski, T., Katzer, J., Bugdol, M., & Rudzki, M. (2015). Steel fibre spacing in self-compacting concrete precast walls by X-ray computed tomography. *Materials and Structures*, 48(12), 3863-3874.

[129] Herrmann, H., Pastorelli, E., Kallonen, A., & Suuronen, J. P. (2016). Methods for fibre orientation analysis of X-ray tomography images of steel fibre reinforced concrete (SFRC). *Journal of Materials Science*, 51, 3772-3783.

[130] Lin, Y. Z. (1999). Tragverhalten von Stahlfaserbeton, Deutscher Ausschuss für Stahlbeton. *Heft 494, Berlin, Beuth Verlag GmbH*.

[131] Bonzel, J., & Schmidt, M. (1984). Verteilung und Orientierung von Stahlfasern im Beton und ihr Einfluss auf die Eigenschaften von Stahlfaserbeton. *Beton*, 34, 463-470.

[132] Edgington, J., & Hannant, D. J. (1972). Steel fibre reinforced concrete. The effect on fibre orientation of compaction by vibration. *Matériaux et Construction*, 5(1), 41-44.

[133] Güneyisi, E., Gesoğlu, M., Akoi, A. O. M., & Mermerdaş, K. (2014). Combined effect of steel fiber and metakaolin incorporation on mechanical properties of concrete. *Composites Part B: Engineering*, 56, 83-91.

[134] Poon, C. S., Shui, Z. H., & Lam, L. (2004). Compressive behavior of fiber reinforced high-performance concrete subjected to elevated temperatures. *Cement and Concrete Research*, 34(12), 2215-2222.

[135] Kaïkea, A., Achoura, D., Duplan, F., & Rizzuti, L. (2014). Effect of mineral admixtures and steel fiber volume contents on the behavior of high performance fiber reinforced concrete. *Materials & Design*, 63, 493-499.

[136] Khaliq, W., & Kodur, V. (2011). Thermal and mechanical properties of fiber reinforced high performance self-consolidating concrete at elevated temperatures. *Cement and Concrete Research*, 41(11), 1112-1122.

[137] Zhu, H. B., Yan, M. Z., Wang, P. M., Li, C., & Cheng, Y. J. (2015). Mechanical performance of concrete combined with a novel high strength organic fiber. *Construction and Building Materials*, 78, 289-294.

[138] Song, P. S., & Hwang, S. (2004). Mechanical properties of high-strength steel fiber-reinforced concrete. *Construction and Building Materials*, 18(9), 669-673.

[139] Ding, Y., Liu, H., Pacheco-Torgal, F., & Jalali, S. (2011). Experimental investigation on the mechanical behaviour of the fiber reinforced high-performance concrete tunnel segment. *Composite Structures*, 93(4), 1284-1289.

[140] Eren, Ö., & Celik, T. (1997). Effect of silica fume and steel fibers on some properties of high-strength concrete. *Construction and Building Materials*, 11(7), 373-382.

[141] Köksal, F., Altun, F., Yiğit, İ., & Şahin, Y. (2008). Combined effect of silica fume and steel fiber on the mechanical properties of high strength concretes. *Construction and Building Materials*, 22(8), 1874-1880.

[142] Mehta, P. K., & Monteiro, P. J. (2014). Concrete: microstructure, properties, and materials. Fourth edi. McGraw-Hill.

[143] Li, V. C. (2002). Large volume, high-performance applications of fibers in civil engineering. *Journal of Applied Polymer Science*, 83(3), 660-686.

[144] Edgington, J. (1973). Steel Fibre Reinforced Concrete Volume B. *Doctoral dissertation*, University of Surrey.

[145] Shallal, M. A., & Al-Owaisy, S. R. (2007). Strength and Elasticity of Steel Fiber Reinforced Concrete at High Temperatures. *Journal of Engineering and Development*, 11(2), 125–133.

[146] AL-Ameeri, A. S. (2013). The Effect of Steel Fiber on Some Mechanical Properties of Self Compacting Concrete. *American Journal of Civil Engineering (AJCE)*, 1(3), 102-110.

[147] Ibrahim, I. S., & Bakar, M. C. (2011). Effects on mechanical properties of industrialised steel fibres addition to normal weight concrete. *Procedia Engineering*, 14, 2616-2626.

[148] Noumowe, A. (2005). Mechanical properties and microstructure of high strength concrete containing polypropylene fibres exposed to temperatures up to 200 C. *Cement and Concrete* Research, 35(11), 2192-2198.

[149] Salih, S. A., Rejeb, S. K., & Najim, K. B. (2005) Improving The Modulus of Elasticity of High Performance Concrete by Using Steel Fibers. *Anbar Journal for Engineering Sciences*, 205–216.

[150] Ozger, O. B., Girardi, F., Giannuzzi, G. M., Salomoni, V. A., Majorana, C. E., Fambri, L., Baldassino, N., & Di Maggio, R. (2013). Effect of nylon fibres on mechanical and thermal properties of hardened concrete for energy storage systems. *Materials & Design*, 51, 989-997.

[151] Tassew, S. T., & Lubell, A. S. (2014). Mechanical properties of glass fiber reinforced ceramic concrete. *Construction and Building Materials*, 51, 215-224.

[152] Wang, S., Zhang, M. H., & Quek, S. T. (2012). Mechanical behavior of fiber-reinforced high-strength concrete subjected to high strain-rate compressive loading. *Construction and Building Materials*, 31, 1-11.

[153] Giner, V. T., Baeza, F. J., Ivorra, S., Zornoza, E., & Galao, Ó. (2012). Effect of steel and carbon fiber additions on the dynamic properties of concrete containing silica fume. *Materials & Design*, 34, 332-339.

[154] Beigi, M. H., Berenjian, J., Omran, O. L., Nik, A. S., & Nikbin, I. M. (2013). An experimental survey on combined effects of fibers and nanosilica on the mechanical, rheological, and durability properties of self-compacting concrete. *Materials & Design*, 50, 1019-1029.

[155] Suhaendi, S. L., & Horiguchi, T. (2006). Effect of short fibers on residual permeability and mechanical properties of hybrid fibre reinforced high strength concrete after heat exposition. *Cement and Concrete Research*, 36(9), 1672-1678.

[156] Aulia, T. B. (2002). Effects of polypropylene fibers on the properties of high-strength concretes. *Institutes for Massivbau and Baustoffechnologi*, University Leipzig, Lacer, (7).

[157] Nelson, J. K., & McCormac, J. C. (2005). Design of Reinforced Concrete. Atlantic Highland.

[158] Neville, A. M. (2005). Properties of concrete. *14th edition. New York : J. Wiley*.

[159] Berra, M., & Ferrerra, G. (1990). Normal weight and total-lightweight high-strength concretes: a comparative study. *ACI Special Publication*, 121, 701-734.

[160] Bencardino, F., Rizzuti, L., Spadea, G., & Swamy, R. N. (2008). Stress-strain behavior of steel fiber-reinforced concrete in compression. *Journal of Materials in Civil Engineering*, 20(3), 255-263.

[161] Libre, N. A., Shekarchi, M., Mahoutian, M., & Soroushian, P. (2011). Mechanical properties of hybrid fiber reinforced lightweight aggregate concrete made with natural pumice. *Construction and Building Materials*, 25(5), 2458-2464.

[162] Hsu, L. S., & Hsu, C. T. (1994). Stress-strain behavior of steel-fiber high-strength concrete under compression. *ACI structural journal*, 91(4), 448-457.

[163] Wafa, F. F., & Ashour, S. A. (1992). Mechanical properties of high-strength fiber reinforced concrete. *ACI Materials Journal*, 89(5), 449-455.

[164] Marar, K., Eren, Ö., & Celik, T. (2001). Relationship between impact energy and compression toughness energy of high-strength fiber-reinforced concrete. *Materials letters*, 47(4), 297-304.

[165] Ünal, O., Demir, F., & Uygunoğlu, T. (2007). Fuzzy logic approach to predict stress–strain curves of steel fiber-reinforced concretes in compression. *Building and environment*, 42(10), 3589-3595.

[166] Ezeldin, A. S., & Balaguru, P. N. (1992). Normal-and high-strength fiber-reinforced concrete under compression. *Journal of materials in civil engineering*, 4(4), 415-429.

[167] Bai, J. (2013). Advanced fibre-reinforced polymer (FRP) composites for structural applications. Elsevier.

[168] Nataraja, M. C., Dhang, N., & Gupta, A. P. (1999). Stress–strain curves for steel-fiber reinforced concrete under compression. *Cement and concrete composites*, 21(5), 383-390.

[169] Zain, M. F. M., Mahmud, H. B., Ilham, A., & Faizal, M. (2002). Prediction of splitting tensile strength of high-performance concrete. *Cement and concrete research*, 32(8), 1251-1258.

[170] Li, G. (2004). The effect of moisture content on the tensile strength properties of concrete. Doctoral dissertation, University of Florida.

[171] Li, Z. (2011). Advanced concrete technology. John Wiley & Sons.

[172] Dewar, J. D. (1964). The indirect tensile strength of concrete of high compressive strength. Cement and Concrete Association.

[173] Lu, X., & Hsu, C. T. T. (2006). Behavior of high strength concrete with and without steel fiber reinforcement in triaxial compression. *Cement and Concrete Research*, 36(9), 1679-1685.

[174] Yazıcı, Ş., İnan, G., & Tabak, V. (2007). Effect of aspect ratio and volume fraction of steel fiber on the mechanical properties of SFRC. *Construction and Building Materials*, 21(6), 1250-1253.

[175] Sivakumar, A., & Santhanam, M. (2007). Mechanical properties of high strength concrete reinforced with metallic and non-metallic fibres. *Cement and Concrete Composites*, 29(8), 603-608.

[176] Altun, F., Haktanir, T., & Ari, K. (2007). Effects of steel fiber addition on mechanical properties of concrete and RC beams. *Construction and Building Materials*, 21(3), 654-661.

[177] Van Chanh, N. (2004). Steel fiber reinforced concrete. In Faculty of Civil Engineering Ho chi minh City university of Technology. Seminar Material, 108-116.

[178] Gül, R., Okuyucu, E., Türkmen, İ., & Aydin, A. C. (2007). Thermo-mechanical properties of fiber reinforced raw perlite concrete. *Materials Letters*, 61(29), 5145-5149.

[179] Gao, J., Sun, W., & Morino, K. (1997). Mechanical properties of steel fiber-reinforced, high-strength, lightweight concrete. *Cement and Concrete Composites*, 19(4), 307-313.

[180] Yao, W., Li, J., & Wu, K. (2003). Mechanical properties of hybrid fiber-reinforced concrete at low fiber volume fraction. *Cement and concrete research*, 33(1), 27-30.

[181] Song, P. S., Hwang, S., & Sheu, B. C. (2005). Strength properties of nylon-and polypropylene-fiber-reinforced concretes. *Cement and Concrete Research*, 35(8), 1546-1550.

[182] Mohammadi, Y., Singh, S. P., & Kaushik, S. K. (2008). Properties of steel fibrous concrete containing mixed fibres in fresh and hardened state. *Construction and Building Materials*, 22(5), 956-965.

[183] Shihada, S. (2011). Mechanical Properties of Ultra High Performance Fiber Reinforced Concrete (UHPFRC). *The Islamic University Journal*, 19(2), 57-69.

[184] Kim, D. J., Park, S. H., Ryu, G. S., & Koh, K. T. (2011). Comparative flexural behavior of hybrid ultra high performance fiber reinforced concrete with different macro fibers. *Construction and Building Materials*, 25(11), 4144-4155.

[185] Yap, S. P., Bu, C. H., Alengaram, U. J., Mo, K. H., & Jumaat, M. Z. (2014). Flexural toughness characteristics of steel–polypropylene hybrid fibre-reinforced oil palm shell concrete. *Materials & Design*, 57, 652-659.

[186] Xie, J. H., Guo, Y. C., Liu, L. S., & Xie, Z. H. (2015). Compressive and flexural behaviours of a new steel-fibre-reinforced recycled aggregate concrete with crumb rubber. *Construction and Building Materials*, 79, 263-272.

[187] Gopalaratnam, V. S., & Gettu, R. (1995). On the characterization of flexural toughness in fiber reinforced concretes. *Cement and concrete composites*, 17(3), 239-254.

[188] Yi, C. K., & Ostertag, C. P. (2001). Strengthening and toughening mechanisms in microfiber reinforced cementitious composites. *Journal of materials science*, 36(6), 1513-1522.

[189] Wang, J. Y., Chia, K. S., Liew, J. Y. R., & Zhang, M. H. (2013). Flexural performance of fiber-reinforced ultra lightweight cement composites with low fiber content. *Cement and Concrete Composites*, 43, 39-47.

[190] Balaguru, P., & Najm, H. (2004). High-performance fiber-reinforced concrete mixture proportions with high fiber volume fractions. *ACI Materials Journal*, 101(4), 281-286.

[191] Balaguru, P., Narahari, R., & Patel, M. (1992). Flexural toughness of steel fiber reinforced concrete. *ACI Materials Journal*, 89(6), 541-546.

[192] Toutanji, H. A. (1999). Properties of polypropylene fiber reinforced silica fume expansive-cement concrete. *Construction and Building Materials*, 13(4), 171-177.

[193] Banthia, N., & Sappakittipakorn, M. (2007). Toughness enhancement in steel fiber reinforced concrete through fiber hybridization. *Cement and Concrete Research*, 37(9), 1366-1372.

[194] Blunt, J. D., & Ostertag, C. P. (2009). Deflection hardening and workability of hybrid fiber composites. *ACI Materials Journal*, 106(3), 265-272.

[195] Kwon, S. H., & Shah, S. P. (2008). Prediction of early-age cracking of fiber-reinforced concrete due to restrained shrinkage. *ACI Materials Journal*, 105(4), 381-389.

[196] Soliman, A. M., & Nehdi, M. L. (2011). Effect of drying conditions on autogenous shrinkage in ultra-high performance concrete at early-age. *Materials and Structures*, *44*(5), 879-899.

[197] Gribniak, V., Kaklauskas, G., Kliukas, R., & Jakubovskis, R. (2013). Shrinkage effect on short-term deformation behavior of reinforced concrete–When it should not be neglected. *Materials & Design*, 51, 1060-1070.

[198] Cheung, A. K., & Leung, C. K. (2011). Shrinkage reduction of high strength fiber reinforced cementitious composites (HSFRCC) with various water-to-binder ratios. *Cement and Concrete Composites*, 33(6), 661-667.

[199] Bentz, D. P., Geiker, M. R., & Hansen, K. K. (2001). Shrinkage-reducing admixtures and early-age desiccation in cement pastes and mortars. *Cement and concrete research*, 31(7), 1075-1085.

[200] Folliard, K. J., & Berke, N. S. (1997). Properties of high-performance concrete containing shrinkage-reducing admixture. *Cement and Concrete Research*, 27(9), 1357-1364.

[201] Nmai, C. K., Tomita, R., Hondo, F., & Buffenbarger, J. (1998). Shrinkage reducing admixtures. *Concrete International*, 20(4), 31-37.

[202] Shah, S. P., Weiss, W. J., & Yang, W. (1998). Shrinkage cracking-Can it be prevented? *Concrete International*, 20(4), 51-55.

[203] Swamy, R. N., & Stavrides, H. (1979). Influence of fiber reinforcement on restrained shrinkage and cracking. *In ACI Journal proceedings*, 76(3), 443-460.

[204] Paul, B. K., Polivka, M., & Mehta, P. K. (1981). Properties of fiber reinforced shrinkage-compensating concrete. *In ACI Journal Proceedings*, 78(6), 488-492.

[205] Swamy, R. N. (1986). Steel fibre concrete for bridge deck and building floor applications. *Structural Engineer. Part A*, 64, 149-157.

[206] Kim, B., & Weiss, W. J. (2003). Using acoustic emission to quantify damage in restrained fiber-reinforced cement mortars. *Cement and Concrete Research*, 33(2), 207-214.

[207] Grzybowski, M., & Shah, S. P. (1990). Shrinkage cracking of fiber reinforced concrete. *ACI Materials Journal*, 87(2), 138-148.

[208] Sargaphuti, M., Shah, S. P., & Vinson, K. D. (1993). Shrinkage cracking and durability characteristics of cellulose fiber reinforced concrete. *ACI materials journal*, 90(4), 309-318.

[209] Banthia, N., & Yan, C. (2000). Shrinkage cracking in polyolefin fiber-reinforced concrete. *ACI Materials Journal*, 97(4), 432-437.

[210] Banthia, N., Azzabi, M., & Pigeon, M. (1995). Restrained shrinkage tests on fiber reinforced cementitious composites. *ACI Special Publication*, 137-151.

[211] Wang, Y. D., & Fan, X. C. (2011). Experimental research on physical and mechanical properties of steel fiber high-strength concrete. *In Advanced Materials Research*, 168, 1061-1064.

[212] Jafarifar, N., Pilakoutas, K., & Bennett, T. (2014). Moisture transport and drying shrinkage properties of steel–fibre-reinforced-concrete. *Construction and Building Materials*, 73, 41-50.

[213] Güneyisi, E., Gesoğlu, M., Mohamadameen, A., Alzeebaree, R., Algın, Z., & Mermerdaş, K. (2014). Enhancement of shrinkage behavior of lightweight aggregate concretes by shrinkage reducing admixture and fiber reinforcement. *Construction and Building Materials*, 54, 91-98.

[214] Zhang, P., & Li, Q. F. (2013). Effect of polypropylene fiber on durability of concrete composite containing fly ash and silica fume. *Composites Part B: Engineering*, 45(1), 1587-1594.

[215] Bywalski, C., Kamiński, M., & Maszczak, M. (2015). Influence of steel fibres addition on mechanical and selected rheological properties of steel fibre high-strength reinforced concrete. *Archives of Civil and Mechanical Engineering*, 15(3), 742-750.

[216] Choi, S. Y., Park, J. S., & Jung, W. T. (2011). A study on the shrinkage control of fiber reinforced concrete pavement. *Procedia Engineering*, 14, 2815-2822.

[217] Sun, W., Chen, H., Luo, X., & Qian, H. (2001). The effect of hybrid fibers and expansive agent on the shrinkage and permeability of high-performance concrete. *Cement and Concrete Research*, 31(4), 595-601.

[218] Mangat, P. S., & Azari, M. M. (1984). A theory for the free shrinkage of steel fibre reinforced cement matrices. *Journal of materials science*, 19(7), 2183-2194.

[219] Ranaivomanana, N., Multon, S., & Turatsinze, A. (2013). Basic creep of concrete under compression, tension and bending. *Construction and Building Materials*, 38, 173-180.

[220] Buratti, N., Mazzotti, C., & Savoia, M. (2010). Long-Term Behaviour of Fiber-Reinforced Self-Compacting Concrete Beams. *In Design, Production and Placement of Self-Consolidating Concrete*, 439-450.

[221] Rouse, J. M., & Billington, S. L. (2007). Creep and shrinkage of high-performance fiber-reinforced cementitious composites. *ACI materials journal*, 104(2), 129-136.

[222] ACI 209R-97. (1997). Prediction of creep, shrinkage, and temperature effects in concrete structures.

[223] ACI 544.5R-10. (2010). Report on the physical properties and durability of fiber-reinforced concrete.

[224] Rossi, P., Tailhan, J. L., & Le Maou, F. (2013). Comparison of concrete creep in tension and in compression: Influence of concrete age at loading and drying conditions. *Cement and Concrete Research*, 51, 78-84.

[225] Chen, C. T., Chang, J. J., & Yeih, W. C. (2014). The effects of specimen parameters on the resistivity of concrete. *Construction and Building Materials*, 71, 35-43.

[226] Jalal, M., Mansouri, E., Sharifipour, M., & Pouladkhan, A. R. (2012). Mechanical, rheological, durability and microstructural properties of high performance self-compacting concrete containing $SiO_2$ micro and nanoparticles. *Materials & Design*, 34, 389-400.

[227] Aït-Mokhtar, A., Belarbi, R., Benboudjema, F., Burlion, N., Capra, B., Carcasses, M., Colliat, J. B., Cussigh, F., Deby, F., Jacquemot, F., De Larrard, T., Lataste, J. F., Le Bescop, P., Pierre, M., Poyet, S., Rougeau, P., Rougelot, T., Sellier, A., Séménadisse, J., Torrenti, J. M.,Trabelsi, A.,Turcry, P., & Yanez-Godoy, H. (2013). Experimental investigation of the variability of concrete durability properties. *Cement and concrete research*, 45, 21-36.

[228] Sanish, K. B., Neithalath, N., & Santhanam, M. (2013). Monitoring the evolution of material structure in cement pastes and concretes using electrical property measurements. *Construction and Building Materials*, 49, 288-297.

[229] Polder, R. B. (2001). Test methods for on site measurement of resistivity of concrete-a RILEM TC-154 technical recommendation. *Construction and building materials*, 15(2), 125-131.

[230] Basheer, P. A. M., Gilleece, P. R. V., Long, A. E., & Mc Carter, W. J. (2002). Monitoring electrical resistance of concretes containing alternative cementitious materials to assess their resistance to chloride penetration. *Cement and Concrete Composites*, 24(5), 437-449.

[231] Pacheco, J., Šavija, B., Schlangen, E., & Polder, R. B. (2014). Assessment of cracks in reinforced concrete by means of electrical resistance and image analysis. *Construction and Building Materials*, 65, 417-426.

[232] Torres-Luque, M., Bastidas-Arteaga, E., Schoefs, F., Sánchez-Silva, M., & Osma, J. F. (2014). Non-destructive methods for measuring chloride ingress into concrete: State-of-the-art and future challenges. *Construction and Building Materials*, 68, 68-81.

[233] Ahmad, S., Adekunle, S. K., Maslehuddin, M., & Azad, A. K. (2014). Properties of self-consolidating concrete made utilizing alternative mineral fillers. *Construction and Building Materials*, 68, 268-276.

[234] Boulay, C., Dal Pont, S., & Belin, P. (2009). Real-time evolution of electrical resistance in cracking concrete. *Cement and Concrete Research*, 39(9), 825-831.

[235] ACI 222R-01. (2001). Protection of metals in concrete against corrosion.

[236] Audenaert, K. (2006). Transportmechanismen in zelfverdichtend beton in relatie met carbonatatie en chloridepenetratie. *Doctoraalstudie, Universiteit Gent, Gent*.

[237] Polder, R., Andrade, C., Elsener, B., Vennesland, Ø., Gulikers, J., Weidert, R., & Raupach, M. (2000). Test methods for on site measurement of resistivity of concrete. *Materials and Structures*, 33(10), 603-611.

[238] De Rooij, M. R., Polder, R. B., & Van Oosten, H. H. (2007). Validation of service life performance of in situ concrete by TEM and RCM measurements. *Heron*, 52 (4), 1-14.

[239] Bertolini, L., Elsener, B., Pedeferri, P., Redaelli, E., & Polder, R. B. (2013). Corrosion of steel in concrete: prevention, diagnosis, repair. *John Wiley & Sons*.

[240] Sabet, F. A., Libre, N. A., & Shekarchi, M. (2013). Mechanical and durability properties of self consolidating high performance concrete incorporating natural zeolite, silica fume and fly ash. *Construction and Building Materials*, 44, 175-184.

[241] Smith, K. M., Schokker, A. J., & Tikalsky, P. J. (2004). Performance of supplementary cementitious materials in concrete resistivity and corrosion monitoring evaluations. *ACI Materials Journal*, 101(5), 385-390.

[242] Baroghel-Bouny, V., Kinomura, K., Thiery, M., & Moscardelli, S. (2011). Easy assessment of durability indicators for service life prediction or quality control of concretes with high volumes of supplementary cementitious materials. *Cement and Concrete Composites*, 33(8), 832-847.

[243] Ramezanianpour, A. A., & Jovein, H. B. (2012). Influence of metakaolin as supplementary cementing material on strength and durability of concretes. *Construction and Building materials*, 30, 470-479.

[244] Tsai, C. T., Li, L. S., Chang, C. C., & Hwang, C. L. (2009). Durability design and application of steel fiber reinforced concrete in Taiwan. *The Arabian Journal for Science and Engineering*, 34(1B), 57-79.

[245] Nili, M., & Afroughsabet, V. (2012). Property assessment of steel–fibre reinforced concrete made with silica fume. *Construction and Building Materials*, 28(1), 664-669.

[246] Frazão, C., Camões, A., Barros, J., & Gonçalves, D. (2015). Durability of steel fiber reinforced self-compacting concrete. *Construction and Building Materials*, 80, 155-166.

[247] Kakooei, S., Akil, H. M., Jamshidi, M., & Rouhi, J. (2012). The effects of polypropylene fibers on the properties of reinforced concrete structures. *Construction and Building Materials*, 27(1), 73-77.

[248] Nili, M., & Afroughsabet, V. (2012). The long-term compressive strength and durability properties of silica fume fiber-reinforced concrete. *Materials Science and Engineering: A*, 531, 107-111.

[249] Söylev, T. A., & Özturan, T. (2014). Durability, physical and mechanical properties of fiber-reinforced concretes at low-volume fraction. *Construction and Building Materials*, 73, 67-75.

[250] Lim, T. Y. D., Teng, S., Bahador, S. D., & Gjørv, O. E. (2016). Durability of very-high-strength concrete with supplementary cementitious materials for marine environments, *ACI Materials Journal*, *113*, 95-104.

[251] Banthia, N., Zanotti, C., & Sappakittipakorn, M. (2014). Sustainable fiber reinforced concrete for repair applications. *Construction and Building Materials*, 67, 405-412.

[252] Ghafoori, N., Najimi, M., Sobhani, J., & Aqel, M. A. (2013). Predicting rapid chloride permeability of self-consolidating concrete: A comparative study on statistical and neural network models. *Construction and Building Materials*, 44, 381-390.

[253] Zhang, M. H., & Li, H. (2011). Pore structure and chloride permeability of concrete containing nano-particles for pavement. *Construction and Building Materials*, 25(2), 608-616.

[254] Živica, V. (1997). Relationship between pore structure and permeability of hardened cement mortars: on the choice of effective pore structure parameter. *Cement and Concrete Research*, 27(8), 1225-1235.

[255] Tanaka, K., & Kurumisawa, K. (2002). Development of technique for observing pores in hardened cement paste. *Cement and Concrete Research*, 32(9), 1435-1441.

[256] Chao, S., & Lin, W. (2013). Effects of silica fume and steel fiber on chloride ion penetration and corrosion behavior of cement-based composites. *Journal of Wuhan University of Technology-Mater. Sci. Ed.*, 28, 279-284.

[257] Gagné, R., Aïtcin, P. C., & Lamoth, P. (1993). Chloride-ion permeability of different concretes. *In Proceedings of the Sixth International Conference on Durability of Building Materials Components*, Omiya, Japan, 1171-1180.

[258] Aıtcin, P. C. (2003). The durability characteristics of high performance concrete: a review. *Cement and Concrete Composites*, 25(4), 409-420.

[259] ASTM C1202-05. (2005). Standard test method for electrical indication of concrete's ability to resist chloride ion penetration.

[260] Nilsson, L., Ngo, M. H., & Gjørv, O. E. (1998). High-performance repair materials for concrete structures in the port of Gothenburg. *In Second international conference on concrete under severe conditions: environment and loading*, 2, 1193-1198.

[261] Gruber, K. A., Ramlochan, T., Boddy, A., Hooton, R. D., & Thomas, M. D. A. (2001). Increasing concrete durability with high-reactivity metakaolin. *Cement and concrete composites*, 23(6), 479-484.

[262] Choi, Y. S., Kim, J. G., & Lee, K. M. (2006). Corrosion behavior of steel bar embedded in fly ash concrete. *Corrosion Science*, 48(7), 1733-1745.

[263] Lu, X., Li, C., & Zhang, H. (2002). Relationship between the free and total chloride diffusivity in concrete. *Cement and Concrete Research*, 32(2), 323-326.

[264] Thomas, M. D., & Bamforth, P. B. (1999). Modelling chloride diffusion in concrete: effect of fly ash and slag. *Cement and Concrete Research*, 29(4), 487-495.

[265] Manera, M., Vennesland, Ø., & Bertolini, L. (2008). Chloride threshold for rebar corrosion in concrete with addition of silica fume. *Corrosion Science*, 50(2), 554-560.

[266] Yang, C. C., & Cho, S. W. (2003). An electrochemical method for accelerated chloride migration test of diffusion coefficient in cement-based materials. *Materials chemistry and physics*, 81(1), 116-125.

[267] Shekarchi, M., Rafiee, A., & Layssi, H. (2009). Long-term chloride diffusion in silica fume concrete in harsh marine climates. *Cement and Concrete Composites*, 31(10), 769-775.

[268] Uysal, M., Yilmaz, K., & Ipek, M. (2012). The effect of mineral admixtures on mechanical properties, chloride ion permeability and impermeability of self-compacting concrete. *Construction and Building Materials*, 27(1), 263-270.

[269] Deboodt, T., Fu, T., & Ideker, J. H. (2015). Durability assessment of high-performance concrete with SRAs and FLWAs. *Cement and Concrete Composites*, 57, 94-101.

[270] Şahmaran, M. (2007). Effect of flexure induced transverse crack and self-healing on chloride diffusivity of reinforced mortar. *Journal of Materials Science*, 42(22), 9131-9136.

[271] Van Niejenhuis, C. B., Walbridge, S., & Hansson, C. M. (2016). The performance of austenitic and duplex stainless steels in cracked concrete exposed to concentrated chloride brine. *Journal of Materials Science*, 51(1), 362-374.

[272] Boughanem, S., Jesson, D. A., Mulheron, M. J., Smith, P. A., Eddie, C., Psomas, S., & Rimes, M. (2015). Tensile characterisation of thick sections of Engineered Cement Composite (ECC) materials. *Journal of Materials Science*, 50(2), 882-897.

[273] Rokugo, K., Kanda, T., Yokota, H., & Sakata, N. (2009). Applications and recommendations of high performance fiber reinforced cement composites with multiple fine cracking (HPFRCC) in Japan. *Materials and structures*, 42(9), 1197-1208.

[274] Di Prisco, M., Plizzari, G., & Vandewalle, L. (2009). Fibre reinforced concrete: new design perspectives. *Materials and Structures*, 42(9), 1261-1281.

[275] ACI Committee 224R. (2001). Control of cracking in concrete structures. *ACI 224-01. American Concrete Institute, Detroit, Michigan*.

[276] ACI Committee 318. (1995). Building code requirements for reinforced concrete. *ACI 318-95. American Concrete Institute, Detroit, Michigan*.

[277] CEB-FIB Model Code 1990. (1993). CEB information report no. 213/214. *Committee Euro-International DuBeton, Lausanne*.

[278] JSCE. (1986). Standard specification for design and construction of concrete structures-part 1 (Design). *Japan Society of Civil Engineers, SP- 1, Tokyo, Japan.*

[279] Mangat, P. S., & Gurusamy, K. (1987). Chloride diffusion in steel fibre reinforced marine concrete. *Cement and Concrete Research*, 17(3), 385-396.

[280] Aldea, C. M., Shah, S. P., & Karr, A. (1999). Effect of cracking on water and chloride permeability of concrete. *Journal of materials in civil engineering*, 11(3), 181-187.

[281] Balouch, S. U., Forth, J. P., & Granju, J. L. (2010). Surface corrosion of steel fibre reinforced concrete. *Cement and Concrete Research*, 40(3), 410-414.

[282] Karlsson, J. (2014). Alternative Reinforcement Approaches-Extended service life of exposed concrete structures. *Master of Science Thesis, Chalmers University of Technology*.

[283] De Rivaz, B. (2008). Steel Fiber Reinforced Concrete (SFRC): The use of SFRC in precast segment for tunnelling. *Water and Energy International*, 65(3), 47-56.

[284] Tazaly, Z. (2012). Punching Shear Capacity of Fibre Reinforced Concrete Slabs with Conventional Reinforcement: Computational analysis of punching models. *Master of Science Thesis, KTH University*.

[285] Berrocal, C. G., Lundgren, K., & Löfgren, I. (2015). Corrosion of steel bars embedded in fibre reinforced concrete under chloride attack: State of the art. *Cement and Concrete Research*, 80, 69-85.

[286] Berrocal, C. G., Löfgren, I., Lundgren, K., & Tang, L. (2015). Corrosion initiation in cracked fibre reinforced concrete: influence of crack width, fibre type and loading conditions. *Corrosion Science*, 98, 128-139.

[287] Abbas, S., Soliman, A. M., & Nehdi, M. L. (2015). Exploring mechanical and durability properties of ultra-high performance concrete incorporating various steel fiber lengths and dosages. *Construction and Building Materials*, 75, 429-441.

[288] Granju, J. L., & Balouch, S. U. (2005). Corrosion of steel fibre reinforced concrete from the cracks. *Cement and Concrete Research*, 35(3), 572-577.

[289] Lawler, J. S., Zampini, D., & Shah, S. P. (2002). Permeability of cracked hybrid fiber-reinforced mortar under load. *ACI Materials Journal*, 99(4), 379-385.

[290] Blunt, J., Jen, G., & Ostertag, C. P. (2015). Enhancing corrosion resistance of reinforced concrete structures with hybrid fiber reinforced concrete. *Corrosion Science*, 92, 182-191.

[291] ASTM C 143. (2010). Standard test method for slump of hydraulic-cement concrete.

[292] ASTM C 39. (2003). Standard test method for compressive strength of cylindrical concrete specimens.

[293] ASTM C 469. (2014). Standard test method for static modulus of elasticity and Poisson's ratio of concrete in compression.

[294] ASTM C 496/C 496M-11. (2011). Standard Test Method for Splitting Tensile Strength of Cylindrical Concrete Specimens.

[295] BSEN 14651. (2007). Test method for metallic fibre concrete-measuring the flexural tensile strength (limit of proportionality (LOP), residual).

[296] ASTM C 642-13. (2013). Standard Test Method for Density, Absorption, and Voids in Hardened Concrete.

[297] ASTM C 157/C 157M-08. (2014). Standard test method for length change of hardened hydraulic-cement mortar and concrete.

[298] ASTM C 876-91. (1991). Standard test method for half-cell potentials of uncoated reinforcing steel in concrete.

[299] BS EN 480-14. (2006). Admixtures for concrete, mortar and grout. Test methods. Determination of the effect on corrosion susceptibility of reinforcing steel by potentiostatic electro-chemical test.

[300] Kjellsen, K. O., Monsøy, A., Isachsen, K., & Detwiler, R. J. (2003). Preparation of flat-polished specimens for SEM-backscattered electron imaging and X-ray microanalysis—importance of epoxy impregnation. *Cement and concrete research*, *33*(4), 611-616.

[301] Ramachandran, V. S., & Beaudoin, J. J. (2000). *Handbook of analytical techniques in concrete science and technology: principles, techniques and applications*. Elsevier.

[302] Calvo, J. G., Revuelta, D., Carballosa, P., & Gutiérrez, J. P. (2017). Comparison between the performance of expansive SCC and expansive conventional concretes in different expansion and curing conditions. *Construction and Building Materials*, *136*, 277-285.

[303] Shuguang, H., & Yue, L. (1999). Research on the hydration, hardening mechanism, and microstructure of high performance expansive concrete. *Cement and concrete research*, *29*(7), 1013-1017.

[304] Afroughsabet, V., Biolzi, L., & Ozbakkaloglu, T. (2016). High-performance fiber-reinforced concrete: a review. *Journal of Materials Science*, *51*(14), 6517-6551.

[305] Chung, D. D. L. (2002). Review: improving cement-based materials by using silica fume. *Journal of Materials Science*, 37(4), 673-682.

[306] Corinaldesi, V., Nardinocchi, A., & Donnini, J. (2015). The influence of expansive agent on the performance of fibre reinforced cement-based composites. *Construction and Building Materials*, *91*, 171-179.

[307] Fib Bulletin 65. (2010). Model Code 2010-Final Draft, 1, 234–247.

[308] He, H. A., Dong, W., & Wu, Z. M. (2011). Study on long-term expansive deformation of self-stressing concrete with combined restrictions of steel fibers and steel bar. In *Key Engineering Materials*, 452, 533-536.

[309] Ioannou, S., Paine, K., Reig, L., & Quillin, K. (2015). Performance characteristics of concrete based on a ternary calcium sulfoaluminate–anhydrite–fly ash cement. *Cement and Concrete Composites*, *55*, 196-204.

[310] Markovich, I., Van Mier, J. G. M., & Walraven, J. C. (2001). Single fiber pullout from hybrid fiber reinforced concrete. *Heron*, *46*(3), 191-200.

[311] Park, S. H., Ryu, G. S., Koh, K. T., & Kim, D. J. (2014). Effect of shrinkage reducing agent on pullout resistance of high-strength steel fibers embedded in ultra-high-performance concrete. *Cement and Concrete Composites*, *49*, 59-69.

[312] Panesar, D. K., & Francis, J., (2014). Influence of limestone and slag on the pore structure of cement paste based on mercury intrusion porosimetry and water vapour sorption measurements. *Construction and Building Materials*, *52*, 52-58.

[313] Señas, L., Priano, C., & Marfil, S., (2016). Influence of recycled aggregates on properties of self-consolidating concretes. *Construction and Building Materials*, *113*, 498-505.

[314] Sharma, R. L., & Pandey, S. P., (1999). Influence of mineral additives on the hydration characteristics of ordinary Portland cement. *Cement and Concrete Research*, *29*(9), 1525-1529.

[315] Lumley, J. S., Gollop, R. S., Moir, G. K., & Taylor, H. F. W., (1996). Degrees of reaction of the slag in some blends with Portland cements. *Cement and Concrete Research*, *26*(1), 139-151.

[316] Yu, R., Spiesz, P., & Brouwers, H. J. H. (2015). Development of an eco-friendly Ultra-High Performance Concrete (UHPC) with efficient cement and mineral admixtures uses. *Cement and Concrete Composites*, *55*, 383-394.

[317] Divsholi, B. S., Lim, T. Y. D., & Teng, S. (2014). Durability properties and microstructure of ground granulated blast furnace slag cement concrete. *International Journal of Concrete Structures and Materials*, *8*(2), 157-164.

[318] Afroughsabet, V., & Ozbakkaloglu, T., (2015). Mechanical and durability properties of high-strength concrete containing steel and polypropylene fibers. *Construction and Building Materials*, *94*, 73-82.

[319] Yoo, D. Y., Yoon, Y. S., & Banthia, N., (2015). Predicting the post-cracking behavior of normal-and high-strength steel-fiber-reinforced concrete beams. *Construction and Building Materials*, *93*, 477-485.

[320] Simões, T., Octávio, C., Valença, J., Costa, H., Dias-da-Costa, D., & Júlio, E., (2017). Influence of concrete strength and steel fibre geometry on the fibre/matrix interface. *Composites Part B: Engineering*, *122*, 156-164.

[321] Gonzalez-Corominas, A., & Etxeberria, M., (2016). Effects of using recycled concrete aggregates on the shrinkage of high performance concrete. *Construction and Building Materials*, *115*, 32-41.

[322] Coumes, C. C. D., Courtois, S., Peysson, S., Ambroise, J., & Pera, J. (2009). Calcium sulfoaluminate cement blended with OPC: a potential binder to encapsulate low-level radioactive slurries of complex chemistry. *Cement and Concrete Research*, *39*(9), 740-747.

[323] Ogawa, K., & Roy, D. M. (1982). C4A3S hydration, ettringite formation, and its expansion mechanism: II. Microstructural observation of expansion. *Cement and Concrete Research*, *12*(1), 101-109.

[324] Kou, S. C., Poon, C. S., & Etxeberria, M., (2014). Residue strength, water absorption and pore size distributions of recycled aggregate concrete after exposure to elevated temperatures. *Cement and Concrete Composites*, *53*, 73-82.

[325] Elahi, A., Basheer, P. A. M., Nanukuttan, S. V., & Khan, Q. U. Z. (2010). Mechanical and durability properties of high performance concretes containing supplementary cementitious materials. *Construction and Building Materials*, *24*(3), 292-299.

[326] Martin, L. H., Winnefeld, F., Müller, C. J., & Lothenbach, B. (2015). Contribution of limestone to the hydration of calcium sulfoaluminate cement. *Cement and Concrete Composites*, *62*, 204-211.

[327] Liao, Y., Wei, X., & Li, G. (2011). Early hydration of calcium sulfoaluminate cement through electrical resistivity measurement and microstructure investigations. *Construction and building materials*, *25*(4), 1572-1579.

[328] Ramezanianpour, A. A., Pilvar, A., Mahdikhani, M., & Moodi, F. (2011). Practical evaluation of relationship between concrete resistivity, water penetration, rapid chloride penetration and compressive strength. *Construction and Building Materials*, *25*(5), 2472-2479.

[329] Janotka, I. V. A. N., Krajci, L., & Mojumdar, S. C. (2002). Influence of Portland cement addition to sulphoaluminate-belite cement on hydration and mechanical properties of hardened mortars. *Ceramics-Silikaty*, *46*(3), 110-116.

[330] Aranda, M. A. G., & De la Torre, A. G. (2013). Sulfoaluminate cement. *Eco-efficient concrete*, 488-522.

[331] Huang, R., Chang, J. J., & Wu, J. K. (1996). Correlation between corrosion potential and polarization resistance of rebar in concrete. *Materials Letters*, *28*(4-6), 445-450.

[332] Scrivener, K. L., Crumbie, A. K., & Laugesen, P. (2004). The interfacial transition zone (ITZ) between cement paste and aggregate in concrete. *Interface Science*, *12*(4), 411-421.

[333] Erdem, S., Dawson, A. R., & Thom, N. H. (2012). Impact load-induced micro-structural damage and micro-structure associated mechanical response of concrete made with different surface roughness and porosity aggregates. *Cement and Concrete Research*, *42*(2), 291-305.

[334] Cwirzen, A., & Penttala, V. (2005). Aggregate–cement paste transition zone properties affecting the salt–frost damage of high-performance concretes. *Cement and Concrete Research*, *35*(4), 671-679.

[335] Hu, C., Hou, D., & Li, Z. (2017). Micro-mechanical properties of calcium sulfoaluminate cement and the correlation with microstructures. *Cement and Concrete Composites*, *80*, 10-16.

[336] Arjunan, P., Silsbee, M. R., & Roy, D. M. (1999). Sulfoaluminate-belite cement from low-calcium fly ash and sulfur-rich and other industrial by-products. *Cement and Concrete Research*, *29*(8), 1305-1311.

[337] Mudbhatkal, G. A., Parmeswaran, P. S., Heble, A. S., Pai, B. V. B., & Chatterjee, A. K. (1986). Non-Alitic Cement from Calcium Sulphoaluminate Clinker-Optimisation for High Strength and Low Temperature Application. In *UIn: U Proceedings of the 8P th P International Congress on the Chemistry of Cement*, 364-370.